

COMPARISON OF UNIVERSITY OF MICHIGAN CIREN CASES TO EXISTING TYPES OF CRASH TESTS

Bridget O'Brien-Mitchell

Kacy Bailey

Daniel Faust

Jack Jensen

Julie Kleinert

Christine Wodzinski

Stewart Wang

University of Michigan Program for Injury Research and Education

United States

Paper Number 09-0185

ABSTRACT

A comparison of U-M CIREN (University of Michigan Crash Injury Research and Engineering Network) cases to crash tests used in the automotive industry is presented in this paper. 442 U-M CIREN crashes were compared to crash test configurations used throughout the industry. Of those 442 cases, 49% were similar in crash configuration and crash extent to industry crash tests. 32% of the cases were similar to one of the industry crash tests in configuration but had greater extent. 20% of the cases did not match any of the current industry crash tests.

This analysis concluded that the majority of injuries in this study occurred in crash configurations similar to existing crash tests while only 20% of cases had crash configurations that were not represented by current crash tests. Any consideration of increasing test severity to address those crashes that produce a greater extent of crash deformation than that produced in crash tests must consider a broader spectrum of collisions including non-injury producing crashes. This analysis must be done in a way that does not increase the risk to the current uninjured population that is not included in the CIREN database.

INTRODUCTION

Studies have demonstrated that fatality rates from motor vehicle crashes in the United States have been reduced over the last several decades. As an example the fatality rate per 100 million miles driven was 5.5 in 1966 and steadily declined to 1.41 in 2006. In addition, injuries have been reduced from 169 injuries per 100 million miles driven in 1988 to 85 in 2006. Despite the significant improvements in automotive safety, there continues to be about 38,500 annual fatalities due to motor vehicle crashes [1]. Therefore there is benefit to investigating the

remaining fatalities and serious injuries due to motor vehicle crashes.

The goal of this project was to compare the crashes in the U-M CIREN database to existing industry crash tests. CIREN is a multi-center research program involving a collaboration of clinicians and engineers in academia, industry, and government. There are currently eight CIREN centers around the United States that each pursues in-depth studies of crashes, injuries, and treatments. The UMPIRE (University of Michigan Program for Injury Research and Education) team specifically investigates crashes in Southeast Michigan in which the victims are brought to the University of Michigan Trauma Center in Ann Arbor, Michigan and serves as the CIREN center in Michigan.

BACKGROUND

Industry Crash Test Library

Auto manufacturers routinely conduct crash tests for a number of reasons. Tests are conducted to insure compliance to crash test regulations not only for the United States but for any country in which a vehicle may be marketed. In addition, tests may be conducted to evaluate a vehicle's performance to consumer metric tests such as those conducted at the Insurance Institute of Highway Safety (IIHS) or those conducted as part of the New Car Assessment Program (NCAP). Crash tests may also be conducted by a vehicle manufacturer to evaluate a vehicle's performance in crash tests which are neither government regulated nor consumer metric tests. Crash tests may be supplemented or replaced with component level tests, subsystem tests, math based computer modeling, or engineering judgment.

For the above reasons it is expected that different manufacturers may test to different matrices of crash

tests. However, certain impact test types are generally common throughout the industry. The majority of auto manufacturers who sell vehicles in the United States consider these configurations when designing vehicles.

Table 1 lists the crash test types that were chosen for comparison to the U-M CIREN cases for this study.

Table 1.
Included Industry Crash Tests

0 Degree Frontal (FMVSS 208 [2] and Frontal NCAP)
Left Angle (FMVSS 208 [2])
Right Angle (FMVSS 208 [2])
40% Offset Deformable Barrier (FMVSS 208 [2] and IIHS [3])
Frontal Center Pole
Frontal Offset Pole
Bumper Underride
IIHS Side Impact [4]
Side Impact (FMVSS 214 [5] and Side NCAP)
Side Pole [6]
Rollover

Limitations

It is important to acknowledge that this study is based solely on cases documented in the U-M CIREN database. As such, the uninjured population is not included for comparison. By the definition of the CIREN selection criteria (Appendix A), all of the case occupants are severely injured patients. Those crashes in which there are no injuries or only minor injuries are not included in the CIREN database or the U-M CIREN database, and are not referenced in this study. Thus it is not appropriate to use the CIREN database or the U-M CIREN database in isolation to estimate risk to the driving public.

To help put the CIREN database into context, Figure 1 shows a comparison of the data in the National Automotive Sampling System – Crashworthiness Data System (NASS-CDS) to CIREN cases. More than half of the crashes in NASS-CDS are MAIS 0 crashes because the NASS selection criteria specifies a ‘tow-away’ crash whereas CIREN contains mostly MAIS 3, 4 and 5 cases.

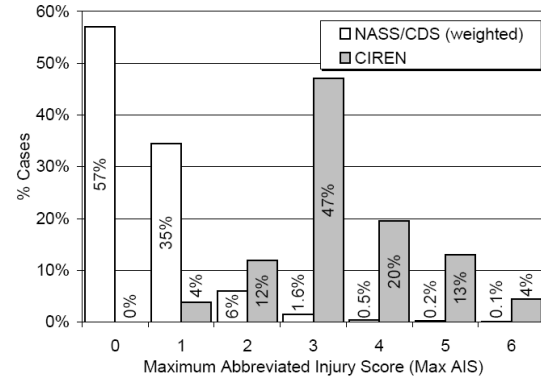


Figure 1. Comparison of CIREN to NASS-CDS. [7]

Figure 2 shows a comparison of AIS 3+ NASS-CDS cases to CIREN cases. Both databases show a similar distribution of Maximum AIS.

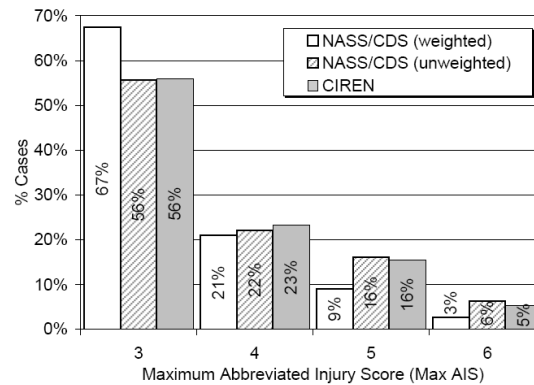


Figure 2. Comparison of AIS 3+ CIREN and NASS-CDS. [7]

Due to these database limitations, this study cannot be used to quantify the relative safety of vehicles, the effectiveness of government regulations, or the effectiveness of the vehicle design process. It has already been documented that motor vehicles have become much safer over the last few decades. This study did not attempt to quantify or verify that conclusion. Instead this study investigated the crash configurations of U-M CIREN cases and compared them to existing crash test configurations. This allowed for conclusions to be drawn about how the industry crash tests match to those injury producing crashes in the U-M CIREN database.

Another limitation of the study is that the vehicles included in the U-M CIREN database were designed at different times to different requirements. Government regulations have changed during the time span of the case vehicles. In addition, different manufacturers may have differing in-house, crash test requirements.

Database

The dataset used for this comparison included all of the 442 CIREN cases that resided in the U-M CIREN database as of August 2007.

To be selected as a CIREN case, the occupant needs to be air bag, or air bag and seat belt restrained and sustain serious injury (Abbreviated Injury Severity [AIS] 3 or greater, or AIS 2 injuries in two or more body regions with medical significance [8]). Currently, the case vehicle must be less than 6 years old and involved in a frontal, side, or rollover crash as described in Appendix A.

Figure 3 indicates that the case vehicles' age ranged from 1989 — 2006 model years with 63% of the vehicles from 1995 — 2000 model years. Most of the vehicles (84%) were produced by GM, Ford, or Chrysler.

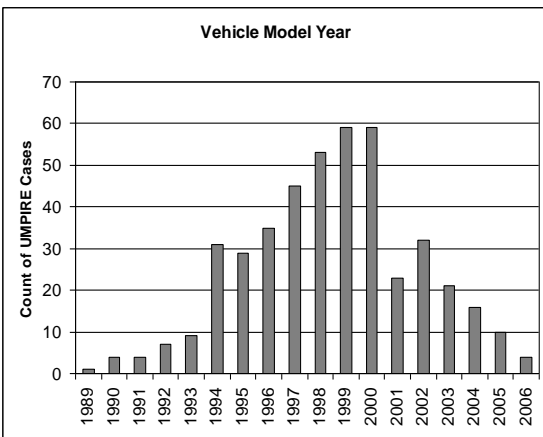


Figure 3. Case Vehicle Model Year Distribution.

METHOD AND RESULTS

The study consisted of two major tasks. First, crash tested vehicles were reviewed and Collision Deformation Classifications (CDCs) were assigned to the crash test types identified in Table 1. Next, U-M CIREN cases were reviewed and matched to test types and/or categorized into new crash categories.

CDC Coding of Crash Tests

Assigning CDCs to laboratory tests from post-test photographs CDCs were assigned to crash tests of midsize sedans, small sedans, small coupes, and large SUVs.

A variety of vehicles were evaluated to determine if there were differences in deformation patterns based

on vehicle type. The team reviewed photographs of vehicles that had been crash tested in the laboratory according to standard test procedures and assigned CDCs as a team.

The method for assigning CDCs is defined in SAE recommended practice J224 [9]. The CDC is a method to classify the extent of residual vehicle deformation in a motor vehicle collision, and consists of three numeric and four alpha-numeric characters, arranged as shown in Figure 4.

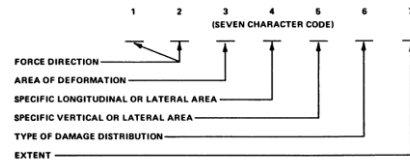


Figure 4. CDC Code

Frontal Crash Test Types — CDCs from Post Test Photographs Figure 5 shows a schematic of a 0 degree frontal crash test and an actual crash tested vehicle.

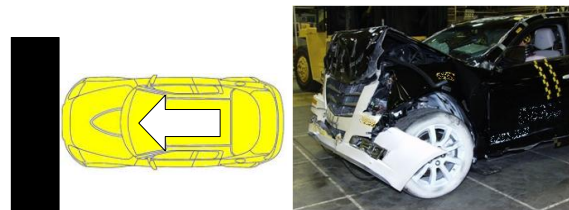


Figure 5. 0 degree Frontal Test.

The CDC for this crash test was 12FDEW3. 0 degree frontal crash tests conducted in the laboratory will always have a 12 o'clock Principle Direction of Force (PDOF). UMPIRE crash case PDOFs of 1 o'clock and 11 o'clock were also considered as similar to a 0 degree frontal laboratory tests. The remaining characters describe a crash that is front (F), distributed across the vehicle (D), everything below the beltline (E) and a wide damage distribution (W).

Figure 6 shows a schematic of a left angled frontal barrier crash test and an actual crash tested vehicle.



Figure 6. Left Angle Barrier Test.

The CDC for this crash test is 12FYEW3. The principal difference between the 0 degree frontal crash test and a left or right angle crash test or offset deformable barrier tests is in the lateral area of deformation. The angled barrier crashes have a force direction of 11 or 12 o'clock force direction (left) or 12 or 1 o'clock force direction (right.) The angled barrier crash tests have a frontal (F) area of deformation but instead of the deformation being distributed across the entire front of the vehicle, it is more localized on the left or right side of the vehicle.

Figure 7 shows a schematic of a left offset deformable frontal barrier crash test and an actual crash tested vehicle.

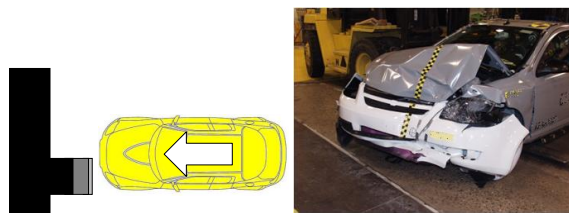


Figure 7. Offset Deformable Barrier Test.

The CDC for this crash test is 12FYEW3. In comparing the deformation pattern between angled frontal barriers to that in the offset deformable barrier test, although the shape of the barrier face differs in these two test modes, the deformation pattern, as defined by the CDC methodology cannot discriminate between the two. Using left angle tests and left offset deformable barriers as an example, the character in position 4 would be L if the area of deformation comprised up to 1/3 of the lateral area of the vehicle or Y if the deformation was between 1/3 and 2/3 of the left side of the vehicle. For a 40% overlap offset deformable barrier, the code for this position would, by definition, be Y as it would for a left angle crash test where the area of deformation is closer to 2/3 of the vehicle.

Figure 8 shows a schematic of a frontal center pole crash test and an actual crash tested vehicle.

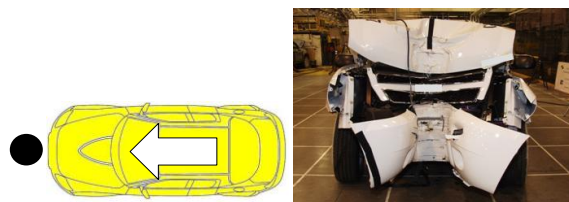


Figure 8. Frontal Center Pole Test.

The CDC for this crash test is 12FCEN3. A frontal center pole test has a 12 o'clock force direction and a

frontal (F) area of deformation. The lateral area of deformation is in the center third of the vehicle (C), everything below the beltline (E) and narrow, less than 16", distribution.

Figure 9 shows a schematic of a bumper underride crash test and an actual crash tested vehicle



Figure 9. Bumper Underride Test.

The CDC for this crash test is 12FDMW3. The frontal underride evaluation results in a deformation pattern that is described with a 12 o'clock force direction, front (F) distributed across the vehicle (D) crash, but the key difference between this crash test type and a 0 degree frontal barrier is that the vertical deformation is from the top of the bumper to the beltline/hood (M). This crash type engages the entire front of the vehicle for a wide damage distribution (W).

After the CDCs were assigned to the crash tests, cases in the U-M CIREN database were compared to the list of CDCs before evaluating the extent of deformation (CDC character 7). Table 2 shows the number of U-M CIREN cases assigned to each frontal crash test type and associated CDCs assigned to the tests.

Table 2. Distribution of Frontal Cases by CDC

Crash Test Type	CDC 1-6	Total
0 degree frontal	12FDEW	78
	11FDEW	14
	01FDEW	6
left angle or offset	12FYEW	52
	12FLEW	12
	11FYEW	7
right angle or offset	12FZEW	16
	01FZEW	5
	12FREW	3
	01FREW	1
frontal center pole	12FCEN	10
bumper underride	12FDMW	3
Total		207

Side Impact Crash Types — CDCs from Post Test Photographs Figure 10 shows a schematic of an IIHS side impact crash test and an actual crash tested vehicle.

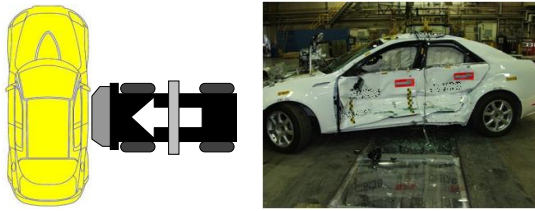


Figure 10. IIHS Side Impact Test.

The CDC for this crash test is 9LPAW3. IIHS side impact tests are conducted with a moving deformable barrier that strikes the vehicle on the side at a 90 degree angle leading to a force direction and area of deformation of 3 o'clock on the right (3R) or 9 o'clock on the left (9L). The moving deformable barrier is aligned with the goal of maximizing the contact with the passenger compartment leading to deformation of P (passenger compartment) or Y (passenger compartment and area forward of passenger compartment) for character 4. The vertical deformation in this crash type can extend above the beltline leading to an A or E for character 5. The lateral extent of the deformation in this crash type is greater than 16", or wide (W) for character 6.

Figure 11 shows a schematic of a side NCAP crash test and an actual crash tested vehicle.

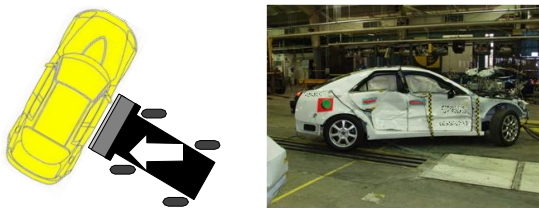


Figure 11. Side NCAP Test.

The CDC for this crash test is 10LPAW3. The key difference between the IIHS side impact test and the side NCAP test is that the side NCAP test uses a moving deformable barrier that is crabbed (at an angle of 27 degrees) with respect to the impacted vehicle. The crabbed impact results in a 10 o'clock left (10L) or 2 o'clock right (2R) as opposed to 3 and 9 o'clock for the IIHS test. The remaining characters are the same as for the IIHS test.

Figure 12 shows a schematic of a side impact pole crash test and an actual crash tested vehicle.

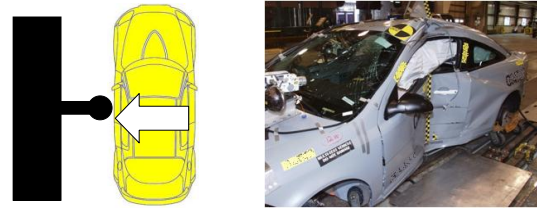


Figure 12. Side Impact Pole Test.

The CDC for this crash test is 9LPAN3. The side impact pole test that can be conducted as an evaluation for FMVSS 201 defines a perpendicular impact with a 254mm pole centered at center of gravity of the head of the Anthropomorphic Test Device (ATD, or test dummy). The differences in deformation pattern between this type and the IIHS side impact test type is that the pole impact results in a narrow (N), less than 16", deformation pattern in character 6, and has a vertical deformation pattern of the entire vehicle (A) in character 5.

Table 3 shows the number of U-M CIREN cases assigned to each side impact crash test type and associated CDCs assigned to the tests.

**Table 3.
Distribution of Side Impact Cases by CDC**

Crash Test Type	CDC 1-6	Total
IIHS side impact	09LPAW	12
	09LYAW	9
	03RPAW	9
	09LPEW	5
	03RPEW	4
	03RYAW	3
	09LYEW	3
	03RYEW	1
side NCAP	10LYAW	13
	02RPAW	8
	02RYAW	7
	02RYEW	3
	10LPAW	3
	10LYEW	3
	02RPEW	1
side pole	09LPAN	2
	03RPAN	1
	09LPAW	1
Total		89

Table 4 shows CDCs from non-arrested rollover crash cases that have deformation patterns that are similar to those generated in laboratory crash tests.

Table 4.
Non-arrested rollover crash CDCs

Crash Test Type	CDC 1-6	Total
rollover	00TDDO	6
	00TYYO	1
	00TYZO	1
Total		8

Laboratory rollover crash tests [10] are used in developing rollover sensor calibrations. These tests focus on the initiation portion of the rollover and therefore often involve tethered vehicles so there is no body damage, or the vehicle rolls one full roll or less. These kinds of tests result in a CDC that is defined as non-horizontal (00) for the force direction and an area of deformation of top (T). Deformation in laboratory rollover tests is typically distributed over the vehicle (D) or skewed slightly forward (Y) due to the location of the engine in the front of the vehicle. Character 5 can be either distributed (D) or the left (Y) or right (Z) 2/3 of the vehicle. Finally, character 6 is always O for a rollover. An example of a rollover laboratory tested vehicle is shown in Figure 13 (a) with a comparable U-M CIREN case in Figure 13 (b)



Figure 13. Laboratory Rollover Crash Tested Vehicle and Non-Arrested Rollover Case Vehicle-00TDDO3.

Additional Case CDCs Matched to Front and Side Impact Crash Test Types during In-depth Review

The next step was an in-depth case-by-case review of the remaining U-M CIREN cases to determine if the cases had deformation that appeared visually to match that generated in crash tests. Table 5 shows the number of additional U-M CIREN frontal cases that had deformation patterns that were determined to be similar to frontal crash test types and the associated CDCs.

Table 6 shows the number of additional U-M CIREN side impact cases that had deformation patterns that were determined to be similar to side impact crash test types and the associated CDCs.

Table 7 shows examples of additional frontal and side impact crashes. These examples are explained in the following section.

Table 5.
Distribution of Additional Frontal Impact Cases by CDC

Crash Test Type	CDC 1-6	Total
frontal offset pole	12FZEN	5
	12FYEN	4
	12FLEN	3
	12FZAN	1
	12FRAN	1
	12FREN	1
left angle or offset	11LYEW	6
	11LYAW	5
	12FYAW	1
	11FYAW	1
0 degree frontal	11FDAW	5
	12FDAW	3
	01FDAW	1
right angle or offset	01RZEW	2
	12FZAW	1
frontal center pole	12FCEW	2
Total		42

Table 6.
Additional Side Impact Cases by CDC

Crash Test Type	CDC 1-6	Total
IIHS side impact	09LZAW	4
	08LZAW	1
side NCAP	10LZAW	3
	01RPAW	1
side pole	09LPEN	1
Total		10

Table 7.
Examples of Additional Frontal and Side Impact Crash Types

Frontal Impact	Side Impact
(a) Offset Pole - 12FZEN3	(d) IIHS Side Impact - 09LZAW4
(b) 0 Degree Frontal - 12FDAW5	(e) Side Pole - 09LPEN3
(c) Left Angle - 11LYEW4	(f) Side NCAP - 10LZAW3

Table 7 Figure (a) shows an example of a 12 o'clock frontal (12N) narrow impact (N, character 6) that was similar to a frontal pole test. Table 7 Figure (b) demonstrates a vertical deformation area that extends above the beltline (A, character 5) was similar to the deformation that is generated in a 0 degree frontal crash but coded as everything below the beltline (E, character 5). Table 7 Figure (c) is an example from the left angle or offset category. There was an overlap between the deformation defined by an 11 o'clock frontal (11F) and an 11 o'clock left side (11L) and therefore the 11 o'clock left impacts were added to this category. A similar overlap was noted on the right side of the vehicle. In addition, for angled impacts that engaged up to 2/3 of the lateral vehicle structure (Y or Z, character 4), vertical deformation that extended above the beltline (A, character 5) was also similar to that seen in the frontal angle and offset crash tests, everything below the beltline (E, character 5).

The two additional CDCs assigned to the IIHS side impact test type reflect a slight shifting of the impact rearward in the vehicle so that the area of deformation includes the passenger compartment but extends rearward (Z, character 4) as demonstrated in Table 7 Figure (d). In addition there was one case with an 8 o'clock force direction that had deformation similar to that generated in an IIHS side impact test.

For the side NCAP test type, the additional CDCs were assigned in a similar fashion — a slight rearward shifting in deformation area (Z, character 4) shown in Table 7 Figure (e) as well as a force direction that that was one 'hour' different than assigned from crash test pictures (1 o'clock versus 2 o'clock).

For the side pole test, one case, Table 7 Figure (f), had a deformation pattern of everything below the beltline (E, character 5) instead of extending up above the beltline as is typical in a side pole crash test.

Cases with Crash Configurations Different from Laboratory Tests

The remaining cases which could not be matched to existing crash tests were grouped into new crash configuration categories. In this step, 77 cases were assigned to these additional crash configurations without a matching crash test and 9 cases were so unique that they could not be categorized into any crash category.

The distribution of frontal crash cases without a corresponding crash test is shown in Table 8.

Table 8.
Distribution of Frontal Crash Cases without an Associated Crash Test by CDC

Crash Type	CDC 1-6	Total
left small overlap	12FLEE	9
	12FLAE	8
	11FLEE	3
	12FLAW	3
	11LFEW	2
right small overlap	12FREE	5
	02FREE	1
underride	12FDAA	3
	12FZAA	1
high undercarriage	12FDLW	2
	12FRLN	1
sideswipe	12LDAS	1
corner underride	12FRAE	1
offset underride	12FLME	1
Total		41

The distribution of side impact cases without a corresponding laboratory crash test is shown in Table 9.

Table 9.
Distribution of Side Crash Cases without an Associated Crash Test by CDC

Crash Type	CDC 1-6	Total
side imp. non-occ. comp.	10LFEW	2
	02RFEW	2
	09LFEW	1
	09LBEW	1
	03RBEW	1
IIHS side - shifted rwd	03RZAW	2
	02RZAW	2
	09LZEW	2
oblique side	01RDAW	2
	11LDAW	1
IIHS side - distributed	09LDAW	2
side NCAP - shifted rwd	02RZEW	2
IIHS side - shifted fwd	01RYAW	2
side oblique pole	10LPAN	1
side NCAP - distributed	02RDAW	1
Total		24

The rear impact crash cases are shown in Table 10

Table 10.
Distribution of Rear Crash Cases without an Associated Crash Test by CDC

Crash Type	CDC 1-6	Total
full overlap rear impact	06BDEW	3
partial overlap rear impact	06BZAW	1
	06BYAW	1
rear angle	07BLAW	1
narrow overlap rear impact	06BRAE	1
Total		7

Table 11 shows examples of cases without a corresponding crash test. These examples are explained in the following section.

The left and right small overlap crashes (Table 11 Figure (a)) had deformations that were typically outside of the longitudinal rails. These were primarily frontal crashes (F, character 3) with damage limited to the left (L, character 4) or right (R, character 4) 1/3 of the vehicle. The vertical damage ranged from the entire vehicle (A, character 5) or everything below the beltline (E, character 5) with a corner (from corner to 16" inboard) (E, character 6) type of damage distribution. In addition, the overlap seen between the FL and the LF (characters 3 and 4) resulted in an additional CDC and two cases assigned to this crash type.

The corner underride case (Table 11 Figure (b)) was different from a right angle or offset test in that although there was deformation below the beltline, the majority of deformation was above the beltline. This is a detail that is not evident in the CDC but was visible during review of the post-crash photographs.

The high undercarriage cases (Table 11 Figure (c)) had deformation that was from the top to the bottom of the vehicle frame (L, character 5), which discriminated these cases from 0 degree frontal and pole tests which have residual deformation from the beltline down (E, character 5).

The one offset underride case (Table 11 Figure (d)) was distinguished from other case types by the M for character 4, meaning from the top of the frame to the beltline. The sideswipe crash (Table 11 Figure (e)) was categorized by the S in character 6 which is defined as a sideswipe with 0 to 4" of lateral overlap. The underride crash types (Table 11 Figure (f)) were categorized by the A in character 6 defined as an overhanging structure or inverted step.

The side impact cases without a corresponding crash test type primarily involved damage that involved either more of the side of the vehicle (D, character 4, as shown in (Table 11 Figure (g)) or was shifted forward or rearward of the occupant compartment. In addition, there were variations in the force direction (characters 1 and 2) as compared to laboratory tests.

The oblique side impacts (Table 11 Figure (h)) were defined by the somewhat frontal force directions of 11 and 1 o'clock combined with a distributed loading along the side of the vehicle. The side impacts that did not involve the compartment (Table 11 Figure (i))

Table 11.
Examples of Cases Without a Corresponding
Crash Test

<p>(a) Left Small Overlap - 12FLEE9</p> 	<p>(g) IIHS Side Impact - Distributed - 09LDAW4.</p> 
<p>(b) Corner Underride - 12FRAE7</p> 	<p>(h) Oblique Side Impact - 01RDAW3</p> 
<p>(c) High Undercarriage - 12FDLW1</p> 	<p>(i) Side Impact Non-Occupant Compartment - 10LFEW3.</p> 
<p>(d) Offset Underride - 12FLME5</p> 	<p>(j) Side Oblique Pole Impact - 10LPAN4</p> 
<p>(e) Sideswipe - 12LDAS2</p> 	<p>(k) Full Overlap Rear Impact - 06BDEW3</p> 
<p>(f) Underride - 12FDAA6</p> 	

were either in front of the occupant compartment (F, character 4) or behind the occupant compartment (B, character 4). The side oblique pole was characterized by a non-perpendicular 10 o'clock impact with a

narrow damage distribution (N, character 6, Table 11 Figure (j)).

The rear impact cases were characterized by force directions from the rear of the vehicle (6 and 7 o'clock) and a rear area of deformation (B, character 3, Table 11 Figure (k)). Although rear impact crash test evaluations are performed to evaluate vehicle structural performance, occupant performance is not evaluated in these tests.

The arrested rollover crash cases are shown in Table 12. Cases with deformation patterns that are so unique that they could not be categorized are shown in Table 13 and Table 14.

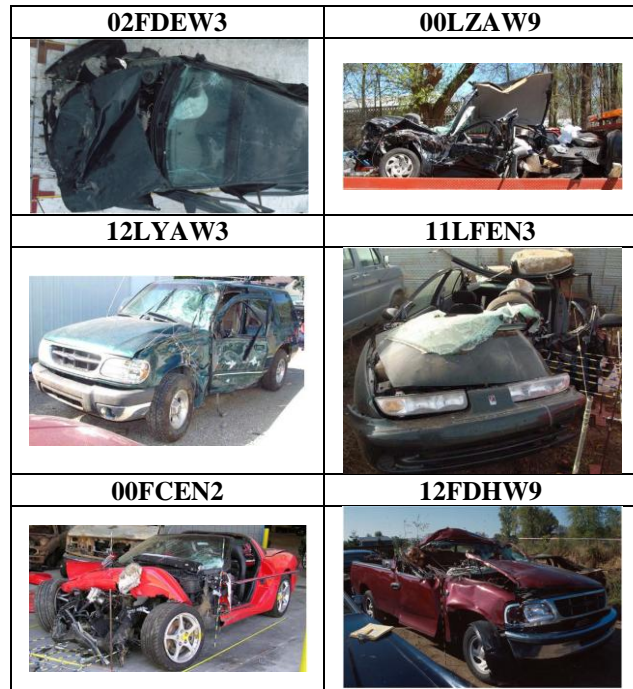
Table 12.
Distribution of Arrested Rollover Crash Cases without an Associated Crash Test by CDC

Crash Type	CDC 1-6	Total
arrested rollover	00TZDW	1
	00TYDN	1
	00TPDN	1
	00TFDO	1
	00TZZO	1
Total		5

Table 13.
Non-categorized Crash Cases by CDC

Crash Test Type	CDC 1-6	Total
not categorized	02FDEW	3
	12LYAW	2
	00FCEN	1
	00LZAW	1
	11LFEN	1
	12FDHW	1
Total		9

Table 14.
Examples of Crash Damage in U-M CIREN Cases Non-categorized Cases by CDC



Extent (CDC Character 7) After categorizing the U-M CIREN cases by crash configuration and crash category, the CDC extent, character 7, was analyzed. The maximum extent for the laboratory crash test types is shown in Table 15. The maximum extent was consistent across laboratory tests of different vehicle types.

Table 15.
CDC Extent for Crash Tests

Crash Test Type	Maximum Extent in Laboratory Testing
0 degree frontal	3
bumper underride	3
frontal center pole	4
frontal offset pole	4
left angle or offset	3
right angle or offset	3
IIHS side impact	3
side NCAP	3
side pole	3
rollover	3

Appendix B shows the distributions of U-M CIREN crash types by CDC characters 1-6 and CDC extent above or below that generated in laboratory crash tests.

DISCUSSION

In many cases, crash damage in U-M CIREN cases closely resembled deformation from laboratory crash tests. Table 16 shows a comparison of three crash types to the associated case vehicle where the pattern of deformation is visually similar.

Table 16.
Examples of Crash Damage in U-M CIREN Cases Similar to Crash test Damage

Laboratory Crash Test	U-M CIREN Case CDC
0 Degree Frontal	12FDEW3
	
Frontal Center Pole	12FCEN4
	
IIHS Side Impact	9LPAW3
	

In some cases, crash damage within a CDC category varied from crash test deformation. Table 17 shows a comparison of two crash types to the associated crash test types where the pattern of deformation is not visually similar. The first example, shows a U-M CIREN case coded 12FYEW3, or similar to a left angle or offset laboratory test. There is an obvious difference in deformation patterns, but because the impact in the U-M CIREN case engaged part of the left and center thirds of the front of the vehicle and was wider than 16”, the case must be coded as wide (W, character 6) as opposed to narrow (N, character 6).

The second example shows a 0 degree frontal laboratory crash test coded as 12FDEW3. Visually, the deformation pattern in the U-M CIREN case looks more similar to a frontal angle test, but because

the damage is distributed across the front of the vehicle, this case is categorized as a 0 degree frontal.

There were cases in which the ‘classic’ picture of a given CDC did not exactly match the actual vehicle deformation. These examples demonstrate the coarseness of using CDCs to describe vehicle deformation.

Table 17.
Examples of Crash Damage in U-M CIREN Cases Different from Crash test Damage

Laboratory crash test	U-M CIREN Case CDC
Left Angle Frontal	12FYEW3
	
0 degree Frontal	12FDEW3
	

SUMMARY

As shown in Figure 14, 48.9% of the 442 U-M CIREN cases studied matched an existing crash test configuration with an extent less than or equal to the test, 31.7% of the frontal cases matched an existing crash test configuration but with greater extent, and 19.5% did not match an existing crash test configuration.

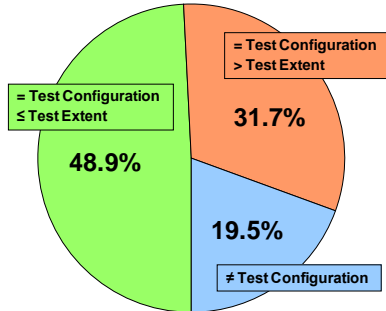


Figure 14. Distribution of U-M CIREN Cases.

A comparison was made to determine if the distribution of the U-M CIREN cases was consistent with the entire set of cases from all of the CIREN centers. Of the 2089 CIREN cases analyzed, the CDCs placed 47.5% in the groups which matched an existing crash test type with an extent less than or equal to the test, 25.8% of the cases matched an existing crash test configuration but with greater extent, and 14.4% did not match an existing crash test configuration. There were 12.3% of the CIREN cases that had CDCs that did not match those found in U-M CIREN cases (Figure 15). Those cases were not

analyzed further in this study. The distribution of cases was similar between the U-M CIREN and CIREN datasets, which gave confidence that the U-M CIREN dataset is reasonably representative of the entire CIREN dataset.

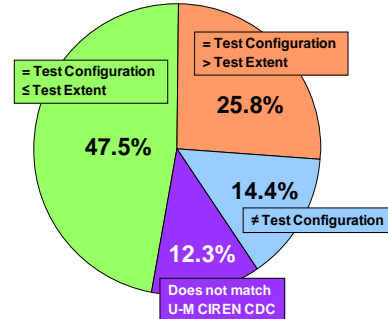


Figure 15. Distribution of all CIREN Cases.

Cases Matching Test Configuration and Extent

Figure 16 shows the distribution of the 48.9% of U-M CIREN crash cases that had configurations similar to current laboratory tests with extents less than or equal to the test. For frontal crashes, the 0 degree frontal impact category was the most represented followed by the left angle or offset category. For side impact crashes, the percentage of cases in the Side NCAP and IIHS Side Impact categories were similar. These categories were the most prevalent type of side impact configuration. There were a limited number of rollover cases in the CIREN database which is influenced by the CIREN selection criteria.

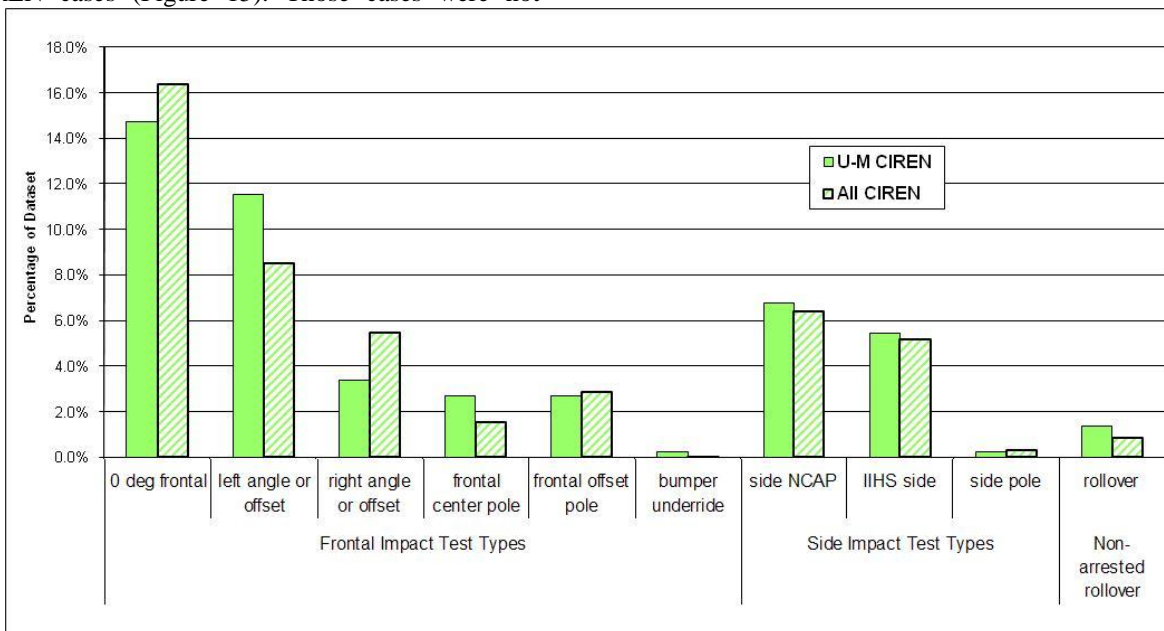


Figure 16. Distribution of U-M CIREN and CIREN cases versus Crash Test Type for crashes with similar configurations and extents less than or equal to a current industry crash test

Cases matching Test Configuration but with Greater Extent

Figure 17 shows the distribution of the 31.7% of U-M CIREN crash cases that had configurations similar to current laboratory tests with extents greater than current crash tests. Similar to the cases with lesser

extents, the 0 degree frontal was the most prevalent frontal impact, followed by the left angle or offset category. Side NCAP was the most represented side impact category, followed by the Side IIHS configuration. There were very few frontal pole crashes with extents greater than the industry crash tests.

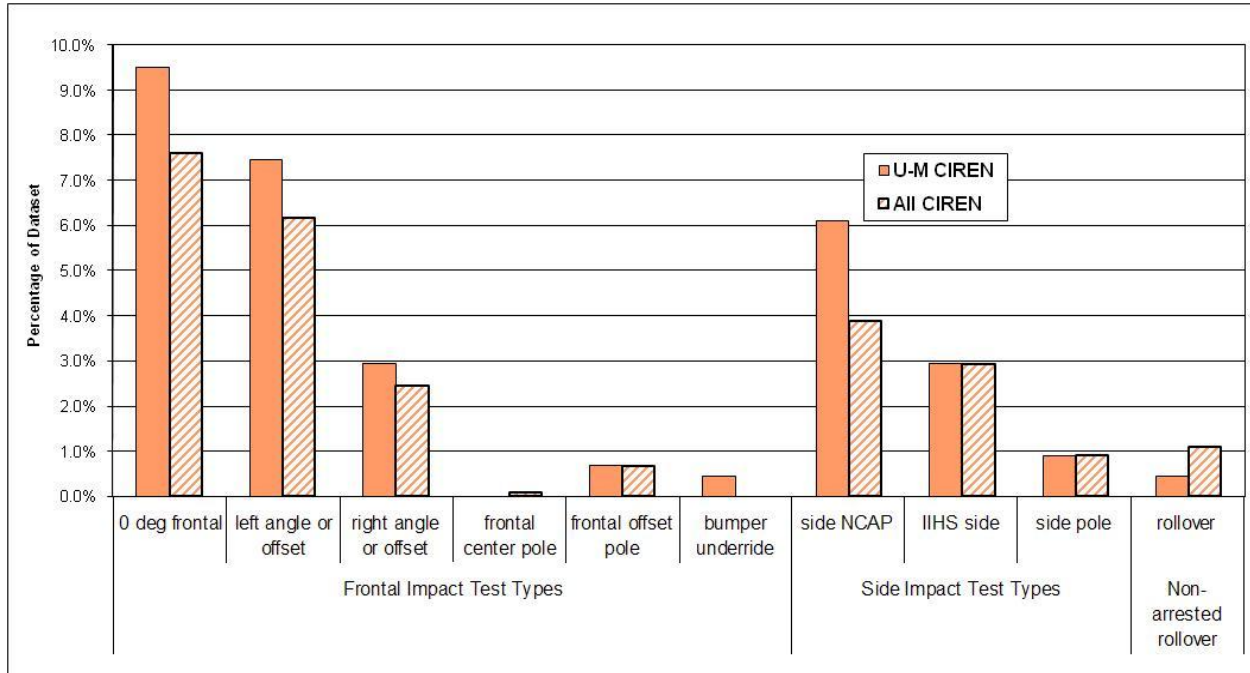


Figure 17. Distribution of U-M CIREN and CIREN cases versus Crash Test Type for crashes with similar configurations and extents greater than a current industry crash test.

There are several possible measures of crash severity including delta V, Equivalent Barrier Speed (EBS), and Extent of Deformation. CDC extent (Character 7), or extent of crash deformation, was used in this analysis as an indicator of crash severity because delta V and EBS were not available for all cases. Overall, the distribution of cases that had an extent greater than the crash test extent was very similar to the distribution of cases that had an extent less than or equal to the crash test extent. The maximum regulated frontal crash test speed is currently 35 mph which encompasses 99% of all frontal tow away crashes by delta V as illustrated by Figure 18.

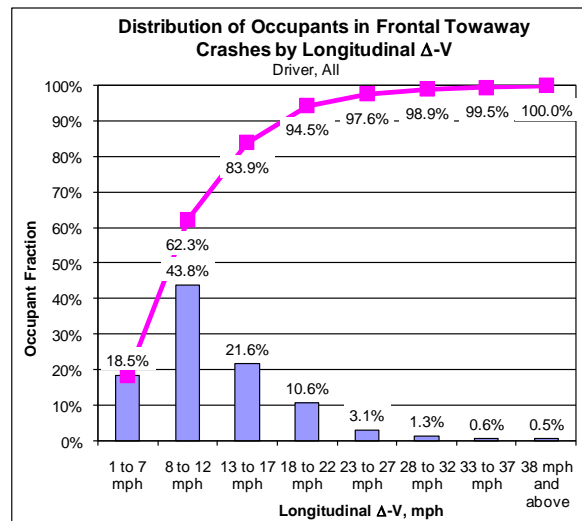


Figure 18. Frontal Crash Severity Distribution - 1997-2006 NASS CDS.

Cases Not Matching Test Configuration

Figure 19 shows the distribution of the 19.5% of U-M CIREN crash cases that did not match a current industry crash test configuration. The majority of these cases were Left or Right Small Overlap crashes. Left (FLEE) and right (FREE) small overlap crashes totaled 10.7% of all frontal cases in the U-M CIREN

database. The next largest category contains crashes with deformation patterns that were so unique that they could not be categorized. The majority of side impacts in this group were similar to current industry side impact crash tests, but with the impact location shifted more forward or rearward of the occupant compartment.

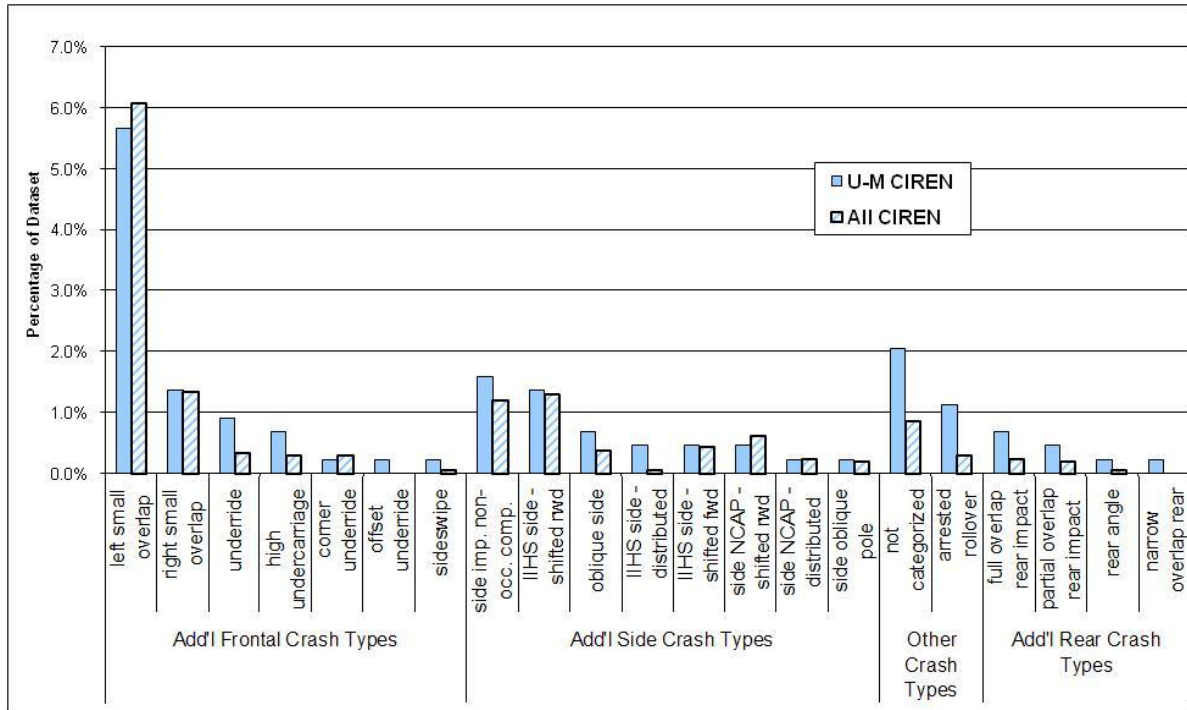


Figure 19. Distribution of U-M CIREN and CIREN cases versus Crash Test Type for crashes that do not match a current industry crash test.

Figure 20 shows the distribution of frontal crash test extents for cases with frontal crash configurations that were different from existing test types. Figure 21

shows the distribution of frontal crash test extents for cases with configurations similar to current test types.

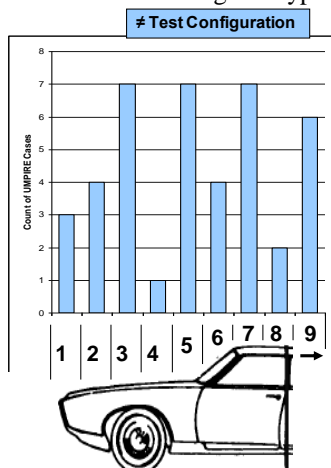


Figure 20. Extent Distribution \neq Test Configuration.

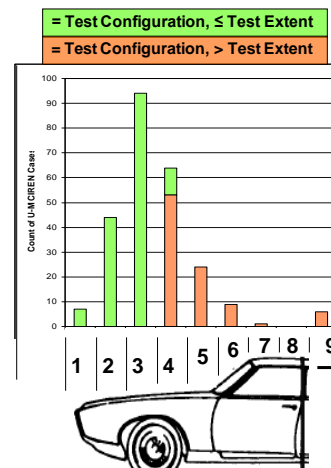


Figure 21. Extent Distribution = Test Configuration.

Frontal crashes that had configurations different from current laboratory tests tended to involve localized vehicle deformation. The concentrated loads engaged less of the vehicle's front structure and resulted in maximum crush extending farther rearward on the vehicle. Measures of crash severity other than the extent of maximum crush, such as delta V, are less likely to show the same increase and may even decrease.

CONCLUSIONS

The conclusions of this research are:

- The majority of cases in this study had crash configurations similar to existing industry crash tests.
- Only 19.5% of cases had crash configurations that were not represented by current crash tests.

Any consideration of increasing test severity to address those crashes that produce a greater extent of crash deformation than that produced in crash tests must consider a broader spectrum of collisions including non-injury producing crashes. This analysis must be done in a way that does not increase the risk to the current uninjured population that is not included in the CIREN database.

ACKNOWLEDGMENT

This work was supported by grants #DTNH22-00-H-07444 and #DTNH22-05-H-31001 from the US Department of Transportation – National Highway Traffic Safety Administration as well as educational grants from General Motors. The views expressed are those of the authors and not necessarily those of the sponsor.

REFERENCES

- [1] "Traffic Safety Facts 2006", US Department of Transportation, National Highway Traffic Safety Administration, Publication No. DOT HS 810 818.
- [2] National Highway Traffic Safety Administration Standard No. 208; Occupant Crash Protection 49 CFR 571.208
- [3] Frontal Offset Crashworthiness Evaluation, Offset Barrier Crash Test Protocol (Version XIII), Insurance Institute for Highway Safety, 2008
- [4] Side Impact Crashworthiness Evaluation, Crash Test Protocol (Version V) Insurance Institute for Highway Safety, 2008
- [5] National Highway Traffic Safety Administration Standard No. 214; Side Impact Protection 49 CFR 571.214
- [6] National Highway Traffic Safety Administration Standard No. 201; Occupant Protection in Interior Impact 49 CFR 571.201
- [7] A Population-Based Comparison of CIREN and NASS Cases Using Similarity Scoring, Stitzel JD, Kilgo P, Schmotzer B, Gabler HC, Meredith JW, 51st Annual Proceedings Assoc. for the Advancement of Automotive Medicine 2007, 51:395-417
- [8] Trauma.org
<http://www.trauma.org/archive/scores/ais.html>
- [9] SAE Surface Vehicle Standard J224 Collision Deformation Classification, Rev 1980-03, SAE International, Warrendale, PA
- [10] Rollover Sensor Signature Test Development, O'Brien-Mitchell BM, Horn CK, Lange RC, SAE 2007-01-0375, SAE International, 2007

APPENDIX A: CIREN ADULT INCLUSION CRITERIA (OCTOBER 2006)

Case Type	Crash Direction	Vehicle Criteria	Restraint Criteria	Occupant Positions	Injury Thresholds
Frontal	10 to 2 o'clock Full frontal Offset frontal	CY-6 yrs* (Priority on newest vehicles)	Air bag, Air bag and 3-point belt	Row 1	AIS _≥ 3 or **
			Must be in 3-point belt and gross misuse not documented	Rows 2+	
Side	8 to 10 o'clock 2 to 4 o'clock	CY-6 yrs* (Priority on newest vehicles)	Any and all, including unrestrained on struck side and far side	Any	AIS _≥ 3 or **
Rollover	All	CY-6 yrs* (Priority on newest vehicles)	Any and all, including unrestrained (EXCEPTION = 100% EJECTION)	Any	AIS _≥ 3 or **
Pregnant Occupant (total enrollment limited)	10 to 2 o'clock Full frontal Offset frontal	CY-8 yrs* (Priority on newest vehicles)	Must be in a 3-point belt and gross misuse not documented Avoid out-of-position cases. (call NHTSA on non-belted cases for consideration)	Any	AIS2+ AIS1 (with moderate to severe impact)
PI Special Interest ***	Any	Any	Any	Any	Any
Success Case****	Any	CY-6 yrs*	Appropriate restraint usage (belt and/or air bag)	Any	Any
Fire	All	Any	Any and all, including unrestrained	Any	AIS _≥ 2

* Cases where the vehicle is >6 yrs old may be considered for enrollment if the vehicle contained advanced safety components – NHTSA approval required

** AIS of 2 in 2 or more body regions with medical significance (avoid concussive type injury for inclusion)

* AIS of 2 in the lower extremity with significant articular injury (pilon/talus/calcaneus/Lisfranc/Choparts)

*** Max. PI SI cases allowed per site per year would be 5 based on a 50 case enrollment (10%)

**** Cases must be extraordinary for consideration – NHTSA approval required

APPENDIX B: CDC EXTENT

Table 18.
U-M CIREN Cases Matched to Frontal Impact Crash Test Types

Crash Test Type	CDC 1-6	≤ Test Extent	> Test Extent	Total
0 degree frontal	12FDEW	51	27	78
	11FDEW	10	4	14
	01FDEW	4	2	6
	11FDAW		5	5
	12FDAW		3	3
	01FDAW		1	1
0 degree frontal Total		65	42	107
left angle or offset	12FYEW	33	19	52
	12FLEW	7	5	12
	11FYEW	2	5	7
	11LYEW	4	2	6
	11LYAW	4	1	5
	11FYAW	1	1	2
12FYAW	1		1	
left angle or offset Total		51	33	84
right angle or offset	12FZEW	7	9	16
	01FZEW	5		5
	12FREW	1	2	3
	01RZEW	1	1	2
	12FAW		1	1
	01FREW	1		1
right angle or offset Total		15	13	28
frontal offset pole	12FZEN	5		5
	12FYEN	4		4
	12FLEN	3		3
	12FZAN		1	1
	12FRAN		1	1
	12FREN		1	1
frontal offset pole Total		12	3	15
frontal center pole	12FCEW	10		10
	12FCEW	2		2
frontal center pole Total		12		12
bumper underride	12FDMW	1	2	3
bumper underride Total		1	2	3
Total		156	93	249

Table 19.
U-M CIREN Cases Matched to Side Impact Crash Test Types

Crash Test Type	CDC 1-6	≤ Test Extent	> Test Extent	Total	
IIHS side impact	09LPAW	7	5	12	
	09LYAW	4	5	9	
	03RPAW	3	6	9	
	09LPEW	3	2	5	
	03RPEW	3	1	4	
	09LZAW		4	4	
	03RYAW		3	3	
	09LYEW	2	1	3	
	08LZAW	1		1	
	03RYEW	1		1	
	IIHS side impact Total		24	27	51
	side NCAP	10LYAW	7	6	13
02RPAW		5	3	8	
02RYAW		6	1	7	
02RYEW		2	1	3	
10LPAW		3		3	
10LYEW		3		3	
10LZAW		3		3	
01RPAW		1		1	
02RPEW			1	1	
10LPEW			1	1	
side NCAP Total		30	13	43	
side pole	09LPAN		2	2	
	90LPAW		1	1	
	03RPAW		1	1	
	09LPEN	1		1	
side pole Total		1	4	5	
Total		55	44	99	

Table 20.
U-M CIREN Cases Matched to Non-Arrested Rollover Crash Tests

Crash Test Type	CDC 1-6	≤ Test Extent	> Test Extent	Total
rollover	00TDDO	5	1	6
	00TYYO	1		1
	00TYZO		1	1
rollover Total		6	2	8
Total		6	2	8

Priorities for Enhanced Side Impact Protection in Regulation 95 Compliant Cars

P. Thomas, Chair EEVC WG 21 Accident Studies

R. Welsh

Loughborough University, UK

E. Lenguerrand, G. Vallet

INRETS, France

D. Otte

Medical University of Hanover, Germany

J. Strandroth

Swedish Roads Administration, Sweden

09-0156

Abstract

This paper summarises the main results of an analysis of accident data conducted for the European Enhanced Vehicles Committee (EEVC) WG13 "Side Impact" to inform the further development of side impact test procedures for cars. The analysis of data from three countries was coordinated by EEVC WG 21 "Accident Studies".

The national datasets of the UK, France and Sweden from the year 2005 were analysed containing a total of 411,311 cars. In each country side impacts typically represented 33% of all fatalities but less than 25% of casualties of all severities. Struck-side occupants represented typically 60% of all side impact casualties regardless of injury severity while the remainder of the casualties were seated away on the non-struck-side.

Amongst single vehicle side impacts, collisions with poles were most commonly specified, although there was considerable variation between countries. In multi-vehicle crashes the collision partner was a car in about 75% of cases. The relative involvement of each type of collision partner varied by casualty severity and in both the UK and France there were similar numbers of fatalities in collisions with poles as with cars. A comparison of injury risks suggested the risk of serious injury in newer cars struck by other newer cars was similar to older, pre-Regulation 95, cars struck by older cars. This indicates the improvements in side protection since the introduction of Regulation 95 may have been at least partially offset by increases in front stiffness of cars due to the introduction of Regulation 94 and EuroNCAP.

The paper presents other details on the circumstances of side impacts and the different driver populations involved in loss-of control and intersection collisions.

It links to two other papers concerning car-to-car and car-to-pole side collisions using in-depth data.

Background

This paper is a summary of the key findings of an analysis of accident data concerning side impacts. The analysis has been conducted by the European Enhanced Vehicle Safety Committee, Working Group 21 Accident Studies and has been requested by EEVC Working Group 13 Side Impact as part of its work to raise the level of side impact protection of cars.

This paper describes the results of an overview analysis focussing on the accident data from the UK, France, and Sweden. A related paper¹ summarises the results of the analysis of side impacts of cars with poles using in-depth data from Germany, GB and Sweden while a second paper² summarises the equivalent results of an analysis of car to car side collisions.

The European side impact test procedure is enacted within Directive 96/27/EC³ and requires cars to maintain a specified level of protection when struck in the side by a mobile barrier travelling at 50km/hr. There have been a number of previous studies^{4 5 6} that have evaluated the frequency and characteristics of side impacts although few have covered more than a single member State. The EU Directive included a requirement that it be evaluated after two years and Edwards et al⁷ did this under the auspices of the EEVC. They concluded that the test speed should be increased and that the use of a pole test be considered. Similar conclusions were reached by Hassan et al⁸ who examined both UK Co-operative Crash Injury Study (CCIS) data and US national Automotive Sampling System (NASS) data files. Frampton et al⁹ highlighted the frequency of injuries to non-struck (far) side occupants. Thomas et al¹⁰ reviewed UK in-depth accident data and confirmed that more car occupants died as a result of side

impacts than frontal crashes, impacts with poles were nearly as frequent as car to car side collisions and that the side impact test speed was substantially below that of the majority of fatal crashes.

Data sources

The task of EEVC WG 21 is to conduct accident data studies and incorporate as wide a range of EU accident data sources as possible compatible with the objectives of the research focus. Data from three countries, UK, France and Sweden was used for this analysis. Each of these datasets defined “fatality” as death within 30 days of the crash but differences exist for the “serious” category. These are defined below.

GB accident data – STATS 19

The British national accident database, STATS 19, is based on the reports for every police reported crash in Great Britain. Data for the year 2005 was used with a total of 271,017 casualties. Side impacts were defined on the basis of the police assessment of the first point of impact and seriously injured casualties are defined as those with a fracture or an overnight stay in hospital. Accident data for Northern Ireland is stored separately so the dataset refers to Great Britain rather than the United Kingdom.

French accident data - BAAC

The data for France is also based on the police reports of crashes in the year 2005. The BAAC (Bulletin d’Analyse des Accidents Corporels de la Circulation) classifies impact direction in a similar manner to the UK but the “serious” category is defined on the basis of hospitalisation. The technical basis of BAAC has been revised since the 2005 dataset to minimise issues concerning under-reporting.

Sweden - STRADA

The Swedish STRADA system (Swedish Traffic Accident Data Acquisition) is based on police reports of each crash occurring nationally. Impact direction is based on the police assessment of the first point of

impact. The data is enhanced by linkage with hospital files and details of vehicle inspections.

Frequency of side impacts

The total cases for each dataset are shown in Table 1 for all road user types and Table 2 shows the distribution of impact direction of car impacts according to each national definition.

In GB 24.3% of all car occupants were injured in impacts while in France and Sweden they represented 21.9% and 25.9% respectively. In each country the most common impact type was a frontal collision. However amongst fatalities side impacts were more common, in GB they represented 0.4% of all car occupant casualties compared with 0.5% in frontal collisions. In France side impact fatalities constituted 1.5% of all casualties compared with 3.5% in frontal impacts and in Sweden they represented 0.3% of all casualties.

Seating position

Car occupants seated on the struck side are the target of current safety requirements as they may be exposed to intruding structures with higher risk of injury. Table 3 shows the seating position of occupants in side impacts in each of the three countries. In all three countries and irrespective of the severity of injury typically between 54% (Sweden) and 59% (France) of all casualties were seated on the side of the impact with little variation according to injury severity.

Selection of cars compliant with Regulation 95.

National accident databases do not include a record of the regulatory compliance of cars so the selection of this group of cars was achieved by indirect methods. All new cars produced after 2003 were required to meet the side impact regulatory requirements however this would have resulted in a very small number of relevant vehicles in the 2005 dataset. It was not feasible to utilise the Vehicle Identification Number as it was not available on the national accident databases and following consultation with EuroNCAP and the industry

Table 1 National database casualty counts - 2005

	UK		France*		Sweden	
	STATS 19 - GB		BAAC		STRADA	
Fatal	3,201	1.2%	5,319	4.7%	440	1.6%
Serious	28,954	10.7%	39,811	35.1%	3,915	14.6%
Slight	238,862	88.1%	68,265	60.2%	22,544	83.8%
Total	271,017	100%	113,395	100%	26,899	100%

*serious - in-patient, slight - out-patients

Table 2 - Distribution of car occupant casualties by impact type and injury severity

	GB** (n=169,670)			France* (n=52,634)			Sweden (n=9,180)**		
	Front	Side	Rear	Front	Side	Rear	Front	Side	Rear
Fatal	0.5%	0.4%	0.1%	3.5%	1.5%	0.3%	0.7%	0.3%	0.0%
Serious	4.9%	1.9%	0.5%	22.0%	6.5%	3.3%	6.5%	2.5%	1.0%
Slight	44.1%	22.0%	25.6%	34.9%	13.9%	14.1%	45.9%	23.1%	20.0%
Total	49.5%	24.3%	26.2%	60.4%	21.9%	17.7%	53.1%	25.9%	21.0%

*serious in-patients, slight out-patients - no multiple impacts

**may include multiple impacts - based on first point of impact

Table 3 Proportion of struck side and non struck side casualties among all side impacts

	GB		France*		Sweden	
	SS	NSS	SS	NSS	SS	NSS
Fatal	61%	39%	61%	39%	100% n=4	0
Serious	56%	44%	59%	41%	61%	39%
Slight	57%	43%	58%	42%	54%	46%
All severities	57%	43%	59%	41%	54%	46%

*serious in-patients, slight out-patients

members of WG 21 it was considered that the most effective definition was to consider vehicles registered after 1998 to represent the group compliant with Regulation 95. A later part of the analysis, to be reported elsewhere, focussed on the cars registered since 2003.

Collision partner

The test conditions under consideration by WG 13 relate to car to car and car to pole side impact conditions and the analysis of the datasets was therefore framed around these factors. Table 4 shows the frequency of each main impact configuration for each of the three countries.

Within the complete group of side impact casualties as occupants of cars registered since 1998 car to car side collisions were the most common, between 45% (Sweden) and 65% (France) of crashes were in this category. Collisions involving buses or goods vehicles, possibly within separate phases of the collision sequence, typically accounted for 13% (GB and Sweden). Car to pole collisions only represented between 3% (Sweden) and 6% (France) of all side impacts and collisions with other roadside objects were more common.

Table 5 shows the corresponding table for fatally injured casualties. 24% of GB casualties were killed in car to pole single vehicle collisions compared with 25% in car to car side impacts. Similarly in France there were 30% who died in collisions with poles and 37% in collisions with other cars. Other single

vehicle crashes and impacts with trucks or buses were also frequent causes of fatality. There were a total of only 8 fatalities in the Swedish data so these are not presented.

Casualty reduction resulting from Reg 95

The introduction of the European side impact performance requirements included a specification that a consequent casualty reduction be evaluated. An interim evaluation was conducted but there was insufficient accident data available to support an estimate of effectiveness.

To accomplish this the national data from the UK, France and Sweden was analysed separately. Given the relatively low proportion of fatalities in each dataset the killed and seriously injured (KSI) groups of casualties have been combined. It should be noted that the national definitions of "serious" differ so that the countries cannot be directly compared.

Table 4: Collision partner, all side impacts, post-1998 registered cars, all casualties

Collision Partner	GB		France		Sweden	
Pole	764	4%	269	6%	18	3%
Other SVA*	2,176	13%	329	7%	244	37%
Car	9,170	54%	2,989	63%	299	45%
Bus/GV**	2,148	13%	533	11%	86	13%
Other TVA***	748	4%	340	7%	21	3%
Three + vehicles	2,029	12%	250	5%	0	0%
Total	17,035	100%	4,710	100%	668	100%

*SVA – Single Vehicle Accident

** GV – Goods Vehicle

*** TVA – Two Vehicle Accident

Table 5: Collision partner, all side impacts, post-1998 registered cars, fatally injured casualties

Collision Partner	GB		France	
Pole	50	24%	95	30%
Other SVA	42	20%	37	12%
Car	52	25%	116	37%
Bus/GV	25	12%	41	13%
Other TVA	6	3%	8	3%
Three + vehicles	30	15%	18	6%
Total	205	100%	315	100%

Table 6 shows the rates of killed and seriously injured casualties (KSI) comparing vehicles registered after 1998 with those earlier. Vehicles registered on or after 2003 will all comply with the side impact requirements and the KSI rates of these vehicles are also compared with the rates experienced by older cars. To represent the conditions of the test configuration, the dataset was restricted only to the crashes involving side impacted cars struck by other cars.

Table 6 - KSI rates % (sample size) by vehicle registration year

	GB	France	Sweden
Pre 1998	4.2 (1244)	27.8(909)	11.0 (91)
1998 onwards	3.5 (1921)	20.0(904)	5.2 (116)
Pre 2003	3.8 (2448)	25.0(1523)	10.0 (130)
2003 onwards	3.7 (677)	18.6(290)	3.9 (77)

Data from each of the three countries showed a reduction in the rate of killed or serious injury comparing the modern vehicles against the older cars although the magnitude of the reduction varied. The UK showed a reduction of 17% comparing the post-

1998 cars with earlier models and reduction of 3% comparing post-2003 with earlier models. Reductions in France and Sweden were larger ranging from 26% to 61% (post-2003 cars).

Other factors relating to injury rates

Regulation 94 side impact was introduced in the same year as Regulation 96 frontal impact and over the period of the comparisons of KSI rates it is possible that other changes to vehicles, such as the stiffness of the car front, may have occurred. Tables 7 and 8 by registration year groups, pre-1998, post-1998 and post-2003 for cars struck in the side by the front of the opponent cars.

Table 7 UK - KSI rates % (sample size) by struck and bullet car age.

Bullet car \ Struck car	Pre 1998	Post 1998	Post 2003
Pre 1998	4.3 (441)	3.8 (533)	3.9 (179)
Post 1998	4.0 (659)	3.5 (879)	3.5 (258)
Post 2003	4.6 (219)	3.6 (330)	4.1 (97)

The GB STATS 19 data shows that the reference rate of killed and seriously injured casualties of pre-regulation cars when struck by a similar aged car was 4.3%. The KSI rates for this oldest category of car

when struck in the side by the newest cars, post-2003, was reduced to 3.9%. However the rate for the newest cars when struck on the side by the front of the newest cars was little changed from the reference category at 4.1%.

Table 8 France - KSI rates (sample size) by struck and bullet car age

Bullet car	Pre 1998	Post 1998	Post 2003
Struck car			
Pre 1998	26.3(498)	29.7(411)	28.9(128)
Post 1998	16.7(450)	23.4(454)	24.5(151)
Post 2003	14.7(143)	22.5(147)	26.8(56)

The French BAAC data, shown in Table 8, indicated a similar pattern. The reference group of older cars struck in the side by the front of older cars showed a KSI rate for the occupants of 26.3%. The newer groups of car, when struck by the same oldest car group, showed decreasing rates down to 14.7%. However when this same category of cars was struck by the front of more recent cars the KSI rates did not reduce and the rate for the post-2003 cars struck by the front of post-2003 cars was marginally greater than the reference group.

Matched samples

The characteristics of the drivers of cars varies according to the age of the vehicle reflecting the social groups that purchase new and used cars. In many countries, including the UK and Sweden, many new cars are bought for business use. Older cars are generally cheaper and may more often be bought by drivers who are less well off, such as younger drivers. It is therefore possible the drivers of the newer cars in the sample may have a different gender, age and other distributions from those in older cars and that these differences could account for the different KSI rates.

Tables 9 and 10 show the age and gender distributions of the drivers of the side impacted cars in GB and France. The distributions of these factors for each of the vehicle age groups in each of the countries showed that the characteristics of drivers of newer cars were generally similar to those of older cars..

Table 9 Struck vehicle GB

		Struck Vehicle Age			
		Pre 1998	1998 onwards	Pre 2003	2003 Onwards
Driver Gender	Male	62%	55%	58%	56%
	Female	37%	44%	41%	43%
	N/K	1%	1%	1%	1%
Driver Age	17-40	61%	53%	58%	49%
	41-60	20%	29%	24%	31%
	61+	15%	14%	14%	16%
	N/K	4%	4%	4%	4%

Table 10 Struck vehicle France

		Struck Vehicle Age			
		Pre 1998	1998 onwards	Pre 2003	2003 Onwards
Driver Gender	Male	60%	59%	58%	66%
	Female	40%	41%	42%	34%
	N/K	0	0	0	0
Driver Age	17-40	55%	49%	53%	49%
	41-60	28%	34%	30%	37%
	61+	17%	16%	17%	13%
	N/K	0.1%	1%	0.2%	1%

Discussion

The availability of representative accident data is fundamental to the development of relevant performance criteria for cars to reduce the impact of crashes. Whenever changes are introduced to test criteria it is essential that the social impact, including changes in casualties, is assessed. Where the test requirements are intended to reduce fatalities then these crashes should be assessed in detail.

As part of the development of new test requirements EEVC WG 13 has asked EEVC WG 21 to review the conditions of side impact across as broad a number of EU Member States as possible. The objectives were specifically to assess the overall frequency of side collisions amongst the wider crash population and also to examine the characteristics of crashes of all injury severities including those killed and seriously injured. WG 21 has responded by bringing together a range of accident sources for analysis and has particularly focussed on three aspects in direct relation to the considerations of future test procedures – the overall importance of side impacts, the characteristics of car to car collisions and the characteristics of car to pole crashes. This paper is based on the first of these three analyses and specifically examines the national accident datasets, the other reports are based on the analysis of in-depth

accident data. The full reports will be published at <http://eevc.org/publicdocs/publicdocs.htm>.

The national accident databases of EU Member States only have a limited comparability. The work of the European Commission CARE programme within the European Road Safety Observatory¹¹ has done much to harmonise data but there are still many differences in practise and the use of relatively untrained data gatherers normally determines further constraints. Nevertheless the national accident data can give very useful indications about the details of crash characteristics.

The data from the GB, France and Sweden all indicate that side impacts remain an important crash configuration, especially when serious or fatal injuries are sustained. In the three countries side impacts accounted for between 28% (France) and 40% (GB) and between 20% (France) and 26% (GB) of seriously injured. In GB in 2005 there were a total of 679 casualties who died in a side collision, 790 in France and 28 in Sweden.

The existing side impact test procedures, defined in ECE Regulation 95, represent the conditions of a car struck mid-door by the front of another car. The injury risks are evaluated for the front seat occupant on the struck side, immediately impacted by intruding side structures. Despite this the data from the three countries demonstrates that typically 40% of casualties in side impacts are seated away from the collision on the non-struck (far) side of the car regardless of injury severity. There is no published information available on the relationship between improved performance in regulatory side impact tests and changes in non-struck side injury risks, it cannot be therefore concluded that reductions in struck side injury risks as a consequence of Reg. 95 will automatically result in the same changes to non-struck side occupants.

Within the population of post-1998 side impacts collisions with other cars were substantially the most common, being between 45% (Sweden) and 63% (France) of the total. Impacts with poles ranged between 3% and 6%. Collisions with buses and trucks represented between 11% and 13% of side impacts while other types of single vehicle crash accounted for between 7% (France) and 37% (Sweden). The distribution of collision partner for fatal side crashes of post-1998 cars was different. While car to car collisions were the most frequent in France and GB impacts with poles were also frequent as were other single vehicle collisions. This distribution confirms the emphasis placed on

protection in car to car side collisions but also reaffirms the importance of protection in car to pole crashes. Currently there is no European regulatory crash test requirement for pole side impacts and until recently the EuroNCAP test has only examined head injury risks. The characteristics of car to pole collisions are examined in a linked paper.

The data from the three countries indicates that there have been improvements in safety following the introduction of Regulation 95, although there is little consistency between countries. Reductions ranged from 3% to 61% and it is believed these are in part a consequence of different sampling practises. However closer scrutiny of this positive picture reveals the possibility that other changes in vehicle characteristics may have had unintended consequences, although at a non-significant level statistically. In particular the French data indicates that the injury risk to occupants of a newer car (post-2003) when struck in the side by another newer car are slightly larger than those when an old (pre-1998) car is struck by another old car. A similar, although less pronounced, pattern was observed in the GB data. This contradicts the hypothesis that injury rates would be lower in newer cars. It is possible from the results that improvements in side impact protection have been counterbalanced by increases in aggressivity of car front ends however further experimental research is required to clarify the factors. On the other hand when a newer car was struck by an older car, on which the mobile deformable barrier was based, injury risks were lower in both GB and French data.

Conclusions

Examination of the national accident databases of Sweden, France and GB have been undertaken in support of the development of revised crash test procedures for side impact conducted by EEVC WG 13. The main conclusions are:-

1. Side collisions remain a frequent cause of fatal and serious injury
2. Non-struck side occupants are a frequently injured group who are not covered by existing test procedures.
3. Impacts with other cars are marginally the most common type of side collision.
4. Although rare overall, pole impacts are a frequent cause of death.
5. There are indications that improvements in side protection may have been counterbalanced by other changes in car structural performance, one of which is an increase in car front stiffness although these need to be evaluated

experimentally together with an identification of any differences in driver factors.

References

¹ Otte, D., Haasper, C., Welsh, R., Thomas, P., Sferco, R., Schaefer, R., Assessment of Injury Severity of Nearside Occupants in Pole Impacts to Side of Passenger Cars in European Traffic Accidents - Analysis of German and UK In-depth data. Enhanced Safety Vehicles conference 2009

² Welsh, R., Morris, A.P., Thomas, P., Lenard, J., Otte, D., Strandroth, J., Car to car struck side impacts - a comparison between European Accident data and Regulation 95, Welsh et al. International Research Council for the Bio-mechanics of Impact, York, 2009

³ [96/27/EC](#) Protection of occupants of motor vehicles in the event of a side impact and amendment of Directive [70/156/EEC](#),

⁴ Thomas, P.D. and Bradford, M.A., Side impact regulations - how do they relate to real world accidents? 12th International Technical Conference on Experimental Safety Vehicles. 1989 Gothenburg

⁵ Frampton, R.J., Brown, R.H., Thomas, P.D. and Fay, P., The importance of non struck side occupants in side impacts. 42nd Conference of the Association for the Advancement of Automotive Medicine. 1998

⁶ Morris, A.P., Welsh, R., Thomas, P., Kirk, A. Head and chest injury outcomes in struck-side crashes. International Research Council on Biomechanics of Impact 2005

⁷ Edwards, M., Fails, A., Davies, H., Lowne, R., Hobbs, A. "Review of the European Frontal and Side Impact Directives" Proceedings of the 17th International Technical Conference on the Enhanced Safety of Vehicles, Amsterdam 2001.

⁸ Hassan, A., Mackay, M., Padmanaban, J. Stone Davis, M., Comparison of Real World Side Impact Collisions which Occurred in the United Kingdom and United States, 43rd Annual Proceedings, Association for the Advancement of Automotive Medicine, September 20-21, 1999 Barcelona (Sitges), Spain

⁹ Frampton, R. J., Welsh, R., Thomas, P., Fay, P. The Importance of Non Struck side Occupants in Side Collisions. Journal of Crash Prevention and Injury Control., Vol. 2, No. 2, pp. 151-163, 2000.

¹⁰ Thomas, P., Frampton, R., Crash Testing For Real-World Safety - What Are The Priorities For Casualty Reduction?, 18 Enhanced Safety Vehicle Congress, 2003, Nagoya, Japan

11

http://ec.europa.eu/transport/road_safety/observatory/observatory_en.htm

WG21 Membership at time of review

Pete Thomas	Chairman UK
Dietmar Otte	Secretary/National Representative, Germany
Raimondo Sferco	Technical Advisor Germany
Gilles Vallet	National Representative France
Yves Page	Technical Advisor France
Johan Strandroth	National Representative Sweden
Javier Paez	National Representative Spain
Giancarlo Della Valle	National Representative Italy
Matteo Giunti	Technical Advisor Italy
Richard Cuerden	National Representative UK

QUANTIFICATION OF THE SCATTERING DUE TO THE DUMMY SET-UP IN SIDE POLE IMPACT

Céline Adalian,
Nathalie Nowakowski,
Richard Zeitouni
PSA Peugeot Citroën
France
Paper number 09-0096

ABSTRACT

Up to 2008, in the Euro NCAP rating, the assessment of the adult protection in pole test was only made through the head criteria. From 2009, the pole test in the new "overall rating" Euro NCAP protocol will take into accounts all body regions (head, chest, abdomen and pelvis).

The aim of this study is to analyse the scatter of biomechanical criteria linked to these different body regions. Three phases were defined:

- Phase 1: analysis of a large number of pole tests in order to identify what body region was the most scattered.

- Phase 2: quantification of the scatter linked to the car, seat and dummy set-up. Ten trials of dummy set-up in three laboratories and on three types of vehicles were analysed. The first one of these trials was for reference, since it followed rigorously the vehicle and dummy set-up protocols proposed by Euro NCAP. The other trials were made to assess the scattering by varying several parameters such as vehicle mass, type of dummy, operator. These trials gave us the maximum scattering that could exist and that can be reproduced in dynamic tests.

- Phase 3: quantification of the consequences of the dummy positioning on the pole test's dummy readings. Indeed, several pole tests will be carried out on identical vehicles with different dummy positioning. The results of this study will have to be linked to their consequences on the biomechanical criteria, in particular on the chest and abdomen. Recommendations are given to improve the dummy set-up procedure by taking into account these possible scattering of the dummy positioning and by proposing counter measure to avoid them in a future protocol.

INTRODUCTION - AIM OF THE STUDY

A new balance appears with the brand new Euro NCAP overall rating, since new criteria or new tests come into force. One of the important changes is the pole test assessment which has been widely extended [1], [2]. Indeed, now all the body regions

are rated (head, chest, abdomen and pelvis). By studying into details this new protocol and the results measured on the different body regions, it can be noticed a large scattering that needs to be quantified and controlled. This study takes place in this context.

In order to determine the reliability of the current Euro NCAP pole test assessment (4 body regions: head, chest, abdomen and pelvis), a test programme had been defined. The purpose is :

- to assess the scattering on dummy set-up
- to find the key test parameters/ conditions which influence repeatability and reproducibility of the contemplated test procedure.
- to assess the impact of the scattering on dummy set-up on the biomechanical criteria
- to prepare recommendations for the dummy pole test procedure.

Before going further into the details of this study, it should be wise to recall the main requirements of the Euro NCAP pole test impact protocol.

MAIN REQUIREMENTS OF THE POLE TEST IMPACT PROTOCOL

Car Preparation

The first part of the protocol is the preparation of the car. A reference weight is defined through the vehicle kerb weight. And after preparation, dummy and data acquisition system installations, the test mass is measured. It is important to notice that some tolerances are allowed between the reference weight and the test mass. For instance, 50 kg of difference on the front and rear axles can be OK.

Initial Seat Position

The impact line between the pole and the car is directly derived from the ES2 dummy's head position (Head Center of Gravity, named Head CG for the rest of the study).

For this purpose, it is needed first to define the initial position of the driver seat.

The driver seat is put in its mid rails / fully down position. The torso angle is measured on the H-Point Machine (named Oscar for the rest of the study). It has to be set to the manufacturer design position generally around to 22-25°. Then, the H-point is measured on the Oscar, in order to position the ES2 in its initial position. As a reminder, it may be interesting to recall that the initial ES2 H-point coordinates should be inside a 10 mm circle from the Oscar H-point ones. We called this initial seat position: **“Step 1”**

Final Seat Position

When the ES2 is installed in its initial position, a specific distance has to be measured: the “daylight opening distance”. This distance is measured between a reference point on the car and the rearmost point of the dummy head. Both of them have to be taken at the same height as the Head CG.

Note: At this stage, it is easy to notice that if between two cars, the dummy Head CG is not at the same height, then, two different reference points will be taken on the two cars (the front door daylight opening). Indeed, most of the time, the front door daylight opening is not vertical, therefore, these two points will probably not be at the same position in X.

If the daylight opening distance is 50 mm or more, the dummy will stay in its initial position and the impact point will be the initial Head CG position in X.

But if the daylight opening distance is less than 50 mm, it is required to change the seat set-up. There is a definite order to follow:

- first, the seat back has to be put upright, but it cannot be more than 5° change from the initial position. We call this action: **“Step 2”**
- if the daylight opening distance is still less than 50 mm, the seat is moved forward until the 50 mm is achieved or until the knees of the dummy contact the dashboard. We call this action: **“Step 3”**
- if the daylight opening distance is still less than 50 mm, the seat back have to be put upright again. On the vast majority of our cars, we do not need to go into this step.

At the end of this part, we can measure the Final ES2 H-point.

Impact Line Definition

The car has to impact the pole along the vertical line that passes through the ES2 dummy’s head position (the Final Head CG).

Partial Conclusion

Since the main parameter is the daylight opening distance, one can easily imagine that if a dummy has a different initial head position, or if the seat back initial angle is set in a different way, the impact line can differ as well as the biomechanical results. This is what we will show in the next chapter.

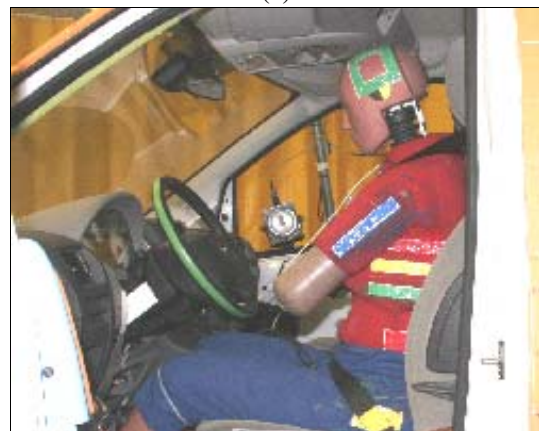
PHASE 1: ANALYSIS OF A LARGE NUMBER OF POLE TESTS

The first need to carry out such a study came from the comparison of two tests made on a PSA car in two different laboratories. These laboratories strictly followed the Euro NCAP protocol, and one of them is even Euro NCAP accredited. The difference in the dummy test position and therefore in the pole impact line between the two tests are shown in Figure 1 (a) and (b).

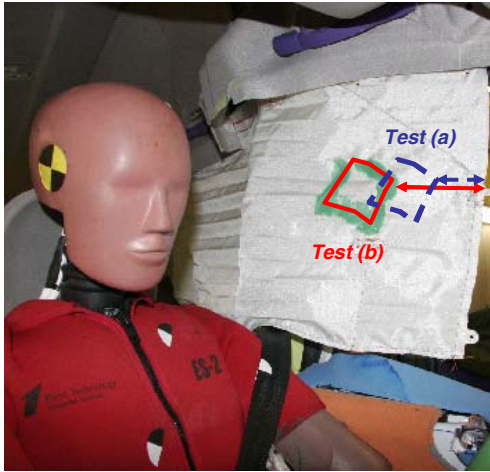
Because of this difference in the dummy positioning, the head impacted a different zone on the curtain airbag. The head impact in the first test was twice forward from the extreme front of the curtain airbag as shown in Figure 1 (c).



(a)



(b)



(c)

Figure 1. Dummy test position for a same car in two different test laboratories (a) and (b), and its consequences on the impact against the curtain airbag (c).

This paragraph presents analyses on pole test realised with several PSA Peugeot Citroën's vehicle models. The results taken into account come from at least 4 pole tests carried out in different test laboratories. This means with different operators, different ES2 dummies and different cars of the same model.

The main outcomes are presented by taking an example on three vehicles that belongs to three different marketing segments:

- Car A: a small family car
- Car B: a family car – SUV type
- Car C: an executive car

Table 1 presents the overall scattering results from these 3 cars on the main test parameters. The scattering is reckoned as the difference between the maximum value measured on the different tests and the minimum value.

Table 1. Overall scattering results from these 3 cars on the main test parameters.

Scattering	Car A	Car B	Car C
Final Head CG (mm)	8	33	-
Final H-point X (mm)	27	32	25
Final H-point Z (mm)	6	20	3
Test Mass (kg)	18	7	-
Pole test score (pts) Max. score = 16 points	2.98	2.9	1.2
% from max score	19 %	18 %	8 %

We can notice that for a car model, the overall scattering of the pole test can give a variation of 20% on the total score that can be obtained (16

points). This is really important and needs to be decreased. If we go a little bit further into the analysis, we can see the scattering in the biomechanical max values used in the Euro NCAP pole test rating.

But we also need to identify if there is a specific body region that sustained the most scattering. For instance, it is clear from our analysis that the scattering on the head results (HIC or head resultant acceleration) has no effect on the Pole Test Rating.

On the other hand the three other body regions can be considered as sensitive to the scattering as it can be shown in Table 2.

Table 2 presents the biomechanical scattering results for these 3 cars. Here again, the scattering is reckon as the difference between the maximum value measured on the different tests and the minimum value.

Table 2. Biomechanical scattering results from these 3 cars on the main test parameters.

Scattering	Car A	Car B	Car C
Pole test score (pts) Max. score = 16 points	2.98	2.9	1.2
Chest Compression (mm)	13.6	8.8	11.8
Back Plate force (kN)	0.2	0.14	0.25
T12 Force (kN)	0.61	1.07	0.34
T12 Moment (kN)	31	36	35
Abdomen Peak force (kN)	0.36	0.79	0.16
Pubic Symphysis force (kN)	0.51	0.91	0.35

As an example, it is interesting to stress that a difference of 13.6 mm in maximum chest compression can give a score from 2.72 points to 0 point, out of a maximum of 4 points.

In the same way, a difference of 0.8 kN in the Abdomen Peak force can lead to a score that goes from 2.13 points to 0 point, out of a maximum of 4 points.

Finally, a difference of 0.9 kN in the Pubic Symphysis force can lead to a score that goes from 1.2 points to 0 point, out of a maximum of 4 points.

Partial Conclusion

This first phase of the analysis clearly show that there is a significant scattering of the pole test results that can gives a high difference of Euro NCAP rating score.

Therefore, there is a need to better control the test parameters and to know which parameters are

linked to this scattering. This is the purpose of the next chapter that presents the 2nd phase of our analysis.

PHASE 2: QUANTIFICATION OF THE SCATTER

Presentation Of The Study

The study was performed on three different car models:

- Car 1: a small family car
- Car 2: a family car
- Car 3: an executive car

For each vehicle model, the same car was circulated to three different test laboratories (Lab 1, Lab 2 and Lab 3). So, we already removed the scattering due to the difference in car production. These three test laboratories are Euro NCAP crash test accredited.

For each car, we asked the labs to perform 10 different trials. Some of the trials were purely identical, in order to assess full **repeatability**.

Whereas some others were voluntarily modified, in order to take into account a difference of mass, a different operator, a different Oscar or a different ES2 dummy while still following the official pole impact test protocol.

These trials will give an assessment of the **reproducibility** within each lab.

Finally the comparison of the three labs will give the full assessment of reproducibility; what we can call the **overall reproducibility** (or overall scattering).

For each trial, we asked the lab to completely start as if it was a new car. Therefore, even the initial seat set-up was carried out again (e.g. setting the seat rail in mid position, finding the initial seat torso angle).

The only parameters we imposed were the car XYZ reference and axes and three points of measurement on the seat and on the seat back. The three seat reference points were used to quantify the change between step 1, step 2 and step 3 (see definition in Chapter “Main requirements of the pole test impact protocol”).

Note: all the car models selected needed to go up to step 3 to get the proper daylight opening distance.

The complete test matrix, for each lab and each car is given in Table 3.

For each trial, we defined the parameters to measure and we used a common and unique datasheet to gather all the parameters.

Table 3.
The complete test matrix carried out for each lab and each car.

Test reference number and description		Operator n°1	Oscar n°1	ES2 n°1	Mass n°1	+50 kg front axle	+50 kg rear axle	Operator n°2	ES2 n°2	Oscar n°2
RA	Reference	X	X	X	X					
RB	Reference (repetition test)	X	X	X	X					
RC1 - 3	Partial repetition test	X	X	X	X					
OP1	Operator change		X	X	X			X		
OP2	Operator change (repetition test)		X	X	X			X		
E1	ES2 dummy change	X	X		X				X	
E2	ES2 dummy change (repetition test)	X	X		X				X	
OS1	Oscar change	X		X	X					X
MA1	Front axle tolerance	X	X	X		X				
MA2	Rear axle tolerance	X	X	X			X			

For each main change, we asked for a repetition test. This is the reason why there is an OP1 and an OP2, as well as an E1 and E2, and an MA1 and an MA2.

For test RC1-3, the idea was to keep the seat position as initially defined by the first dummy set-up (in RC1).

Then, after the full RC1 test was carried out, RC2 and RC3 started with the positioning of the ES2 in the final seat position defined in RC1 to measure the final H-Point, the final Head CG and the final daylight opening distance.

The main parameters that were gathered are:

- H-Point X and Z initial as well as for each step (including the final H-Point)
- Head CG X and Z initial as well as for each step (including the final Head CG)
- Seat back Angle initial as well as for each step
- Number of seat back notches for Step 2
- Number of seat rail notches for Step 3
- Daylight opening distance initial as well as for each step
- Seat reference point 1, 2 and 3 initial as well as for each step

Overall Results Of The Study

A quick analysis showed that counting the notches (for the seat back angle as well as for the seat rails) is not reliable and can lead to errors. Indeed, when one tries to put the seat back upright with the ES2 dummy in the seat, it is quite easy to miss one notch. Therefore it is far much more reliable to measure an angle in degrees or a forward movement in millimetres than to count notches. This is the reason why we will not show in this study any value linked to the number of notches.

The first drawings we created were to compare the four main parameters for each car:

- the initial Oscar H-Point
- the final ES2 H-Point
- the initial Head CG
- the final Head CG

In these drawings, we do not try to distinguish the lab or the other changes in the test parameters.

This gives the results shown in Figure 2 to 4.

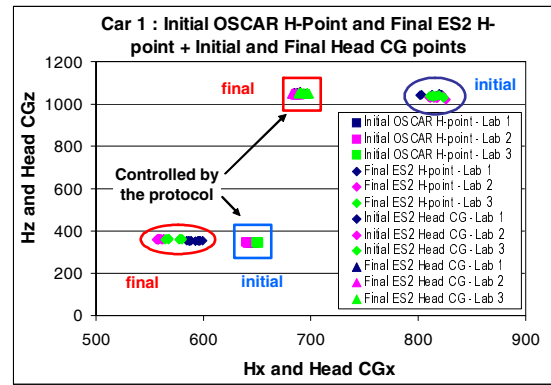


Figure 2. Overall scattering of the 4 main parameters for Car 1.

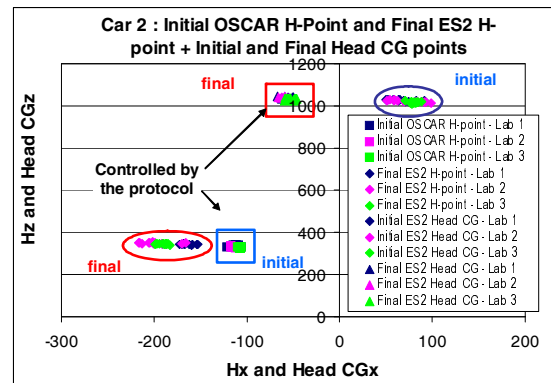


Figure 3. Overall scattering of the 4 main parameters for Car 2.

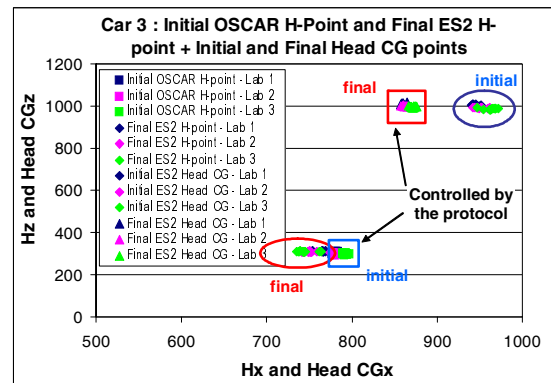


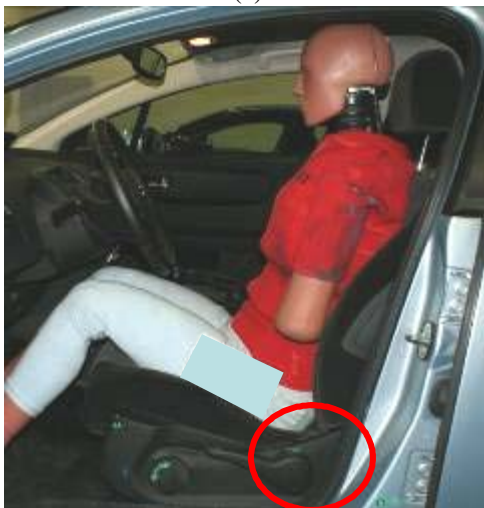
Figure 4. Overall scattering of the 4 main parameters for Car 3.

By looking at these drawings, one can notice that the initial Oscar H-Point and the final Head CG are less scattered than the initial Head CG and the final ES2 H-Point. This is completely linked to the test protocol that controls the initial H-Point and the Final Head CG through the daylight opening distance.

But if the two other parameters are scattered, this means that the dummy is not in the same final position. This is shown by one example presented in Figure 5.



(a)



(b)

Figure 1. Dummy test position for a same car in the same test laboratory but with two different test configurations (a) and (b) both fulfilling the Euro NCAP test protocol.

So, we need to know what the differences are in the dummy position, which extent and if it is due to the bad repeatability of the test procedure or to the bad reproducibility.

Figure 6 to 9 give some examples of the extent of the overall reproducibility for the 4 parameters without distinguishing the labs.

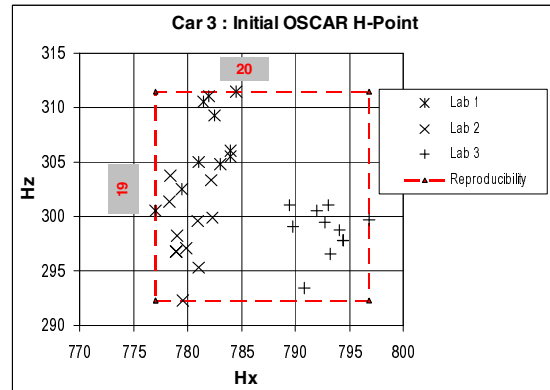


Figure 6. Overall scattering of the Initial Oscar H-Point for Car 3.

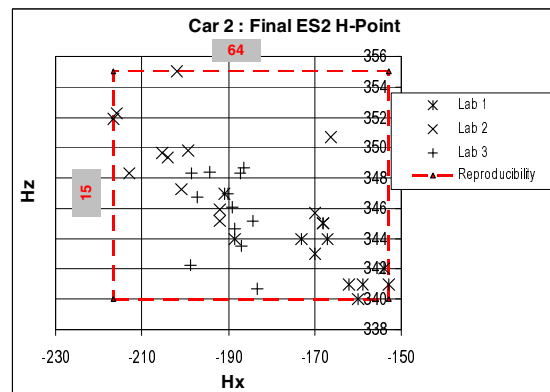


Figure 7. Overall scattering of the Final ES2 H-Point for Car 2.

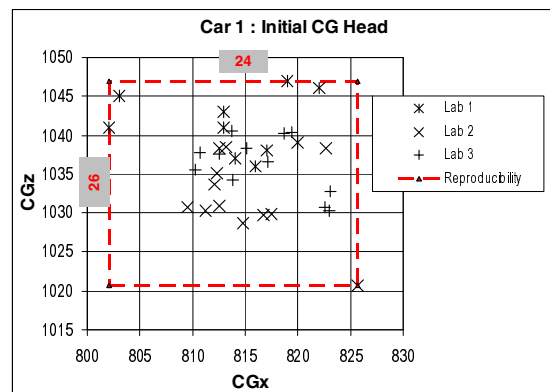


Figure 8. Overall scattering of the Initial Head CG for Car 1.

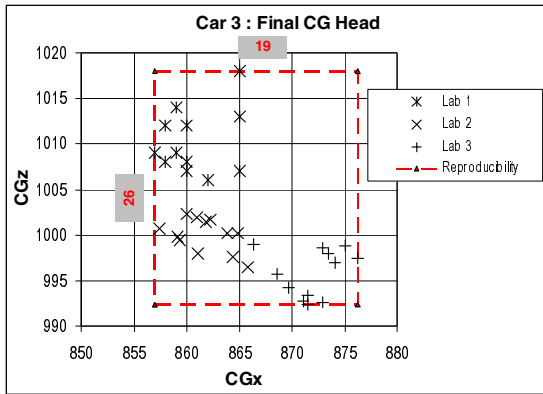


Figure 9. Overall scattering of the Final Head CG for Car 1.

Table 4 gives the complete results of the overall reproducibility scattering for the 4 main parameters.

Table 4. Overall scattering results (reproducibility) for the 3 cars on the 4 main parameters.

Scattering (mm)	Car 1	Car 2	Car 3
Initial Oscar H-Point X	13	15	20
Initial Oscar H-Point Z	7	15	19
Final ES2 H-Point X	43	64	39
Final ES2 H-Point Z	13	15	11
Initial Head CG X	24	49	31
Initial Head CG Z	26	21	28
Final Head CG X	16	21	19
Final Head CG Z	13	20	26

From Table 4, we can notice that there is no car more scattered than the two others.

Overall Reproducibility And Best Repeatability Analysis

Before going into details to identify if there is one test parameter more sensitive than another, we decided to define what could be the minimum repeatability scattering. For this purpose, we looked at the results lab by lab and we found that Lab 3 gave less scattering than the others for the reference tests. Therefore, we decided to say that the repeatability cannot be lessened more than the scattering measured in lab 3 on the reference tests (RA, RB, RC1-3). We called the Lab 3 repeatability, the “best repeatability”.

Combining this definition of repeatability with the distinction between the different test parameters, we got graphs that show that the overall reproducibility (by taking all the labs) is from 1.3 to 4.8 times larger than the best repeatability (Lab 3 repeatability). Examples are shown in Figure 10 to 13.

The other points shown on the graphs present the extreme values of each repeated test parameter (change of operator, change of Oscar, change of ES2, change of Mass) taking the three labs into account.

Figure 10 shows the case of a reproducibility scattering 4.8 times larger than repeatability (initial Oscar H-point X). And Figure 11 shows the case of a reproducibility scattering 1.3 times larger than repeatability (Final ES2 H-point Z). These are the extreme values we got in our study.

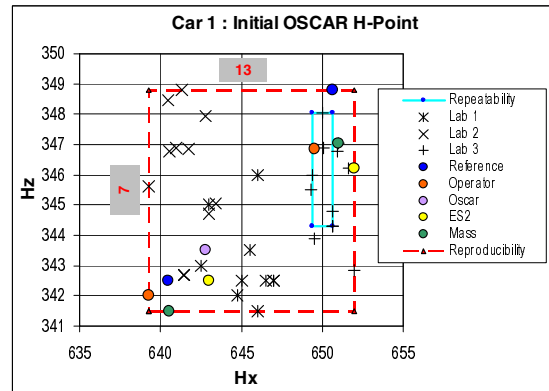


Figure 10. Overall scattering of the Initial Oscar H-Point for Car 1.

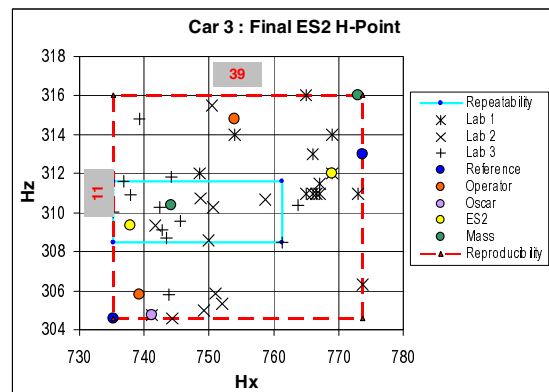


Figure 11. Overall scattering of the Final ES2 H-Point for Car 3.

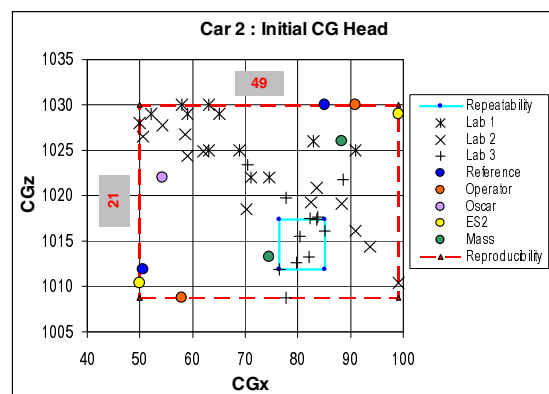


Figure 12. Overall scattering of the Initial Head CG for Car 2.

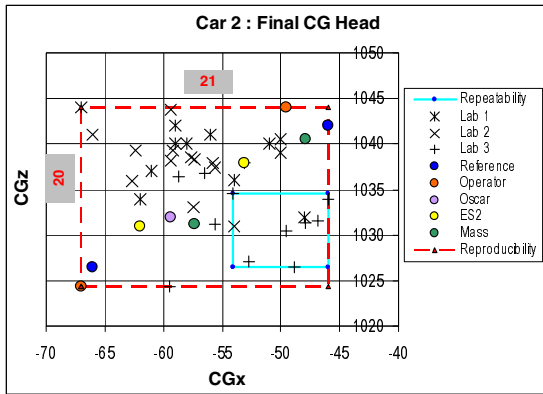


Figure 13. Overall scattering of the Final Head CG for Car 2.

The distinction between the different test parameters does not give clear trends.

If we look at the reference scattering (blue circles) we can find that it highly contributes to the overall reproducibility. This conclusion is logical since the reference scattering is made of the reference tests carried out in the three labs. So, it already includes a different Operator, a different Oscar and a different ES2 dummy between the three laboratories. So, we logically find the contribution of three test parameters in the scattering named reference scattering.

Analysis Of The Best Repeatability And Its Reproducibility

To get a trend of the influence of each test parameters, we studied the results of Lab 3 only. Some of the results are presented in Figures 14 to 18.

For some exceptional cases, Lab 3 repeatability and Lab 3 reproducibility are identical. This is the case for Car 1 Initial CG Head (Figure 16). In this case, changing the dummy didn't give an extra scattering to add to the scattering measured by repeating the reference test.

On the other hand, for the same parameter, but for Car 2, changing the ES2 doubles or triples the scattering (Figure 17).

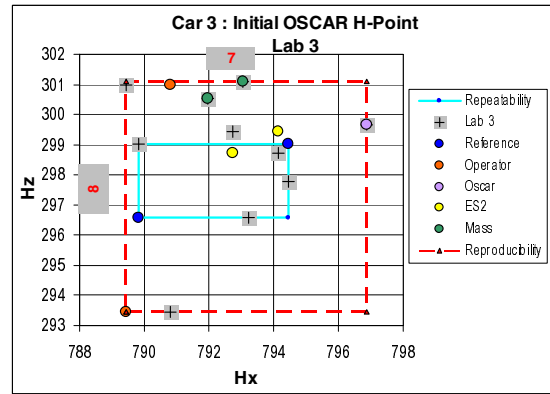


Figure 14. Scattering of the Initial Oscar H-Point for Car 3 in Lab 3 (Best Repeatability).

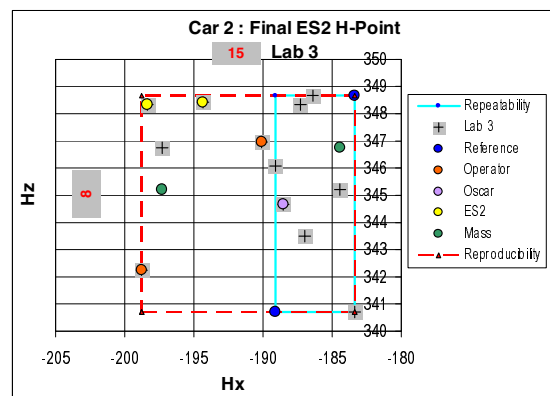


Figure 15. Scattering of the Final ES2 H-Point for Car 2 in Lab 3 (Best Repeatability).

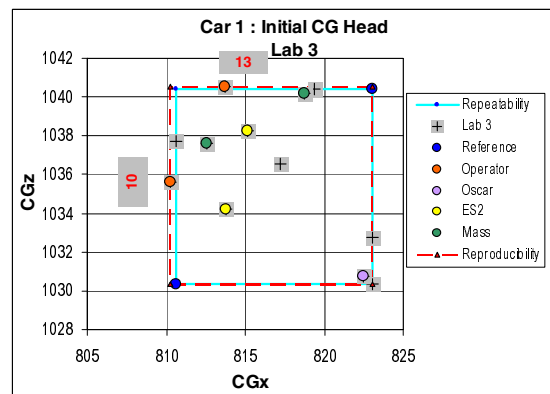


Figure 16. Scattering of the Initial Head CG for Car 1 in Lab 3 (Best Repeatability).

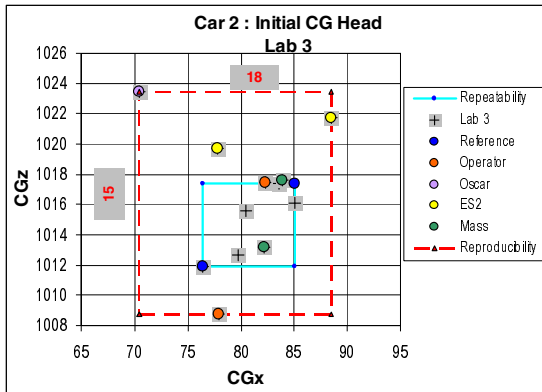


Figure 17. Scattering of the Initial Head CG for Car 2 in Lab 3 (Best Repeatability).

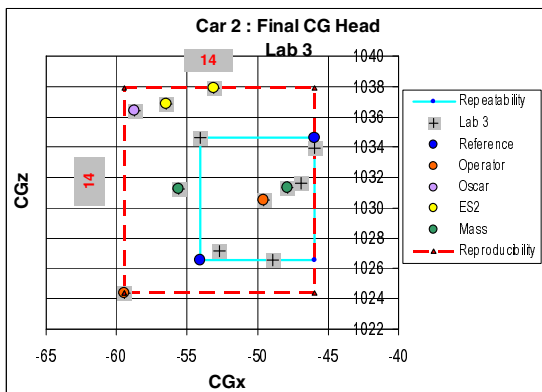


Figure 18. Scattering of the Final Head CG for Car 3 in Lab 3 (Best Repeatability).

DISCUSSION

Assessment Of The Scattering

First of all, from all our analysis, we couldn't highlight a car that gives more scatter than the two others.

We measured the scattering of repeating a same test, with the same tools in the three laboratories and we found that there is one lab that gives better results than the two others. From this remark we can assume that repeatability cannot be lessened more than what we got in Lab 3, without changing the test protocol.

So we know that the **best repeatability** scattering can be:

- a Final H-Point within 26 mm in X and 8 mm in Z
- a Final Head CG within 8 mm in X and 8 mm in Z

But we also measured, within the same lab; a higher scattering as soon as one parameter is changed (whether it is the Oscar, the ES2, the mass or the Operator).

Therefore, the assessment of the best reproducibility (within one lab) is:

- a Final H-Point within 28 mm in X and 9 mm in Z
- a Final Head CG within 14 mm in X and 14 mm in Z

So, even by looking only at the results obtained in Lab 3, we can have up to 28 mm of scattering on the Final ES2 H-Point in X.

For information, this value comes from a change in the mass with respect to a reference test.

In addition, the 14 mm of scattering found on the Final Head CG in X does not come from a change in the ES2 dummy but from a change of Operator! This will change by 14 mm the pole impact line against the car whereas the set-up was carried out in the same laboratory.

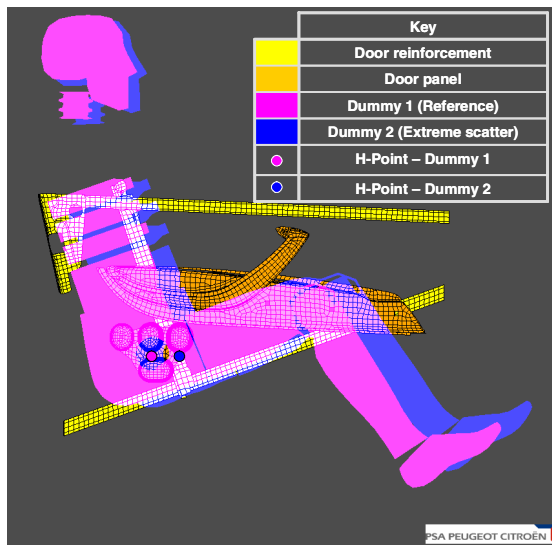
Now, if we look at the **overall reproducibility** - a case we can easily encounter when we develop a car in one lab and we assess its performance in the Euro NCAP rating in another lab - we find:

- a Final H-Point within 64 mm in X and 15 mm in Z
- a Final Head CG within 21 mm in X and 26 mm in Z

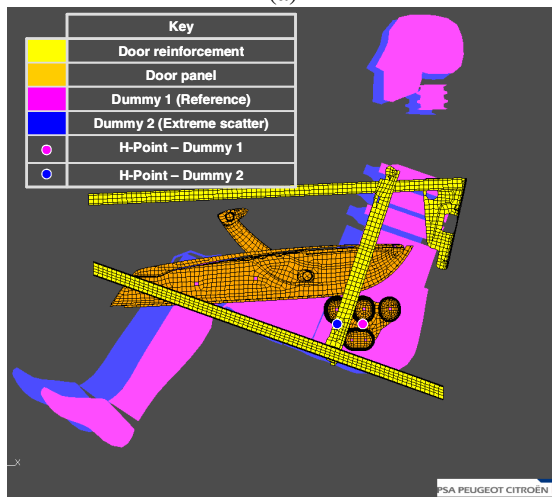
So, between two laboratories, the pole impact line may change by up to 21 mm while fulfilling all the Euro NCAP requirements. And at the same time, we can also have a final H-Point X scatters at 64 mm!

To try to represent the consequences of these two extreme positions a dummy can have in one car, we can get what is shown in Figure 19:

- Dummy 1 is the reference dummy
- Dummy 2 shows the dummy position with the extreme scatters
- Figure 19 shows the superposition of the dummies with the door reinforcements and door panel



(a)



(b)

Figure 19. Drawing of the two extreme positions a dummy can have in one car following the results of our study – (a) view from the car inside and (b) view from the car outside.

Now, we need to quantify exactly the consequences on the dummy readings. We will take the extreme positions defined in the study. But we already know that these dynamic tests will also give some extra scatterings since two different dummies will not have the same dynamic behaviour. This will be made in a future phase, not yet realised.

Parameters To Measure Or Control During The Test Preparation

By following the tests in the different laboratories, it has been highlighted that some extra parameters have to be measured and controlled.

We need to avoid checking the changes between step 1, step 2 and step 3 by counting the number of notches in the seat back angle or in the seat rails.

Clearly, if we have something to check, we need to ask for the seat back angle change in degrees and the seat forward motion in millimetres. In addition, for the seat back angle change, we also need to clearly define how to measure it (on the head restraint stem angle, for instance, with an inclinometer or directly through some CMM measurements).

Moreover, the test protocol could also be better defined. Some pictures could be added to the different steps; to be sure operators will follow the same set-up. This is especially true for the definition of the daylight opening distance (we saw some hesitation between the way to take the reference point: door open or door closed?).

In the same way, some tolerances need to be added. For instance, the protocol states that for step 2 the angle could not be changed by more than 5° . But in some cars we have seat back articulation that moves 1.8° by 1.8° (one more notch gives a 1.8° change in seat back angle). Therefore, being less than 5° means two notches = 3.6° . On the other hand, going to the third notch will give 5.4° total change which is quite closer to 5° than the initial 3.6° change. Do we allow some tolerance to the maximum change of 5° ? Or do we need to be strict even if only 3.6° are taken out of 5° ?

Finally, the dummy intrinsic head position is of extreme importance. We already showed that in the phase 1 of our study. A specific zoom is given in Figure 20.



Figure 20. Two extreme final positions of the ES2 dummy head in real Euro NCAP-like pole impact tests.

This head position is not controlled by the dummy calibration and no specific device can be used to adjust it. The only explanation of the difference in the angle is the fact that there is the possibility of using three types of nodding blocks (rubber elements) of different stiffness. But the stiffness of these nodding blocks has to be chosen to fulfil the neck corridor. Normally, when using a brand new neck, the softer nodding blocks are used. Then, after several tests, there is a need to come to the mid-softness nodding blocks. And finally after some more tests, it is required to use the harder

nodding blocks to be sure the neck corridor is still fulfilled.

So, changing the nodding blocks or imposing one specific type of nodding blocks will not be possible unless multiplying by three the number of neck to buy and replace.

CONCLUSIONS

In order to assess the scattering of the pole test, we conducted a study on the dummy set-up and impact line set-up of three different car models in three different laboratories. Each laboratory used a same reference set-up (same Operator, same Oscar, same ES2 dummy and same mass repartition) and repeated it three to five times. Each lab also followed our demand to change one parameter after the other while still fulfilling the Euro NCAP pole test impact requirements. Every time, the measurements were repeated once.

With the whole database, we derived an assessment of the scattering and we shown that the final position of the dummy can be scattered from 64 mm in the ES2 final H-Point X coordinate and 21 mm in the ES2 Head CG X coordinate. This will change the position of the whole dummy with respect to the car inside (door panel, side airbag, curtain airbag) as well as a change in the pole impact line on the car.

We were able to assess the overall reproducibility but also what we can call the best repeatability. Indeed, we found one lab which gives less scatters than the others when repeating the test measurements with the same tools. But on the other hand, even in this lab, changing only one parameter gave an extra scatters.

This analytical study will also be analysed with a specific statistical tool which will be presented in the oral document. This will help to highlight if one test parameter, or tool, is more sensitive than the others.

Finally, the full study will be finished when we reproduce the extreme dummy positions in dynamic tests and we quantify the changes in the dummy measurements. This is planned to be carried out later this year.

But even without performing these extreme test positions, we already have an assessment of the scattering in the dummy readings, through dynamic tests carried out at different test labs, as presented in the phase 1 of our study. The maximum scattering we had, without trying to assess an extreme scattering, was 2.98 points out of 16. This is already of enough importance to pay attention and try to reduce the scatter.

We hope other studies will be carried out on the same topic, so that more expertise will be added, and probably the test protocol will be improved to control and restraint the overall scattering of the pole test impact.

ACKNOWLEDGMENTS

The authors wish to thank all the labs involved in this study as well as the PSA research team. We also wish to thank V. Boisgard, from Matra, for his help on this study.

REFERENCES

- [1] Euro-NCAP-Pole-Protocol-Version-4.2
- [2] Euro NCAP Assessment Protocol v.4

LATERAL GLAZING CHARACTERIZATION UNDER HEAD IMPACT: EXPERIMENTAL AND NUMERICAL INVESTIGATION

Marie Munsch
Nicolas Bourdet
Caroline Deck
Rémy Willinger

University of Strasbourg – IMFS-CNRS
France
Paper number 09-0184

ABSTRACT

In case of lateral impacts, the most frequent contact source is the side window. This window is also the most frequent aperture through which occupants are partially or fully ejected during a lateral crash. In order to keep occupant within the vehicle during a collision, laminated side glasses have been developed to gradually replace tempered glasses. Three-layered laminated glazing is composed of two glass layers separated by a plastic PolyVinylButyral (PVB) interlayer. The aim of the present work is to improve the understanding of the side window's mechanical behaviour during a head impact. An experimental study is undertaken which consists of an impact of a Hybrid III dummy head on both laminated and tempered side glazing. It appears that at same velocity, impact against laminated glass leads to a significant lower injury head risk than a tempered glass. The principal role of laminated glazing has been preserved as PVB layer never fails. A laminated side glass FE model is then proposed based on experimental validation, with the PVB interlayer implemented by an elastoplastic law with failure criteria. A parametric study is carried out to define the influence of the laminated glass mechanical characteristics on the head response. The parametric study pointed out the importance of the glass layer thickness on head responses in terms of head injury criteria.

INTRODUCTION

In case of lateral car crash, the most frequent contact source is the side window. This side window is also the most frequent (40 %) apertures through which occupants are partially or fully ejected during a crash (Clarke *et al.* 1989, Morris *et al.* 1993, Hassan *et al.* 2001). Occupant ejection from vehicles is often considered to be a contributor to death and serious injury. The head/neck region is

the most frequently injured body region of ejected occupants (Hassan *et al.* 2001). In order to keep occupant within the vehicle during a collision, laminated side glass has been developed to gradually replace tempered glasses. This security glass is composed of two layers of heat-strengthened glass (2.1 mm thick) with a plasticised interlayer membrane of PolyVinylButyral or PVB (0.76 mm thick). This enhanced protective glass offers a good resistance for breaking and entering. It can resist an aggressive attack for 20-30 seconds compared to tempered glass which would resist the attack for only 1-2 seconds (Lu *et al.* 2000).

In the late 1980's, Clarke *et al.* conducted rollover tests on vehicle containing bi-layer glazing in the side window openings. The authors demonstrated the potential of glass-plastic glazing to significantly reduce ejections through motor vehicle windows. Clarke provides acceptable neck loads under severe glazing contact conditions. Advanced glazing systems may reduce partial and complete ejections through side window, according to the same authors. In 2002, Sances *et al.* simulated rollover accidents consisting of a Hybrid III dummy test device impacting side windows with three-layered laminated glazing. This glazing contained the dummy assembly. Head-neck biomechanical parameters were below the critical value injury tolerance limits value. The dummy assembly never went through this security glazing. More recently, other authors stated that production laminated side glass is not an efficient barrier to occupant ejection during rollover (Kramer *et al.* 2006, Pierce *et al.* 2007). Evaluations were made against laminated glazing by drop tests on door-glass systems. Rollover accidents typically include multiple impacts and potentially long duration forces on the side glazing. For this reason, some authors (Piziali *et al.* 2007, Luepke *et al.* 2007) do not associate laminated glazing as a suitable candidate for occupant containment during rollovers. However the use of laminated side glazing in automobiles is

increasing. To understand the retention characteristics of laminated glazing, several mathematical and numerical models have been developed in order to model the laminated glass behaviour. Concerning numerical aspects, Mukherjee *et al.* studied impacts of pedestrians against windscreens. The authors implemented an isotropic elastic brittle law for the glass and an elastic law for the PVB layer with the mechanical characteristics of glass and PVB extracted from Haward's study in 1975. Du Bois *et al.* in 2003 and more recently Timmel *et al.* 2007 modelled windscreens for crash simulations with a hyperelastic law for PVB, such as Blatz-Ko's, Mooney-Rivlin's or Ogden's laws. The two glass layers with small plastic deformations until rupture have been implemented by a linear plastic law. To represent the three-layered glass behaviour, shell elements were used for glass layers and a membrane for PVB interlayer. Zhao *et al.* (2006) studied impact resistance of laminated glazing under head impact. PVB has been modelled as linear elastic in this study. Dharani *et al.* investigated failure modes of a laminated glass subjected to head impact using a linear viscoelastic material for PVB interlayer. According to Wei (2004), difference in stress obtained by treating the PVB as linear viscoelastic and linear elastic is less than 2 %. Considering the PVB plastic behaviour, Parsa *et al.* (2005) are the only one to suggest an isotropic viscoplastic model for laminated glass to study the glass creep forming process.

All these models are applied to windscreens. Laminated side glazing has not yet been numerically investigated under head impact. In a first step an experimental study was carried out to compare effectiveness and advantages of the two current types of side glazing used, tempered and laminated glasses. In a second step a finite element model of a laminated side window will be proposed and validated against experimental data. Finally a parametric study on four mechanical parameters of the lateral window will be conducted in order to propose a tool for lateral window optimisation against head criteria.

METHODOLOGY

An experimental study is undertaken which consists in impacting a Hybrid III dummy head against both, a laminated and a tempered side glasses. A set of 15 laminated windows and 5 tempered windows were

studied. Head impact velocities ranged between 3 and 9.5 m/s, which is a realistic level of real head velocity during side impact crash (Bosch *et al.* 2005).

A laminated side glass FE model is then proposed based on isolated experimental data. Same boundary and initial conditions as for the experimental tests were. A parametric study is carried out to define the influence of the laminated glass mechanical characteristics on the head response.

Experimental approach

Testing is performed on an impact test bench, which principle scheme is given in Figure 1. This device consists of catapulting a headform against the glazing thanks to a jack supplied in compressed air. This air propels a carriage on which the head is set. The carriage is rapidly stopped letting slip the headform freely before impact. This device enables it to get propulsion velocities in a range of 5 to 10 m/s. Two devices enable to determine head velocity. The first one consists of a photodiode which is blocked up during the carriage passing. The carriage velocity is calculated just before head releasing by the length of the shutter divided by the blocking up time duration. The second device consists of a head tracking from a video obtained by a high-speed camera. The Photron Fastcam Ultima APX records 1000 frames per second at resolution of 1024x1024 pixels. Four targets fixed on the headform surface permit to compute head angular and linear velocity before and during, by tracking methods. Data acquisition system is performed by a PC-based platform PXI-1010 National Instruments with Labview software. Sampling frequency for data recording is set at 10 kHz. The headform is a Hybrid III dummy head developed by Foster *et al.* in 1977. The headform is composed of an aluminium structure covered by a vinyl synthetic skin with a total mass of 4.53 kg. In order to record the head linear acceleration, a triaxial linear accelerometer (Kistler) with a sensitivity of 10 mV/g and a measure range of ± 500 g is set at its centre of gravity. Accelerations data are filtered with a cut-off frequency of 1 kHz. Figure 2 represents Hybrid III headform with the different targets, the accelerometer location in the headform and its reference frame. Finally, in addition to head kinematics, HIC is computed with the linear acceleration data.

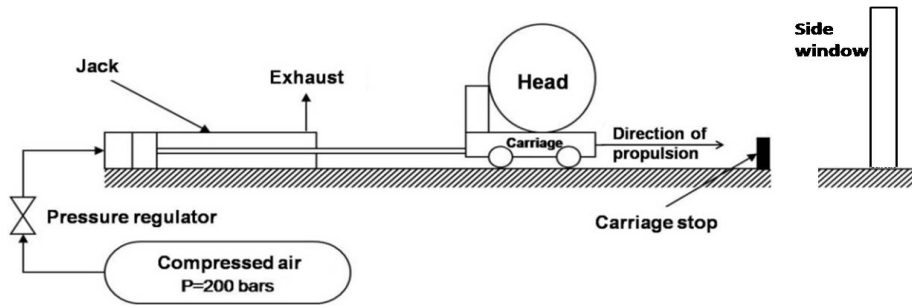


Figure 1. Impact test bench: Principle scheme.

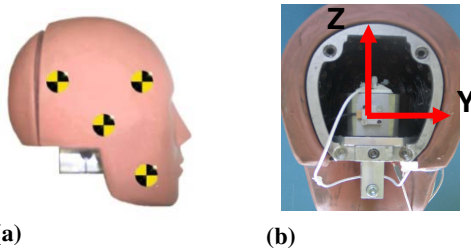


Figure 2. Hybrid III headform: (a) location of targets, (b) accelerometer location and reference frame.

The windows used in this study are front right side windows of a Volvo S80. In order to respect window boundary condition, the windows are encased, closed in the lateral door which is fixed thanks to rubber stripes. Figure 3a represents the window setting in the door. The lateral door is hold screwed on the bench at point A, as represented in Figure 3b. Jambs of the door are maintained at points B and C. The door body is maintained on its slopes to avoid translations along impact direction.

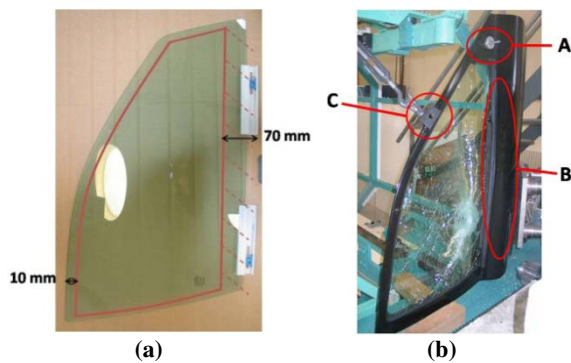


Figure 3. Side window: (a) Window frame in door, (b) Door setting on test bench (screw: A, wedge: B,C).

Tests are performed on 15 laminated glasses and 5 tempered glasses. Table 1 summarizes the different tests with impact velocity and type of glazing used. Nine tests are realised on tempered glazing at impact velocity ranging from 6.6 m/s to 9.4 m/s. A total of fifteen tests are performed on laminated

glazing in an impact velocities range of 2.9 m/s and 11.3 m/s.

The description of the different tests results on laminated and tempered glazing will be presented. Results will be then analysed in terms of head response and injury assessment for both type of glazing.

Table 1. Tests realised on both laminated and tempered glasses with impact velocity.

	Test n°	Velocity [m/s]		Test n°	Velocity [m/s]
Laminated glasses	1	2,9	Tempered glasses		
	2	3,4			
	3	3,9			
	4	4,0		1	6,6
	5	5,0		2	6,7
	6	6,3		3	7,4
	7	6,4		4	7,5
	8	6,8		5	7,7
	9	7,4		6	7,8
	10	7,4		7	7,9
	11	7,4		8	9,1
	12	7,4		9	9,4
	13	8,5			
	14	8,9			
	15	11,3			

Numerical aspects

The second step of this study is to develop a laminated side glass FE model validated against experimental data.

The side window Finite Element model is presented in Figure 4. This model is based on CAO geometry and is meshed with Hypermesh software. It consists of 16613 shell elements modelling the laminated glazing and 8443 brick elements modelling the rubber band. Glazing is modelled under Radioss code by a three layered composite shell with three

different thicknesses: 2.1 mm (glass), 0.76 mm (PVB), 2.1 mm (glass). Glass layers are assigned to an elastic brittle law. An elastoplastic law is implemented for PVB interlayer based on Johnson Cook material for rupture simulation. Rubber band is assigned to an elastic law. Concerning material properties, start point is to consider windscreen properties performed by Mukherjee et al (2000). Young modulus of glass is set at 74000 MPa with a yield stress of 3.8 MPa. PVB is assigned to a Young modulus of 50 MPa, a yield stress of 30 MPa and a failure strain at 0.51. These reference properties will be fitted in order to reproduce mechanical behaviour of laminated glazing during experimental testing.

The mechanical behaviour of the FE lateral laminated window model will be validated against experimental test number five with an initial velocity about 5m/s For this the HIII head FE model was used in simulations. This model consists of shell elements modelling the skull covered by a layer of brick elements. A linear elastic law is implemented for bricks modelling the skin. Mechanical parameters of the HIII FE head model are listed in Table 2 and the total mass of the head model is 4.53 kg.

Equivalent initial conditions and boundary conditions as experimental ones have been applied. These conditions are represented on Figure 5. Interface between window and rubber band is considered as elastic. The validation of the lateral window FEM is made in terms of maximum linear acceleration at the centre of gravity of the head, HIC criterion, glass permanent strain and glass and PVB cracks.

Finally, in order to define the influence of the laminated glass mechanical characteristics on the head response, a parametric study at 5 m/s was undertaken. Four mechanical parameters have been varied: the glass and PVB elastic limit, the thickness of the glass and the PVB interlayer. Each parameter has been set on three different values: a reference value, a high (+ 30 %) and a low (- 30 %) value. The head response was computed in terms of maximum linear acceleration of its center of gravity and HIC value. To analyze and to refine all results, a principal component analysis (PCA) was performed (Volle, 1997) to analyse head response as a function of laminated glass characteristics.

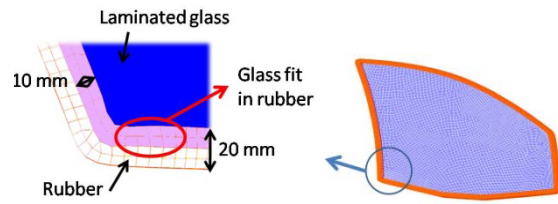


Figure 4. Lateral Window Finite Element Model (16 613 shells, 8 443 bricks).

Table 2. HIII FEM mechanical properties.

component	law	elements	Mechanical properties
skull	Linear elastic	408 shells	$\rho = 260 \text{ Kg/m}^3$ $E = 210\,000 \text{ MPa}$ $\nu = 0,29$
skin		1224 bricks	$\rho = 99 \text{ Kg/m}^3$ $E = 60 \text{ MPa}$ $\nu = 0,409$

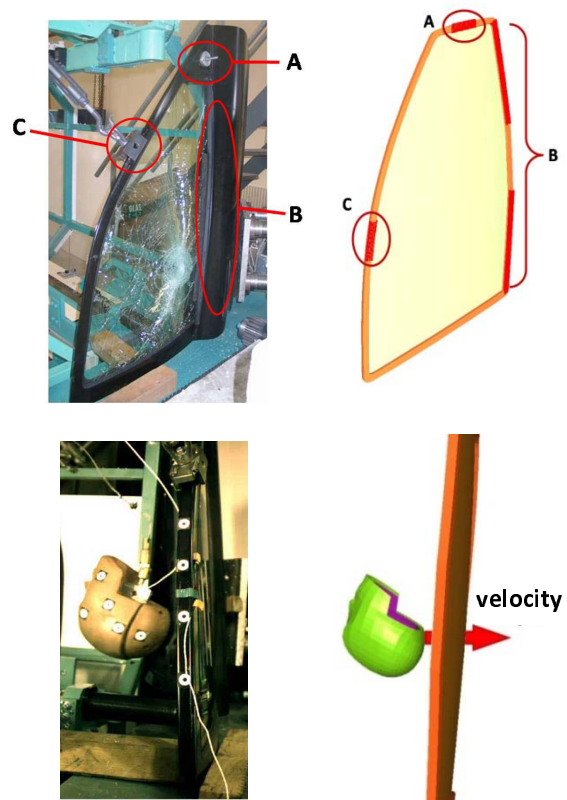


Figure 5. Initial and boundary conditions applied to the window FEM comparing to experimental conditions.

RESULTS

In this section experimental results will be presented by comparing tempered and laminated glass results. Results concerning the FEM of the lateral laminated glass windows validation will be proposed by reproducing test number 5. Finally results concerning the numerical parametric study will be analyzed.

Experimental results

This section presents comparative experimental tempered-versus laminated windows impacts. Tables 3 and 4 lists the different tests performed on tempered and tempered side glazing respectively. These tables report head velocity at impact, maximum linear acceleration at center of gravity of the head and HIC values. Lines in grey represent tests leading to a window failure. Testing was performed on impact test bench at velocity range of 3 to 11 m/s. A pendulum system was used for velocity under 5 m/s on laminated glazing as exposed in the methodology (tests n°1-4).

Table 3. Tests on tempered glazing with maximal linear acceleration and HIC; grey tests led to a glass failure.

Test n°	v [m/s]	γ_{max} [g]	HIC
1	6,6	258	1190
2	6,7	293	1327
3	7,4	525	3347
4	7,5	431	2481
5	7,7	279	1451
6	7,8	356	1646
7	7,9	198	321
8	9,1	357	1772
9	9,4	586	3698

Further observations about broken laminated glasses are detailed in Table 6. In case of failure, cracks appear in both glass layers. An example of coordinates of impact location, cracks after impact and permanent strain is represented in Figure 7 for test n° 5.

In the two last presented cases, there was a duplicated impact of head on the window. In only one case (test n°14), PVB interlayer broke. The rupture location corresponds to the nose impact. Window permanent strain go from 5 to 15 mm. One can notice that there is no correlation between window permanent deformation and impact velocity.

Table 4. Tests on laminated glazing with maximal linear acceleration and HIC; grey tests led to a glass failure.

Test n°	v [m/s]	γ_{max} [g]	HIC
1	2,9	503	2827
2	3,4	545	4041
3	3,9	429	1015
4	4,0	511	2264
5	5,0	104	101
6	6,3	428	2892
7	6,4	126	148
8	6,8	139	211
9	7,4	483	1893
10	7,4	306	1374
11	7,4	324	1383
12	7,4	402	1177
13	8,5	284	702
14	8,9	98	249
15	11,3*	143	2041

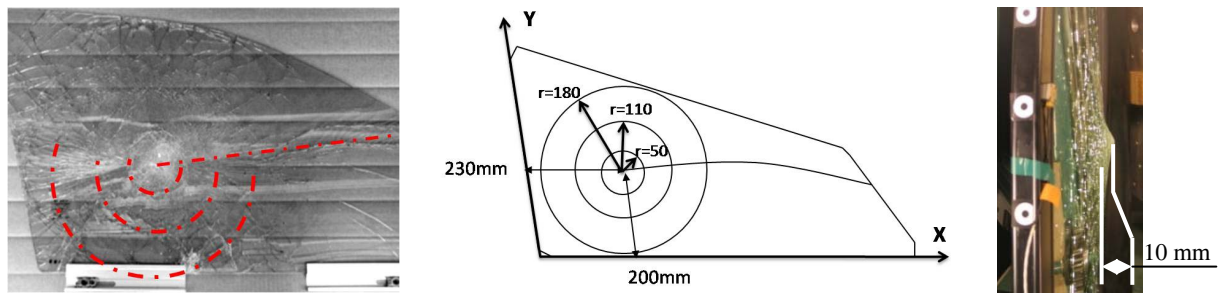


Figure 7. Window condition after impact at test n°5, coordinates of impact location and window permanent strain

Table 6. Observations on broken laminated glasses, permanent strain and impact location.

N° Test	Observations	Per. Strain. [mm]	Impact location
5	Window initially cracked Concentric cracks: r=50, 110, 180 mm No PVB rupture	10	X = 230 Y = 200
7	Concentric cracks: r=50, 180mm Linear cracking No PVB rupture	5	X = 210 Y = 200
8	nape impact Concentric cracks: r=50,140, 170, 300 mm No PVB rupture Long linear crack on rear glass layer	13	X = 230 Y = 225
12	Linear cracking No PVB rupture	10	X = 230 Y = 220
13	Linear cracking Concentric cracks : r=30, 70 mm No PVB rupture	10	X = 230 Y = 225
14	duplicated impact : chin (1) and nose (2) Concentric cracks : r=80, 200 mm PVB rupture (2) Long linear crack	13	X1 = 230 Y1 = 225 X2 = 300 Y2 = 250
15	duplicated impact : nape (1) and chin (2) Concentric cracks : r=140, 190, 300 mm Long linear crack	15	X1 = 180 Y1 = 150 X2 = 260 Y2 = 210

Histograms reported in Figure 8 represent maximal linear acceleration at the center of gravity of the head and HIC values for all tests on tempered glazing. Tests are sorted by increasing velocity. Bars in dark grey represent broken windows. Tolerance limit of 1000 is also represented for HIC criterion. Maximal linear accelerations values stand between 198 g to 586 g. In general, all tests on tempered glazing led to HIC values greater than the tolerance limit, with values from 1190 to 3698. For impact n°7 on tempered glass, predated by tests n°3 and 4, it appears a significant decrease in peak linear acceleration and HIC value. This could be associated with an initiation of micro-cracks due to a repetition of impact. Broken windows (in dark grey) appear at impact velocity from 7.9 m/s (test n°7). Histograms on Figure 9 represent respectively maximal linear acceleration at the center of gravity of the head and HIC values for all head impact tests against laminated glazing. Tests are sorted by increasing velocity. Bars in dark grey represent broken windows.

In tests leading to no rupture for laminated glasses, maximal linear accelerations stand around 400 g (bars in light grey) and HIC values stand all over the tolerance limit of 1000. Mostly tests leading to rupture present HIC values lower than the tolerance limit except test n°12 and 15.

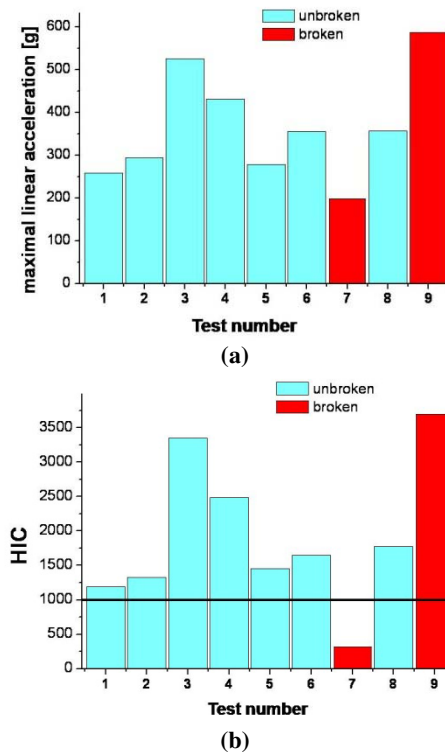


Figure 8. (a) Maximal linear acceleration and (b) HIC for impact tests on tempered glazing classified by increasing velocity, in light grey for unbroken windows, in dark grey for broken windows.

There appear three distinct areas for laminated glazing as a function of velocity (Figure 9):

- A first area (I) where there is no rupture for laminated glasses, tests n°1-4 at impact velocity lower than 5 m/s.
- the third one (III) include brken windows over an impact velocity of 7,5 m/s for tests n°13 to 15.
- The second area is referring to tests n° 5 to 12 between impact velocity of 5 m/s to 7,4 m/s. These cases led to unpredictable glass rupture.

It appears that if the windows failed, the HIC is generally lower than if there is no rupture. It should also be recalled that if the tempered glass break, partial ejection exist which is not the case when laminated glass failed

For laminated glazing, HIC values stand under the limit of 1000 except for test n° 9 at 7.4 m/s and test n°12.

In case n°9 the laminated window did not break. For tempered glazing, HIC values exceed HIC tolerance limit, except for test at impact velocity of 9 m/s where the tempered glass broke.

In most of these cases, maximal linear acceleration and HIC values are lower for laminated glazing. HIC values go from around 200 to 2000 for laminated glazing against 300 to 3500 for tempered glazing. Only one comparison presents the opposing trend. In the fifth comparison (white bars around 9 m/s), values remain greater for laminated glazing (70) than for tempered glazing (321). At this velocity, tempered glass broke and there was a head defenestration. Laminated glazing plays its principal role which is to hold the head inside the car and to fail with HIC value under 1000.

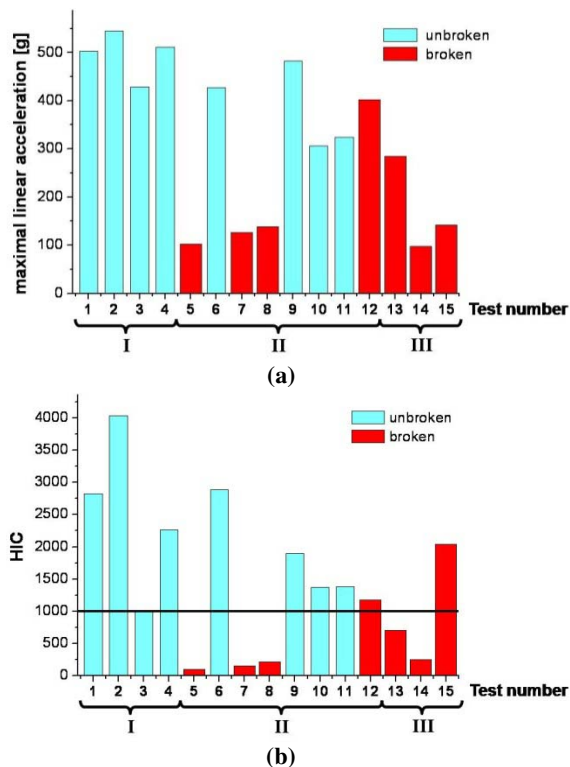


Figure 9. (a) Maximal linear accelerations and (b) HIC for impact tests on laminated glazing classified by increasing velocity, in light grey for unbroken windows, in dark grey for broken windows. I: rupture, II: unpredictable rupture, III: no rupture.

Figure 13 and 14 represent respectively maximal linear acceleration at the center of gravity of the head and HIC criterion for 6 cases of laminated glazing and 6 other cases of tempered glazing. These twelve cases are comparable in terms of head impact velocity.

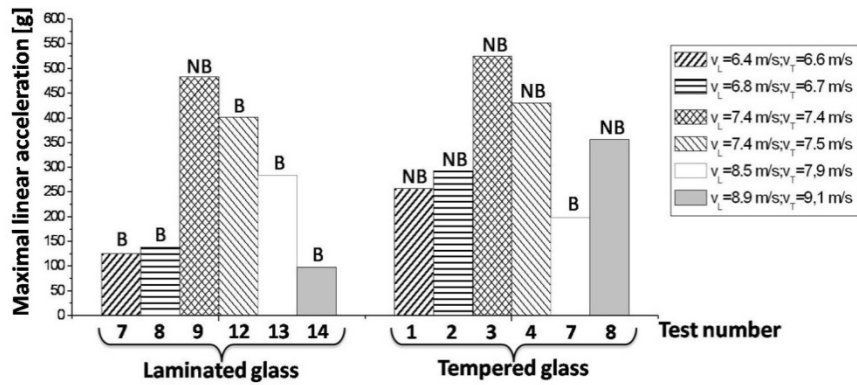


Figure 13. Maximal linear accelerations for tests on laminated and tempered glasses for 12 similar cases (B for broken, NB for not broken), v_L : velocity for Laminated window impact, v_T : velocity for Tempered window impact.

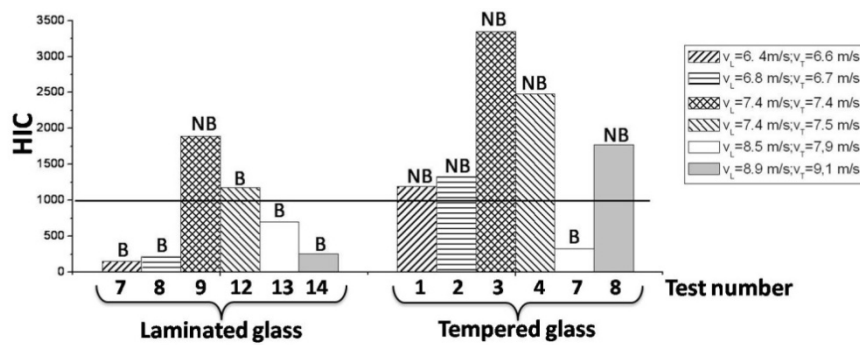


Figure 14. HIC values for tests on laminated and tempered glasses for 12 similar cases (B for broken, NB for not broken), v_L : velocity for Laminated window impact, v_T : velocity for Tempered window impact.

Numerical results

The laminated side window model validation is based on experimental data from test n°5 at 5 m/s. In order to validate laminated behaviour, the mechanical parameters are fitted on both laminated glass and PVB properties.

During this fitting, it appeared that initials conditions in door clumping influenced the model response in a significant way in terms of PVB strain and crack propagation in glass layers. Different ways of clumping were analysed in order to come closer to experimental cracks represented in Figure 7.

In parallel to this clumping analyse, the fit of mechanical parameters have been performed in terms of Young modulus, yield stress and failure strain. The aim of this fitting would be to reproduce cracks in glass layers and strain in PVB interlayer. Variations in Young modulus of both materials do not influence results. The variation of the yield stress of the two materials combined (glass and PVB) influenced the permanent plastic strain of the

laminated glazing. A more accurate optimisation of these mechanical parameters has been made in terms of maximal linear acceleration and HIC criterion.

Final mechanical properties of glass, PVB and rubber listed in Table 7 give the best values compared to experimental results. Results in terms of maximal linear acceleration, HIC criterion and permanent strain are detailed in Table 8 for experimental testing and numerical simulations.

It results for linear acceleration an error of 20 %. HIC values go from 101 in experimental case to 138 in numerical simulation. Figure 15 shows the cracks of window after experimental impact and numerical simulation at impact velocity of 5 m/s. It can be observed two principal concentric cracks at radius equal to 97 mm and 163 mm on numerical picture compared to values equal to 1100 mm and 180 mm on testing window. We also observed a beginning of long linear cracks in accordance with experimental results. The PVB interlayer remains intact in both cases (experimental and numerical results).

Table 7. Final mechanical properties for glass and PVB layers and rubber bands applied to the laminated window FEM.

Constituent	Propriety	Mechanical parameters	Values	Element type	Thickness
Glass	Elastic brittle	Density	2500 Kg.m ⁻³	Shell	2.1 mm
		Young Modulus	70000 MPa		
		Poisson's ratio	0.2		
		Yield stress	50 MPa		
		Maximum strain	0.0007		
PVB	Elastoplastic with rupture	Density	950 Kg.m ⁻³	Shell	0.76 mm
		Young modulus	50 MPa		
		Poisson's ratio	0.4		
		Yield stress (a)	20 MPa		
		Hardening modulus (b)	20		
		Hardening exponent (n)	0.9		
Rubber	Elastic	Density	1052 Kg.m ⁻³	Bricks	5 mm
		Young Modulus	3.91 MPa		
		Poisson's ratio	0.4		

Table 8. Experimental and numerical results for impact at 5 m/s on laminated glass.

Parameter	Experimental	Numerical	Error %
Impact velocity [m/s]	5	5	0
Maximum linear acceleration [g]	103,82	125	20
HIC	101	138	37
Window permanent strain [mm]	10	12	20

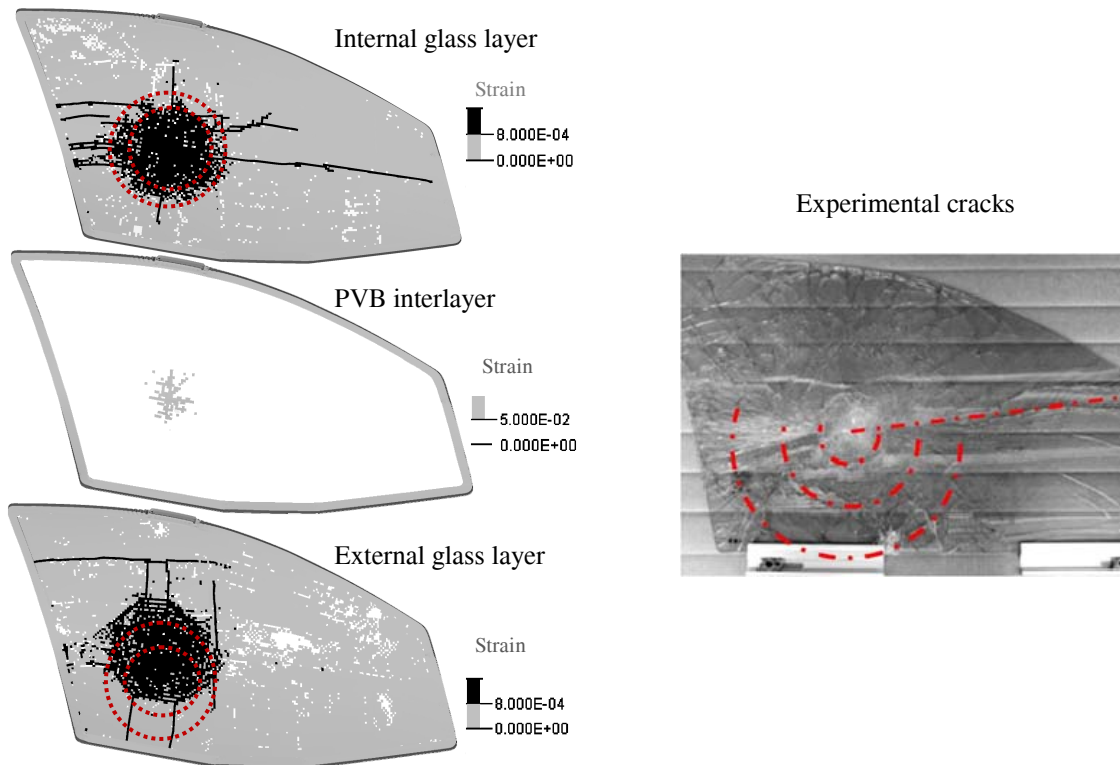


Figure 15. Cracks on laminated side window for impact at 5 m/s with HIII headform, comparison of experimental and numerical simulation.

Parametric study

Four mechanical parameters have been varied: the glass and PVB elastic limit (C and D), the thickness of the glass (A) and the PVB interlayer (B). Each parameter has been set on three different values: the reference value used in the model validation, a high (+ 30 %) and a low (- 30 %) value. The tests used for the parametric study remain in the same boundary conditions at 10 m/s reference velocity for normative impacts. Head response for a given simulation was calculated in terms of maximum linear acceleration at the center of gravity of the head and HIC value. A total of 16 simulations were run with a simulation protocol illustrated on Table 9.

Histograms shown in Figure 16a and b represent respectively the maximum linear acceleration at the center of gravity of the head and HIC values calculated for each simulation. While the reference value in term of maximum linear acceleration reaches 292 g, one of two results stand around a value of 180 g, the others around a value of 400 g. This variation corresponds to the A parameter. We

can already conclude that the glass thickness influences head response in terms of linear acceleration. The same trend is observed concerning HIC values.

The principle of the PCA is to research the best data representation with the less possible dimensions to reduce the number of variables or the initial space dimension number. This consequently allows to explain and to display data with a reduced number of axes in order to facilitate the interpretation of synoptic results. The first result is the correlation matrix reported in Table 10. From this we can observe that some of the variables are highly correlated which means that they move together (boxes in dark grey). We can mention for example that input variables B and D have less correlation with output variables. On the other hand, the glass thickness (A), as observed before, is highly correlated with head responses, maximum linear acceleration (0.98) and HIC (0.85). The variable C is moderately correlated with HIC criterion (0.5). Finally maximum linear acceleration and HIC values are naturally correlated (0.92).

Table 9. Simulation protocol indicating for each of the 17 simulations, the window characteristics retained: +/- stand +30% or -30% of the reference window properties values.

	REF	S1	S2	S3	S4	S5	S6	S7	S8	S9	S10	S11	S12	S13	S14	S15	S16
A (Glass thickness - mm)	2,1	-	+	-	+	-	+	-	+	-	+	-	+	-	+	-	+
B (PVB thickness - mm)	0,76	-	-	+	+	-	-	+	+	-	-	+	+	-	-	+	+
C (Glass elastic limit - MPa)	50	-	-	-	-	+	+	+	+	-	-	-	-	+	+	+	+
D (PVB elastic limit - MPa)	20	-	-	-	-	-	-	-	-	+	+	+	+	+	+	+	+

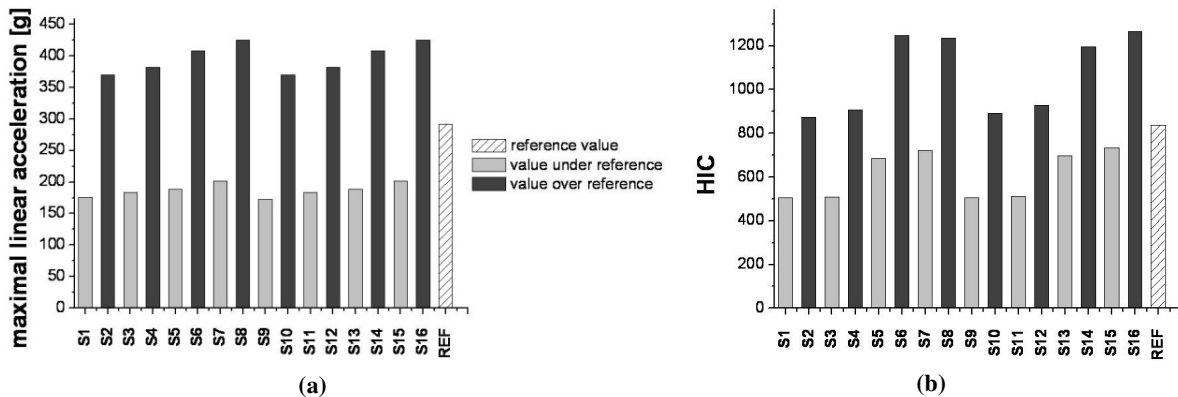


Figure 16. Maximal linear acceleration (a) and HIC values (b) calculated for each simulation.

The next step is then to calculate the principal components. Here the correlation matrix (Table 10) is considered in a mathematical point of view. For this symmetric matrix (6x6) the eigenvalues and eigenvectors are then determined. These eigenvalues reflect the quality of the projection from the N-dimensional initial table (N=6 in this study) to a lower number of dimensions. Each eigenvalue corresponds to a factor which is a linear combination of the initial variables, and all the factors are un-correlated ($r=0$). The eigenvector associated with the largest eigenvalue has the same direction as the first principal component. The eigenvector associated with the second largest eigenvalue determines the direction of the second principal component. These axes are defined by linear forms (1) and (2).

Ideally the first two or three eigenvalues will correspond to a high percentage of the variance, ensuring us that the maps based on the first two or three factors are a good quality projection of the initial multi-dimensional table. In this study, the

first two factors allow us to represent 66.6 % of the initial variability of the data.

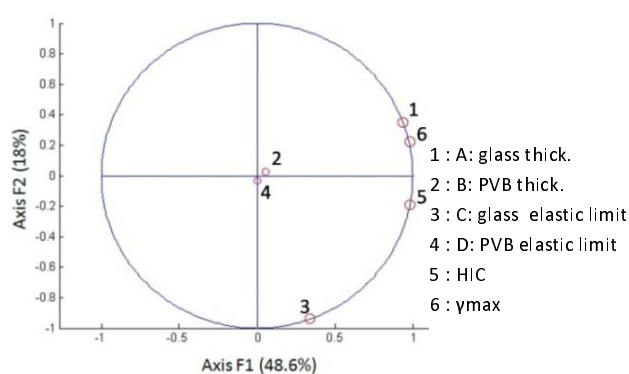
The correlation circle represented in Figure 17a is useful in interpreting the meaning of the axes. It shows a projection of the initial variables in the factors space. In this study, the horizontal axis which represents 48.6 % of the variability is linked with the glass thickness (0.552), HIC criterion (0.573) and maximum linear acceleration (0.575). Along F2 which describes 18 % of the variability, the main important parameter is the glass elastic limit (-0.910). Figure 17 b is the ultimate goal of the PCA. It permits to look at the data on a two-dimensional map, and to identify trends. We can see that simulations are classified from the left (less value) to the right (high value) along the first axis from S1 to S16; S17 represents the simulation of reference. We can note that the best simulations in terms of HIC criterion and maximum linear acceleration are localized in the portion of space described by $F1 \leq 0$ and more accurately by $F2 \geq 0$. The space described by $F1 \leq 0$ corresponds to the influence of glass thickness. The refinement in space corresponds to glass elastic limit.

Table 10. Correlation matrix between the N=6 variables.

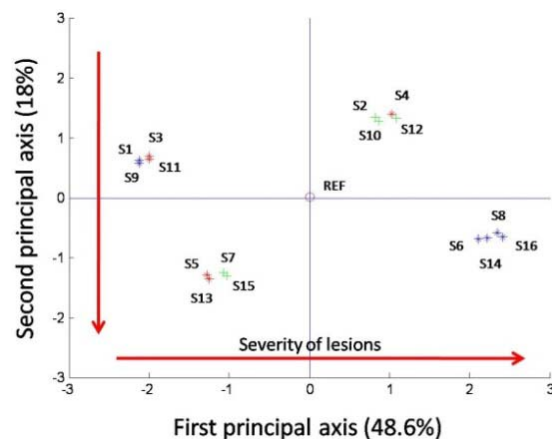
	A	B	C	D	HIC	γ_{max}
A (Glass thickness)	1	0	0	0	0,85	0,98
B (PVB thickness)	0	1	0	0	0,04	0,06
C (Glass elastic limit)	0	0	1	0	0,50	0,13
D (PVB elastic limit)	0	0	0	1	0,01	-0,001
HIC	0,85	0,04	0,50	0,01	1	0,92
γ_{max}	0,98	0,06	0,13	-0,001	0,92	1

$$\text{AxisF1} = 0.552 A + 0.032 B + 0.190 C + 0.003 D + 0.573 \text{HIC} + 0.575 \gamma_{max} \quad (1)$$

$$\text{AxisF2} = 0.314 A + 0.027 B - 0.910 C - 0.030 D - 0.189 \text{HIC} + 0.188 \gamma_{max} \quad (2)$$



(a)



(b)

Figure 17. PCA correlation circle of the 6 variables (a), factorial plane (b).

DISCUSSION & LIMITATIONS

This study shows that side windows with laminated glazing are safer than tempered glazing. For the same velocity, laminated glass windows broke and thereby decreased head injury risks in case of impact, whereas tempered glass did not. At an impact velocity from 6 m/s to 9 m/s against tempered glass windows, HIC values stood over a limit of 1000, which is the normalized value for pedestrian head impact at 10 m/s (Directive 2003/102/EC). The PVB interlayer has never broken at impact velocities of 3 m/s to 9 m/s, contrary to tempered glass. Therefore, laminated glass avoids partial ejection. The developed model even if validated against experimental results need further investigation for the optimization of its behaviour against both HIC and more biofidelic head injury criteria based on human head FE modelling (Marjoux *et al.* 2006, Deck *et al.* 2008).

The parametric study pointed out the prevailing part of the glass layer thickness (A parameter) on head responses in terms of maximal linear acceleration at the center of gravity of the head and HIC criterion. The thicker the glass is the more critical HIC criterion becomes. Therefore head injury risks increases. Yield stress of glass has a lesser influence on maximal linear acceleration and HIC. The PVB thickness and its yield stress have no influence on head response. These findings follow the results from Zhao *et al.* (2006). Glass ply thickness plays a very critical role however the PVB interlayer thickness has no significant effect on the impact resistance of a laminated glass. Simulations which give the less injury risk in term of HIC criterion require a lower glass thickness and a lower glass yield stress.

A main limitation resides in reproducibility of experimental testing. Mode of transport, production line and stochastic nature of glass are parameters not controlled. Only new laminated and tempered glasses were used in this study. Each test involves a change in boundary conditions of the window, a manual repositioning of the head on the carriage. Some difficulties appeared also during the experimental testing, mainly in the velocity fitting and in the control of head rotation at the time of impact, which lead to minor errors in linear acceleration peaks. In the numerical impact reconstructions, the window vibrations due to the framing and the changes of windows were not

considered. The limitation of this experimental study is the range of velocity. The propulsion system does not allow lower and greater impact velocities and could not reproduce same velocities.

CONCLUSIONS & PERSPECTIVES

The experimental tests consisted of a Hybrid III headform which impacts either laminated or tempered glasses side windows. Characteristics of the impact were investigated: velocity of the head, mechanical behaviour of the window (cracks, rupture, and plastic strain), linear acceleration at the center of gravity of the head and HIC criterion. The different tests were performed within a velocity range of 3 m/s to 9.5 m/s. A comparison between the laminated and tempered glass was performed. At same velocity, impact against laminated glass lead to less injury risk than a tempered glass with lower HIC values. The principal role of laminated glazing has been preserved; PVB layer never broke and laminated glazing led to lower injury risks. Laminated glass broke from 5 m/s and tempered glass broke from 8 m/s. In parallel of these experiments, a finite element model of laminated side window has been developed, validated and improved by a parametric study.

In order to ensure the validation of the side window FE model in a large range of impact velocity more experiments with smaller speed increment must be conducted. In a further step the boundary condition of the head at neck level should be considered as this weak point is important in case of glazing braking and partial ejection.

Finally in deep investigation of head injury risk and realistic laminated glass optimization should be conducted by coupling the windows model to a human head FE model.

ACKNOWLEDGEMENTS

The authors wish to acknowledge AAGMA (Advanced Automotive Glazing Manufacturers Association) for their support.

REFERENCES

- Bosch-Rekvelde M, Griotto G, van Ratingen M, Versmissen T, Mooi H, *Head impact location, angle and velocity during side impact: A study based on virtual testing*, SAE, vol.114, n°6, pp. 51-57, 2005.

- Clarke CC, Sursi P, *Rollover Crash and Laboratory Tests of Ejection Reduction by Glass-Plastic Side Windows and Windshields*, SAE Technical Paper # 890218, 1989.
- Deck C, Willinger R, *Improved Head Injury Criteria Based on Head FE Model*, International Journal of Crashworthiness, Vol. 13, N°6, pp.667-679, 2008.
- Dharani LR, Mettu SR, Zhao S, Barbat SD, Chai L, *Modelling fracture in laminated automotive glazing impacted by spherical featureless headform*, SAE Technical Paper 2003-01-1225, 2003.
- Directive 2003/102/EC du Parlement Européen*, Journal officiel de L'Union Européenne, 17 Novembre 2003.
- Du Bois PA, Kolling S, Fasnacht W, *Modelling of safety glass for crash simulation*, Computational Materials Science 28 (2003), 675-683.
- Foster JK, Kortge JO, Wolanin MJ, *Hybrid III – a biomechanically based crash test dummy*, Proceedings of the 21st Stapp Car Crash Conference, SAE 770938, Warrendale, PA, 1977.
- Hassan AM, Mackay M, Foret-Bruno J-Y, Langwieder K, *Laminated side glazing implications for vehicle occupant safety*, Proceedings of Ircobi Conference, Isle of Man, United Kingdom, 2001.
- Haward RN, *Strength of plastics and glass*, Cleaver Hume Press Ltd, New York, 1975.
- Kramer RN, Loibl JM, Morrison RL, Saunby CS, Roberts VL, *A comparative study of automotive side window occupant containment characteristics for tempered glass*, SAE Technical Paper 2006-01-1492, 2006.
- Lu J, Moran JR, Esposito RA, *Enhanced protective glass for higher security automotive glazing*, International Body Engineering Conference, SAE Technical Paper Series 2000-01-2695, Detroit, Michigan, 2000.
- Luepke P, Carhart M, Croteau J, Morrison R, Loibl J, Ridenour J, *An evaluation of laminated side window glass performance during rollover*, SAE Technical Paper 2007-01-0367, 2007.
- Marjoux D, Baumgartner D, Deck C, Willinger R, *Head injury prediction capability of the HIC, HIP, Simon and ULP Criteria*, Accident Analysis and Prevention, vol.40, pp.1135-1148, 2006.
- Morris AP, Hassan AM, Mackay M, Hill J, *Head injuries in lateral impact collisions*, Proceedings of Ircobi Conference, Eindhoven, Netherlands, 1993.
- Mukherjee S, Chawla A, Mahajan P, Mohan D, Mane NS, Singh M, Sakurai M, Tamura Y, *Modelling of head impact on laminated glass Windshields*, Proceedings of Ircobi Conference, Montpellier, France, 2000.
- Parsa MH, Rad M, Shahhosseini MR, Shahhosseini MH, *Simulation of windscreen bending using viscoplastic formulation*, Journal of Materials Processing Technology, vol.170, pp. 298-303, 2005.
- Pierce J, Carhart M, Bare HC, Blakeslee A, Heald J, *Retention characteristics of production laminated side windows*, SAE Technical Papers 2007-01-0376, 2007.
- Piziali RL, Fox JC, Girvan DS, Raphael EH, Ridenour J, *A review and analysis of the performance of laminated side glazing in rollover accidents*, SAE Technical Papers 2007-01-1166, 2007.
- Sances A, Carlin F, Kurnaresan S, *Biomechanical Injury Evaluation of laminated glass during rollover conditions*, SAE Technical Paper 2002-01-1446, 2002.
- Timmel M, Kolling S, Osterrieder P, Du Bois P.A., *A finite element model for impact simulation with laminated glass*, International Journal of Impact Engineering vol.34, pp. 1465-1478, 2007.
- Volle M, *Analyse des données*, 4ème edition Economica, 1997.
- Wei J, *Dynamics and failure analysis of architectural glazing subjected to blast loading*, PhD thesis, University of Missouri-Rolla, 2004.
- Zhao S, Dharani LR, Chai L, Barbat SD, *Analysis of damage in laminated automotive glazing subjected to simulated head impact*, Engineering Failure Analysis vol.13, pp. 582-597, 2006.

Results of NHTSA's Comparison of the Offset Deformable Barrier and the Progressive Deformable Barrier Test Procedures

James Saunders

National Highway Traffic Safety Administration

Pascal Delannoy

Teuchos-Safran Group , UTAC Passive Safety Department

Paper Number 09-0549

ABSTRACT

Over the past several years, NHTSA has conducted testing to evaluate a high-speed fixed offset deformable barrier crash test. It was preliminarily determined that the benefits from such a crash test could lead to an annual reduction in approximately 1,300 to 8,000 MAIS 2+ lower extremity injuries. NHTSA also conducted vehicle-to-vehicle crash tests to investigate the potential for disbenefits from a fixed offset deformable barrier crash test. This testing demonstrated that, for some sport utility vehicles, structural changes that improved their performance in high-speed frontal offset crash tests may also result in adverse effects on the occupants of their collision partners.

The Directorate for Road Traffic and Safety (DSCR) of France developed and proposed a Progressive Deformable Barrier test procedure (PDB) to upgrade the current offset deformable barrier test procedure in the United Nations Economic Commission for Europe (UNECE) R.94 regulation. DSCR is proposing the PDB to potentially improve the barrier performance in testing of the current and future fleet. Therefore, NHTSA is investigating the use of the PDB in the offset test procedure by comparing the current offset deformable barrier test procedure specified in FMVSS No. 208 (ODB) to the PDB. This paper also investigates the performance of each barrier

to predict lower extremity injuries and the ability of the PDB to absorb more energy for heavy vehicles found in the United States (U.S.) fleet.

The PDB performed as designed for heavy vehicles and produced approximately the same occupant compartment intrusions. Both the ODB and PDB did not produce the same lower extremity injuries as seen in the real-world.

The general trend across each body region had a similar trend for each barrier. That is the magnitude of each IAV for each body region was approximately the same for each barrier, but one barrier is not always the maximum.

INTRODUCTION

In the U.S., driver and right front passenger air bags are required in all passenger cars and light trucks under FMVSS No. 208. However, NHTSA estimates that over 8,000 fatalities and 120,000 Abbreviated Injury Scale (AIS) 2+ injuries will continue to occur in frontal crashes even after all passenger cars and light trucks have frontal air bags (Docket number NHTSA-2003-15715). Therefore, NHTSA has focused on the development of performance tests not currently addressed by FMVSS No. 208, particularly a high severity frontal offset crash. These tests are intended to evaluate

occupant compartment intrusion that could compromise occupant survival space and thus increase the potential for lower leg injury. NHTSA is currently evaluating the potential for both the ODB and the PDB test procedures to predict lower leg injuries and to minimize the potential risk of increasing the aggressivity of heavier vehicles.

The EU Directive 96/79 for frontal crash protection went into effect in 1998. The Directive uses the R.94. The UNECE R.94 test procedure was developed to represent a vehicle-to-vehicle frontal offset crash and to generate occupant compartment intrusions similar to that seen in real world crashes of passenger cars. The deformable element of the R.94 barrier was designed to absorb energy and limit severe contact of the vehicle structure against the wall. The stiffness of the R.94 barrier represents the average stiffness of European passenger cars 15 years ago. The current R94 barrier has been shown to bottom out for European small cars, which is a possible concern for the larger-size U.S. fleet (Delannoy et al., 2005).

Many consumer rating programs have adopted the use of a fixed ODB crash test procedure to rate vehicle performance in a 64 kph frontal offset crash test (Euro NCAP (European New Car Assessment Program), Australian NCAP and Insurance Institute for Highway Safety (IIHS)). Some studies have suggested that using this test procedure to rate vehicles may increase their aggressivity, especially for heavier vehicles (Verma, et al., 2003 and Saunders, 2005).

The Directorate for Road Traffic and Safety (DSCR) of France developed and proposed a PDB to upgrade the current offset deformable barrier in the UNECE R.94 regulation to mitigate the potential for the offset test procedure to increase aggressivity

of larger vehicles. The PDB-XT progressively increases in stiffness as it is crushed, which contributes to its name. The barrier was designed to represent a vehicle structure with sufficient force level and energy absorption capacity to mitigate any occurrences of bottoming out. In doing so, the PDB may be able to better harmonize test severity among vehicles of different masses. The approach aims to encourage lighter vehicles to be stronger without increasing the force levels of large vehicles [Delannoy, 2005].

This paper investigates the performance of ODB and the PDB to predict lower extremity injuries and the ability of the PDB to absorb more energy for heavy vehicles.

TEST PROCEDURE

A “dummy-based” seating procedure was used for both the ODB and the PDB tests. This seating procedure uses a step-by-step process that mimics the procedure used by humans to position themselves in their vehicles. Basically the dummy is placed in the seat and the feet are in neutral position. The seat is moved forward until the right foot contacts the accelerator pedal. The left is placed symmetric to the right unless the left foot interacts with the pedal. If there is interaction with the pedal, the left foot is moved to avoid the pedal. A complete description of the “dummy-based” seating procedure can be found in Saunders et al., 2007.

All testing utilized the Hybrid III 50th percentile male dummy with Thor-Lx lower legs. Throughout the rest of the paper this dummy will be referred to as 50 HIII. The upper of the part 50 HIII was instrumented with three axis head and chest accelerometers, and a chest pot. The Thor-Lx was instrumented with upper and lower

tibia load cells and three ankle rotational potentiometers.

The ODB was conducted using the procedure defined in FMVSS No. 208 (S18) with two modifications. The test speed was increased to 56 kph, and the “dummy-based” seating procedure was used instead of the mid-track.

The PDB tests were conducted at 60 kph, overlap of 50 percent, and utilized the “dummy-based” seating procedure.

Figure 1 shows the properties and dimensions of the ODB barrier (Figure 1a) and PDB-XT barrier (Figure 1b). The PDB-XT is taller and thicker than the ODB barrier. The ODB barrier has two layers of honeycomb, both with constant stiffness. The PDB-XT has three layers: two layers with constant stiffness and a middle section that has four stiffness zones. The front two zones of this middle section get stiffer as the thickness increases and the back two sections have a constant stiffness. It should be noted that the PDB-XT height from the ground was 200 mm, for these tests, instead of 150 mm as specified in the PDB test procedure from UTAC.

TEST MATRIX

To compare the two test procedures paired vehicle tests were conducted. The vehicle selection tried to cover all classes of vehicles. Table 1 shows the final matrix.

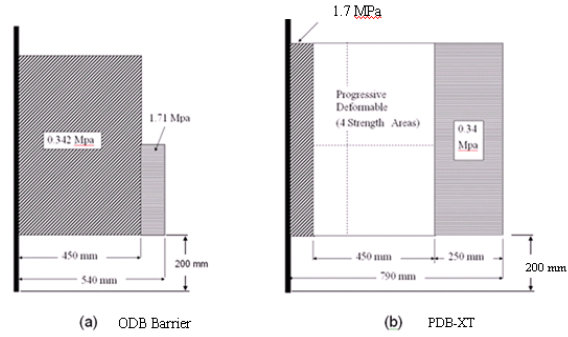


Figure 1. Properties and dimensions of the ODB barrier and PDB-XT barrier

Table 1. Vehicle test matrix for barrier comparison

Vehicle	Vehicle Class	Test Weight (kg)
2008 Chevrolet Aveo	Small passenger car	1,443
2008 Ford Escape	Small unibody SUV	1,781
2008 Saturn Outlook	Large unibody SUV	2,408
2007 Ford F-250	Heavy pickup	3,291

RESULTS

Occupant Compartment Intrusions

To evaluate intrusion the toepan points were measured pre- and post-test by using a 4 by 3 grid (Figure 2). Row 3 of the toepan grid is located at the intersection of the toepan and floorboard.

It can be seen from Figure 3 and Figure 4 that the PDB test procedure produced higher occupant compartment intrusions for the Aveo and Escape when compared with the ODB test procedure. The deformation pattern was similar for both test procedures. The Outlook had a small amount of intrusion for both procedures (Figure 5). For the F250 the ODB procedure pushed the toepan back in the x-direction, whereas, the PDB pushed the toepan up in the z-direction (Figure 6).

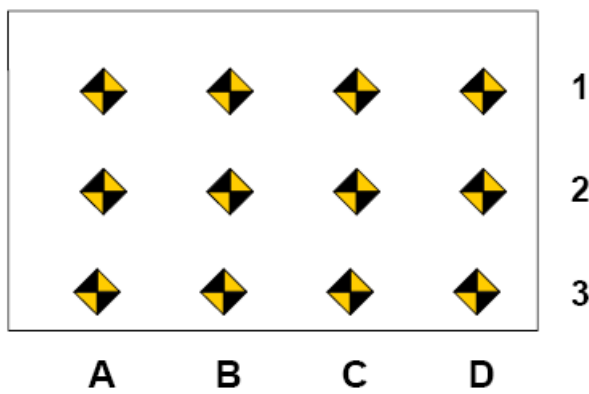


Figure 2. Toepan intrusion measurement points

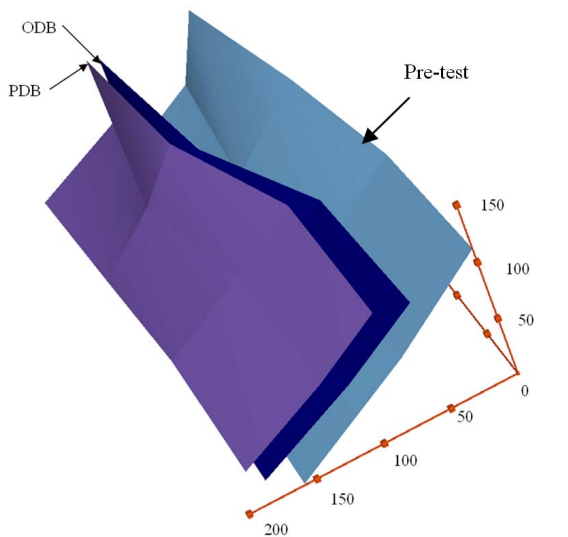


Figure 3. Aveo toepan intrusion mm

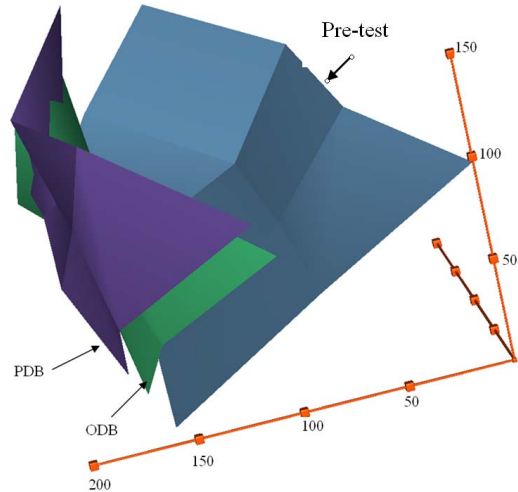


Figure 4. Escape toepan intrusion mm

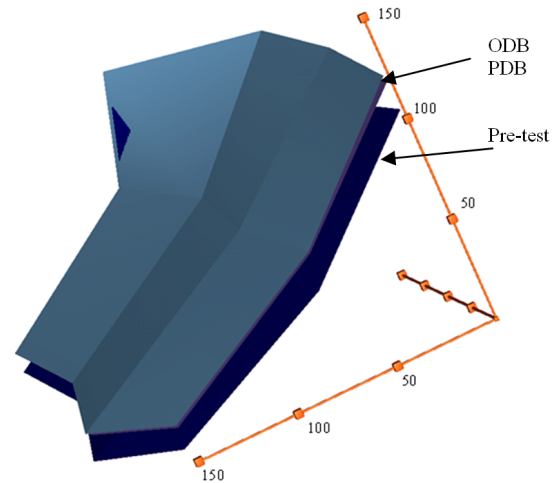


Figure 5. Outlook toepan intrusion (mm)

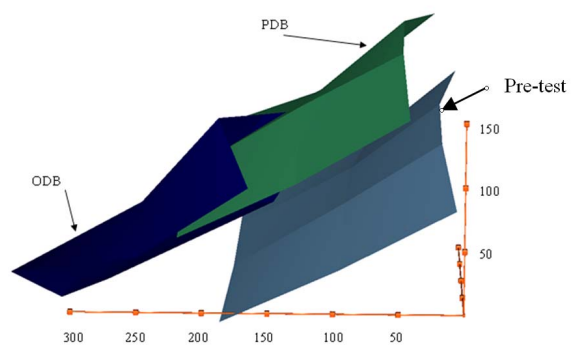


Figure 6. F250 toepan intrusion (mm)

Lower Extremity IAVs

This section compares the lower extremity (LE) Injury Assessment Values (IAVs) for the 50 HIII for each paired vehicle. The femur Injury Assessment Reference Values (IARV) for the 50 HIII are from the FMVSS No. 208 Advanced Air Bag Final Rule. The other IARVs were based upon Kuppa et al., (2001b). The IARVs used to assess LE injuries are presented in Table 2. The definitions for ankle rotations are as follows: Ankle Rot Y is the maximum positive y rotation and Ankle Rot X is the maximum of either the positive or negative x rotation. The highest value from the left or right legs IAV is presented in the following figures and tables.

The PDB procedure produced higher Injury Assessment Values (IAVs) for all body regions except for Ankle Rot Y for the Aveo (Figure 7). There is no comparable trend in the IAVs for both the Escape and Outlook (Figure 8 and Figure 9). The Outlook's high Ankle Rotation X may be due to the geometry of the toepan. Using the "dummy based" seating procedure the left foot partially overlapped the footrest which may have contributed to the rotation. Finally, the trend for the F250 was that the ODB procedure produced higher IAVs for all regions except Upper Tibia Index (Figure 10).

The general trend across each body region had a similar trend for each barrier. That is the magnitude of each IAV for each body region was approximately the same for each barrier, but one barrier is not always the maximum.

The Aveo, Escape, and the Outlook had similar post-test toepan contours for both test procedures, but the trends in IAVs were not the same. The impact speed, overlap, and barrier were different for each paired

and may have affected the IAVs due to the vehicle interaction with the barrier during the test. The differences in the vehicle interaction with the barriers may have changed the rate of the toepan and therefore affecting the IAVs.

Table 2. Injury Assessment Reference Values for lower extremity injuries (Kuppa et al., 2001a, 2001b)

Injury Criteria	IARV for 50 HIII
Femur	10,000 N
Knee Shear	15 mm
Upper Tibia Force	5600 N
Lower Tibia Force	5200 N
Tibia Index	0.91
Ankle Rot Y	35 deg
Ankle Rot X	35 deg

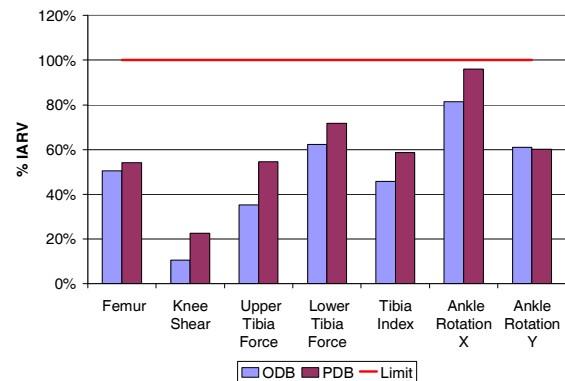


Figure 7. Lower extremity IAVs for the Chevrolet Aveo

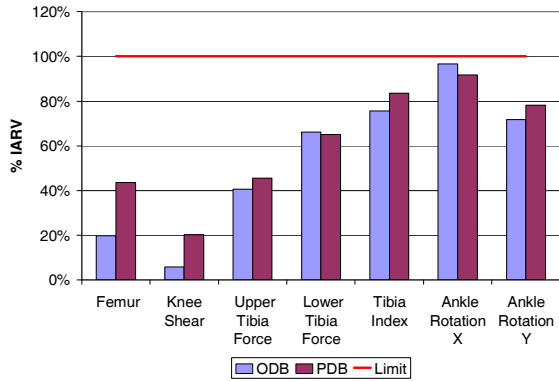


Figure 8. Lower extremity IAVs for the Ford Escape

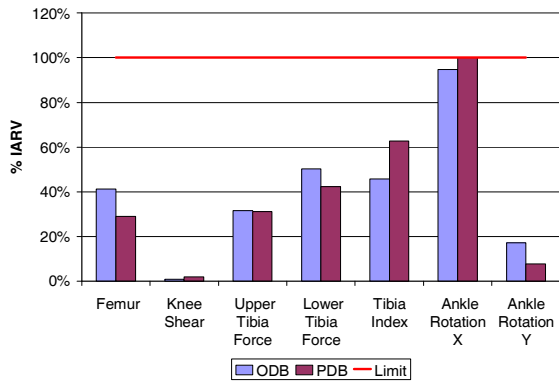


Figure 9. Lower extremity IAVs for the Saturn Outlook

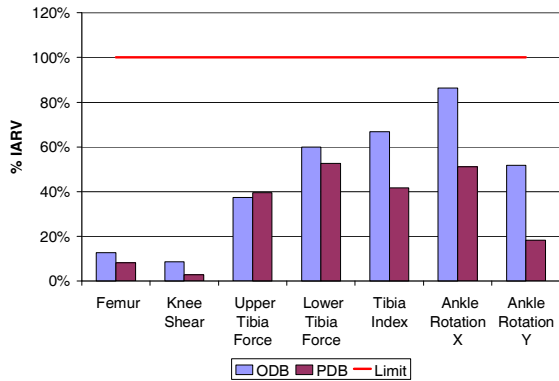


Figure 10. Lower extremity IAVs for the Ford F-250

Barrier Comparison

When comparing the crush of the ODB barrier and the PDB-XT, the ODB bottoms out even with a small car (Figure 11a), whereas the PDB-XT did not bottom out for the same small car (Figure 11b). Also, the ODB barrier bottomed out for the F250 (Figure 12a) and the PDB-XT stayed intact (Figure 12b). From Figure 13 it can be seen that the frame of the F250 punctured the PDB.



(a) ODB barrier



(b) PDB-XT barrier

Figure 11. Aveo barrier crush comparison

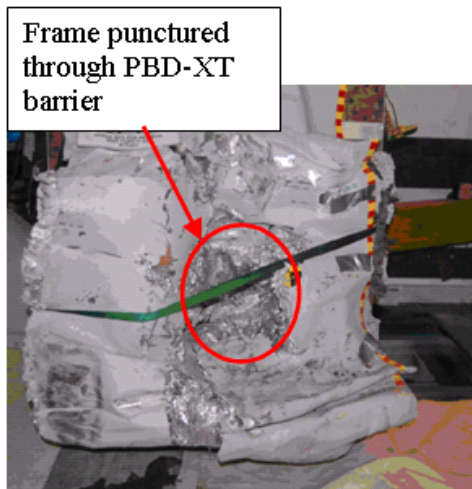


(a) ODB barrier



(b) PDB-XT barrier

Figure 12. Ford F-250 barrier crush comparison



Frame punctured through PDB-XT barrier

Figure 13. Front view of PDB-XT barrier for the F250

Crash Severity

Since both test procedures use a deformable element, the test speed is not a good indication of the test severity. A method for evaluating the test severity is with the Equivalent Energy Speed (EES). The EES is

the initial kinetic energy minus the energy absorbed by the barrier. Details of EES are explained in Pascal et al., 2005.

The EES for the paired vehicles were calculated and the results are shown in Figure 14. The lightest vehicle, Aveo, was the only vehicle tested with the PDB to have a higher EES than the paired vehicle tested with the ODB.

The Aveo tested with the PDB had a higher EES than the Aveo tested with the ODB implies that the Aveo had to absorb more of the crash energy. Which is opposite from the other vehicles tested. The PDB allows the heavier vehicles to absorb less energy when compared to the ODB, which may allow manufactures to soften the structures of heavier vehicles.

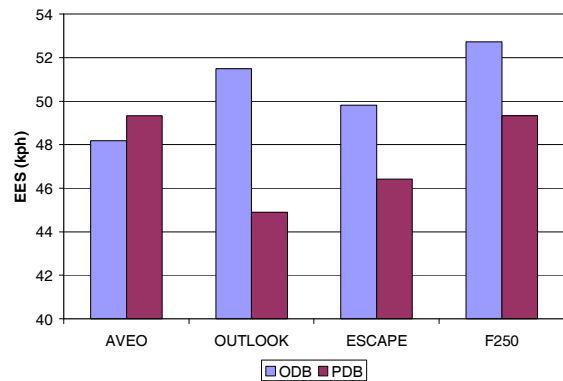


Figure 14. EES for the paired vehicles

DISCUSSION

Vehicle Severity

Pascal 2005 showed that the PDB is able to make the vehicle severity of the PDB procedure approximately equal for all vehicle weights. Figure 15 shows the EES for vehicles tested by NHTSA using the ODB and PDB. This plot includes all vehicles tested by NHTSA, not just the paired vehicles. It is seen from this figure

that the EES for the ODB test increases as the mass of the vehicle increases. For the PDB the EES is basically the same for all size vehicles when a linear fit is applied to the data.

The scatter in the data for the vehicles tested with the PDB is probably due to the vehicles being designed to the ODB test. The ODB barrier collapses during the test and it becomes like hitting a rigid wall. Therefore, these vehicles may not be fully optimized to a progressively deformable element.

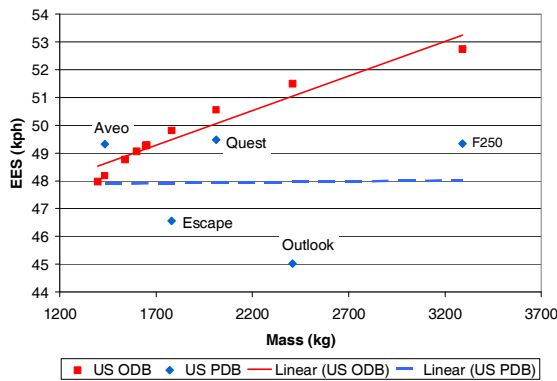


Figure 15. Theoretical EES for different test procedures and EES calculated for vehicles tested in US

Lower Extremity Injuries

Saunders, et al., 2004 showed that the ODB procedure reproduced real-world lower extremity injuries. But, the current ODB procedure and the PDB procedure did not show the same trend in lower extremity injuries as reported by Saunders (Table 3).

Some possible reasons for the difference between the tests conducted by Saunders, et al., 2004 and the current tests: 1) lower extremity injuries in the current fleet are different from the older fleet due to being designed to achieve a higher rating from the IIHS and 2) the use of a different seating procedure.

To determine if the trend of lower extremity injuries are different for current vehicles compared to older vehicles the NASS/CDS analysis performed by Saunders, et al., 2004 was reproduced. This analysis used NASS/CDS years 1995 through 2007 files for left offset crashes with DV over 48 kph. The model year cutoff was chosen at 2000 because most vehicles received a “good” or “acceptable” rating from IIHS after 2000. Figure 16 shows that the risk for LE injuries has increased for the newer vehicles for most of the LE body region injuries.

The dummy based seating procedure may have affected the results because it requires the ankles to be in neutral position, which prevents the ankle from being pre-loaded before the test (Saunders, et al., 2007). Also, the new seating procedure normally placed the seat behind mid-track and the left foot was not placed on the footrest. This seating procedure normally placed the feet away from the toepan and allowed the feet to slide forward before impacting the toepan (Figure 17).

The impact speed, overlap, and barrier were different for each paired may have affected the IAVs due to the vehicle interaction with the barrier during the test. The differences in the vehicle interaction with the barriers may have caused a different rate of the toepan and acceleration applied to the dummy.

CONCLUSIONS

The PDB performed as designed for heavy vehicles. It did not bottom out when impacted with a heavy vehicle (F250) and allowed the barrier to absorb more energy as demonstrated by the decrease in EES for heavier vehicles. It also produced approximately the same occupant compartment intrusion as the ODB procedure.

Both test procedures did not produce the same LE injury trend as previously reported (Saunders, et al.). The main reason for this could be due to the seating procedure used in the current testing. The “dummy based” seating procedure did not preload the ankle and normally placed the seat with the 50 HIII behind mid-track.

The general trend across each body region had a similar trend for each barrier. That is the magnitude of each IAV for each body region was approximately the same for each barrier, but one barrier is not always the maximum.

Table 3. Percent of vehicles tested that exceeded the IARV.

IAV	ODB mid-track	ODB “Dummy Based”	PDB “Dummy Based”
# Test	10	9	4
MY Range	96-03	06-07	07-08
Knee Shear	0%	20%	0%
Femur	0%	0%	0%
Tibia Index	40%	10%	0%
Upper Tibia Force	10%	0%	0%
Lower Tibia Force	30%	0%	0%
Ankle X Rot	20%	40%	0%
Ankle Y Rot	50%	0%	17%

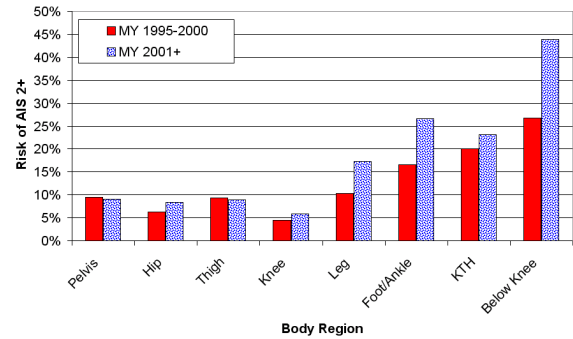


Figure 16. Risk of lower extremity injuries in offset crashes with DV greater than 48 kph

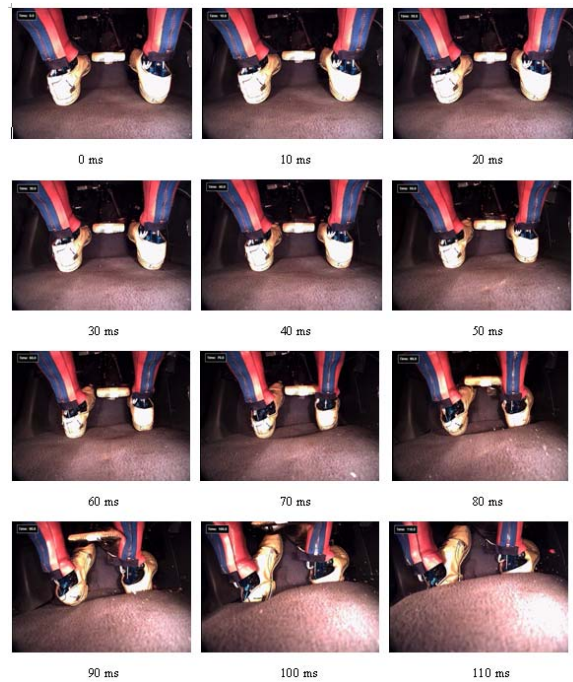


Figure 17. Feet kinematics for the Nissan Quest into the PDB

REFERENCES

Delannoy, P., Faure J., “Compatibility Assessment Proposal Close from Real Life Accidents,” Enhanced Safety of Vehicles Conference, Paper No. 94, May 2003.

Delannoy, P., Martin, T., Castaing, P., Comparative Evaluation of Frontal Offset Tests to Control Self and Partner Protection, Enhanced Safety of Vehicles Conference, Paper No. 05-0010, June 2005.

Kuppa, S., Wang, J., Haffner, M., Eppinger, R., "Lower Extremity Injuries and Associated Injury Criteria," 17th International Technical Conference on the Enhanced Safety of Vehicles, Amsterdam, The Netherlands, June 4-7, 2001a.

Kuppa, S., Haffner, M., Eppinger, R., Saunders, J., "Lower Extremity Response and Trauma Assessment using the Thor-Lx/HIIIr and the Denton Leg in Frontal Offset Vehicle Crashes," 17th International Technical Conference on the Enhanced Safety of Vehicles, Amsterdam, The Netherlands, June 4-7, 2001b.

Saunders, J., Kuppa, S., Prasad, A., "NHTSA's Frontal Offset Research Program," Paper 2004-01-1169, Society of Automotive Engineers, March 2004.

Saunders, J.W., Prasad, A., "NHTSA's Frontal Offset Research Program," Proceedings of the 19th Experimental Safety Vehicles, Paper 05-0206, Washington, DC 2005.

Saunders, J.W., Loudon, A., Prasad, A., "Offset Test Design and Preliminary Results," Proceedings of the 20th Experimental Safety Vehicles, Paper 07-0240, Lyon, France, 2007.

Verma, M., Lange R., Levelle J., "Relationships of Crash Test Procedures to Vehicle Compatibility," Paper 2003-01-0900, Society of Automotive Engineers, March 2003.

DEVELOPMENT OF A HIGH DECELERATION FULL WIDTH FRONTAL IMPACT TEST FOR EUROPE

Mervyn Edwards

TRL

United Kingdom

On behalf of the APROSYS SP1.2 consortium

Paper Number 09-0105

ABSTRACT

To assess a vehicle's frontal impact crashworthiness an integrated set of test procedures is required that assesses both the car's self and partner (compatibility) protection. It has been recommended by the International Harmonisation of Research Activities (IHRA) frontal impact group that the set of test procedures should contain both full overlap and offset tests. Currently, in Europe only an offset test is used in regulation and consumer testing. In 2007, the European Enhanced Vehicle-safety Committee (EEVC) made a number of proposals for a set of test procedures, all of which contain full width and offset tests.

This paper presents the work performed by the European Commission 6th framework APROSYS project to develop a full width test procedure for Europe. It also describes an initial cost benefit analysis for its introduction into the European regulatory regime.

Accident analysis was performed using the UK CCIS and German GIDAS databases to help determine the test speed, what size dummies should be used and the relevance of including rear seated dummies in the test. A matrix of 12 full scale car crash tests was performed to determine the effect of including a deformable face, the effect of including rear seated occupants and to assess the test's repeatability and reproducibility. As all the tests were instrumented with a high resolution Load Cell Wall, the repeatability and reproducibility of proposed metrics to assess a car's compatibility were also assessed.

INTRODUCTION

In Europe, around 10,000 car occupants are killed in frontal impact crashes annually. To assess a vehicle's frontal impact crashworthiness, including its compatibility, an integrated set of test procedures is required that assesses both the car's self and partner (compatibility) protection. To minimise the burden of change to industry the set of procedures should contain a minimum number of procedures that are based on current procedures as much as possible. Also, the procedures should be internationally harmonised to reduce the burden further. The set of test procedures

should contain both a full overlap test and an offset (partial overlap) test as recommended by the IHRA [1]. A full width test is required to provide a high deceleration pulse to control the occupant's deceleration and check that the vehicle's restraint system provides sufficient protection at high deceleration levels. An offset test is required to load one side of the vehicle to check compartment integrity, i.e. that the vehicle can absorb the impact energy in one side without significant compartment intrusion. The offset test also provides a softer deceleration pulse than the full width test, which checks that the restraint system provides good protection for a range of pulses and is not over-optimised to one pulse.

The European Enhanced Vehicle-safety Committee (EEVC) WG15 has helped co-ordinate work in Europe to understand and develop a set of test procedures to improve a vehicle's frontal impact crash performance. It has found that the main factors influencing a vehicle's compatibility are its structural interaction potential, its frontal force levels and its compartment integrity [2]. In 2007, EEVC WG15 made a number of proposals for potential sets of test procedures, all of which contain both full width and offset tests [3]. These were:

Set 1

- Full Width Deformable Barrier (FWDB) test to assess a vehicle's structural interaction potential and provide a high deceleration pulse to test the restraint system.
- Offset Deformable Barrier (ODB) test with EEVC barrier to assess a vehicle's compartment integrity and frontal force levels and also provide a softer deceleration pulse to test the restraint system.

Set 2

- Full Width Rigid Barrier (FWRB) test to provide a high deceleration pulse to test the restraint system.
- Progressive Deformable Barrier (PDB) test to assess a vehicle's structural interaction, frontal force levels and compartment integrity and also provide a softer deceleration pulse to test the restraint system.

Set 3

- Combination of FWDB and PDB

It should be noted that WG15 have formally investigated Sets 1 and 2, but have not explicitly investigated Set 3 to date.

Currently, in Europe only an offset test is used in regulation and consumer testing. This paper reports the work performed by the European Commission 6th framework APROSYS project to develop a full width test procedure for Europe. It also describes an initial cost benefit analysis for its introduction into the European regulatory regime.

The aim was that this test would be suitable for regulatory implementation in the short term and also have potential for further development to include measures to assess and control compatibility in the longer term.

APPROACH

The approach taken to develop the test procedure was to use review of similar procedures, accident analysis, sled and full scale testing to answer the questions to specify the procedure. The main questions and the work performed to answer them were:

- Test speed?
An initial proposal for a test speed of 56 km/h was made on the basis that this was the speed used in similar tests. The Full Width Deformable Barrier (FWDB) test has a speed of 56 km/h. Also, a speed of 56 km/h is currently being phased in for the US FMVSS208 rigid barrier test. Accident analysis was performed to check the appropriateness of this proposal.
- Dummy specification?
The questions to be answered to specify the dummies included: what size dummy (e.g. 5th percentile, 50th percentile) should be used in what seating positions; what injuries should the dummies be capable of assessing; should Hybrid III or THOR-NT dummies be used?
Accident analysis was performed to provide information on the characteristics of the occupants injured and their injuries to help specify the dummy sizes and the type of injuries that should be assessed. Sled testing was also conducted to assess the repeatability and robustness of the THOR-NT dummy and compare its performance with the Hybrid III for a variety of restraint system types to help assess its suitability for its possible inclusion in the test.
- Assessment of rear seated position?
At present it is usually assumed that the cost of providing improved protection for the rear seated

occupant is likely to be greater than the value of the benefit because of the low occupancy rate. Despite this, assessment of the rear seated position may be required in the future because government policies may demand equivalent levels of protection for front and rear seated occupants and/or encourage car sharing which would increase the occupancy rate. To answer questions arising from this debate, accident analysis was performed to quantify the size of the rear seated injury problem and crash test work was carried out to investigate the feasibility of assessing the rear seated position.

- Deformable barrier face?
EEVC WG15 has proposed three potential options for a set of test procedures to assess a vehicle's frontal impact crashworthiness. Set 1 and Set 3 contain a full width test with a 'deformable face' and Load Cell Wall (LCW) to take measures to help assess a vehicle's compatibility, whereas Set 2 does not. Because compatibility research was not advanced far enough to recommend a specific option and hence whether or not the test should have a deformable face, it was decided to use crash testing to evaluate the effect of including it to help inform future decisions.
- Repeatability and reproducibility?
Full scale crash testing was performed to assess the repeatability and reproducibility of the test and to check for any practical or robustness problems. As all the tests were instrumented with a high resolution Load Cell Wall, the repeatability and reproducibility of proposed metrics to assess a car's compatibility were also investigated.

ACCIDENT ANALYSIS

Analysis of the UK CCIS (Co-operative Crash Injury Study) and German GIDAS (German In-Depth Accident Study) accident databases was performed to help answer questions to enable the specification of the draft test procedure [4]. The main criteria used to select cases for the analyses were: vehicles involved in frontal impact with no rollover and occupants belted. Additional criteria were used to select newer vehicles that were Regulation 95 compliant for the majority of the analyses, such as test speed, where including older vehicles was likely to have a significant influence on the results. The criteria used were: for analyses with the CCIS database, vehicles with build year 2000 onwards; for GIDAS, build year 1997 onwards. It was necessary to include a greater proportion of older vehicles in data set for the GIDAS analyses to ensure the sample size was large enough to give statistically meaningful results.

Test Configuration

The CCIS and GIDAS analyses both showed that distributed damage is the most frequent type of damage for all injury severities [Figure 1].

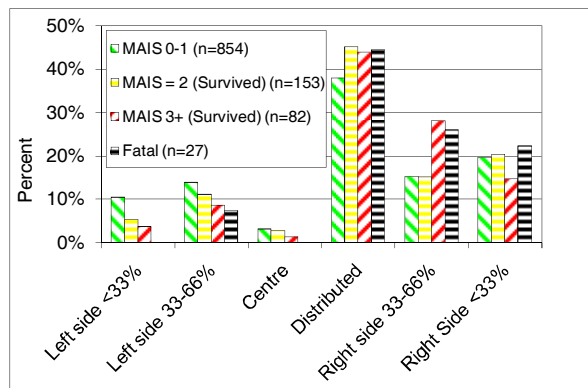


Figure 1. Location of damage by occupant injury severity for belted drivers (CCIS data).

The GIDAS analysis also showed that distributed damage has the highest MAIS 2+ injury risk [Figure 2]. This indicates the need for a full width test in Europe. The injury risk was not calculated for the CCIS analysis because it cannot be easily done because the CCIS data sample is biased.

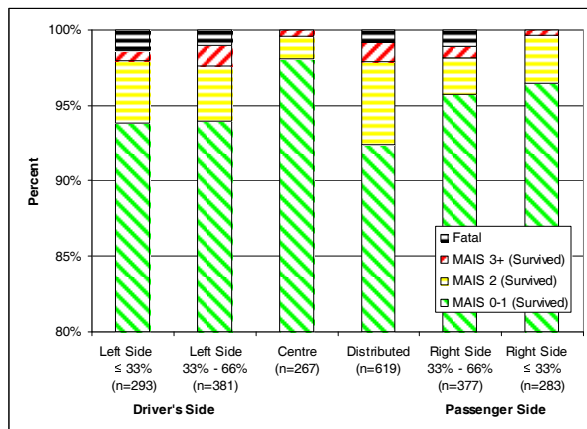


Figure 2. Risk of injury by location of damage for belted drivers.

The CCIS analysis showed that the principle direction of force for the majority of accidents was $0 \pm 15^\circ$ for all injury severities and seating positions. The GIDAS analysis showed similar results. This indicates that a '0° head on' test configuration is the most representative.

Test Speed

The CCIS and GIDAS analyses showed that a test speed of 56 km/h would cover over 80% of MAIS 3+ injuries for belted casualties in frontal impacts with no rollover [Figure 3].

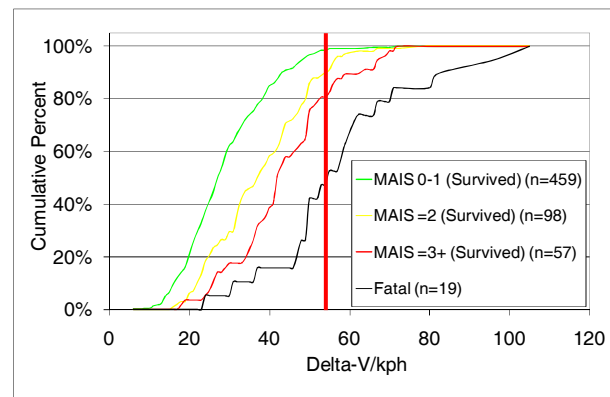


Figure 3. Cumulative frequency plot of distribution of injury against delta V (CCIS data).

Injury type

The CCIS analysis showed that the body regions most frequently injured at the AIS 2 level were the thorax, clavicle and legs for the driver and thorax and clavicle for the front seat passenger. Also, a high number of abdominal (internal organ and lumbar spine) injuries were seen for the front seat passenger. The nature of these injuries requires further investigation to understand why the driver does not also experience this. For the AIS 3+ level the regions were the thorax and legs (femur) for the driver and thorax for the front seat passenger [Figure 4].

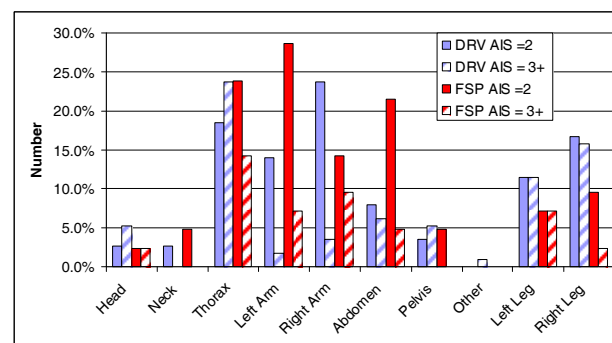


Figure 4. Body region injured for occupants with MAIS 2+ injuries (CCIS data). Note: clavicle injuries are included in arm classification.

The GIDAS analysis showed that the body regions most frequently injured at the MAIS 2+ level were the head and thorax. Further work is required to determine the reason why the GIDAS analysis showed a significantly

higher frequency of head injury than the CCIS analysis. However, it should be noted that the GIDAS data sample contained older vehicles than the CCIS sample (CCIS vehicles build year 2000 onwards, GIDAS 1998 onwards), which may have caused some of this difference.

Occupant characteristics

The GIDAS analysis showed that the driver was usually male (65-77% dependent on injury severity), the front seat passenger usually female (59-69% dependent on injury severity) and the rear seat passenger usually female [Figure 5]. The CCIS analysis gave similar results.

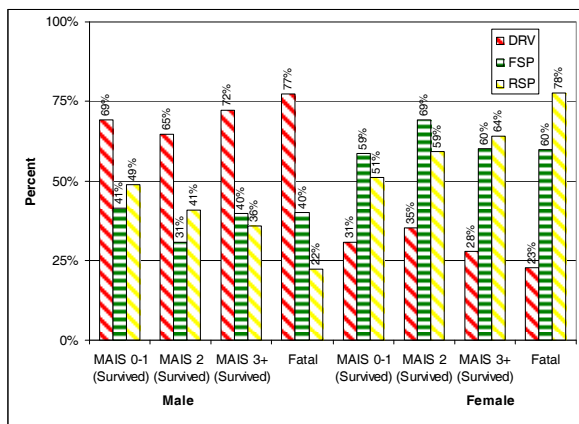


Figure 5. Gender ratio for belted occupants in frontal impacts (GIDAS data).

Further analysis of the GIDAS data showed that the 50th percentile driver was 34 years old, 175 cm tall and weighed 74 kg. The 50th percentile passenger was 30 years old, 169 cm tall and weighed 67 kg. From a choice of the 5th (150 cm, 49 kg) and 50th (175 cm, 78 kg) percentile dummies, the 50th percentile most closely matches these characteristics, indicating that this dummy is the more representative.

For rear seated occupants, the results were similar to those for the front seat passenger indicating that the 50th percentile dummy is the more representative for this position also. It should be noted that children under 12 were excluded from this analysis as it was assumed that they would use a Child Restraint System (CRS). There is a legal requirement in Europe that children under the age of twelve and less than 150 cm tall (135 cm for UK) have to use a CRS.

Rear seated position

Both the CCIS and GIDAS analyses showed that the proportion of occupants wearing a seatbelt was much

lower for rear seated occupants compared to front seated ones [Figure 6]. This clearly indicates that there is a problem with the seat belt wearing rate in the rear.

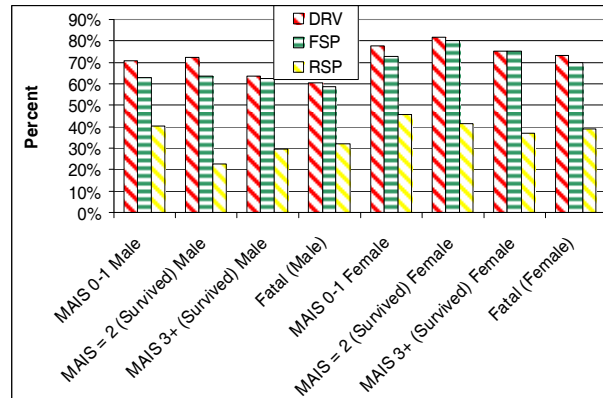


Figure 6. Seat belt usage by injury severity showing relatively low belt usage rate for rear seated occupants.

Further analysis of the GIDAS data showed that the rear seat occupancy rate in collisions was low, about 10% of all occupants involved in collisions are seated in the rear. Also, the analysis showed that if the seatbelt was worn, rear seated occupants have a lower risk of injury than front seated ones.

It was not possible to draw definite conclusions on the type of injury sustained by belted rear seat occupants because of small data sample size. However, the CCIS analysis showed that the body regions injured at the AIS 3+ level for the seven casualties with MAIS 3+ injuries were the thorax, abdomen and legs.

SLED TESTING

A series of sled tests was performed to compare the performance of the THOR-NT dummy to the HYBRID III from the point of view of its robustness, its repeatability and its response to different restraint systems [5]. Because of robustness problems with the THOR-NT dummy, most of which were subsequently solved, test data had to be discarded which resulted in a limited data set for comparison. In terms of injury risk prediction, the limited data showed no significant differences between the dummies. However, in terms of dummy kinematics, slight differences between the dummies were seen. On the basis that specific injury criteria were not available for the THOR-NT dummy and the problems that occurred with THOR-NT in this work, it was decided that the THOR-NT dummy was not well enough developed to include in a test procedure intended for implementation in the short term. Hence it was decided that development of the procedure should continue with the Hybrid III dummy

with an option to upgrade to the THOR-NT dummy in the future.

FULL SCALE CRASH TESTING

Twelve full scale crash tests as shown in Table 1 were performed to investigate the following issues [6]:

- Effect of deformable face compared to rigid wall
- Effect of the introduction of rear seated dummies
- Repeatability and reproducibility
- Practicality and robustness

Table 1. Full scale crash test matrix.

Vehicle	Test Configuration	
	Rigid Wall	Deformable Face
	Test Objective	Test Objective
Supermini 1	Baseline	Baseline
		Reproducibility
Supermini 2	Baseline	Baseline
		Rear occupants
Small Family 1	Baseline	Baseline
	Rear occupants	Rear occupants
		Repeatability
		Reproducibility

Effect of deformable face

The purpose of the deformable face is to make the test more representative of a vehicle to vehicle impact and to enable measures to be taken on a high resolution load cell wall (LCW) to assess a vehicle's compatibility, i.e. its partner protection [7]. The deformable face was designed to achieve this by ensuring that a vehicle's crossbeam structures are loaded in the test as they would be in a vehicle to vehicle impact and that the unrealistic high engine deceleration loads seen in a test with a rigid wall are attenuated, so that the structural loads can be assessed more easily.

Hence as expected, vehicle deformation was different in the tests with and without the deformable face, especially for the front of the lower rails and bumper crossbeam.

The vehicle's compartment deceleration at the start of the impact was slightly lower in the tests with the deformable face compared with those with the rigid wall [Figure 7]. This resulted in a later airbag firing time for the tests with Supermini 2 [Table 2], but made little difference for the other cars tested. This shows that a deformable face may be useful in a full width

test to ensure a more realistic assessment of a vehicle's crash sensing capability.

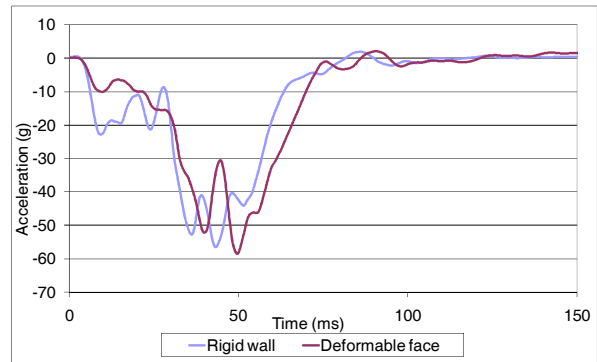


Figure 7. Compartment deceleration for test with 'Supermini 2'.

Table 2. Airbag firing time for test with 'Supermini 2'.

	Driver	Passenger
Rigid wall	12 ms	12 ms
Deformable face	33 ms	33 ms

The dummy injury criteria values were generally similar between the test with the deformable face and the rigid wall test, indicating that the deformable element had little effect on the overall severity of the test [Figure 8]. The exception was for Supermini 2, where the later airbag firing time resulted in substantially higher dummy injury values for the head.

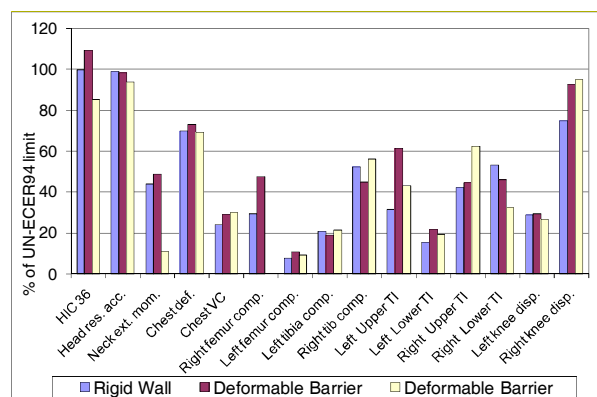


Figure 8. Driver dummy injury criteria values for tests with 'Small family 1'.

The Load Cell Wall (LCW) results also showed significant differences with the deformable face attenuating the engine inertial 'dump' loading seen in the rigid wall test, as expected [Figure 9].

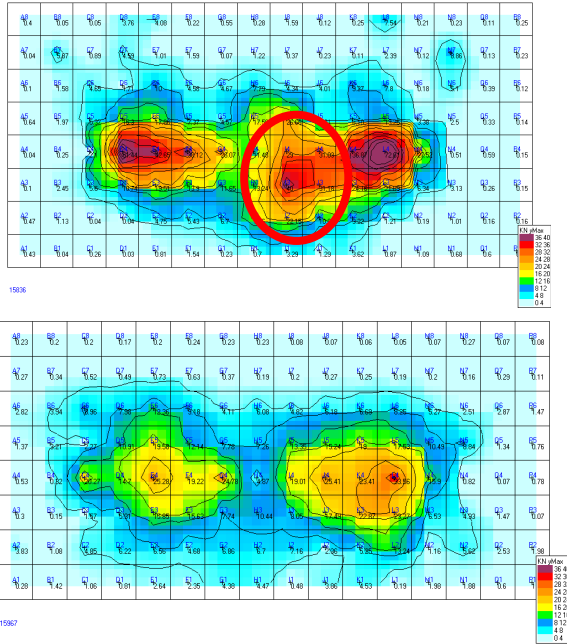


Figure 9. LCW force distribution for tests with 'Small family 1' for rigid wall (top) and deformable face (bottom) tests showing attenuation of engine dump loading for 'Small family 1' tests.

Effect of rear seated dummies

The performance of the front seated dummies did not vary significantly in the tests with and without the rear seated dummies [Figure 10]. Any differences seen could be explained by factors within the range of test repeatability, e.g. the difference between the knee slider values in the 'Small family 1' test was probably caused by the difference in knee interaction with the steering wheel column trim cover.

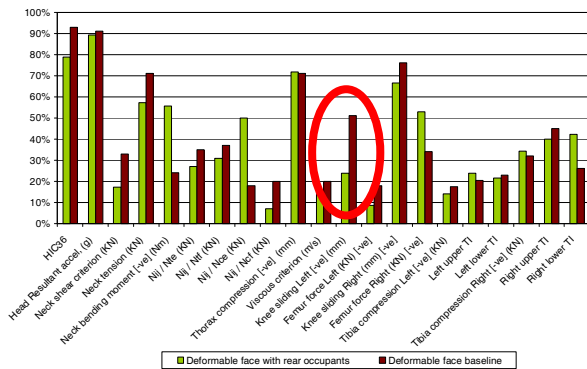


Figure 10. Driver dummy injury criteria values for tests with and without rear seated dummies for test with 'Small family 1'.

There were significant differences for the performance of the rear seated dummies compared to the front seated dummies [Figure 11].

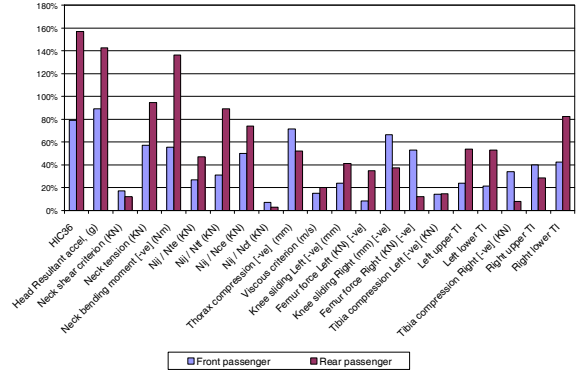


Figure 11. Comparison of front and rear seated dummy performance for driver side dummies for test with 'Small family 1'.

The main differences were the higher head, neck and tibia injury criteria values for the rear seated dummies, which were often substantially higher than the UNECE Regulation 94 performance limits. The higher head and neck values were probably caused by the lack of airbag support for the rear dummies as there was no evidence of interaction of the dummies' heads with the rear of the front seat in any of the tests. The higher tibia values were caused by the interaction of the dummies' lower legs with the rear of the front seat pan.

However, remarkably, even though the shoulder belt loads were substantially higher for the rear seated dummy [Figure 12] the thorax compression values were similar. This is an unexpected result as chest injury is known to be related to seat belt load [8, 9].

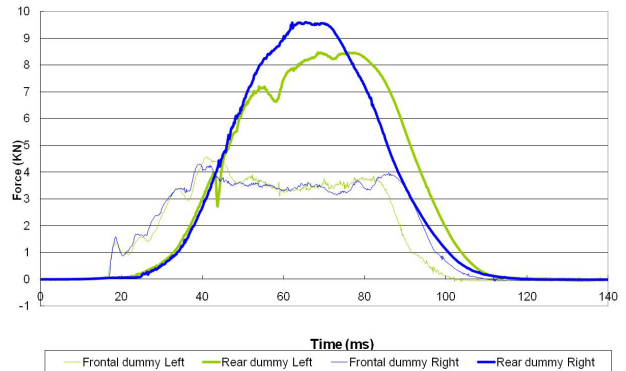


Figure 12. Shoulder belt loads in test with rear seated dummies for test with 'Small family 1'. Loads are substantially higher for rear seated dummies as rear belts do not have load limiters.

Possible contributory factors to this observation include:

- Submarining of the rear seated dummy leading to reduced upper body loading. Note that although there was strong evidence of submarining for the

test with the ‘Small family 1’ [Figure 13], there was no definite post test evidence of submarining for the test with the ‘Supermini 2’. However, there were no onboard cameras to monitor dummy motion or iliac load cells to monitor belt loading to the pelvis.

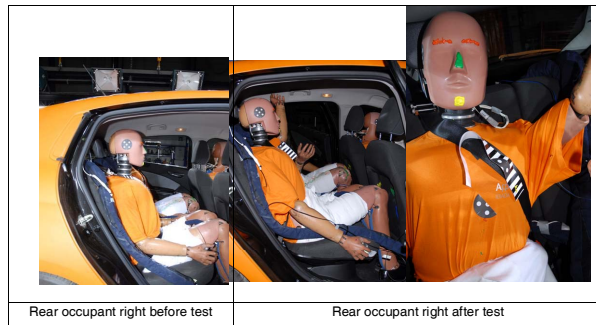


Figure 13. Comparison of belt positioning pre and post 'Small family 1' test for right seated dummy showing evidence of submarining, i.e. lap belt has ridden up off pelvis into abdomen area.

- Difference in routing of the belt for the front and rear seated dummies.
- Capability of Hybrid III dummy to assess thorax injury using the thorax deflection measure. Kent has shown that the relationship between Hybrid III thorax deflection and injury risk is substantially different for belt only, bag only and combined restraint conditions, whereas the injurious level of cadaver chest deflection is not highly sensitive to the load distribution on the chest (i.e. the type of restraint system) [10].

Repeatability and reproducibility

The repeatability and reproducibility of the test with the deformable face was assessed as the repeatability of the test with the rigid face is already well known. Repeatability is defined as the difference between identical tests performed at the same laboratory and reproducibility the difference between tests performed at difference laboratories.

Considering self protection measures, such as dummy injury criteria, it was found that the repeatability and reproducibility were at least as good as for the current UNECE Regulation 94 frontal impact test procedure [Figure 14].

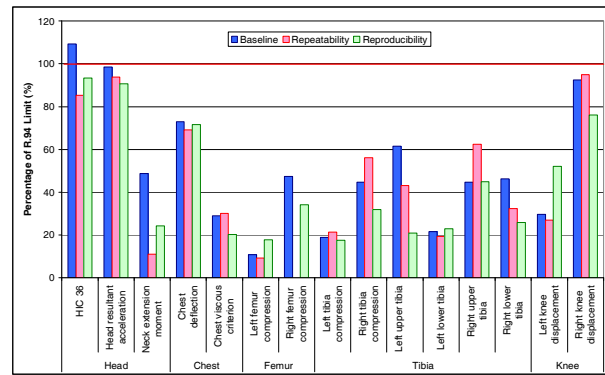


Figure 14. Driver dummy performance for tests with 'Small family 1'.

Considering compatibility (partner protection) measures, such as Load Cell Wall (LCW) force it was found that the global load cell wall force was repeatable and reproducible [Figure 15].

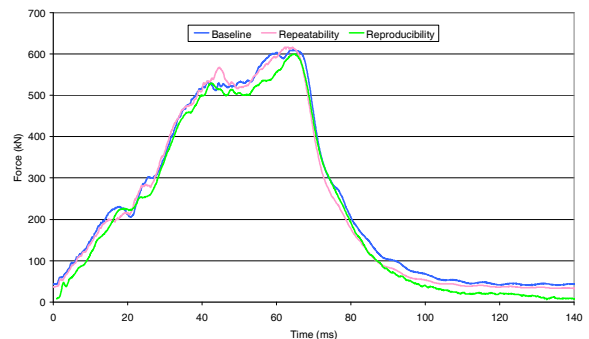


Figure 15. Load Cell Wall (LCW) total force for tests with 'Small family 1'.

For tests with ‘Supermini 1’ the LCW force distribution was repeatable. However, for the tests with ‘Small family 1’ the force distribution was not repeatable because of different collapse modes of the left main longitudinal rail [Figure 16].

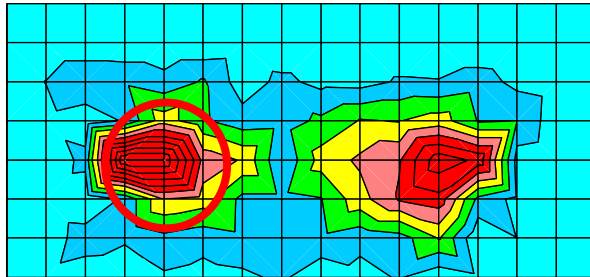
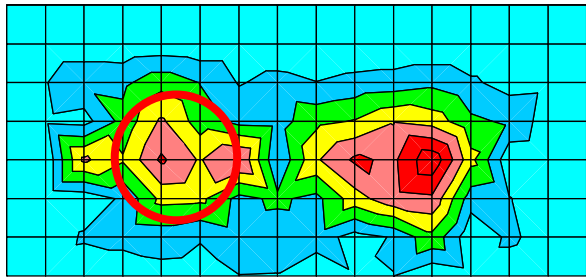


Figure 16. Difference in LCW force distribution in tests with 'Small family 1' caused by different collapse mode of left main longitudinal rail (Note: grid cross points represent centre of load cells).

Recently, the Structural Interaction (SI) metric has been proposed for the assessment of a vehicle's compatibility, in particular its structural interaction potential [11]. The SI metric consists of two components a vertical one (VSI) and a horizontal one (HSI). The repeatability of this metric was assessed for the tests with 'Supermini 1', in which the LCW force distribution was repeatable [Figure 17]. It was found that although the vertical component of the Structural Interaction (VSI) metric was repeatable, the horizontal component (HSI) was not [Table 3]. Note: Borderline value to distinguish between good and poor performing bumper crossbeams is somewhere between 2 and 4.

Table 3. Structural Interaction (SI) metric values for tests with 'Supermini 1'.

	VSI	HSI
Test 1	0.0	4.93
Test 2	0.0	3.26

Further investigation revealed that this was because of the high sensitivity of HSI to small variations (< 5 kN) in individual cell loads. Further development of the SI metric will be necessary to resolve this problem because good repeatability and reproducibility is required for regulatory application.

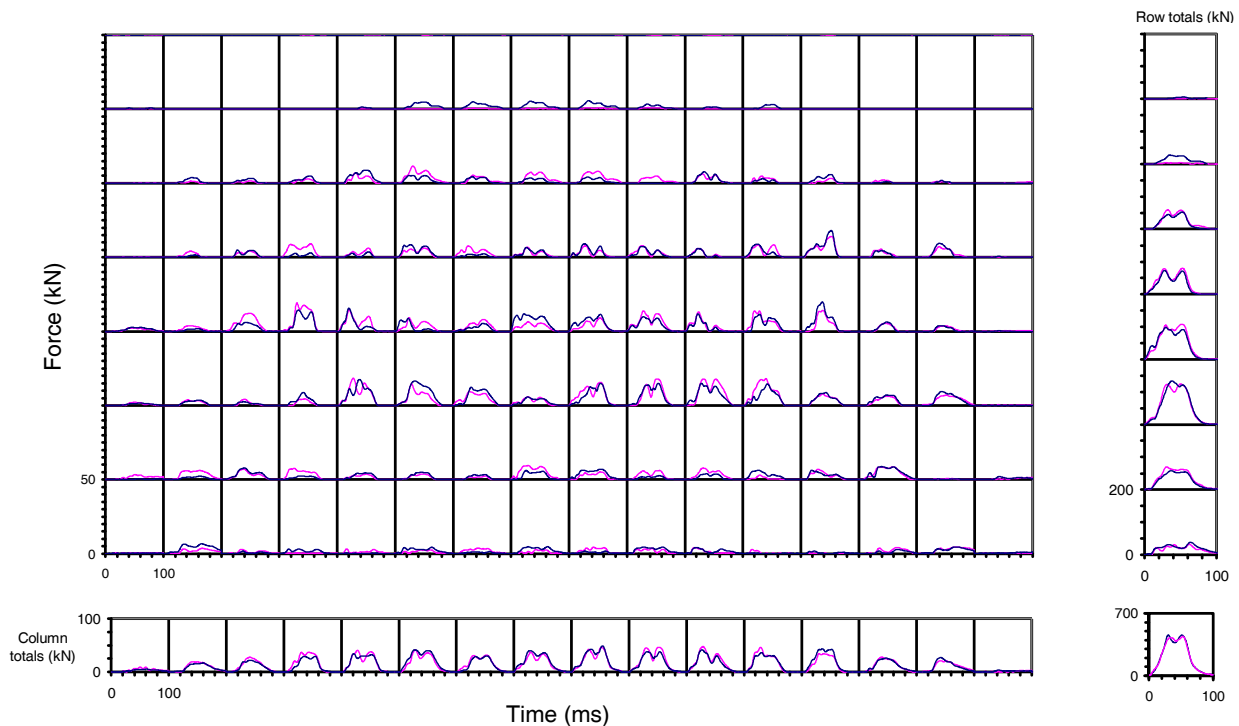


Figure 17. Load Cell Wall (LCW) force distribution for tests with 'Supermini 1'.

Practicality and robustness

No major practical or robustness problems were encountered in the test programme. However, from the experience gained positioning rear seated dummies in 5-door cars used in the test programme, it was thought that for 3-door cars there may be dummy access problems for taking measurements such as pelvic angle.

COST BENEFIT ANALYSIS

An initial cost benefit analysis was performed for the introduction of a full width test into the European regulatory regime [12].

Benefit analysis

The benefit for Europe was estimated by scaling the results from a study which estimated the benefit for GB [13]. Another study, based on German accident data, was also considered for use in this work. However, it was not used because a review of the analysis found that it did not take into account a key confounding factor which, most likely, significantly influenced the results [12].

It is known that a full width test produces a higher compartment deceleration in a car than the offset deformable barrier test, and so it is a more severe test for the restraint systems in the car. Following this argument, the GB benefit analysis was based on the assumption that the introduction of a full width test in Europe would encourage improved restraint systems, which would in turn reduce restraint-induced injury. It was assumed that the main body regions that would benefit from a reduction in restraint-induced injury would be those normally loaded by the webbing of a three-point seat belt, namely the thorax and abdomen. Restraint induced injuries were identified as those which occurred in impacts where the occupant was loaded by the restraint system only, i.e. those where there was little or no steering wheel or compartment intrusion.

The analysis could not be performed using the GB national accident database (STATS19) alone, because it did not contain sufficient information about the casualties' injuries. To resolve this problem, the detailed CCIS database, which contains information about the casualties' injuries for each body region by AIS, was used to estimate a proportional benefit which was scaled to calculate the national benefit.

The following steps were used to calculate the benefit:

- Identify target population in CCIS accident database.

- Calculate proportional benefit in terms of MAIS for casualties in target population.
- Transform benefit in terms of MAIS to police severity scale (fatal, serious, slight, non-injured).
- Scale proportional benefit calculated in CCIS to estimate national benefit.

The Target Population was identified as casualties who were belted and aged less than 65 years involved in frontal impacts with an impact severity less than the test severity (56 km/h) with little or no occupant compartment intrusion (< 5 cm).

The Proportional Benefit was calculated by assessment of the injuries sustained by individual casualties in the target population and how they would be reduced if an improved restraint system was present. The casualties were assessed in terms of both their overall MAIS level and the AIS injury levels sustained by the thorax and abdomen. The MAIS for these casualties was recalculated assuming that thorax and abdomen injuries would be reduced by a maximum of 2 AIS levels, with no injuries being reduced to a level lower than AIS 1 [Table 4].

Table 4. Change in MAIS levels for CCIS data set with restraint induced thorax and abdomen injuries reduced.

MAIS	Original data set (No. of occupants)	Data set with injury reduction (No. of occupants)	Change (No.)
0	296	296	0
1	1084	1174	+90
2	280	219	-61
3	135	115	-20
4	37	29	-8
5	35	34	-1
6	2	2	0
Total	1869	1869	0

This assumption was based on previous work by Cuerden [14] in which expert judgement was used to derive subjective estimates of potential reductions in the severity of an AIS injury to given body regions for the fitment of improved restraint systems. Examples of how this calculation works are given below:

If a casualty had an AIS 5 thorax or abdomen injury, it was reduced to AIS 3. However, if a casualty had an AIS 2 thorax or abdomen injury it was reduced to AIS 1 and there was no reduction for AIS 1 injuries. If the

casualty had an AIS 5 thorax injury and also an AIS 5 head injury even though the AIS 5 thorax injury was reduced to an AIS 3, there was no reduction for the head injury and thus the casualty's MAIS remained at 5.

The distribution of these 'new' MAIS levels was compared with the original MAIS distribution to give an estimated benefit in terms of reduction in MAIS for the casualties in the CCIS target population [Table 4].

Transformation of the Benefit calculated above into the police severity scale (fatal, serious, slight and uninjured) was performed. This was achieved by calculating the percentage distribution of fatal, serious and slight injuries for each MAIS level in the original target population, and using these figures to transform the proportional benefit in terms of MAIS into a proportional benefit in terms of the police injury severity scale.

The National Benefit was estimated by scaling the proportional benefit. This required the definition of equivalent data sets in the CCIS and national (STATS19) data samples to account for factors, such as seat belt use, which are not recorded in STATS19. The benefit for GB was estimated to be a reduction in annual car occupant fatalities of approximately 3 percent (47 occupants) and serious casualties of approximately 6 percent (812 occupants) [Table 5].

Table 5. Annual reduction in car occupant casualties for GB.

	GB National Benefit		
	Original number	Reduction No	Reduction %
Fatalities	1695	47	3
Serious Casualties	14,512	812	6

An additional interesting finding was that if the calculation was repeated using a target population that included elderly casualties, i.e. those over 65 years old, the benefit predicted increased substantially to a 5 percent reduction in fatalities and a 7 percent reduction in seriously injured casualties. This indicates a large potential benefit for restraint systems that could provide better protection to elderly occupants.

The Benefit for Europe (EU15, EU25, EU27) was estimated by simple scaling of the GB benefit. It should be noted that scaling of benefit in this manner will only give an order of magnitude estimate of the benefit for Europe. This is because the accident pattern varies

considerably from country to country and hence this type of direct scaling can introduce large errors.

The Monetary Value of this benefit was calculated using GB quoted values for each life saved (£1,489,450) and serious injury avoided (£167,360) [15]. An exchange rate of 1.2 € per £ was assumed. It should be noted that, in general, the GB values are higher than those used for other European countries as they include a 'Willingness to Pay' element. However, they were still used for this analysis because other published values were not readily obtainable. For the EU15 countries the monetary value of the benefit was about €2,000 million per year [Table 6].

Table 6. Estimated benefit for Europe for introduction of full width test.

	Casualties Prevented		Financial Benefit (€Million)
	Fatal	Serious	
EU15	430	6,017	€1,976
EU25	574	8,038	€2,640
EU27	625	8,756	€2,876

Cost analysis

The analysis was based on the cost to modify a typical European car to meet either UNECE Regulation 94 or US FMVSS208 performance limits in a full width test [Table 7]. The 'Small family 1' car tested by APROSYS was assumed to represent a typical European car.

Table 7. Summary of UNECE Regulation 94 and US FMVSS208 performance limits.

Criteria	Regulation 94 Limits	FMVSS208 Limits
HIC ₃₆	1000	1000
HIC ₁₅		700
Head Acceleration (3 ms exceedence)	80g	
Neck Extension Moment	57 Nm	
Neck tension +Z		4.17 kN
Neck compression -Z		4.00 kN
N _j		1.0
Chest Deflection	50 mm	63mm
Viscous Criterion	1.00	
Chest acceleration (3 ms exceedence)		60g
Femur Compression	9.7 kN	10.0 kN
Knee Displacement	15 mm	
Tibia Compression	8 kN	
Tibia Index	1.3	

The crash test results for ‘Small family 1’ were examined. It was seen that to consistently meet Regulation 94 performance limits the driver dummy head and knee injury criteria values would need to be reduced [Figure 18]. It should be noted that it was assumed that manufacturers would set a design target of around 80 to 85% of the performance limit to give a safety margin to allow for factors such as test repeatability.

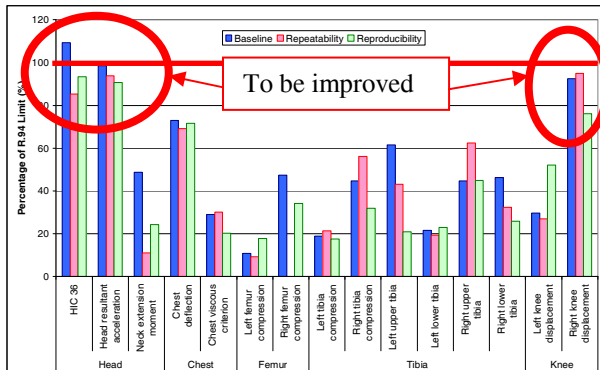


Figure 18. Driver dummy injury criteria values shown as a percentage of the UNECE Regulation 94 performance limits.

From further examination of the results and expert judgement, modifications to the driver restraint system to improve the dummy performance and meet the Regulation 94 performance limits were identified. These modifications included the introduction of a degressive load limiter to improve the head performance and introduction of a double pretensioner to improve the knee performance. This process was repeated for the passenger dummy to identify necessary modifications to the passenger restraint system. Following this, the cost of these modifications was estimated to determine the total cost per car to meet Regulation 94 limits in a full width test. This whole process was repeated to determine the costs per car to meet FMVSS208 limits in a full width test.

These costs were scaled to give an estimate of the total cost per year for the EU15 countries [Table 8]. This was achieved by multiplying the cost per car by the average number of new cars registered per year in the EU15 countries. ACEA data showed this to be 14,221,978 for the years 1999 to 2004 inclusive.

Table 8. Cost of restraint system modifications to meet US FMVSS208 or UNECE Regulation 94 performance limits per car and for the EU15 countries.

Performance limit	Cost per car (€)	Total Cost for EU15 per year (€)
FMVSS208	17	242 Million
UNECE R94	32	455 Million

Many cars sold in Europe are also sold in countries, such as the US, where a full width test is already part of the regulatory requirements. These cars are likely to perform better in a full width test than the typical European ‘Small family 1’ car on which the analysis was based and therefore require fewer modifications to meet the performance requirements. Hence the costs estimated are likely to be high.

Cost benefit

For EU15, a potential benefit of up to approximately €2,000 million per year was estimated for the introduction of a full width test. A cost of €242 million was estimated to meet FMVSS208 limits in the test and €455 million to meet Regulation 94 limits. Assuming that performance limits similar to the Regulation 94 ones are required to deliver the potential benefit, this results in a benefit to cost ratio of about 4:1. However, more stringent performance limits and other measures are likely to be needed to deliver all of the estimated benefit, which would require additional modifications to the car and inevitably increase the cost. These modifications may include adaptive restraint systems. Further work is required to determine appropriate performance limits and update the cost benefit analysis.

DISCUSSION

The decisions taken related to the main questions to help specify the full width test are discussed and summarised below.

- Test speed – 56 km/h.
A test speed of 56 km/h was chosen for the following two reasons. Firstly, the accident analysis showed that it covered a large proportion of casualties with life threatening and fatal injuries (over 80% of MAIS 3+ injuries) for belted occupants in frontal impacts with no rollover. Secondly, it is the same speed as the US FMVSS208 test. This should help to harmonise crash tests worldwide to reduce the testing burden on manufacturers.

- Dummy specification – 50th percentile Hybrid III driver and passenger (front seat and rear seat).
The Hybrid III dummy was chosen on the basis that specific injury criteria were not available for the THOR-NT and the limited data from the sled testing performed showed no significant advantage to using the THOR-NT dummy compared to the Hybrid III. However, an upgrade to the THOR-NT dummy could be considered at a later date if significant advances are made in its development, in particular regarding assessment of restraint induced thorax injury.

50th percentile male dummies were chosen for driver and passenger (front and rear seated) occupant positions on the basis of the results from the analysis with the German GIDAS database. However, it is advised that further analysis is performed using data from European countries besides Germany to verify this choice. For the driver, the analysis showed that the gender median height and weight all corresponded well to the 50th percentile male. For the front and rear seat passengers, the analysis showed that a slightly shorter, lighter female dummy would be a better match to the median occupant, but the 5th percentile female dummy was too short and light to represent a median occupant.

The accident analysis also indicated that key body regions to protect were the head, thorax, femur and clavicle, with emphasis on the head and thorax to reduce fatalities.

- Assessment of rear seated position – undecided.
The crash testing work showed that the inclusion of rear seated dummies did not influence the assessment of the front seated position, indicating that testing this seat position is feasible. Comparison of the injury criteria values for the front and rear seated dummies showed that the main differences were higher head, neck and tibia values for the rear seated dummies. The tests with the ‘Small family 1’ car showed strong evidence of submarining. In addition, it was noticed that the thorax deflection values were similar for the front and rear seated dummies even though the belt loads were substantially higher for the rear seated dummies. Several possible contributory factors were identified to explain this observation, one of them being the different relationship between thorax deflection and injury risk for the Hybrid III dummy for belt only and combined airbag and belt restraint systems identified by Kent [10]. This factor has interesting consequences, namely if it was decided to test the rear seat position and to drive an equivalent level of

safety protection for the thorax to that offered in the front, then different performance limits would be needed for the chest deflection for the rear dummies to account for the different injury risk functions for belt only and belt and airbag restraints.

The main finding from the accident analysis was that the proportion of rear seated occupants wearing a seatbelt was much lower than for front seated occupants. This clearly indicates that there is a problem with the seat belt wearing rate in the rear. The accident analysis also found that the rear seat occupancy rate in collisions was low, about 10% of all occupants. The analysis with the GIDAS database showed that the risk of injury for belted occupants in the rear was lower than for the front. However, other recent studies have indicated that for the elderly the risk of injury is higher in the rear than the front [16].

In summary, the crash tests performed showed no major technical obstacles to include rear seated dummies in the test. However, the accident analysis work showed that the seat belt wearing rate in the rear was substantially lower than for the front and the rear seat occupancy rate is currently low. One way to help improve the seat belt wearing rate could be the fitment of seat belt reminder systems for rear occupants. These and other factors need to be considered further, in particular from a cost benefit point of view, before a decision can be made whether or not to assess the rear seated position.

- Deformable barrier face – undecided.
As mentioned previously, the main purpose of the deformable face is to help take measurements of a vehicle’s compatibility potential and to make the test more representative of a vehicle to vehicle impact, in particular at the beginning of the impact [4]. EEVC WG15 has proposed three potential options for a set of test procedures to assess a vehicle’s self and partner (compatibility) protection, two of which include a full width test with a deformable face. However, the research is not far enough advanced to decide which of these options should be taken forward and hence whether or not a deformable face is required to take compatibility measurements. If a full width test was to be introduced in the longer term it is expected that this research would be complete and hence the decision made. However, the aim of APROSYS was to develop a test that could be introduced in the short term and hence test work was performed to assess the effect of the deformable face on the assessment of a vehicle’s self protection capability.

For the three cars tested the dummy injury criteria values were generally similar between the tests with and without the deformable face indicating that the deformable element had little effect on the overall severity of the test. However, for one car the airbag fired later in the test with the deformable face which resulted in substantially higher dummy injury values for the head. This was most likely caused by the lower compartment deceleration at the beginning of the impact, which is more representative of a vehicle to vehicle impact. This shows that a deformable face may be useful in a full width test in the short term to ensure a more realistic assessment of a vehicle's crash sensing capability. However, the author is not aware of studies showing that there is a problem with late airbag firing in these types of accidents in the real world. Moreover, it should be noted that current regulatory full width tests, such as FMVSS208, do not have a deformable face, so for harmonisation purposes it would be best not to include one in a test for Europe. To make a decision these advantages and disadvantages will have to be weighed up, most likely by governmental and/or regulatory bodies.

- Repeatability and reproducibility
Full scale crash testing was performed to assess the repeatability / reproducibility of the test. As all the tests were instrumented with a high resolution Load Cell Wall, the repeatability and reproducibility of proposed metrics to assess a car's compatibility were also investigated.

For self protection measures, such as dummy injury criteria, it was found that the repeatability and reproducibility were at least as good as for the current UNECE Regulation 94 test procedure.

For partner protection measures, it was found that although the global Load Cell Wall (LCW) force was repeatable for all tests, the LCW horizontal force distribution was not because of different failure modes of the vehicle's main rail. For the Structural Interaction (SI) metric it was found that although the vertical component was repeatable, the horizontal one was not even when the LCW horizontal force distribution was repeatable. This indicates that although assessment of a vehicle's partner protection using LCW measurements and associated metrics shows promise, further development is required to improve repeatability to ensure suitability for regulatory application.

CONCLUSIONS

The APROSYS project has developed a full width test procedure suitable for regulatory application in Europe in the short term to assess a vehicle's self protection capability. An initial cost benefit analysis has also been performed.

However, some issues remain to be resolved to complete the specification of the procedure. These include:

- Definition of performance criteria and limits.
The cost benefit analysis indicated a benefit to cost ratio of 4:1 assuming that performance limits similar to the Regulation 94 ones are required to deliver the estimated benefit. However, more stringent performance limits and other measures are likely to be needed to deliver all of the estimated benefit. These may include adaptive restraint systems and an improved dummy for the assessment of thorax protection. Further work is required to determine appropriate performance limits and update the cost benefit analysis.
- Deformable face
The crash tests results showed that a deformable face could be useful to help ensure a more realistic assessment of a vehicle's crash sensing capability. However, a deformable face is not currently included in any worldwide regulatory or consumer testing and hence would be disadvantageous from the point of view of harmonisation. To decide whether or not to include a deformable face these advantages and disadvantages need to be weighed up, most likely by governmental and/or regulatory bodies.
- Rear seat position
The crash tests performed showed no major technical obstacles to include rear seated dummies in the test. However, the accident analysis work showed that the seat belt wearing rate in the rear was substantially lower than for the front and the rear seat occupancy rate is currently low. These and other factors need to be considered further, in particular from a cost benefit point of view, to make a decision of whether or not the rear seat position should be tested.

ACKNOWLEDGEMENTS

The author acknowledges the contribution of the members of the APROSYS SP1.2 consortium to this paper:

- BAST, Germany
- Fiat, Italy
- IDIADA, Spain
- Nissan

- TNO, Netherlands
- Toyota
- TRL, UK
- Technical University Graz, Austria
- Volkswagen, Germany

The consortium is grateful for the support of: the European Commission DG-TREN, UK Department for Transport, German Ministry of Transport and Housing, Dutch Ministry of Transport for funding this work.

This paper uses accident data from the United Kingdom's Co-operative Crash Injury Study (CCIS) collected during the period 1998 to 2006 (Phases 6 and 7). Currently CCIS is managed by TRL Limited, on behalf of the United Kingdom's Department for Transport (DfT) (Transport Technology and Standards Division) who fund the project along with Autoliv, Fiat, Ford Motor Company, Nissan Motor Company and Toyota Motor Europe. Previous sponsors include Daimler Chrysler, LAB, Rover Group Ltd, Visteon, Volvo Car Corporation, Daewoo Motor Company Ltd and Honda R&D Europe (UK) Ltd. Data was collected by teams from the Birmingham Automotive Safety Centre of the University of Birmingham; the Vehicle Safety Research Centre at Loughborough University; TRL Limited and the Vehicle & Operator Services Agency (VOSA) of the DfT. Further information on CCIS can be found at <http://www.ukccis.org>

REFERENCES

1. Lomonaco C and Gianotti E (2001). 'IHRA: 5-years Status Report of the Advanced Offset Frontal Crash Protection', 17th ESV conference, Amsterdam, Netherlands, 2001.
2. Faerber E (2003). 'EEVC Research in the field of improvement of crash compatibility between passenger cars', 18th ESV conference, Nagoya, 2003.
3. Faerber E (2007). 'EEVC Approach to develop test procedure(s) for the improvement of crash compatibility between passenger cars', 20th ESV conference, Lyons, France, 2007.
4. APROSYS (2008). 'Accident Analysis for Specification of Advanced European Full Width Test', Deliverable 123A, www.aprosys.com
5. APROSYS (2008). 'Draft Test and Assessment Protocol for Advanced European Full Width Test', Deliverable 121, www.aprosys.com
6. APROSYS (2008). 'Evaluation of Advanced European Full Width Test', Deliverable 122, www.aprosys.com
7. Edwards M, Davies H and Hobbs A (2003). 'Development of Test procedures and Performance Criteria to Improve Compatibility in Car Frontal Collisions', Paper No. 86, 18th ESV conference, Nagoya, 2003.
8. Kent R, Crandall J, Bolton J, Nusholtz G, Prasad P and Mertz H (2001). 'The Influence of Superficial Soft Tissues and Restraint Condition on Thoracic Skeletal Injury Prediction', 45th Stapp Car Crash Conference, pp. 183-204.
9. Foret-Bruno J-Y, Trosseille X, Page Y, Huere J-F, Le Coz J-Y, Bendjellal F, Diboine A, Phalempin T, Villeforceix D, Baudrit P, Guillemot H and Coltat J-C (2001). 'Comparison of Thoracic Injury Risk in Frontal Car Crashes for Occupant Restrained without Belt Load Limiters and Those Restrained with 6 kN and 4kN Load Limiters', 45th Stapp Car Crash Conference.
10. Kent R, Lessley D, Shaw G and Crandall J (2003). 'The utility of Hybrid III and THOR chest deflection for discriminating between standard and force-limiting belt systems', Proc. 47th Stapp Car Crash Conference, n°2003-22-0013, pp. 267-297.
11. Edwards M, Cuerden R and Davies H. (2007). 'Current Status of the Full Width Deformable Barrier test', 20th ESV conference, Lyons, France, 2007.
12. APROSYS (2008). 'Cost benefit Analysis for Introduction of Advanced European Full Width Test', Deliverable 123B, www.aprosys.com
13. Thompson A, Edwards M and Cuerden R (2007). 'Benefit Analysis for the Introduction of a Full Width Frontal Impact Test' TRL Published Project Report PPR 296.
14. Cuerden R, Hill J, Kirk A and MacKay M (2001). 'The Potential Effectiveness of Adaptive Restraints', IRCOBI conference, Isle of Man, UK, 2001. <http://www.ircobi.org/publications.htm>
15. RCGB (2006). 'Road Casualties Great Britain Annual Report'. <http://www.dft.gov.uk/pgr/statistics/datatablespublications/accidents/casualtiesgbar/roadcasualtiesgreatbritain2006>
16. Kent R, Forman J, Parent D and Kuppa S (2007). 'Rear seat occupant protection in frontal crashes and its feasibility', 20th ESV conference, Lyon, France.

© Copyright TRL Limited 2009.

Summary of Activities of the Compatibility Working Group in Japan

Hideki Yonezawa

National Traffic Safety and Environment Laboratory

Koji Mizuno

Nagoya University

Takahiro Hirasawa, Hitoshi Kanoshima

Ministry of Land, Infrastructure, Transport and Tourism

Hideaki Ichikawa, Shuji Yamada, Hideki Koga, Akira Yamaguchi

Japan Automobile Manufacture Association

Yuji Arai

Japan Automobile Research Institute

Atsumi Kikuchi

Institute for Traffic Accident Research and Data Analysis

Japan

Paper Number 09-0203

ABSTRACT

In 2006, the Transport Policy Council's Report in Japan stated that it is necessary to discuss compatibility improvement considering the traffic accident environment in Japan. In response to this report, the MLIT has launched the Compatibility Working Group in Japan. This paper summarizes the activities of the WG toward the compatibility improvement.

In the WG, accident analyses and crash tests were performed to identify the safety problem. From global accident data, it is shown that as the front rail of the opposite (or collision partner) car was higher, the injury risk to the occupant tended to be higher. Full frontal car-to-car crash tests were conducted to investigate height matching and mismatching conditions of front rails. It was suggested that matching the front rail heights between two cars provides an overall safety benefit for occupant protection, though the leg injuries may become worse. From the accident analysis and crash tests, it was recognized in the WG that the matching of the front rail heights could be the first issue to be investigated for compatibility improvement.

To evaluate the height of front rails, geometrical measurements and analysis of crash test data can be considered. The footprint of the front rails can be observed in the measured barrier force distribution of

a full-width rigid barrier test. Accordingly, to evaluate the front rail heights, measurement and evaluation of the barrier force distribution using high-resolution load cells in a full-width rigid barrier test was investigated. Several methods were developed and proposed for evaluating the front rail heights based on the barrier force distributions.

INTRODUCTION

Transport Policy Council's Report in Japan (June 2006) [1] states in the section of "Enhancement of Passive Safety Measures" that "As another passive safety measure, it will be necessary to formulate a compatibility regulation relating to occupant protection in an accident between vehicles of different sizes in keeping with available research results and the drafting of a similar international regulation." In response to this report, the Ministry of Land, Infrastructure, Transport and Tourism (MLIT) has launched the Compatibility Working Group (WG) in Japan to investigate measures of compatibility.

In vehicle compatibility, it is recognized that good structural interaction is a prerequisite to ensure the efficient energy absorption of frontal structures and the integrity of the passenger compartment. For good structural interaction, matching the heights of front rails above the ground is one of the important factors. In compatibility, the aggressiveness of the sports

utility vehicle (SUV) is one of significant issues to be addressed. In 2003, the Front-to-Front Compatibility Technical Working Group (TWG) of the US Alliance announced Phase I requirements for improving geometrical compatibility [2]. In the Phase I, it was required that either (1) the primary energy absorbing structure (PEAS) shall overlap the FMVSS Part 581 bumper zone (Option 1) or (2) a secondary energy-absorbing structure (SEAS) shall be installed, whose lower edge shall be no higher than the bottom of the Part 518 bumper zone (Option 2).

The MLIT has conducted accident analyses and crash tests. The Japan Compatibility WG examined the results of these analyses. The WG focused on the front rail height matching in car-to-car collisions. In order to evaluate the front rail height, candidate test procedures based on measurement and evaluation of the barrier force distribution in a full-width rigid barrier (FWRB) crash test were proposed in the WG.

ACCIDENT ANALYSIS

The relationship between front rail heights and injury risks to drivers were examined using global and in-depth accident data in Japan.

Global Accident Data Analysis

National accident data (police data) in Japan was used to investigate the compatibility situation. Vehicle-to-vehicle collisions, where both vehicle drivers were belted, were selected for the analysis. Table 1 presents the number of injured drivers in head-on collisions. The number of belted drivers in cars involved in car-to-vehicle head-on collisions in the time span from 2001 to 2007 was 119,692, and the probability of fatal and serious injuries was 7.3%. The number of car-to-car collisions during this time was 91,766. In order to examine late model cars, models tested by the Japan New Car Assessment Program (JNCAP) as of 2002 were selected as the subject cars (N=3,856). Furthermore, among these collisions involving the car models tested by JNCAP, the other collision partner cars were limited to those registered as of 2000, which led to the population of 1,308 collisions. This research focused on these 1,308 collisions.

Figure 1 shows the probability of fatal and serious injuries to belted drivers by the curb mass of the subject car. The probability of injury in the subject car decreases and that in the collision partner car increases with increasing subject car mass. The probability of fatal and serious injury of the drivers in the subject and the collision partner cars are comparable when the subject car mass in the range of 1,100 to 1,300 kg.

Table 1. Number and probability of injuries of drivers in cars in head-on collisions (both drivers were belted in collisions)

	Subject car	Number of drivers				Total	Prob. of fatal and serious injury (%)	
		Fatal	Serious	Minor	No injury			
Car-to-vehicle collision		1,056	7,667	62,640	48,329	119,692	7.3	
Car-to-car collision	Car	309	4,990	48,169	38,298	91,766	5.8	
	JNCAP car	Subject	3	187	2,263	1,403	3,856	4.9
		Other	17	202	1,966	1,671	3,856	5.7
	JNCAP car vs. car (registered 2000 or later)	Subject	1	69	753	485	1,308	5.4
		Other	3	62	729	514	1,308	5.0
	Total	4	131	1,482	999	2,616	5.2	

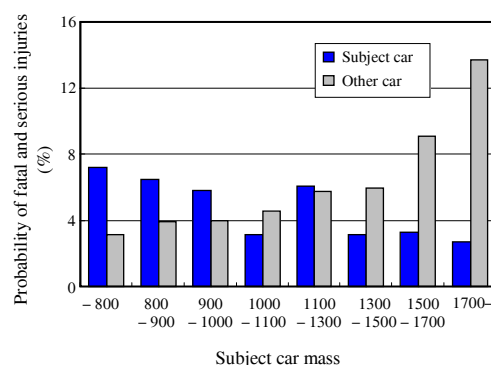


Figure 1. Car curb mass and probability of injuries to belted driver

The number of driver injuries is presented in Table 2 as a function of the front rail ground height of the subject car. The front rail height is defined as the average of ground heights between the upper and lower edges of the front rail front-end. The number of cars with a front rail height ranging from 425 to 475 mm is 1,174, which account for 44.9% in the vehicle fleet. The number of cars with their front rail height ranging from 400 mm or less and from 500 mm or more is 195 and 277, respectively. Front rail heights of many cars in the Japanese car fleet are included in the FMVSS Part 581 bumper zone (i.e., 406 to 508 mm).

Figure 2 shows the probability of injuries to drivers by the front rail height of the subject car. Within the range from 400 to 500 mm of front rail height, the probability of injuries in the subject car tends to decrease with a higher front rail, whereas in the collision partner car the probability tends to increase. However, this tendency is not observed in the ranges where the front rail height is less than 400 mm or when it is greater than 500 mm. One reason may be the number of subject cars is small in these ranges (see Table 2).

Table 2. Front rail height of subject car and the number of belted driver injuries

Front rail height (mm)	Subject car				Other car					
	Fatal	Serious	Minor	No injury	Total	Fatal	Serious	Minor	No injury	Total
-400	10	117	68	195	10	103	82	195		
400-425	1	24	196	128	349	9	207	133	349	
425-450	3	31	291	212	537	2	23	320	192	537
450-475		29	361	247	637	2	37	358	240	637
475-500		31	361	229	621	38	346	237	621	
500-525		6	132	95	233	13	124	96	233	
525-			24	20	44	1	24	19	44	
Total			1482	999	2616	4	131	1482	999	2616

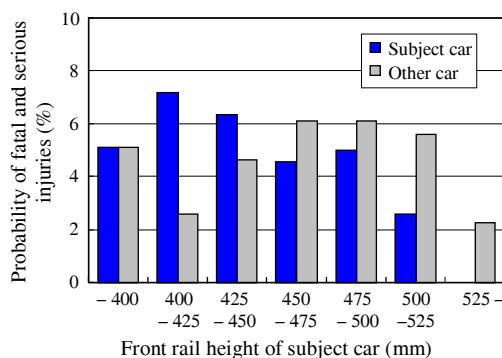


Figure 2. Front rail height of subject car and the probability of belted driver injuries

The injury risks to belted drivers were examined by the relative height (ΔH) of the front rail of the subject car with respect to the collision partner car. When ΔH is positive, the front rail of the subject car is higher than that of the collision partner car; and conversely, when ΔH is negative, the front rail is lower than that of the collision partner.

The number of involved drivers and the probability of fatal and serious injury by relative front rail height ΔH are shown in Figure 3. There is an observable trend that the probability of fatal and serious injury

was lower as the relative front rail height ΔH was lower. The probability of serious injury to belted drivers was 7.7% for cars with ΔH of 70 mm or less. In contrast, it was 4.3% for cars with a ΔH of 70 mm or more.

Figure 4 and Figure 5 show the probability of fatal and serious injuries of belted drivers by subject car mass and the relative front rail height ΔH . The collisions were classified into groups in which ΔH ranged from -40 to 40 mm (see Figure 4) and from -25 to 25 mm (see Figure 5). The probability of driver injury of the subject car and the other car is slightly smaller for collisions in which the relative front rail height ΔH was in the range from -40 to 40 mm. However, this trend was opposite, where the injury risk to drivers was higher for the group where the relative front rail height ΔH ranged from -25 to 25 mm.

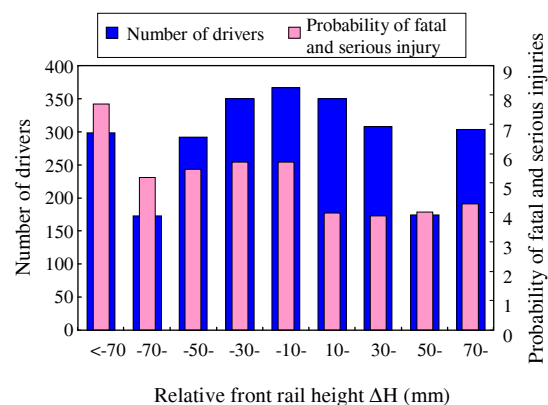


Figure 3. The probability of belted driver injuries by subject car relative front rail height

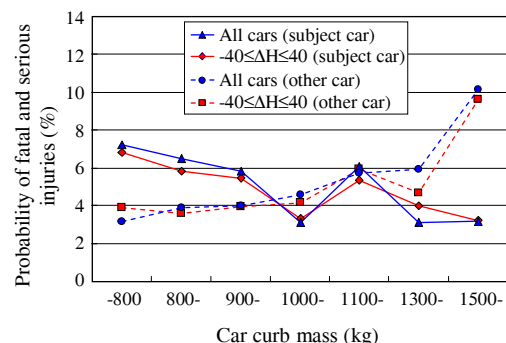


Figure 4. The probability of belted driver injuries by subject car mass and relative front rail height (ΔH) of -40 to 40 mm

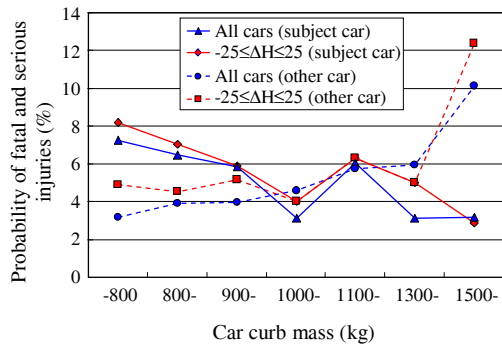


Figure 5. The probability of belted driver injuries by subject car mass and relative front rail height ΔH of -25 to 25 mm

Table 3 presents the probability of fatal and serious injuries to belted drivers classified by subject car types versus the ΔH divided into three ranges—less than 40 mm, -40 to 40 mm, and greater than 40 mm. When the relative front rail height ΔH is in the range from -40 to 40 mm, the injury risks to driver tend to be smaller than for the other two groups.

In accident data, many factors can affect injuries to drivers. The front rail height is one of design factors, which can be associated with vehicle mass, stiffness, and vehicle type. More research on accidents is needed to identify the effectiveness of front rail height matching. The influences of vehicle mass and stiffness also will be investigated in the WG to make clear the problem of compatibility.

Table 3. Probability of fatal and serious injuries to belted drivers in subject cars by relative front rail height differences

Front rail height of subject car from other car	Prob. injury of driver in subject car		
	Minicar	Small car	MPV
$\Delta H \leq -40$ mm	7.5%	6.5%	5.9%
-40 mm $< \Delta H < 40$ mm	6.3%	4.4%	3.2%
$\Delta H \geq 40$ mm	9.1%	3.9%	3.9%

In-Depth Accident Data Analysis

From in-depth accident database of Institute for Traffic Accident Research and Data Analysis (ITARDA) from 1994 to 2008, 34 head-on collisions between cars were extracted. The involved vehicles consisted of 62 cars, 5 Multi Purpose Vehicles (MPVs) or SUVs, and one 1-BOX type vehicles. In

the data, the cross-section height, upper edge and lower edge ground heights of front rails were distributed 60–170 mm, 378–600 mm, and 256–500 mm, respectively.

Figure 6 shows the relation between override/underride occurrence and the relative front rail height. The override/underride occurrences were identified from photographs of cars in accidents by comparing the crush depth of the upper and the lower structures. Although the override or underride tendency is not clearly defined, it may occur when the front rail height difference is 100 mm or more.

The intrusion into the passenger compartment is shown in Figure 7 by the front rail relative height ΔH and the barrier equivalent velocity (BEV). The compartment intrusion started to initiate at a BEV of 25 km/h, and tended to increase with increasing BEV. The compartment intrusion tended to be small as the front rail difference was close to zero. There were cars with intrusions of 450 mm ($\Delta H = -140$ mm) and 500 mm ($\Delta H = 121$ mm) at a BEV of 60 km/h, and where the intrusion was related to the survival space in these accidents.

The injury severities of belted drivers are also shown by the Maximum Abbreviated Injury Scale (MAIS) in Figure 8. The MAIS tended to be large as the front rail height difference was large. However, the MAIS also tended to be large as the front rail height difference was small. When the front rail heights of two collided cars matched each other, the car acceleration can be higher than where there is no matching. The acceleration-related injuries such as the restraint system injury might be one of the causes for this tendency.

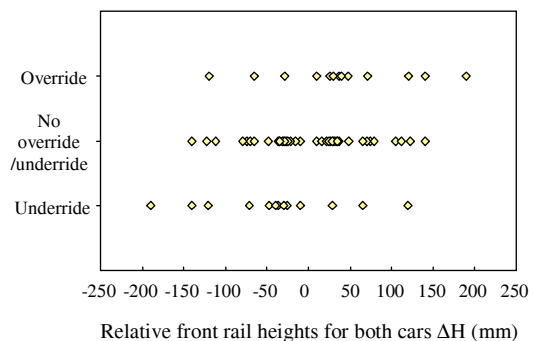


Figure 6. Override/underride based on in-depth accident data

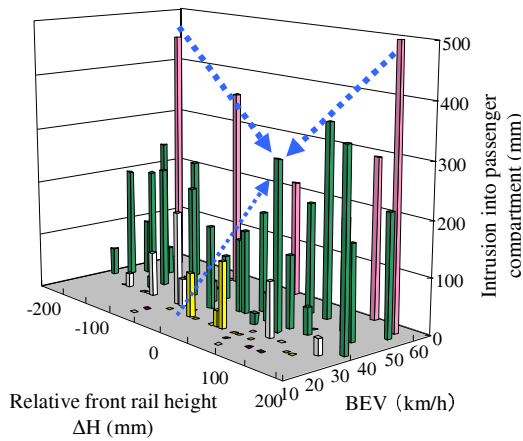


Figure 7. Relation between passenger compartment intrusion, relative front rail height, and barrier equivalent velocity

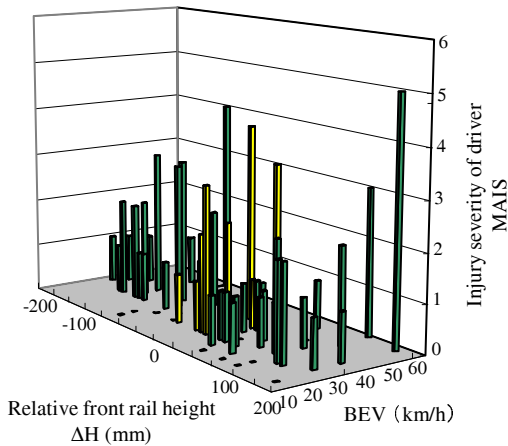


Figure 8. Injury severity of belted driver by front rail ground height and barrier equivalent velocity

CRASH TESTS

Full frontal car-to-car crash tests were conducted for a minicar and a large car, for which the heights of their front rails were different, and for which the ride heights of both cars were adjusted so that the front rail heights were aligned. The car accelerations and dummy responses were examined, and also compared to those in the FWRB test at 55 km/h conducted by JNCAP.

Test Method

A minicar and a large car were impacted center line-to-center line with 100% overlap of the minicar (Figure 9). The velocity of each car at the time of impact was 50 km/h. Figure 2 shows the geometry of the front rails of both cars. In Test 1, the front rail of the large car was higher than that of the minicar by 130 mm, as measured at the location of the center of the cross sections across the front rails. Due to the height difference, the front rails of both cars would not contact (or interact) each other. In Test 2, the ride height of the minicar was raised and that of the large car was lowered so that the geometric centers of the front rails of both cars were aligned. In the lateral direction, the front rails of both cars overlapped each other. In each car, a Hybrid III AM50 dummy was seated in both the driver seat (right) and front passenger seat (left) and was restrained with a seat belt. The test weights of the minicar and the large car were 1024 kg (curb mass 820 kg) and 1695 kg (curb mass 1510 kg), respectively; and the ratio of the large car-to-minicar test mass was 1.6.

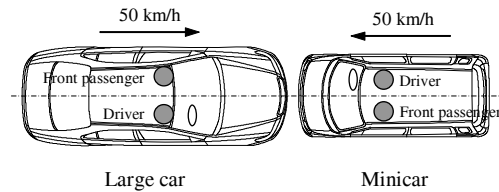


Figure 9. Crash configuration

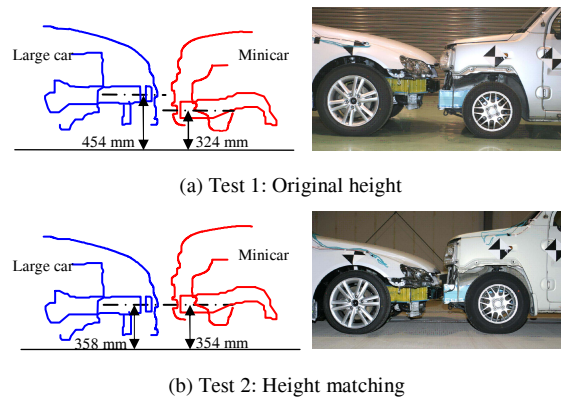


Figure 10. Structure geometry in Test 1 and Test 2

Test Results

Car Behavior

The car behavior during impact in Tests 1 and 2 is presented in Figure 11. In both tests, the minicar was pushed rearward by the large car. In Test 1, it was observed that the large car overrode the minicar. During the first 20 to 60 ms of the crash sequence, the crash interface moved upward and both cars slid relative to each other. At about 50 ms, the front wheels of the large car separated from the ground and overrode the front wheels of the minicar. Beyond 60 ms of the crash sequence, pitching of the minicar occurred with the rear wheel losing contact with the ground. In Test 2, the structures of both cars interacted and the crash interface did not move in a vertical direction. Pitching of the minicar occurred, whereas the attitude of the large car did not change appreciably.

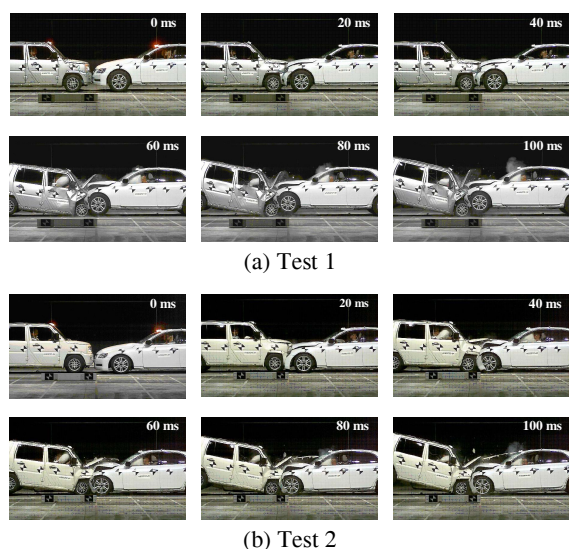


Figure 11. Car behavior in car-to-car full frontal tests

Car Deformation

Figure 12 and Figure 13 present deformation patterns of the minicar and large car after the tests. The measured deformations at selected locations are shown in Figure 14. In Test 1, the deformations of front rails of the minicar car were small due to their height mismatch against the large car. For the minicar, the deformation of the right and left front rails was 180 and 153 mm, respectively. The deformation of the upper structures of the minicar was large, and the engine rotated rearward. Additionally, inside the passenger compartment, the

intrusion of the instrument panel was 39 mm on the right side and 44 mm on the left side, and the steering column moved rearward by 35 mm and upward by 63 mm. As shown in Figure 5, the steering column rotated upward; and, due to dummy contact, the steering wheel bent and fractured.

In Test 2, the front structures of the minicar deformed uniformly. The car deformation mode was comparable with that in the FRWB test in JNCAP. The deformation of the right and left front rail was 302 and 261 mm, respectively, which was large compared to Test 1. The intrusion of the upper part of the passenger compartment was small. The rearward and upward deformation of the steering column was 12 mm and 33 mm. However, in Test 2, the deformations of the lower structures of the minicar were large, particularly for the transmission bottom (110 mm). As a result of the large deformations, the intrusion of the toe board for the front passenger side was large (143 mm).

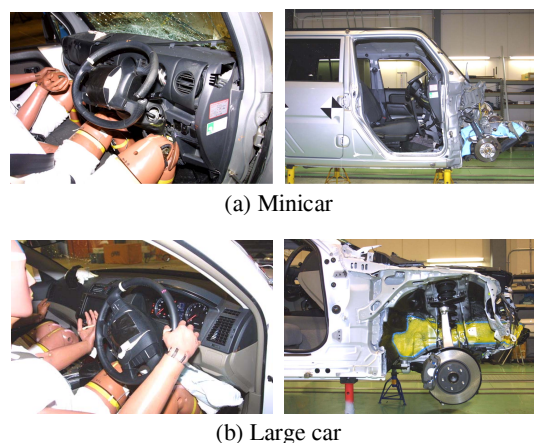


Figure 12. Car deformation (Test 1)

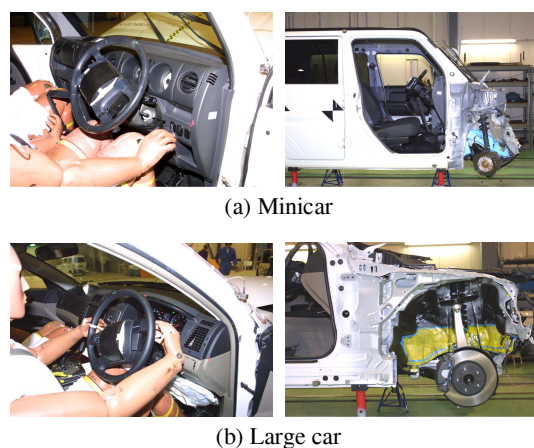


Figure 13. Car deformation (Test 2)

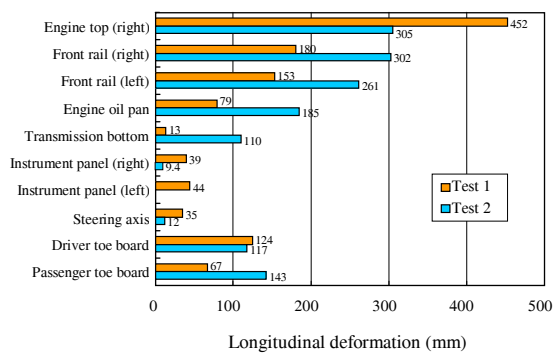


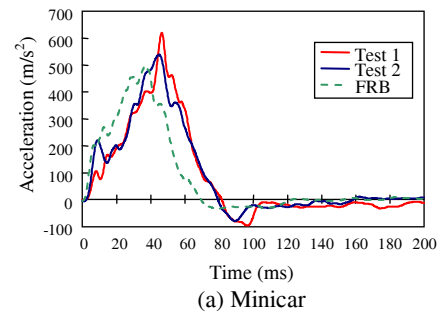
Figure 14. Minicar deformation in Test 1 and 2

Car Acceleration

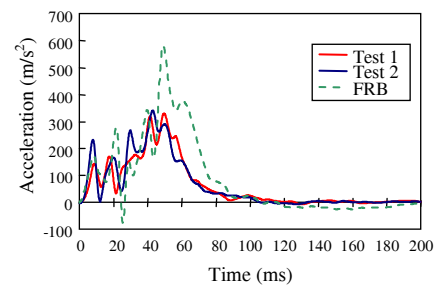
The accelerations of the passenger compartment are shown in Figure 15. In general, the acceleration pulses are comparable between Test 1 and Test 2. However, in Test 1 and Test 2, there are differences in the car accelerations at the time of the initial stage of impact. For the first 15 ms, the minicar acceleration was higher in Test 2 because the front rails of both cars made contact with each other. On the other hand, the peak acceleration of the minicar was higher for Test 1 (619 m/s^2) than for Test 2 (539 m/s^2). For the large car, the car acceleration in the initial stage was also high in Test 1 as compared to that in Test 2. The maximum car acceleration was similar in Test 1 (331 m/s^2) and Test 2 (341 m/s^2). Compared to the JNCAP FWRB 55 km/h tests, the time duration was longer for the minicar and shorter for the large car since the minicar is stiffer than the large car.

Injury Measures

According to the video analysis, the driver airbag of the minicar started to deploy at 24 ms, 17 ms, and 14 ms in Test 1, Test 2, and the FWRB test, respectively. Thus, the timing of the airbag deployment was delayed in Test 1 by 7 ms later than that in Test 2. The shoulder belt tension also started late in Test 1 due to the delay of the seat belt pretensioner activation. As a consequence of this delay of the seat belt forces, the acceleration of the head and chest started later by 7 ms in Test 1 compared to Test 2.



(a) Minicar



(b) Large car

Figure 15. Car acceleration measured at the B-pillar bottom in car-to-car test and full-width rigid barrier test (JNCAP)

The injury measures of the dummies were compared for Test 1 and Test 2. Figure 16 and Figure 17 show the ratios of the injury measures of the driver and front passenger dummies to the injury assessment reference values (IARVs) of ECE R94, respectively. For the minicar, the injury measures of the driver dummy were larger in Test 1 than those in Test 2. In Test 1, some injury measures of the driver dummy in the minicar exceeded the IARVs due to the high acceleration and large intrusion of the car. Especially, the neck extension moment, knee displacement (right), and tibia index (right) exceeded their respective IARVs. In Test 2, the head acceleration, neck extension moment, and chest acceleration also exceeded the IARVs, but these measures were less than those in Test 1. As shown in Figure 12 and Figure 13, the steering column of the minicar rotated upward in Test 1 and Test 2. This steering upward rotation was more apparent in Test 1, so that the HIC, chest acceleration, and neck extension moment were large in Test 1. For the front passenger dummy, the injury measures were also larger in Test 1, with the exception of the left tibia axial force and tibia index (see Figure 17). In Test 2, the toe board intrusion of the front passenger of the minicar was large due to large rearward displacement of the transmission. It is likely that this large intrusion led to the large tibia axial force of the front passenger dummy.

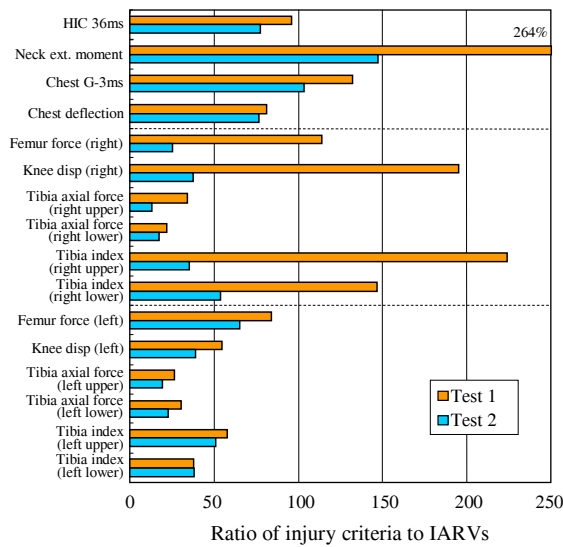


Figure 16. Injury criteria of driver dummy in minicar

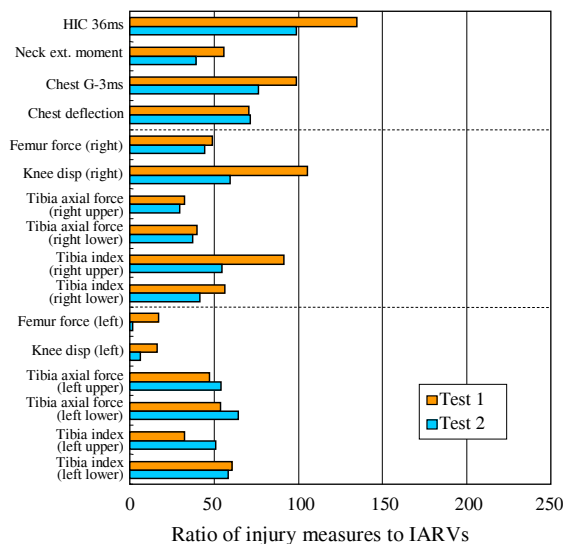


Figure 17. Normalized Injury measures of the front passenger dummy in the minicar

Summary of Crash Test Results

The front rails of the minicar and large car passed by and did not contact each other in Test 1; whereas, they made contact with each other in Test 2. The driver airbag deployment was delayed by 7 ms in Test 1 compared to Test 2 for the minicar. It is likely that the crash sensing at the front rail was affected by the front rail height mismatch. The delayed airbag deployment starting time affected the interaction between the airbag and the dummy head. The height

mismatch of the front rails also led to the large intrusion of the upper part of the passenger compartment of the minicar. When the height of front rails were matched (Test 2), the front structure deformed in a comparable mode as observed in the JNCAP FWRB 55 km/h test. As a result, the car acceleration, deformation, and the dummy kinematics in the car-to-car full frontal crash responded in a controlled manner, which was comparable to those in the FWRB tests. These results confirmed that height matching of front rails has advantages in car-to-car collisions in that the car deformation and dummy response could be predicted in a designed mode in crash tests.

The passenger compartment intrusion of the minicar was more severe for Test 1 where the front rail heights were mismatched. In Test 2, where the front rails heights of the two cars matched, the intrusion and the dummy injury criteria could be improved. The matching of front rail height would have the benefit of preventing serious injuries in severe crashes where the intrusion of the passenger compartment is large. However, it should be noted that in crashes at lower velocities, the risk of minor injuries to occupants could be lower when the heights of the car front rails are mismatched. This is because the car acceleration will be smaller when the front rails of the two cars are mismatched in height and they do not generate large crash forces.

CANDIDATE TEST PROCEDURES TO EVALUATE THE FRONT RAIL HEIGHTS

In the WG, four test procedures were proposed to evaluate the front rail heights (Option 1). These tests are based on the evaluation of the barrier force distribution using high resolution load cells (125 mm) in FWRB tests. The FMVSS Part 581 bumper zone is contained within the 3rd and 4th rows of the load cells (Figure 18). As shown in Figure 19, the effect of an engine impact on the force distribution is large in FRWB tests. Accordingly, it is necessary to eliminate the effect of the engine impact in order to evaluate the heights of the structures. If the front rail heights of cars are higher than an established acceptance level, the SEAS should be installed (Option 2). The scope of the test vehicles will be

minicars, ordinary-size cars, and SUVs. In each candidate test, the criteria and acceptance levels are presented below. In some acceptance levels, parentheses [] were used to show temporal values.

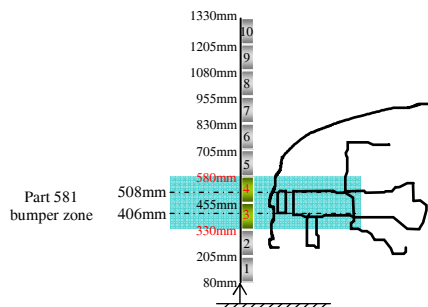


Figure 18. FMVSS Part 581 bumper zone and load cell heights

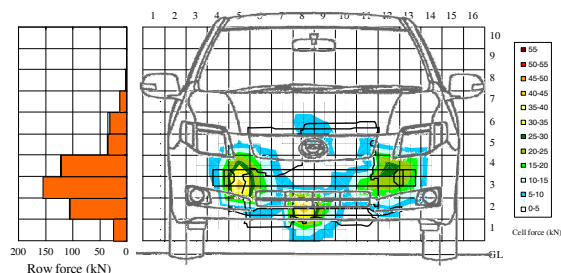


Figure 19. Peak cell force distribution of a small car until car deformation 400 mm in full-width rigid barrier test

Proposed Test 1

In FWRB tests, after the axial collapse of the front rails has commenced, the engine impacts the barrier. Figure 20 plots the barrier force and engine force of cars tested in JNCAP. The engine force is calculated based on the engine mass and acceleration. The engine force is relatively small up to 200 kN of total barrier force. Figure 21 shows the peak cell force distribution of a small car at a total barrier force of 200 kN. The footprint of the front rails is shown clearly. Accordingly, it is likely that the force of these rail structures can be evaluated by analyzing the force distributions up to 200 kN total barrier force.

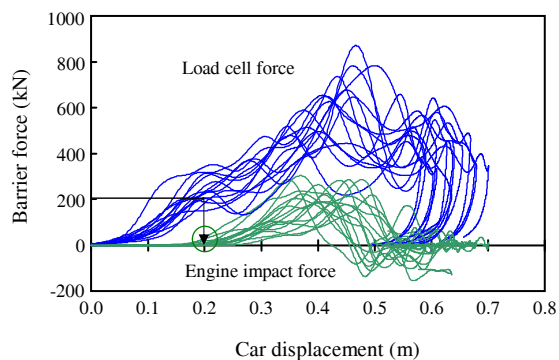


Figure 20. Barrier force and engine impact force in full-width rigid barrier tests (JNCAP 2008)

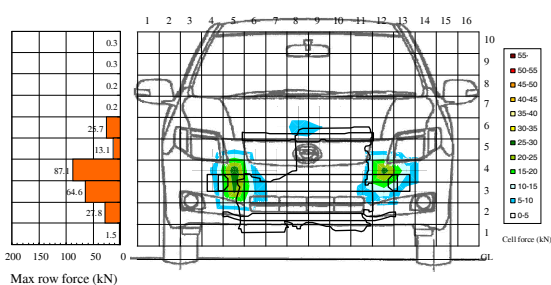


Figure 21. Peak cell force distribution of a small car at total barrier force 200 kN

In a first step, a determination is made whether the front rail height is located between 3rd and 4th row cells. Figure 22 shows the sum of the maximum 3rd and 4th row force at 200 kN total barrier force with the front rail height. The sum of F_3+F_4 tends to be large as the front rail height is close to the 3rd and 4th row boundary line (455 mm). If the acceptance level of F_3+F_4 is too high, then the multiple load path cars may not be accepted. Thus, the acceptance level of [80] kN of F_3+F_4 was used so that only a few cars for which the front rails heights are outside of the 3rd and 4th row are excluded.

In the next step, it is judged that the front rails are located between the 3rd and 4th rows, and whether the front rail cross section includes 455 mm of ground height is examined. Figure 23 shows the relation between the force ratio $F_4/(F_3+F_4)$ and the geometry ratio $U/(L+U)$ (where U is the height between the front rail upper edge and 455 mm, and L is the height between 455 mm and the front rail lower edge). The ratio $F_4/(F_3+F_4)$ is used because the force levels F_3 and F_4 depend on the front rail stiffness. When $0 < U/(L+U) < 1$, the front rail cross

section includes 455 mm height. From Figure 23, the ratio $0 < U/(L+U) < 1$ corresponds to $0.2 < F4/(F3+F4) < 0.8$. The criteria and the acceptance levels of the barrier force for the front rail heights are as follows:

1. $F3+F4 > [80]$ kN
2. $[0.2] < F4/(F3+F4) < [0.8]$

where $F3$ and $F4$ is the 3rd and 4th maximum row force up to the time of 200 kN of total barrier force. If the cars meet the acceptance levels, it is assumed that the cross section of front rail includes the height of 455 mm.

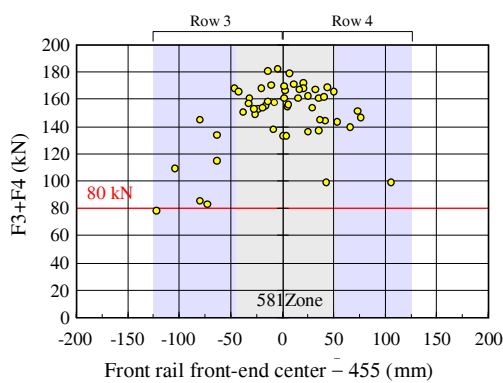


Figure 22. Sum of 3rd and 4th row force and front rail cross section height

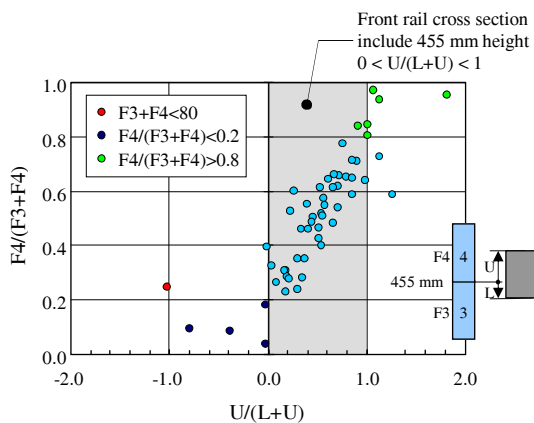


Figure 23. Front rail height and ratio of row force

Figure 24 shows the results of the criteria and the acceptance levels applied to the JNCAP FWRB tests. The cars for which the front rail cross sections do not include 455 mm height were not accepted. It is also shown that the AHOF 400 might not be a good criterion to evaluate the front rail height. The evaluation flow diagram is presented in Figure 25.

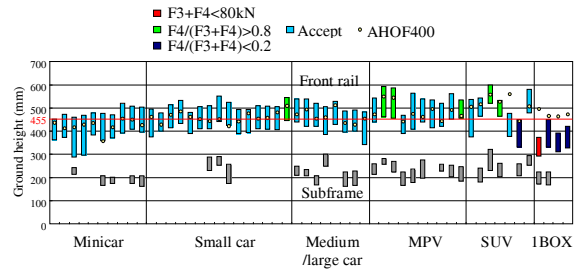


Figure 24. Application of proposed test 1

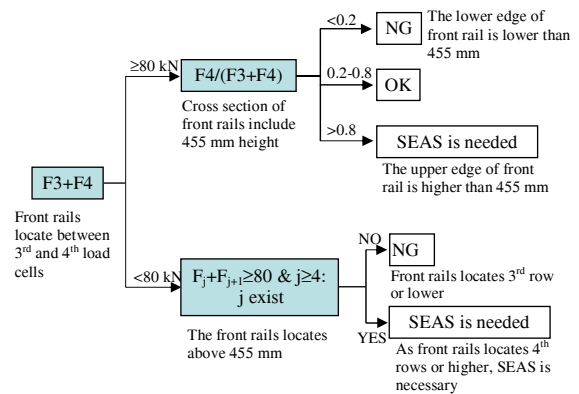


Figure 25. Evaluation flow in proposed test 1

Proposed Test 2

In Option 1, the front rail heights are evaluated. If the cars are not accepted in Option 1, the SEAS will be evaluated in Option 2. The evaluation flow diagram is shown in Figure 26.

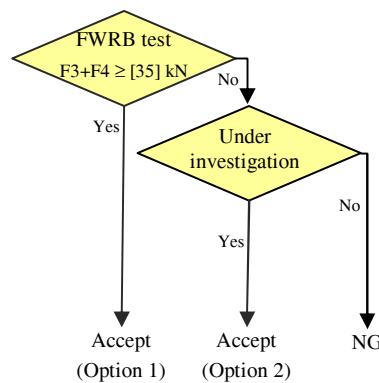


Figure 26. Evaluation flow in proposed test 2

Option 1: The 3rd and 4th row force ($F3$, $F4$) in FRWB test are evaluated so that the influence of a SEAS is excluded. The barrier force distributions before the engine impacts the barrier are used to reduce the influence of engine impact force. The criterion is $F3+F4$, and its acceptance level is [35] kN

as follows (Figure 27):

$$F3+F4 > [35] \text{ kN}$$

where F3 and F4 is the 3rd and 4th maximum row force until 200 kN of total barrier force.

Option 2: Option 2 is dimensional requirement of SEAS, and an evaluation method is under investigation (Figure 28).

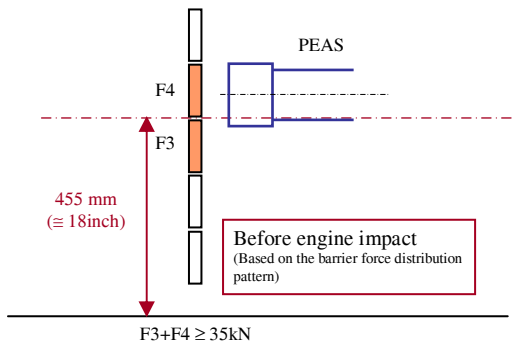


Figure 27. Option 1 test in proposed test 2

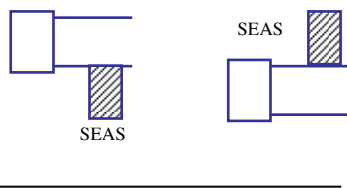


Figure 28. Option 2 test in proposed test 2

Proposed test 3

When a front rail is located in the Part 581 Zone, the force on rows 3 and 4 would be generated mainly by the front-rail stiffness and an engine impact force. Figure 29 shows the $(F3+F4)/2$ within the center 4 columns until the crush depth 400 mm in JNCAP. Since $(F3+F4)/2$ in the center 4 columns is less than 100 kN, in general, the engine impact force is less than 100 kN. Accordingly, the car structural force can be evaluated in the 3rd and 4th rows by using the lower limit of 100 kN of $(F3+F4)/2$.

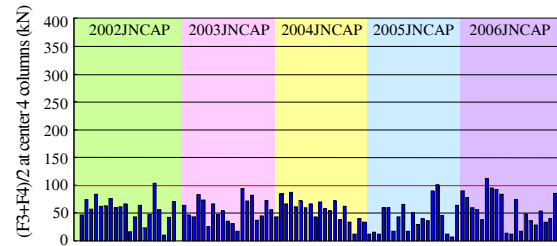


Figure 29. Average of 3rd and 4th rows at center 4 columns in loadcell wall until crush depth 400 mm

In Option 1, the combined force on rows 3 and 4 is evaluated in FWRB test as follows:

$$(F3+F4)/2 \geq 100 \text{ kN (until 400mm of crush depth)}$$

When the forces generated outside the 3rd and 4th rows are large, the 3rd and 4th row force may not be excited and not be measured correctly. Accordingly, if $(F_n + F_{n+1})/2 \geq (F3 + F4)/2$ ($n=4$ to 9) until the crush depth 400 mm, an additional test will be carried out to evaluate structural forces that locate at 3rd and 4th rows (Option 2). A evaluation criteria and a flow diagram of the evaluation is presented in Figure 30 and Figure 31.

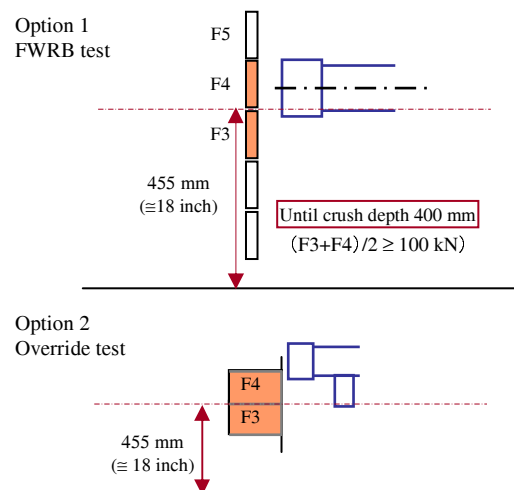


Figure 30. Proposed test 3

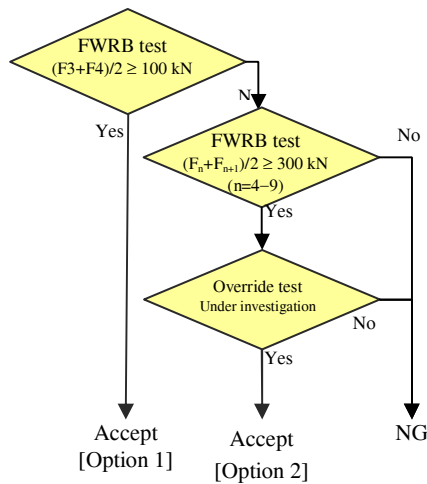


Figure 31. Evaluation flow in proposed test 3

Proposed test 4

Proposed test 4 is similar to proposed test 1 except for the criteria and acceptance levels (Figure 32). In Option 1, the barrier row forces are evaluated in FWRB test as follows:

1. $F_3 + F_4 \geq 100 \text{ kN}$
2. $F_3 \geq 40 \text{ kN}$
3. $F_4 \geq 40 \text{ kN}$

where F_3 and F_4 is the 3rd and 4th maximum row force until 200 kN of total barrier force. If the cars do not meet the Option 1, an override test or underide test is carried out to evaluate the SEAS as the Option 2. Figure 33 presents the evaluation flow diagram.

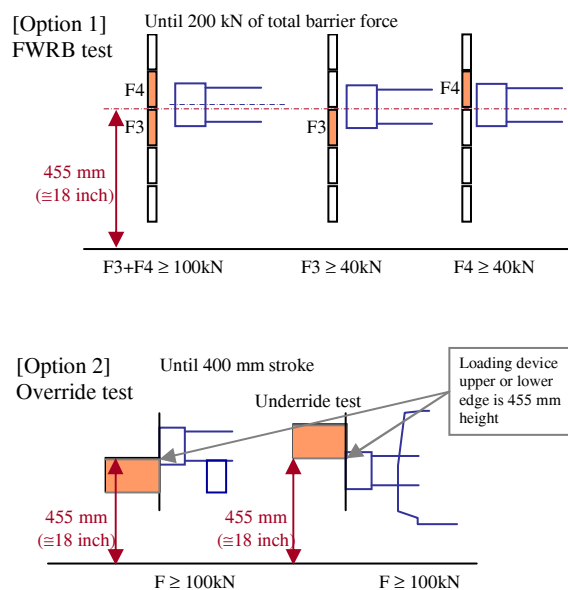


Figure 32. Proposed test 4

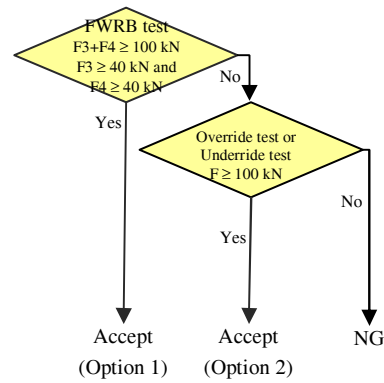


Figure 33. Evaluation flow in proposed test 4

SUMMARY

In the compatibility working group in Japan, the compatibility measures based on the current traffic accident environment in Japan were discussed. The results are summarized as follows.

1. From accident analyses, there is an observed trend that the injury risks increase when the front rail heights are mismatched. However, the front rail heights are related with other factors such as vehicle mass, stiffness, and vehicle class. More research is needed to understand better the effects of front rail height matching.
2. From the full frontal car-to-car crash tests, it was shown that front rail height matching had an advantage of uniform car deformation to prevent large intrusion into the passenger compartment.
3. In the WG, some test procedures to evaluate the front rail heights were proposed that can be used to address one of the identified compatibility problems. In the candidate test procedures, the barrier force distributions were evaluated in full-width rigid barrier tests.

REFERENCES

- [1] The Road Transport Subcommittee of Land Transport Committee of Transport Policy Council, "Vehicle Safety Measures for Building a Society Free from Road Traffic Accidents (Report)", 2006.
- [2] S Barbat, "Status of enhanced front-to-front vehicle compatibility technical working group research and commitments", Paper number 05-463, 19th international conference on Enhanced Safety of Vehicles, 2005.

REPRODUCIBILITY OF AHOF400 AND KW400

Guy Nusholtz
 Lan Xu
 Edith Lugo Velez
 Tim Hsu
 Sadegh Babaii Kocheksarai
 Chrysler LLC.
 USA
 Paper Number 09-0453

ABSTRACT

AHOF400 estimates the average height, from the ground, of the interacting force between a vehicle and the barrier in a rigid barrier crash test. Similarly, KW400 estimates the “stiffness” derived from the force-crush relationship corresponding to a vehicle crashing into a ridge barrier. Both metrics are calculated during the first 400 mm of crush. Although, the formulas for calculating both AHOF400 and KW400 appear simple, the reproducibility for these two measures has not been determined. One area of concern is variations in numerical methodology, signal processing algorithms and/or labs can lead to different results: numerical issues such as, determining time zero of a signal may increase lab to lab variability. In addition, AHOF400 and KW400 may not be the invariants of the system: they may be velocity dependent.

INTRODUCTION

As a part of NHTSA’s compatibility program [1-4], there was an attempt to measure the Average Height Of Force, AHOF. The height of force was defined as [5-6]

$$HOF(t) = \frac{\sum_{i=1}^{i=n} Fi(t) * Hi}{\sum_{i=1}^{i=n} Fi(t)} \quad (1).$$

Where, $Fi(t)$ was the i -th load cell force and Hi was the height of the corresponding load cell. AHOF(t) was obtained by averaging the HOF(t) from the weighting function of total force $F(t)$,

$$AHOF(t) = \frac{\sum_0^t HOF(t) * F(t)}{\sum_0^t F(t)} \quad (2).$$

The summation of HOF to produce AHOF was initiated when the total force exceeded 50kN (Eq2). An alternative of AHOF was introduced in [7]. Instead of using $F(t)$ in Eq1 and Eq2, $F(d)$ was used to obtain the height of force and averaged height of force, where d was the displacement of a vehicle (vehicle crush). The average height of force delivered by a vehicle in the first 400 mm of crush, AHOF400 was formulated as:

$$HOF(d) = \frac{\sum_{i=1}^{i=n} Fi(d) * Hi}{\sum_{i=1}^{i=n} Fi(d)} \quad (3).$$

$$AHOF400 = \frac{\sum_{d=25mm}^{d=400mm} HOF(d) * F(d)}{\sum_{d=25mm}^{d=400mm} F(d)} \quad (4).$$

In addition to the AHOF400, the “stiffness” metric KW400 was used in the analysis in [7]. KW400, defined in [8], was

$$KW400 = \frac{2 \int_{25mm}^{400mm} F(d) dd}{(400^2 - 25^2)} \quad (5).$$

In the analysis presented below, Eq4 and Eq5 were used to calculate AHOF400 and KW400 for the 16 tests presented in the paper by Patel et. al.[7], as well as other NHTSA’s NCAP and FMVSS208 tests[9]. The objective of this study is to understand and investigate the reproducibility of AHOF400 and KW400 and to determine in a qualitative way how these two metrics vary as a function of signal processing and computation methods, usage of different software, and other relevant variables.

METHOD

$HOF(d)$, $AHOF400$ and $KW400$ defined in Eq3 to Eq5 and in [7] were used in this study. The calculation of $AHOF400$ and $KW400$ involves obtaining forces and crush (displacements of the undeformed part of the vehicle during impact) from a full frontal rigid barrier impact. Crush time history data used in this study were obtained from the accelerometers on the left and right rear sills or rear seat brackets. Displacement (d) was obtained by double integrating the acceleration data starting from the initiation of impact (time zero). Total impact force was the sum of all individual load cell data obtained from the rigid barrier. The force was filtered according to SAEJ211. In some cases, in the NHTSA database, the force, the acceleration or both are not aligned with the recorded time zero and either or both may have to be shifted (time-shifted) to bring them into alignment. The Software Matlab® (product of The MathWorks Company) was used for most of the calculations.

RESULTS

In this section, the treatment of the available data and calculation of $AHOF400$ and $KW400$ using the methodology described above will be presented and discussed.

Reproducibility of $AHOF400$ and $KW400$

A comparison of the calculated $AHOF400$ and $KW400$ between the present study and Ref [7] for 16 reported NCAP (New Car Assessment Program) tests from NHTSA's crash test data base is presented in Figures 1 and 2, and in Table 1 below.

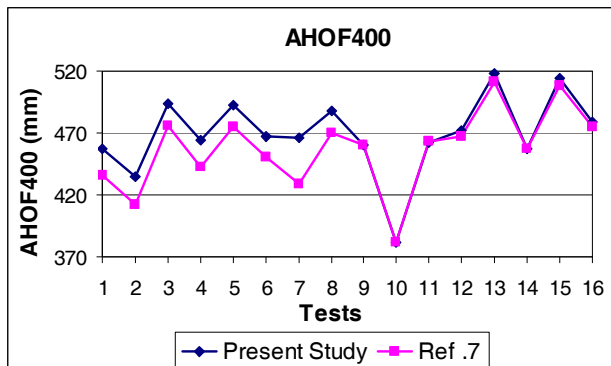


Figure 1. Comparison of $AHOF400$

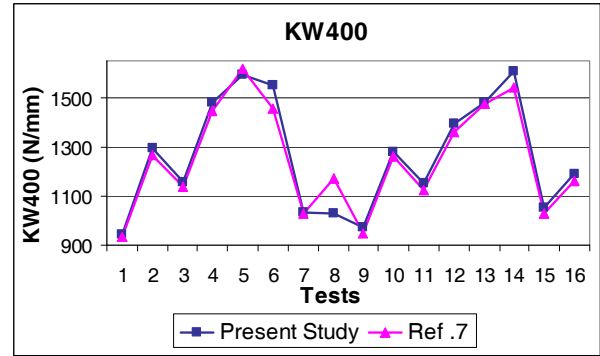


Figure 2. Comparison of $KW400$

These 16 tests can be divided into two sets of 8 tests. The two sets are identical in the aspect that they consist of vehicles of the same make and model. The set of the first 8 tests consists of full frontal barrier impacts using either a 30 or a 36 load cell flat wall. The last 8 tests utilized the same make and model vehicles in impact tests using either a 132 or a 134, or a 128 load cell flat wall [6]. The same time-shifting presented in [7] was applied. The data were processed and the results were obtained by using routines developed in MATLAB®.

A total of four types of load cell walls were used in the 16 tests. The configuration of those different types of walls is shown in Appendix A. In the first set of 8 tests, 1 through 8 in Table 1, there were two different types of load cell walls, as shown in Figures A1 and A2 (Appendix A). The second set, 9 through 16 in Table 1, used two types of load cell walls. One was a nine row barrier, with two different ground heights (from the ground to the bottom of the first row of load cells) and slightly different top row configuration , as shown in Figures A3 and A4 (Appendix A). The other was an eight row barrier, as shown in Figure A5 (Appendix). It should be noted that: the ground height and the size of the load cells and the heights to the top of the load cell wall for the four types of load cell walls are different. The total heights covered by the two rows, four rows, two of the nine rows walls, and the eight rows are 1378mm, 1050mm, 1205, 1255mm, and 1130mm, respectively. These differences result in significant differences to the heights of the center of individual load cells.

The numbers (x-axis, 1-16) in Figures 1 and 2 are the corresponding numbers in Table 1. The percentage difference p between two numbers, a and b , in the Table 1 was calculated using the equation,

$$p = \frac{a - b}{\left(\frac{a + b}{2}\right)} \times 100 \quad (6).$$

The following were observed from those results:

- *AHOF400* results of the first 8 tests differ from the corresponding results published in [7], with the range of difference from 4% to 8%.
- *AHOF400* results from the last 8 tests differ from the published results [7], with the difference no larger than 1.4%.
- *KW400* values differ from the published values [7], with the range of difference from 1% to 13%.

Table 1 –Differences of *AHOF400* and *KW400*

Number	Test No	AHOF400 (Ref. 7) (mm)	AHOF400 (Present Study) (mm)	AHOF400 difference	KW400 (Ref. 7) (N/mm)	KW400 (Present Study) (N/mm)	KW 400 difference
1	4216	436	457	5%	934	942	1%
2	3456	412	435	5%	1265	1296	2%
3	4936	476	494	4%	1137	1156	2%
4	4463	443	464	5%	1448	1477	2%
5	4472	475	493	4%	1619	1593	2%
6	5273	450	467	4%	1456	1548	6%
7	4485	429	466	8%	1027	1031	0%
8	2997	470	488	4%	1172	1029	13%
9	5712	460	460	0%	947	970	2%
10	5710	382	382	0%	1261	1279	1%
11	5713	463	462	0%	1124	1151	2%
12	5144	467	472	1%	1360	1396	3%
13	5711	511	518	1%	1472	1478	0%
14	5714	457	457	0%	1542	1607	4%
15	5062	508	514	1%	1027	1051	2%
16	4990	475	479	1%	1163	1190	2%

Analysis of Numerical Variation

Some factors that could affect the *AHOF400* and *KW400* results are: filtering, resultant total barrier force calculation, integration of the acceleration data, the software used, time shifted, zeroing, and the load cell height information used.

Filtering

The effects of different SAE filters have been investigated in this study using Hypergraph® (a product from Altair Engineering Inc.). Two Hypergraph® built-in filters, SAE60 and SAE (J211) ISO6487 Padding CFC60 were evaluated. Figure 3 shows that different peak values were observed even when the “same” SAE class 60 were used. The difference is about 2%.

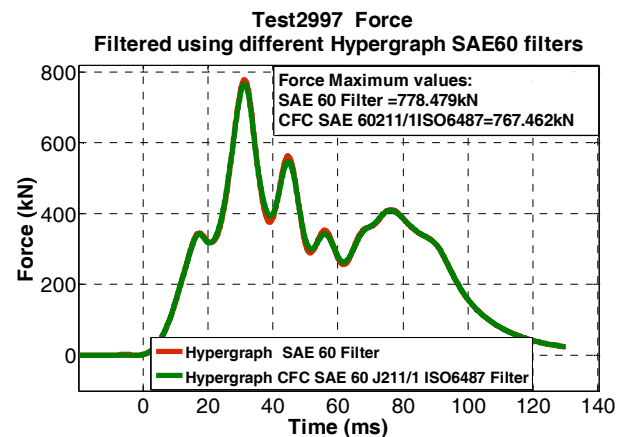


Figure 3. Comparison of Filtering

In general, filtering is shown to have minimal impact due to the fact that only the force signal for the

AHOF400 and *KW400* is affected by filtering and that the force is not directly used in the calculations. *AHOF400* is the result of a force summation process, effectively integration, and *KW400* is obtained from integration of the force and acceleration. Hence unfiltered and filtered signals have for all practical purposes the same integral values.

Software

It was observed that NHTSA has multiple data formats in the database that can be downloaded for use with different software. Two formats/software were used to calculate *AHOF400* and *KW400*. The two softwares were Hypergraph® and Matlab®. The results of *AHOF400* and *KW400* from these two softwares are presented in Table 2. Comparison of those two sets of results indicated that there was no significant difference from using the two softwares. The maximum difference for *AHOF400* is about 2mm, which is about 0.4%. The maximum difference for *KW400* is 5N/mm, which is about 0.5%.

Table 2 – Comparison of Result from Matlab and Hypergraph

Test No.	AHOF400 (mm)		KW400 (N/mm)	
	Matlab	Hypergraph	Matlab	Hypergraph
4216	457	457	942	941
3456	435	434	1296	1297
4936	494	494	1156	1153
4463	464	464	1477	1477
4472	493	493	1593	1592
5273	467	468	1548	1548
4485	466	466	1031	1028
2997	488	488	1029	1025
5712	460	460	970	970
5710	382	380	1279	1283
5713	462	463	1151	1150
5144	472	472	1396	1394
5711	518	518	1478	1473
5714	457	458	1607	1606
5062	514	514	1051	1046
4990	479	478	1190	1185

Influence of Signal “Zero”

The influence of aligning the beginning of the signals, time-zero, is investigated in what follows. It is possible that not all of the conventions used for the time-shifting in Ref. [7] are consistent with what was used in their calculations. It was noted that if the sign of the shifted time is reversed for the test No. 8, v2997, the difference of *KW400* between the two calculations will be as low as 0.3%, instead of 13% as listed in the Table 1.

Figure 4 illustrates that slight alternatives in the FD curve as a consequence of time-shifted change the integration results and the corresponding *KW400* values. The differences in the *KW400* could be as much as 13% between shifted force time-history by 2ms and un-shifted force time-history (orange and blue curves in the Figure 3).

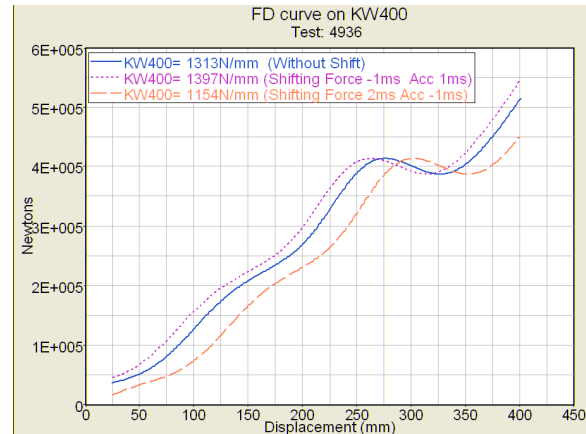


Figure 4. KW400 Sensitive to the Signal Shift

In what follows, *KW400* and *AHOF400* values are calculated using various time-shifts of the force and acceleration time-histories at given intervals prior to the construction of the FD curves. Figures 5 to 8 and Tables 3 to 4 present the influence of the time shift to the *KW400* and *AHOF400*. Applied time-shifts to acceleration and force data were from -2ms to 2 ms, where positive shift represents the movement of the signal from left to right and *vice versa*. Figures 5 and 6 represent the change of *KW400* and *AHOF400* versus time-shifts in force time-histories with zero acceleration time-shift. For other non-zero acceleration times-shifted, the same trends were observed. Figures 7 and 8 represent general trends for

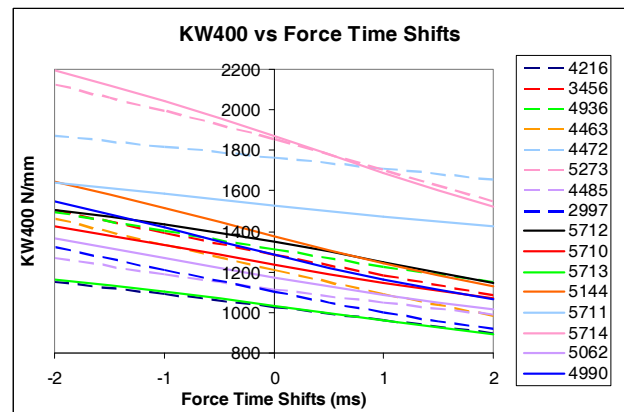


Figure 5. The Influence of Force Signal Shift to KW400

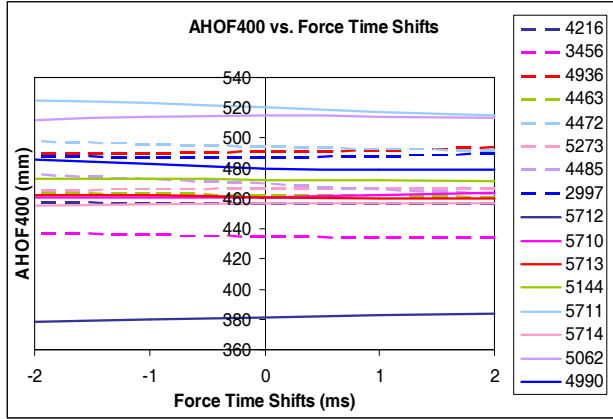


Figure 6. The Influence of Force Signal Shift to AHOF400

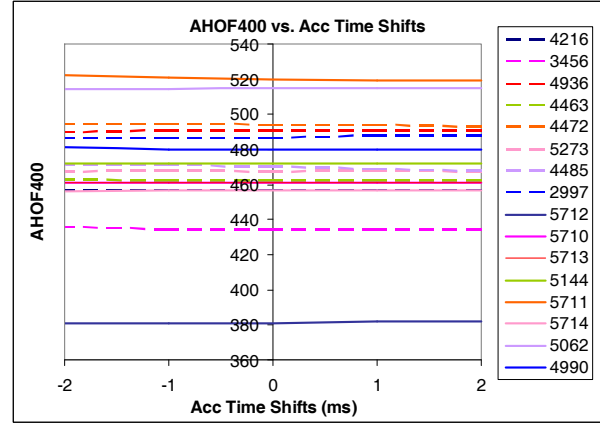


Figure 8. The Influence of Acceleration Signal Shift to AHOF400

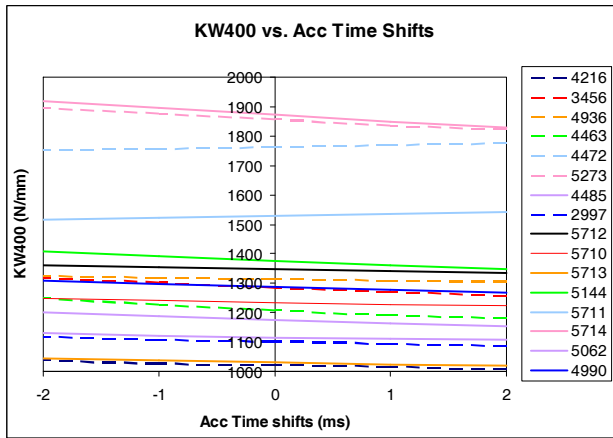


Figure 7. The Influence of Acceleration Signal Shift to KW400

the change of KW400 and AHOF400 versus the time-shifts in acceleration time-histories while the force time-shift was set to zero.

For all the 16 tests investigated, it is observed that:

- Shifting force signals to the left in time (negative shifts) results in increased KW400 values. A shift to the right results in a reduction of KW400. The change could be as much as 10% as shown in Figure 13, test v5714, with 1 ms force signal shift.
- Acceleration time-shifting does not influence KW400 as much as that from force shifts. The changes range from 0.6% to 2% for each 1 ms acceleration signal shift.
- AHOF400 does not show any significant change with time-shifting in either force signal or acceleration signal.

As an example, the KW400 and AHOF400 values from test v5711 are presented in Tables 3 and 4. Using the same equation (Eq1) as used in Table 1, the percentage differences in the table were calculated with a zero shift as the baseline. AHOF400 is found to be less sensitive to the time-shifting than KW400. The maximum change in AHOF400 is about 1.2%, vs. about 8.3% in KW400 for the shift range from -2ms to 2ms.

Table 3 – KW400 Versus Force and Acceleration Signal Shift

VC5711	KW 400	Acc Shift				
		2 ms	1 ms	0 ms	-1 ms	-2 ms
Force Shift	2 ms	-6.14%	-6.63%	-7.12%	-7.68%	-8.25%
	1 ms	-2.52%	-3.06%	-3.60%	-4.14%	-4.76%
	0 ms	0.91%	0.46%	0.00% (1528N/mm)	-0.46%	-0.92%
	-1 ms	4.35%	4.04%	3.66%	3.35%	3.09%
	-2 ms	7.56%	7.37%	7.19%	7.01%	6.89%

Table 4 – AHOF400 Versus Force and Acceleration Signal Shift

VC5711	AHOF 400	Acc Shift				
		2 ms	1 ms	0 ms	-1 ms	-2 ms
Force Shift	2 ms	-1.16%	-1.16%	-0.97%	-0.77%	-0.58%
	1 ms	-0.77%	-0.58%	-0.58%	-0.39%	-0.19%
	0 ms	-0.19%	-0.19%	0.00% (520mm)	0.19%	0.38%
	-1 ms	0.19%	0.38%	0.58%	0.58%	0.77%
	-2 ms	0.77%	0.77%	0.96%	1.15%	1.15%

A manual method similar to what was used in Ref. [7] was utilized to find “zero” in this study. This was done without checking the values in Ref [7] first to avoid bias. Table 5 shows the time-shifts comparison of this study and Ref. [7]. The difference ranges from 0 to 1.7ms, with the RMS (Root Mean Square) about 0.8 ms.

Table 5 – Time-Shifts (ms) Comparison

Test No.	This Study	Ref. [7]
4216	1.5	1.3
3456	-0.9	-0.1
4936	1.5	1.9
4463	-3.1	-2.1
4472	2.7	3.1
5273	1	2
4485	0.2	1.3
2997	0	0.75
5712	0.5	0.9
5710	0	0.7
5713	1	1
5144	0	-0.15
5711	0.3	1
5714	0.5	1.5
5062	-0.2	1.5
4990	0.1	0.8

Effects of Load Cell Height on AHOF400

An almost constant difference of the AHOF400 between this study and Ref. [7] was observed for the first 8 tests. If the AHOF400 values from this study are reduced by 18mm for the first 8 tests, the differences between the two calculations will be in the range of 0% to 4%, instead of 4% to 8% reported in Table 1. The 18mm was determined by minimizing the difference, in a least square sense, of the two calculations. One possibility is that the load cell height from the test report is different from what was

used in [7]. If this is correct, then the 18mm difference could be explained. Otherwise, it is unclear what has caused the differences.

An estimation of errors in AHOF400 induced possibly by inaccurate height information was performed. For a *m*-rowed load cell with the height of each load cell row *H_c* and the ground height of the load cell wall *H_g*, HOF from Eq3 can also be expressed in the following form,

$$HOF = H_g + \frac{H_c}{F} \sum_1^m F_i * (i - \frac{1}{2}) \quad (7).$$

Where *F* is the total barrier force and *F_i* is the force in the *i*-th row.

Based on Eq7, any error in the ground height, *H_g*, will be added onto the HOF, and then AHOF400 directly. The effect of the error in a load cell height *H_c* is roughly estimated in the following example. Figure 9 shows the load cell force from a four row

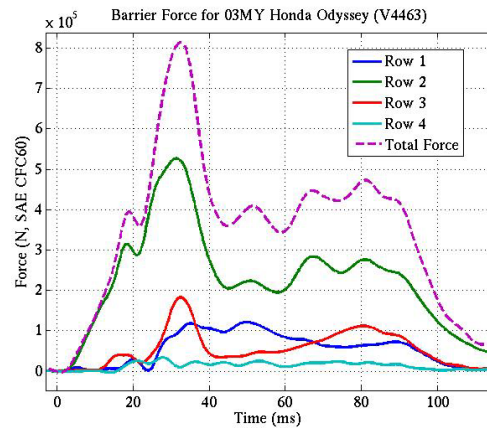


Figure 9. – Barrie Force from Each Load Cell Row in Test v4463

load cell wall test. If the forces distributed among the four load cell rows are approximately 10%, 60%, 25%, and 5% of the total barrier force F before 30ms, which is typically when 400mm displacement occurred, respectively, then approximately, $\Delta HOF = 1.8\Delta Hc$.

To get an estimate, it is further assumed that ΔHc is 10% of load cell height, i.e., approximately 10% of 250mm (which is typical for the barrier in many of the current test labs). Then the estimated error migrated from HOF to $AHOF400$ could be as high as 46mm, which is about 10%.

Analysis of Experimental Variation

In this section, the effects from two variables on the $AHOF400$ were examined. One variable is the vehicle impact speed, and the other is the test to test variation from a pair of repeat tests.

Influence of Impact Speed to $AHOF400$

$AHOF400$ is a measure of the "Average height of force" of a vehicle. The characteristic of this metric is anticipated to be mainly dependent on the characteristics of the vehicle. A preliminary investigation on the influence of impact speeds to $AHOF400$ is also included in this study. $AHOF400$ s for three different vehicles, at two different impact speeds (30 and 35 mph), were calculated and shown in Figure 10. The percentage differences from those results are 8%, 3% and less than 1% respectively, with the $AHOF400$ from 35 mph impact always equal to or greater than those from the 30 mph impact. In addition, one other speed comparison (25, 30 mph) is also presented with the difference being -6%. The 25 to 30mph relationship is opposite to that of the 35mph to 30 mph in that the $AHOF400$ is higher for the lower speed.

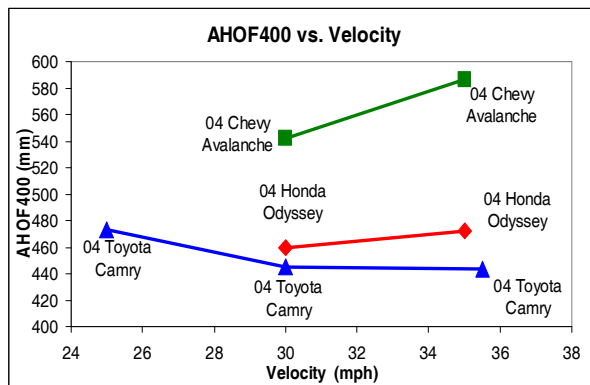


Figure 10. The Influence of Impact Speed to $AHOF400$

The FD curves from those tests are presented in Figure 11. In most of the comparison of the same vehicle at different impact speeds, the total forces in the range of 0 to 400mm are significantly different, which suggests that the barrier forces are dependent on the impact speed. The energy absorbed in the first 400 mm of displacement is presented in Table 6. In general, the higher the speed the greater the energy absorbed in the first 400 mm. The data is not entirely consistent with this relationship. In one test set, test 5216 at 30 mph and test 5071 at 25 mph, the energy absorbed in the first 400 mm is almost the same. In another test set, test 5144 at 35 mph and test 5212 at 30 mph, the energy absorbed in the first 400 mm is higher, about 4%, for the lower speed.

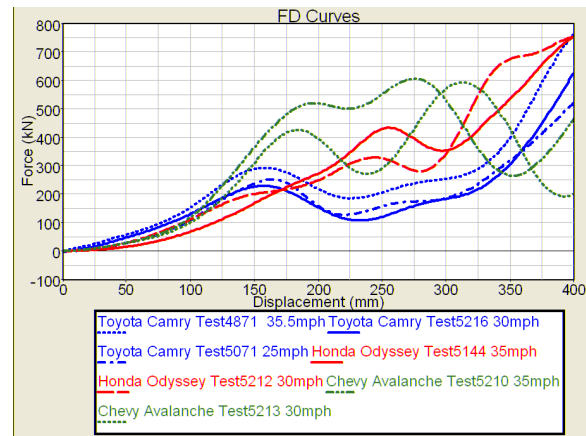


Figure 11. Force-Displacement Curves

Table 6 – Integral from FD Curve in Figure 11

Vehicle	Test No	Velocity (mph)	Integral kN*mm
Toyota Camry	4871	35.5	96891.587
Toyota Camry	5216	30	72348.884
Toyota Camry	5071	25	71919.591
Honda Odyssey	5144	35	110088.569
Honda Odyssey	5212	30	114893.049
Chevy Avalanche	5210	35	128944.091
Chevy Avalanche	5213	30	110257.985

On the other hand, the difference in the height of the individual load cells, the barrier used for the 25mph test (test 5071) in Figure 10 was a two row load cell wall, while for the 30 mph test (test 5216) was a four row load cell wall, could cause significant errors in $AHOF400$, as analyzed in the previous section. Due to the limited availability of load cell data additional analysis was not possible; therefore, from these results it is unclear if there is a trend or not. If in fact the 25 mph impact has a "true" $AHOF400$ value higher than that from the 30 mph impact then this

indicates that $AHOF400$ might be influenced by the impact speed but in a complicated way.

None the less it is also possible that because of the small sample size this could be the effect of test variability and not the effect of impact speed.

Effects of the Experimental Variation on $AHOF400$

The effect of the test variation in barrier force measurement was examined qualitatively in the following: The force in the k -th row is assumed to have an increased ΔF in one of the two repeat tests. Using the same notation from above section, and Eq7, the difference in HOF between those two repeats will be

$$\Delta HOF = \frac{Hc\Delta F}{(F + \Delta F)F} \sum_1^m Fi * (k - i) \quad (9).$$

It is observed from Eq9 that, typically, if k is above the middle of the load cell wall, the HOF will increase or decrease with the increase or decrease of ΔF correspondingly, and *vice versa*.

A random distribution of Fi and k were used to estimate the change of HOF for a four row load cell wall. It was found the change of $\Delta HOF / HOF$, on average, is $0.3 * \Delta F / F$, but in some cases, it could be as much as $1.1 * \Delta F / F$ assuming that the forces in both the top and the bottom rows are no larger than 10% of the total force F .

To qualitatively illustrate the effect of test variation on $AHOF400$, an example of two 30mph repeat tests was used. The barrier force distribution from those two tests, V4646 and V4714, with the $AHOF400$ values 503mm and 522mm (about 4% difference) respectively are presented in Figure 12. The solid lines in the figure represent the load cell forces at each row, A, B, C, and D (which is corresponding to 1,2,3, and 4 in the notation above) for test V4646, and the dashed lines are for test V4714. While the forces in the third and the fourth rows are similar for the two tests, the forces in first and second rows from test V4646 are greater than those from test V4714.

The difference in row 2 (row B) is about 12% of total force, and 5% in row 1 (row A), on an average sense as shown in Figure 13. A difference in HOF and possible $AHOF400$ between those two repeat tests is estimated to be around 5% by assuming

$\Delta HOF / HOF$ is about $0.3 * \Delta F / F$ for this case.

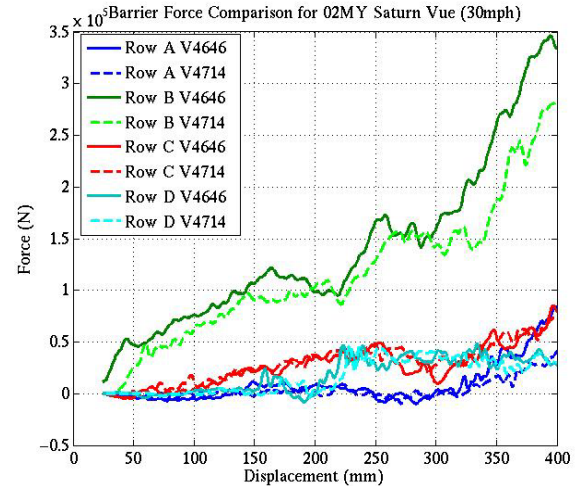


Figure 12. Overlay of Barrie Force from Each Load Cell Row

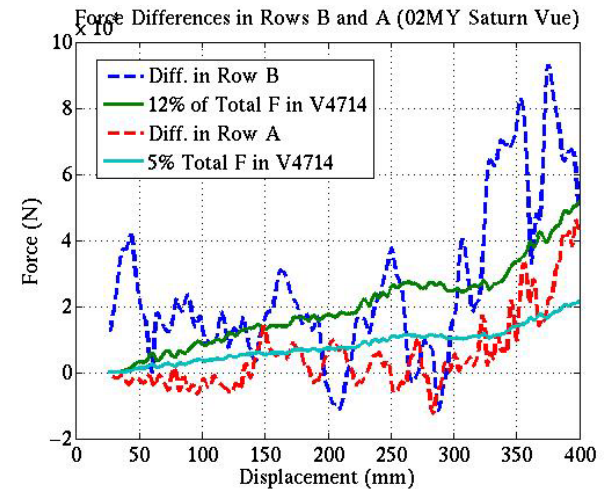


Figure 13. Differences in Barrie Force

DISCUSSION

In many of the tests in the NHTSA database the defined time zero does not coincide with the force and/or acceleration time zero, rather, they can be different by as much as 4ms. Therefore, for both force and acceleration signals, a “true” time zero is needed that can be used in the calculations. This is important because $KW400$ is found to vary significantly with the determination of time zero (time-shift), which is consistent with [7].

In both this study and in [7] time-zero was obtained subjectively. Comparisons of this study and [7] indicate that $KW400$ could differ by as much as 20% because of subjective determination of time-zero. For the purposes of reproducibility, it will be desirable to obtain the “true” signal zero by an objective method.

Typically, in a given signal, there is a certain level of noise before time-zero of the transducer time history. This may limit the ability to determine the “true” time-zero. Consequently, improvements in signal to noise ratio of the force time histories of the barrier load cells may be needed before accurate *KW400* estimation can be made. On the other hand, the “noise” in the test signals may be due to the disturbance of the impact that produces a signal that may not lend itself to objective determination.

It is unclear why there is a need for the perceived re-determining time-zero. One possible reason for re-definition of zeros could be that the contact switch did not work correctly. However, at the initiation of impact, the force and deflection may not start at the same time: re-determining time-zero should not be done. Neither of these can be easily justified.

Another observation from this preliminary study is that *AHOF400* may vary with impact speeds for some vehicles. The hypothesis is that the body materials may be rate sensitive or the number of structural components engaged during the impact varies as the crash progresses and interact differently. Therefore, the “damping” characteristic of the vehicle structure is different which will result in a different load distribution pattern. Detailed analysis on how vehicle structure changes at different impact speed is beyond this study. If *AHOF400* changes with impact speeds, it would be interesting to know whether this has any real world significance.

CONCLUSIONS

This is a limited study on the analysis of possible sources to impediments of reproducibility of *AHOF400* and *KW400*. The results indicate that the determination of the starting time of the signals (time zero) for the different transducers could affect *KW400* values significantly. For some vehicles, it seems that *AHOF400* is dependent on impact speed. In addition, some differences observed in *AHOF400*s could be attributed to inconsistent reporting of barrier information, or experimental variations.

In this study no effort has been made to determine the utility of *AHOF400* and *KW400*, they may only be a scientific curiosity. None the less, regardless of their utility more research would be needed if it becomes necessary to understand the reproducibility of *AHOF400* and *KW400*.

REFERENCES

[1]: Hollowell, W.T. and Gabler, H.C, "NHTSA's

Vehicle Aggressivity and Compatibility Research Program", Proceedings of the Fifteenth International Conference on Enhanced Safety of Vehicles, Paper No. 96-S4-O-01. Melbourne, Australia. May 1996.

[2]: Gabler, H.C and Hollowell, W.T., "NHTSA's Vehicle Aggressivity and Compatibility Research Program", Proceedings of the Sixteenth International Conference on Enhanced Safety of Vehicles, Paper No. 98-S3-O-01, Windsor, Canada. June 1998.

[3]: Hans C. Joksch, University of Michigan Transportation Institute, "Fatality Risk in Collisions Between Cars and Light Trucks" Report, September 1998.

[4]: Hans C. Joksch, University of Michigan Transportation Institute, "Vehicle Design versus Aggressivity", Report, DOT HS 809 194. April 2000.

[5]: Stephen Summers, Alope Prasad, William T. Hollowell, "NHTSA's Compatibility Research Program Update", Society of Automotive Engineers Paper No. 2001-01-1167 March 2001.

[6]: Stephen Summers, Alope, Prasad, "NHTSA Recent Compatibility Program", NAHTS, Proceedings of the Nineteenth International Conference on Enhanced Safety of Vehicles, Paper No. 05-0278, 2005.

[7]: Patel, S., Simith, D, and Prasad, A., Mohan, P., "NHTSA Recent Vehicle Crash Test Program on Compatibility in Front-to-Front Impacts", Proceedings of the Twentieth International Conference on Enhanced Safety of Vehicles, Paper No. 07-0231, 2007.

[8]: Nusholtz, G.S., Xu,L., Shi, Y, and L.D. Domenico, "Vehicle Mass and Stiffness: Search for a Relationship," SAE Technical Paper No. 2004-01-1168, March, 2004

[9]: NHTSA Database Website:
<http://www.nhtsa.dot.gov/portal/site/nhtsa/menuitem.8027fe7cfb6e727568d07a30343c44cc/>

APPENDIX A

Load Cell Wall Configurations

This Appendix details the configurations of load cells on the rigid wall barriers which were used for the vehicle impact tests. The calculation of the *AHOF400* in this study was based on the heights shown in the Figures below.

Evaluating Vehicle Incompatibility Using Center of Velocity Change Methodology

Gowrishankar Srinivasan

URC Enterprises Inc.
United States of America

Joseph Kaniyanthra

National Highway Traffic Safety Administration
(Now retired and a principal of Active Safety Engineering)
United States of America
Paper# 09-0022

ABSTRACT

The concept of compatibility includes not only the safety of the occupants within the subject vehicle itself, but also the safety of occupants in other vehicles that are involved in the collision. The term self-protection describes the safety afforded to the occupants within a vehicle, while partner-protection describes the safety afforded to the occupants of the crash partner vehicle. Early research identified vehicle weight as having a critical but not exclusive role in defining crash outcomes. The geometry and vehicle stiffness or crush characteristics were also observed to play a significant role.

This study uses the New Car Assessment Program¹ (NCAP) frontal barrier test data to find a suitable metric to assess the effect of incompatibility in crashes involving light passenger vehicles. The number of drivers with AIS 3+ injuries in head on crashes between passenger car (PC) and light truck vehicle (LTV) is used to compute the effectiveness of the metric.

NCAP crash test data for 239 vehicles were used in calculating the value of “distance from ground to the center of velocity change”. Ten years of National Automotive Sampling System /crashworthiness data systems² (NASS/CDS) data were used to demonstrate the metric. The crash compatibility metric developed can be used to compare the number of injuries that result in PCs - LTVs head on crashes.

Most safety benefits can be achieved by changes in the metric, specifically, adjusting for vehicle size (height) and the structural characteristics (stiffness). Hence the metric can be used as a measure of compatibility in crashes between vehicles.

This study is limited to investigation of incompatibility in full head-on crashes. This paper

develops a new comprehensive metric that can quantify the compatibility disparity.

BACKGROUND

Throughout much of the 1980's and early 1990's National Highway Traffic Safety Administration's (NHTSA) compatibility research was focused on frontal and side impact safety and how the characteristics of the striking vehicle's front end affected the occupant survivability in the struck vehicle. The genesis of NHTSA's current program began in 1996 with studies investigating the changing vehicle mix in the US fleet and its effect on the vehicle compatibility problem. This problem is related to the introduction of a large number of sport utility, pick-ups (LTV) and minivans into the US fleet. This issue has a long history of research, but has recently received increased attention due to the changing mix of vehicles in the US fleet once again.

Over the last decade NHTSA has been vigorously pursuing some research activity to develop potential strategies to improve vehicle compatibility. Improving structural engagement characteristics in vehicle-to-vehicle crashes through establishment of an average height of force requirement energy management through front end stiffness and crush force parameter specifications, and even the development of a modified compatibility test barrier were all topics in NHTSA's research agenda that were pursued with some level of interest.

In December 2003, the Insurance Institute for Highway Safety³ (IIHS) facilitated a voluntary commitment from the automobile manufacturers through their trade associations, the Alliance and AIAM, to begin designing vehicles to enhance vehicle-to-vehicle crash compatibility. The voluntary agreement included commitments to enhance occupant self protection in front-to-side

crashes through improved head impact protection and design criteria to enhance partner protection in vehicles involved in front-to-front crashes by geometric matching of front structural components in cars and light trucks. This commitment required 100 percent of each participating manufacturers' vehicles to be designed according to the criteria specified for side impact protection and frontal impact protection by September 2009. The details of these commitments are available in a document originally submitted to the agency in December, 2003 and subsequently revised in November, 2005.

In 2006, IIHS completed an analysis of the safety benefits of the front-to-front Compatibility agreement. The Institute examined passenger-car driver death rates in two-vehicle crashes with light trucks. The light trucks were divided into two groups – those designs that met the front-to-front performance criteria and those that did not. The analyses used NHTSA's Fatality Analysis Reporting System (FARS) data for calendar years 2001-2004 involving model years 2000-2003 light trucks.

IIHS⁴ found that in front-to-front crashes involving light trucks into passenger cars, the passenger car driver was 16 percent less likely to be killed if struck by a sport utility vehicle (SUV) with a front-end design that met the compatibility performance criteria specified under the voluntary agreement. Similarly, the passenger car driver was 20 percent less likely to be killed if struck by a pickup truck with a front-end design that met the compatibility performance criteria. The overall reduction in passenger car driver deaths in front-to-front crashes involving both SUVs and pickup trucks was 19 percent.

In front-to-side crashes involving light trucks into passenger cars, the passenger car driver was found to be 30 percent less likely to be killed if struck by a SUV with a front-end design that met the front-to-front compatibility performance criteria. The passenger car driver was 10 percent less likely to be killed if struck by a pickup truck with a front-end design that met the front-to-front compatibility performance criteria. The overall reduction in passenger car driver deaths in front-to-side crashes involving both SUVs and pickup trucks was 19 percent.

METHODS

The analytical effort described in this paper is an attempt to find a suitable metric that could be used to assess front-to-front structural compatibility in vehicle-to-vehicle frontal crashes as well as in front-

to-side crashes. It was also important to determine the potential benefits if such a metric was used to make any or all vehicles in the fleet to be compatible.

NHTSA conducts 30 and 35mph frontal barrier impact tests under Federal Motor Vehicle Safety Standard (FMVSS) No.208, and the New Car Assessment Program (NCAP). These tests are assumed to represent NASS/CDS crash data where the principal direction of force, for the two vehicles involved, is in between 350 and 10 degrees. This study is an attempt to use the NCAP barrier test data to find a suitable metric to address the effect of incompatibility in crashes between passenger cars and light trucks. For this study crash test data for 239 passenger vehicles of model years 2000 - 2007 were used.

The load cell barrier, currently used in the NCAP tests, has a 36 load cell array arranged as a 4 rows and 9 columns matrix as shown in Figure 1

D1	D2	D3	D4	D5	D6	D7	D8	D9
C1	C2	C3	C4	C5	C6	C7	C8	C9
B1	B2	B3	B4	B5	B6	B7	B8	B9
A1	A2	A3	A4	A5	A6	A7	A8	A9

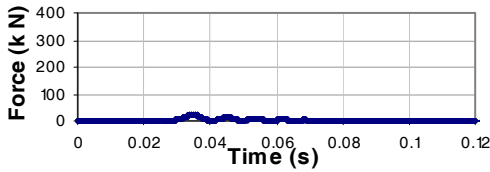
Figure 1: Barrier with 36 load cells used in the front barrier test.

The width of all the cells in the load cell barrier is 9 inches (229mm). While height of the bottom two rows (A&B) is 9 inches (229mm) each, the height of the top two rows (C&D) is 10.2 inches (259mm) each. The bottom edge of the barrier is 2.62 inches (66.67mm) above the ground. The data used in this study is collected from the time of impact until the vehicle velocity reaches zero.

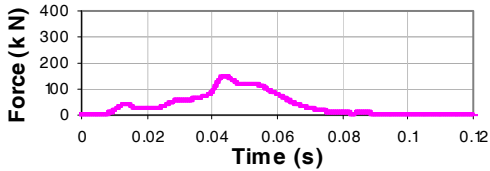
Derivation of Impulse Ratio

Time histories of forces acting on load cell rows A, B, C, and D during NCAP frontal barrier test for a compact car is shown in Figure 2. The area under the curve gives the impulse acting on each of the load cell rows A, B, C, and D (listed from bottom); their values are 2310.6, 17651.9, 4181.1, and 285.3 Newton second respectively. The sum of calculated impulses gives the total impulse acting on the barrier, for the selected example. The sum in this case is equal to 24429 Newton second.

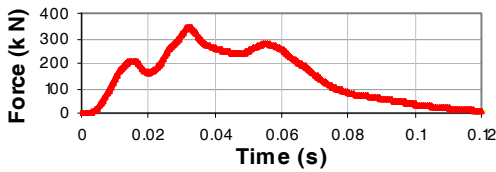
Row D



Row C



Row B



Row A

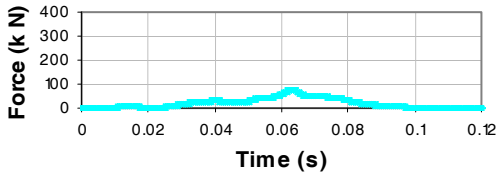


Figure 2: Force acting on the load cell rows from NCAP frontal barrier test for a compact passenger car

The row impulses are assumed to be acting on the center of each of the load cell rows A, B, C, and D. The distances from ground to the center of the load cell rows are 7.13 inches (181.2mm), 16.15 inches (410.2mm), 25.66 inches (651.7mm), and 35.66 inches (905.7mm), for load cell rows A, B, C, and D, respectively.

The ratio of impulse on load cell row A as a fraction of total impulse is given below:

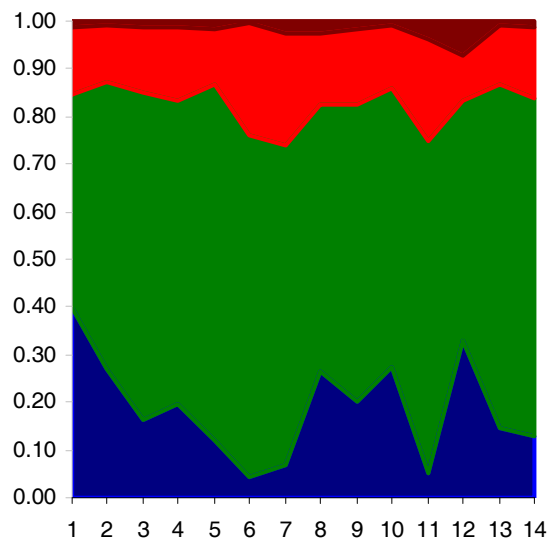
$$F_A = \frac{2310.6}{24429} = 0.09.$$

Similarly the ratio of impulse for each load cell row as a fraction of the total impulse for the compact passenger car example given above are 0.72, 0.17, and 0.01 for rows B, C, and D, respectively.

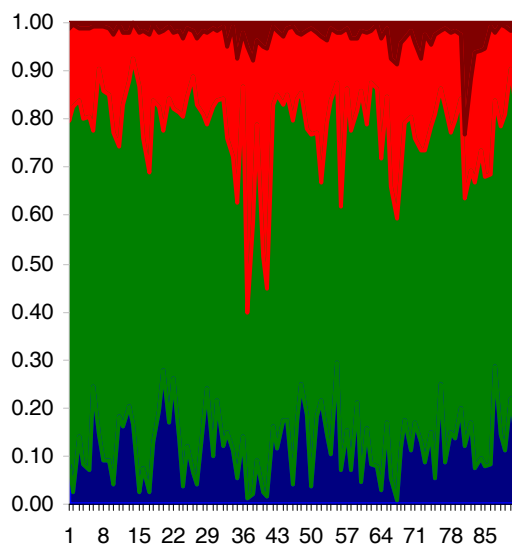
Similarly the ratio of impulse for each of the load cell rows as a fraction of the total impulse for each of the 239 NCAP barrier tested PCs and LTVs were calculated. The impulse ratios for the PCs and LTVs are grouped into three groups each by test weights for PCs and LTVs - less than 3000 lbs, 3000 to 4000 lbs and greater than 4000 lbs for PCs and less than 4000 lbs, 4000 to 5000 lbs and greater than 5000 lbs for LTVs. The distribution of the impulse ratios for each of the PC and LTV weight groups are shown in Figure 3. Impulse ratios are shown on the Y axis and the vehicles tested are shown on the X axis for each weight group.

The impulse data for each vehicle tested is presented row by row for the different weight groups in PCs and LTVs. In Figure 3 the blue region shows the impulse in load cell Row A as a fraction of the total impulse. Similarly the impulse ratios for Rows B, C, and D are given by the areas in green, red and dark red colors, respectively. The data in each graph is ordered by vehicle test weight. It can be inferred from the figure that a large portion of the impulse in PCs is in rows A and B (blue and green) compared to LTV's, especially in the heavier weight groups. But, the LTVs weighing greater than 4000 lbs show a significantly large area covered by red and dark red (rows C and D) in comparison to PCs, implying large and heavy LTVs have impulses acting on a higher plane from the ground relative to the PCs. This is not surprising because of the higher profile of the LTVs.

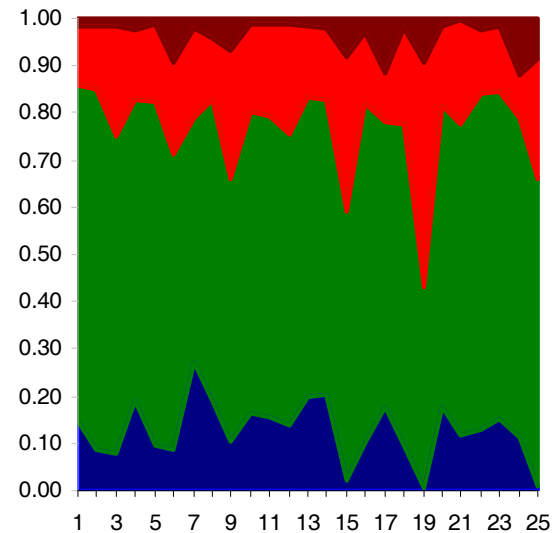
PC < 3000 lb



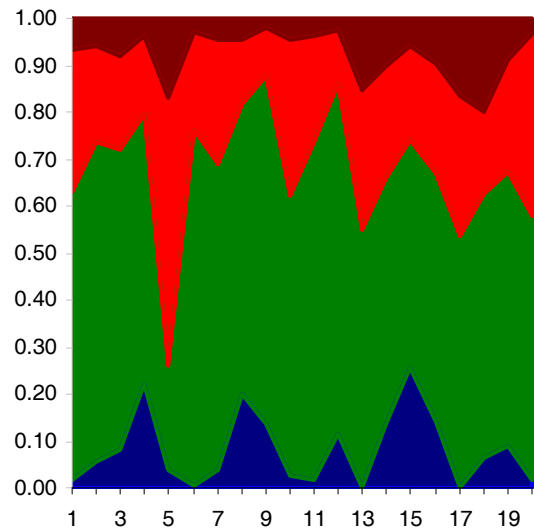
3000 < PC < 4000 lb



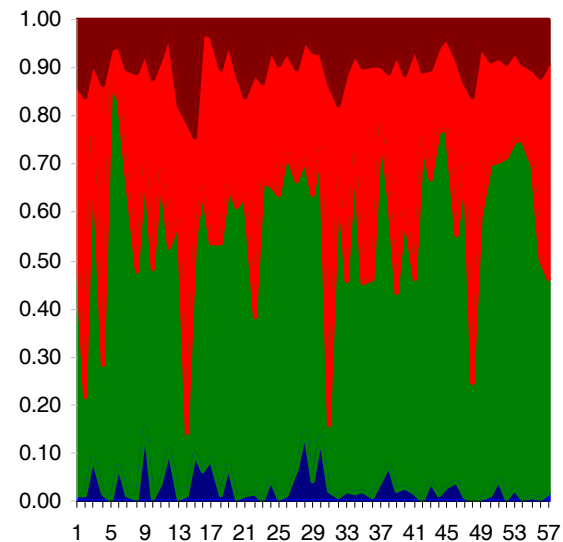
PC > 4000 lb



LT < 4000 lb



4000 < LT < 5000 lb



LT > 5000 lb

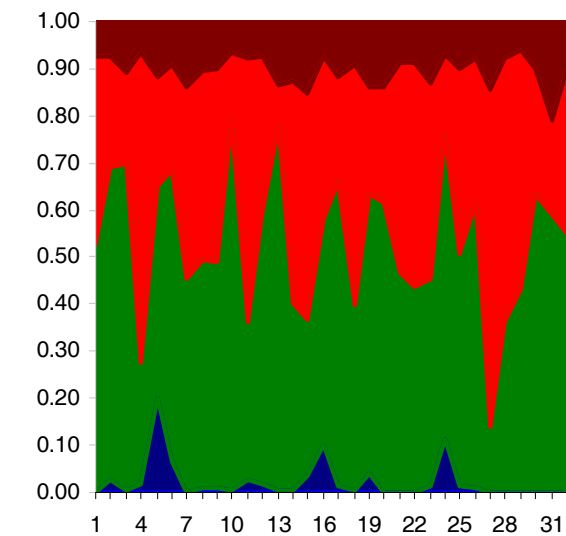


Figure 3, Distribution of Force during a Frontal Fixed Barrier Test

Derivation of a suitable metric from impulse to define compatibility

Impulse is defined as the integral of force with respect to time;

$$I = \int F \cdot dt,$$

where, ‘F’ is force and ‘dt’ is the time increment. I_A , the impulse on load cell row A is determined by $I_A = \int F_A \cdot dt_A$, and is equal to the area below the Force-Time curve for load cell row A in Figure 2. Similarly values for I_B , I_C , and I_D are determined. The time duration dt for each test theoretically starts at the time the test vehicle contacts the load cell barrier (time zero) and ends when the test vehicle velocity crosses zero as the vehicle starts to rebound from the barrier.

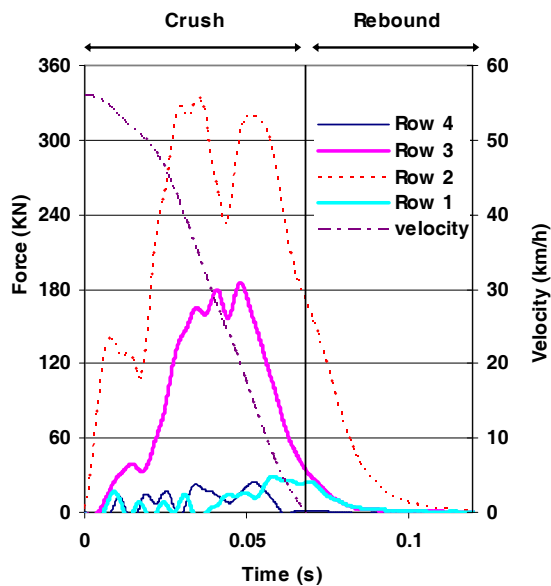


Figure 4, Forces acting on each load cell row along with vehicle velocity.

The total crash duration is made up of crush period, between time zero and the time when the velocity crosses zero and the rebound period as the vehicle bounces off of the barrier (Figure 4). In this study, the impulse is calculated only for the period up to the point of rebound because the load cell readings during the rebound are not consistent and the impulse contribution during rebound as a percent of the total is not significant as seen in Figure 4..

Since the time dt for each load cell row is influenced by the effective stiffness (geometric stiffness distribution) characteristic of the vehicle structure, it can be concluded that the calculated metric for compatibility using the impulse also reflects the effect of stiffness.

A suitable metric can now be derived using the impulse that could define the distinguishing compatibility characteristics of PCs and LTVs during a full frontal head-on crash. For the purpose of deriving this metric, a point located on the vehicle is defined as the center of velocity change. This point is assumed to be the point at which the total impulse I is concentrated as the vehicle contacts the load cell barrier. This point is projected on to the crash foot print on the barrier. It is located at a height X from the ground. The distance to this point defined as the “Center of Velocity Change”, can now be calculated as shown below:

$$I = \int F \cdot dt = \int d(mV) = m \int dv$$

Distance from the ground to the center of velocity change is:

$$X = \frac{I_A \cdot Z_A + I_B \cdot Z_B + I_C \cdot Z_C + I_D \cdot Z_D}{I_A + I_B + I_C + I_D}$$

Where:

- F = crash forces transferred to the barrier
- m = mass of the vehicle
- I_A, \dots = impulse acting on load cell row A, etc.
- Z_A, \dots = distance from ground to the midpoint of the row A, etc.

The ratio of impulse on each load cell row to the total impulse normalizes the effect of mass.

Substituting the values for impulse and its respective distances from the ground for each load cell row in the above equation, the value for X - “the distance from the ground to the center of velocity change”, is determined. The metric “X” is a single measure of height (distance from the ground) at which the net impulse of a vehicle will act during a fixed rigid load cell barrier crash. It can be considered to be the impulse ratio weighted average of the heights Z_1, Z_2, \dots etc. for each row.

For the example using the compact car data that was previously presented, the value X, is calculated to be 435.66 mm or 17.15 inches.

Ideally for compatible vehicle crashes involving passenger cars and LTVs, the value of X for light trucks should be similar to the value of X for passenger cars. This can be achieved by controlling one or both of the following variables: distance from the ground represented by Z_i and the impulse ratios. Since duration of force and level of force constitute the impulse, they can be varied to attain an optimum value for X by appropriate vehicle structural design.

Analysis based on breakdown of vehicle class by test weight

The distance, X, was calculated for all the 239 vehicles that were tested in frontal New Car Assessment Program (NCAP) barrier tests. The correlation between median vehicle test weights and Xs, for all the vehicles tested in NCAP frontal barrier tests were determined.

In this analysis, it was observed that there is a strong correlation between the calculated values of X and the test weights, even though the weights themselves do not enter directly into the calculation of X both in PCs and in the LTVs. However, it is also noted that the vehicles tested in NCAP are not designed for optimal value of X and therefore, the correlation noted above is only because the weights and size are the two most dominant parameters that are well correlated for the vehicles in the current fleet.

The calculated value of X is a reflection of parameters including stiffness and size, that exist in the fleet. However, vehicles that are optimized for the values of X may have better correlation not only to vehicle weights and size, but also to stiffness since other design variables such as the stiffness and geometry could be modified within certain limits to get the desired value of X in future fleets.

The following are the six steps involved in this analysis to obtain estimates of the potential benefits of optimizing the value of X. The first three steps relate to the computation of the compatibility metric X from NCAP data for relevant vehicle classes and calculation of relative injury risk for drivers in real world vehicle-to-vehicle frontal crashes. Steps four through six explain how the relative risks change as the value of X is varied. Step four provides a means to directly compare the relative risk in one class of vehicle as it interacts with all the other vehicle classes in real world crashes.

Step 1

The value of X was computed from 239 NCAP tests that belonged to different vehicle test weight groups. The weight groups in the NCAP data are used in the analysis of real world data.

Crash database NASS/CDS includes the variable, vehicle curb weight. Those weights were used to match the vehicle classes in the real world against the classes in the NCAP data. Ten years of real world crash data in NASS/CDS 1997- 2006, were used in this analysis to determine the injury risk based on the number of injured drivers in head-on crashes of different vehicle classes. The median values and the

average values of X along with the standard deviation are given in Table 1. Both are found to be close and using either of these values would be satisfactory.

Table 1 NCAP front barrier test vehicle classes and X values

Vehicle Class	Test weight range (lbs)	Estimated			Symbol
		Average X (in)	Standard Deviation	Median	
Compact Passenger Car	Less than 3,500	16.9	1.3	16.6	CPC
Full size Passenger Car	Greater than 3,500	17.7	1.6	17.2	FPC
Compact Light Truck vehicle	Less than 4500	20.1	2.4	19.8	CLTV
Large Light Truck Vehicle	Greater than 4500	20.9	1.7	20.7	LLTV

However, the median values of X determined for each vehicle class based on weights were used in this analysis. Since there were only a limited number of crash cases in the NASS/CDS data, the vehicle classes were collapsed into four classes as stated before - two classes of PCs and two of LTVs.

Step 2

Only two-vehicle, head-on crashes were selected as the target crash type from the NASS/CDS crash data as it is similar to the full frontal NCAP barrier tests. The head-on crash data include the crashes in which the frontal area of one vehicle impacts the frontal area of another. The vehicle body types selected are PCs, compact and large utility vehicles, and compact and large pick up trucks. NCAP crash test data for MY 2000-2007 were used in calculating the value of X that provided a direct measure of compatibility characteristics. In order to increase the number of cases available in the NASS/CDS database, all vehicle model years in the NASS/CDS database for ten years were included in the analysis. However, it is noted that the NCAP data used are for newer vehicles tested.

The number of injured drivers with AIS 3+ injuries is used as the outcome measure to calculate the effect of changes in the value of X. Only driver injuries are considered in this analysis to eliminate the errors that could result because of the varying occupancy rates in the vehicles involved.

Table 2 shows number of (un-weighted) drivers with and without AIS 3+ injuries in two vehicle head-on

crashes. The numbers in the upper half of each cell in Table 2 represents the number of injured or uninjured drivers of the subject vehicle, while the numbers in the lower half of each cell represents the number of injured or uninjured drivers in other vehicle. The other vehicle represents the principal other vehicle involved in two vehicle full head on crash with the subject vehicle.

For example, comparing crashes between full size passenger cars (FPC) and compact light truck vehicles (CLTV), it is seen in the un-weighted data (shown in bold for this example) that there are 43 AIS 3+ injured drivers in full size passenger cars. There are also 99 un-injured drivers in FPCs (subject vehicle) in towed vehicles in the database. In the same manner, there are 36 AIS 3+ injured and 108 uninjured drivers in CLTVs (other vehicle).

The uninjured data from Table 2 are not used in any further calculations because odds ratio comparisons could not be made with out knowing the exact count of uninjured drivers in each vehicle class.

Table 2: AIS 3+ Drivers injured in two vehicle head-on crashes in subject vehicles and other vehicles, NASS/CDS 1997 to 2006 (un-weighted).

Subject Vehicle Other Vehicle	Compact Passenger Car (CPC)		Full Size Passenger Car (FPC)		Compact Light Truck Vehicle (CLTV)		Large Light Truck Vehicle (LLTV)	
	Injured	Un-Injured	Injured	Un-Injured	Injured	Un-Injured	Injured	Un-Injured
Compact Passenger Car (CPC)	67	186						
Full Size Passenger Car (FPC)	96	224	23	61				
Compact Light Truck Vehicle (CLTV)	77	94	43	99	9	24		
Large Light Truck Vehicle (LLTV)	87	85	56	65	25	38	10	21

Table 3 gives the weighted number of injured drivers from the same data shown in Table 2, giving the number of injured drivers only.

Table 3 AIS 3+ Drivers Injured in two vehicle head-on crashes, CDS 1997 to 2006 weighted data.

Subject vehicle Other vehicle	Compact Passenger Car (CPC)	Full size Passenger Car (FPC)	Compact Light Truck Vehicle (CLTV)	Large Light Truck Vehicle (LLTV)
Compact Passenger Car (CPC)	5212			
Full size Passenger Car (FPC)	4908	1625		
Compact Light Truck Vehicle (CLTV)	7203	5696	1149	
Large Light Truck Vehicle (LLTV)	6904	3667	2222	959

Step 3

This step calculates relative driver injury risk in two vehicle full head on crash. From Table 2 it is seen that the number of drivers injured in certain vehicle class interactions are small in the ten years of un-weighted NASS/CDS data. In the case of the small number of injured drivers in Table 2, the affect of weighting on calculations of weighted data shown in Table 3 is not well understood. Hence, using weighted data in this analysis is likely to cause larger errors because of the discrepancy in certain weights and, therefore, it was considered desirable to use the un-weighted data. Therefore, the relative risk for drivers is calculated from the un-weighted data. However, for the purpose of estimating benefits, the target populations available from the weighted data were used.

The relative risk of AIS 3+ injuries to the driver using the un-weighted data in each of the above four vehicle groups is calculated and shown in Table 4. Table 4 gives the relative risk of driver injuries in the vehicles classified as the subject vehicle when involved in two vehicle head-on crashes with a vehicle type shown as the other vehicle.

The relative risk for a specific vehicle class is determined by calculating the ratio of number of drivers injured in subject vehicles to those injured in other classes. For example, the relative risk of AIS 3+ driver injury in a CLTV, when involved in a head-on crash with a CPC is 0.39. This is obtained by dividing the number of drivers injured in CLTV by the number injured in CPC (30/77). The inverse of

this number shows the relative risk of AIS 3+ driver injury in CPC when involved in a head-on crash with a CLTV (2.57). The relative risk is equal to 1 along the diagonal of the matrix in vehicle-vehicle interactions that involve vehicles belonging to the same class.

Table 4 Driver injury relative risks in two-vehicle head-on crashes (CDS 1997 - 2006 un-weighted data – Ratios of Injured)

Subject Vehicle \ Other vehicle	Compact Passenger Car (CPC)	Full size Passenger Car (FPC)	Compact Light Truck Vehicle (CLTV)	Large Light Truck Vehicle (LLTV)
Compact Passenger Car (CPC)	1.00	0.61	0.39	0.25
Full size Passenger Car (FPC)	1.63	1.00	0.84	0.41
Compact Light Truck Vehicle (CLTV)	2.57	1.19	1.00	0.56
Large Light Truck Vehicle (LLTV)	3.95	2.43	1.79	1.00

Step 4

The calculated relative risk, from step 3, for the interactions of each vehicle type is then plotted against the height of the center of velocity change X for each of the four vehicle classes. Figure 5 is a plot of the relative risk and the height of the center of velocity change, X in inches. Median value of X for each vehicle class is used in developing the curves.

These plots are the best fit curves based on the four data points that represent the relative risk of driver injuries in each vehicle class in its interaction with all the other vehicle classes. Exponential fit yielded the best correlations and hence is used in generating the curves given in Figure 5. The range of values of X for each class is different. The curves in Figure 5 are plotted using the full range of X and the relative risks as one class of vehicle interacts with other classes of vehicles including its own class. i.e., different curves for each vehicle class indicate the risks of various vehicle class interactions and its relationship to X.

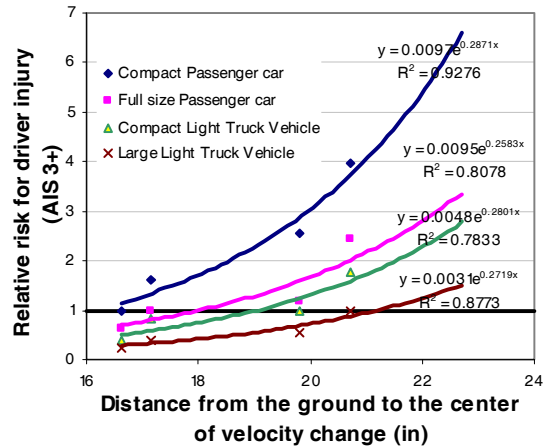


Figure 5: Relative risk vs distance X from the ground to the center of velocity change

Each of the curves for a specific vehicle class above shows the potential risk associated with frontal crashes involving a specific vehicle class and all the other vehicle classes.

For example, the top curve shows the risk of AIS 3+ injuries to compact passenger car drivers as they collide with vehicles in all the other classes. The values of X for the vehicle classes involved fall in a range of approximate 14 to 26 inches. The horizontal line showing a risk of 1.0 is the risk as a vehicle in a specific class collides with another vehicle of the same class. As expected, the curves plotted for each vehicle class is well correlated with the values of X as indicated by the R² values.

Step 5

The risk relationship between the subject vehicle and the other vehicle for PCs is shown in Figures 6 and 7. Figures 6 and 7 shows the change in risk with respect to X for CPC and FPC vehicle classes when they interact with all the other vehicle classes. As seen, when X for the other vehicle class increases, the risk of driver injury in subject vehicle increases. At the same time, the risk to drivers in the other vehicle class decreases. The intersection of the two curves indicates a risk of one. This point represents the risk to drivers in a specific vehicle class as they crash in to another vehicle class having same value for X.

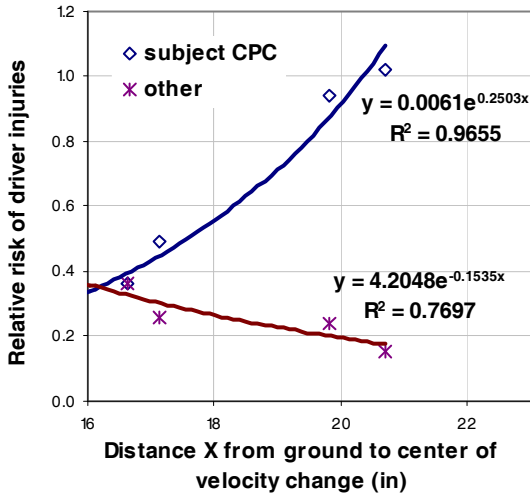


Figure 6 Relative risk for subject vehicle CPC (Using ratios of drivers injured)

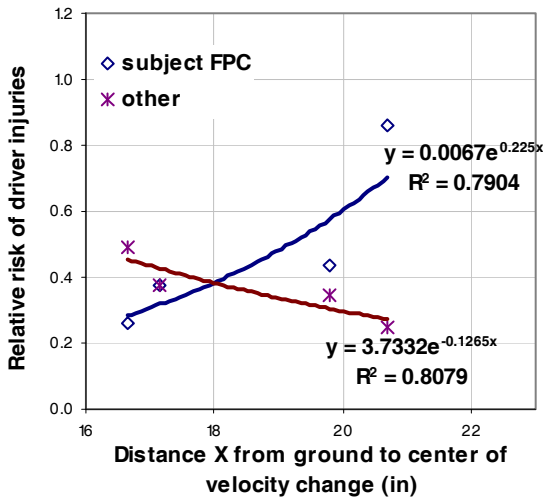


Figure 7 Relative risk for subject vehicle FPC (Using ratios of drivers injured)

Figures 8 and 9 are the same as described above, but, for CLTV and LLTV classes. From Figures 6 -9, it is clear that for PCs and LTVs, as the value of X for the other vehicles is increased, the risk to drivers in the subject vehicle increases, while the risk to drivers in the other vehicle decreases. These curves were generated based on risk calculations using the ratios of the number of injured drivers in pairs of interacting vehicle classes.

The pair of curves, shown in each of the Figures, 6, 7, 8, and 9, is the inverse of the other curve. Comparison of Figures 6 and 7, shows that the rate of increase of risk for subject vehicle CPC class is higher than increase in FPC for PCs. Similarly, for

CLTV and LLTV (Figures 8 and 9), the rate of increase in risk is smaller in comparison to the PCs (Figures 6 and 7).

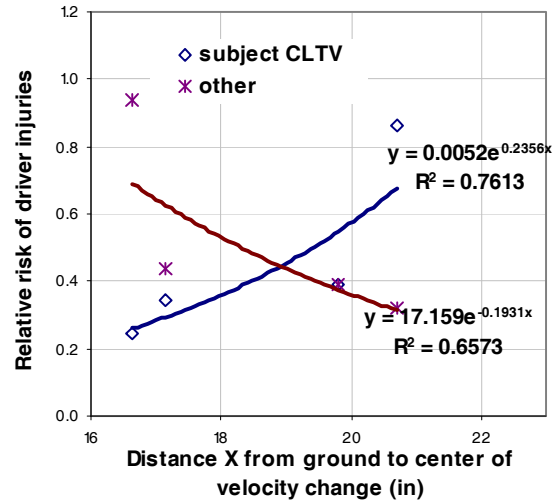


Figure 8 Relative risk for subject vehicle CLTV (Using ratios of drivers injured)

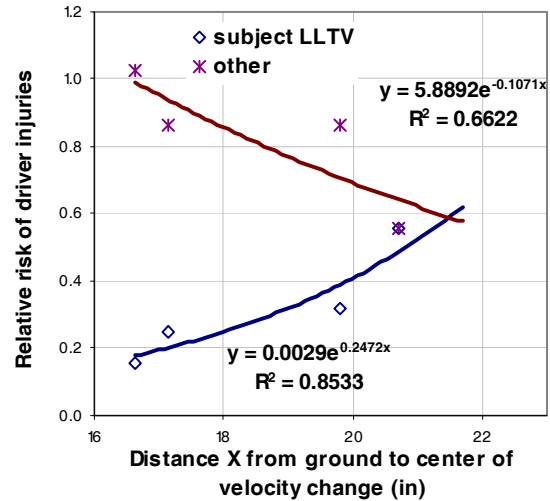


Figure 9 Relative risk for subject vehicle LLTV (Using ratios of drivers injured)

Step 6

In order understand the influence of X on injury risk a new curve for the subject vehicle could be plotted by changing the proportionality constant and the value of X in the exponent. This new curve will intersect with the curve representing the other vehicle classes. The point of intersection of the two curves defines the new risk and also specifies the value of X for the subject vehicle to make them more compatible with the other classes. Rather than changing the constants, it is easier to visualize the curve for other

vehicles remaining constant while the subject vehicle curve is allowed to intersect the curve for the other vehicles as X for the other vehicle class is varied. The risk associated with the intersection points for each value of X can now be compared to the original risk to compute the change in risk.

The change in risk at the new intersection point can now be computed as a fraction of the original risk. This fraction represents the effectiveness for making the subject vehicle class meet a specific value of X. This effectiveness when multiplied by the target population of the total number of injuries that occur in crashes involving a specific subject vehicle class and all other classes will approximate the potential benefits in the specific subject vehicle class.

It is noted that in this analysis, the target population used is all AIS 3+ injuries in a specific vehicle class. These include the injuries that are due to mass disparities as well as differences, possibly in the values of X. Since the target population cannot be split up to separately account for the effect of each variable on the injury outcome in crashes, the estimated benefits are likely to be higher than what may result from changing the value of X.

These steps can now be repeated for each vehicle class to approximate the benefits in each class for the subject vehicles and the other vehicles. As can be seen, when X is varied for one class of vehicles, the benefits that may result in one class may be negated by the negative-benefits for the other. The combined benefits when all vehicle classes are made to comply with specific values of X can be approximated by summing up the benefits and negative benefits obtained class by class.

It is noted that, in this methodology each vehicle class interaction is treated as unique and the benefits calculated are upper bounds, because of the few benefits that result from the double counting involved each time the benefits are computed for interactions of one class of vehicles with all the other classes. Correcting for this discrepancy was not attempted each time. Since only the net benefits are of interest, an estimate of the over prediction is made and the net benefits are expressed as a range.

Assumptions used in the benefit calculations

1. The vehicle classifications developed from the NCAP data are equivalent to the classifications obtained from the NASS/CDS data.
2. The X values computed from the newer vehicles in NCAP data are similar to those vehicles including the older models in the fleet.

3. Relative risks derived from driver injury data in head-on crashes are only influenced by the compatibility metric X. However, in the current analysis, vehicle designs have not taken in to account X as a metric, the injuries that are seen in the fleet as it currently exists may be influenced by other factors such as mass and geometric disparities.
4. When the functional relationship between the risk for the drivers in subject vehicles and X for other vehicle classes is changed, it is assumed that the functional relationship between X and the risk for the other vehicle classes remain unchanged.
5. The benefits determined on the basis of AIS 3+ injuries reduced will equally apply to lesser injuries and fatal injuries irrespective of the crash conditions of speed and other variables.
6. The target population used for above includes the effect of all the variables that affect the injury outcome. Use of these numbers in estimating the benefits is likely to result in higher estimates than can be realized in actuality by changing the value of X
7. The head-on crashes selected from the NASS/CDS crash data have principal direction of force acting between 350 and 10 degrees for both the vehicles and are assumed to be similar to NCAP FMVSS No 208 crash tests.
8. As part of this study no case review (review of the accident case file) was conducted to verify whether the target population used in the benefit calculation would benefit from center of velocity change methodology.

Analytical methodology for evaluating benefits

Potential benefits of changing the value of X for various vehicle classes in the fleet were calculated from the target injuries that occur in all head-on frontal crashes between the subject vehicle class and the other classes including itself. For example, it is seen from Table 3 that there are a total of 24,227 AIS 3+ driver injuries in compact passenger cars in crashes involving all other passenger vehicle classes including other compact vehicles. Similarly, 12,260 AIS 3+ injuries occur in the other vehicle classes also in the ten year period in the NASS database (weighted) involving compact vehicles. Similarly, there are a total of 14,114 AIS 3+ driver injuries in FPC and 11,986 in other classes, 9019 in CLTV and 14,701 in others and 5,339 in LLTVs and 13,752 in other classes, respectively. Since the vehicles in the fleet are not designed by optimizing X, the injuries used in the target population include effect of all variables including mass differences

The relative risk of CPC in crashes involving all other classes were first calculated by varying the values of X in the range of 16.0 to 21.5 inches in increments of 0.5 inch and then in the same range in increments of 0.1 inch. The original relative risk for CPC as indicated by the point of intersection of the two curves seen in Figure 6 is 1.0 (at a value of X = 16.14 inches). Similarly, for each of the other subject vehicle classes FPC, CLTV and LLTV and the other classes, the intersection point and the associated value of X for each class is different. Figure 6 presents the curves for PCs and Figure 6 presents the data for LTVs.

These effectiveness fractions for subject vehicle and other vehicle classes are multiplied by their respective target populations to determine the potential benefits in each class interaction. The net benefits are then determined by adding up the potential benefits for each subject vehicle class and all other classes at a specific value of X.

Based on this analysis, it is concluded that there is no advantage in driving changes in the value of X in FPC and CLTV. On the other hand, there are potential safety benefits to be gained by changes in small passenger cars (CPC) and large light trucks and vans (LLTV) using this metric. As expected, the methodology used in the benefit calculations result in different total benefits as values of X are varied. True relative risks can only be determined if the number of injured and uninjured drivers in each vehicle class is known.

The NASS data provide the uninjured numbers for only the tow-away crashes. In two-vehicle crashes, the uninjured numbers do not include the uninjured in non-tow-away vehicles. Therefore, calculating the relative risk as an odds ratio may exaggerate the potential benefits and is not considered. On the other hand, when the relative risks are calculated on the basis of the injured drivers only, it is assumed that the number of uninjured drivers in the subject vehicles and the other vehicles are the same.

Performance scheme and rationale

While the analysis described is based on head-on crashes only, many other frontal crashes that are not strictly defined as head-on crashes may also derive benefits from the changes in the compatibility metric X. For example, even though the data did not include many other types of frontal crashes that are not included under head-on type, it is reasonable to assume that those crashes would also be helped when vehicles comply with this compatibility metric.

The value of X can be increased by changes in geometry and stiffness characteristics. For example, for small passenger cars, it is not practical to change geometry significantly. However, stiffness of such vehicles may be increased substantially to increase X. Beyond limits, this may require redesign of the restraint systems. Some small cars in today's fleet are already stiffening up their structures and therefore, the compatibility metric X for those vehicles may already be high even though they have a low front-end profile.

Based on the front NCAP test data for vehicles, a value of X can be computed for each vehicle. If those nominal values fall within the prescribed metric +/- a tolerance value, an enhanced rating for such vehicles in the smallest and largest vehicle class could drive compatibility without adding a new test or incurring additional cost for compliance evaluations. The full size passenger cars and the crossover vehicles could be left alone as they do not appear to provide any appreciable benefits when the value of X is changed for those classes.

Conclusion

Using the methodology described the overall safety benefits can be estimated by calculating the reduction in the number of drivers with AIS 3+ injuries in all frontal crashes as well as in side crashes by making the vehicles in the fleet comply with selected values of X. However, initially the benefits are estimated for head-on crashes only after validating the methodology described in this paper.

Additional estimates for side crashes can only be attempted once the necessary data related to side crashes and H-point heights in struck vehicles are obtained. It must be noted that, the relevant metric for side crashes is not likely to be just the value of X for striking vehicles, but also the difference between X for the striking vehicles and the height from the ground to the H-point (h) in struck vehicles. It is assumed that the relative risk of injuries in side crashes will be influenced by the new metric, (X - h). This new metric has to be derived from side NCAP data and a functional relationship between this metric and side crash injuries will have to be developed before applying the methodology for the benefits calculation. Absence of relevant H-point data for various vehicle classes prevented the development of a preliminary benefit estimate for side crashes. However, it is noted that at least for passenger cars, the H-point heights are close to each other, irrespective of the size of the vehicle. Therefore, it is reasonable to assume h to be a constant for passenger cars. Based on this assumption, available side

NCAP data for passenger cars could be used to develop the relationship between (X-h) and the real world relative risks in side crashes as various classes of vehicles strike the sides of passenger cars. Using this methodology, it can be attempted in the future as H-point data become available for light trucks as well.

REFERENCES

1. New Car Assessment Program (NCAP) frontal barrier test data; http://www-nrd.nhtsa.dot.gov/database/nrd-11/veh_db.html
2. Crashworthiness Data System 2007 Coding and Editing manual <http://www-nrd.nhtsa.dot.gov/Pubs/CDS07.PDF>
3. Automaker pledge series of steps to improve crash compatibility, Insurance Institute for Highway Safety, Status Report, Vol. 39, No. 1, January 3 2004.
4. In collision with cars, SUVs are incompatible, Insurance Institute for Highway Safety, Status Report, Vol. 40, No. 5, April 28 2005.

EFFECTS OF ACTIVE STRUCTURES ON INJURIES IN MEDIUM SEVERITY FRONTAL IMPACTS

Bengt Pipkorn

Autoliv Research
Sweden

Anders Kullgren

Folksam Research and Department for Public Health Sciences,
Karolinska Institutet, Sweden

Paper Number 09-0380

ABSTRACT

An evaluation of the influence of crash pulse shape on the risk to sustain injuries in medium severity frontal collisions was carried out by reconstructing a number of real world accidents using mathematical simulations.

Ten crashes with restrained occupants, recorded crash pulses and known injury outcomes were selected for reconstruction. The crashes were selected from the Folksam accident database. Delta-V and mean acceleration were derived from the recorded crash pulses. The injury outcome was collected from hospital records and questionnaires and coded according to the 2005 version of AIS. Only restrained occupants were included.

Computer simulations using a mathematical model of the 50%-ile Hybrid III dummy were used to evaluate the influence of the crash pulse on the loading of the occupants. The restraint system was a state of the art system with a driver side airbag and a belt system equipped with a pretensioner and a load limiter. Simulations were carried out in which the crash pulse shape was varied according to what can be achieved with the frontal longitudinal beam in which the crush force can be varied. Injury reducing benefits for the occupants were achieved by varying the crash pulse shape in medium severity impacts.

The principal technical solution to vary the crash pulse is to pressurize the frontal longitudinal beams in the frontal structure prior to impact. In low and medium-speed impacts, the beams are not pressurized to use the available crush distance of the vehicle front. In high-speed impacts, the beams are pressurized to increase the force level of the beam and use the available crush distance of the vehicle front efficiently.

INTRODUCTION

An evaluation of the CCIS (Co-operative Crash Injury Study) database of front seated occupant injuries in small family cars involved in frontal crashes with an equivalent test speed (ETS) of 20-40 km/h was performed. Thorax injuries (AIS 2+) were found to be more numerous than any other type of injury. The vast majority of chest injuries were skeletal. The sample sizes were limited but there were fewer serious chest injuries to front seat passengers in newer cars (registered 2000 or later) than in old cars (registered 1983 to 1997). There was no such reduction of chest injuries evident for drivers but injuries to other body parts decreased in newer cars. As a matter of fact serious chest injuries to older drivers in newer cars increased sharply. Also there was no decrease of serious chest injuries for young female drivers of newer cars.

The manufacturers of cars are faced with the problem of a continuing down sizing and mass reduction trend to reach low fuel consumption levels and to minimize environmental impact. One limiting factor is the need to provide a sufficiently long deformation zone in the frontal part of the car body. Conventional test methods to perform crash tests into deformable or non-deformable barriers at speeds between 40-64 km/h (25 to 40 mph) have resulted in cars with specific crash pulses and restraint systems tuned to give a low occupant loading. It can be reasoned that in real life, given the many different crash types that occur in real life, the importance of tailored crash pulses do not have such a significant effect. However, it can be stated that the longer the crush depth the lower the loading on the occupants will be, given that the crash pulse is not too heavily skewed with a high deceleration level at the end of the crash.

The concept of crash pulse tuning to reduce occupant loads in barrier testing has been discussed and evaluated previously [1,2]. Recent advances provide the opportunity for crash pulse variation in real time through variable beam buckling force technology. Such technology will have at least a three fold

advantage namely: to enable softer crash pulse at low and medium velocity impacts in order to decrease the loading on the occupants, to produce a square wave crash pulse at high impacts velocities and to make it possible to improve compatibility in vehicle to vehicle impacts.

An effort was made to understand the influence of the crash pulse and vehicle deformation length on the driver occupants in frontal impacts in moderate to high velocity impacts. Mathematical analysis and mechanical sled tests were carried out [3, 4 and 5]. Significant benefits for the occupant were obtained. However, these analyses were carried out on vehicle crashes into a rigid wall. There is a need to evaluate the potential for active crash pulse control for vehicles in real world accidents.

METHOD

Crashes with recorded crash pulses in the Folksam crash recorder database were used. Since 1992, approximately 270 000 CPR's have been installed in vehicles in Sweden, comprising of 4 different car makes and more than 20 models aimed at measuring frontal and rear-end impacts. To date the database contains approximately 700 frontal crashes with a recorded crash pulse. The inclusion criteria and content of the database has been described in previous studies [6, 7].

The crash recorder measures the acceleration in frontal crashes with a sampling frequency of 1000. The crash pulses are filtered at CFC60.

The injuries were collected from hospital records, questionnaires sent to the occupants or from insurance claims. The injuries were classified according to the 2005 revision of the Abbreviated Injury Scale [8].

The inclusion criteria in this study were a vehicle overlap of at least 25% (measured as the proportion of the front that was deformed), a crash angle within +/- 30 degrees, restrained occupants (belt use was verified from inspections of the seat belt systems) and a change of velocity in the interval 40 to 75 km/h.

In total 13 crashes with restrained occupants, known crash pulse and injury outcome were selected for reconstruction. The ΔV varied from 40 – 72 km/h with an average of 50 km/h. The stopping distance varied from 1.3 – 0.5 m with an average of 0.75 m. Peak acceleration varied from 21 – 45 g.

The crash circumstances and injury outcomes are listed in Table 1.

Table 1.
Crash Types, Occupant Age/Gender and Injuries

ΔV (km/h)	Injury	Accident type	Gender / age
72,3	AIS1	Full frontal into a rolled truck trailer	m / 71
55,3	AIS1	Full frontal into side of other vehicle	m / 48
53,1	AIS1	Frontal collision with large car	m / 25
52,9	AIS2	Full frontal into front of small family car	f / 36
52,1	AIS1	Full frontal into a family car	f / 48
51,3	AIS1	Full frontal into front of small family car	m / 35
49,7	AIS0	Front to rear of tractor	f / 36
48,0	AIS1	Single vehicle crash into a concrete culvert	m / 71
44,3	AIS1	Frontal collision into tree	f / 57
43,9	AIS1	Frontal, 30 % overlap with large MPV	f / 64
43,7	AIS2	Single vehicle crash into a rock/stone	m / 51
41,5	AIS2	Frontal into a truck	m / 62
40,2	AIS2	Frontal collision with small car + sideswipe with large car	f / 45

The crash pulses were modified to two levels. The levels were 15g and 20g constant acceleration. An available crush distance (vehicle front length) of 600 mm was assumed. The total crush distance was not altered for the adaptive crush pulses. All crash pulses can be found in Appendix A.

To reconstruct the crashes a mathematical model was used. The geometry of the occupant compartment in the mathematical model was based on the geometry of the occupant compartment of a common mid size vehicle. The mathematical model was a full finite element model (LS-DYNA) that incorporated a 50%-ile HIII-dummy, a windscreen, a ceiling, a seat, a knee bolster, a belt system, an airbag, a steering wheel and a fixed steering column (Figure 1). The belt system incorporated a buckle pretensioner and a load limiter at the retractor. The level of the pretensioner was 1 kN and the load limiter 3.6 kN (at the retractor).

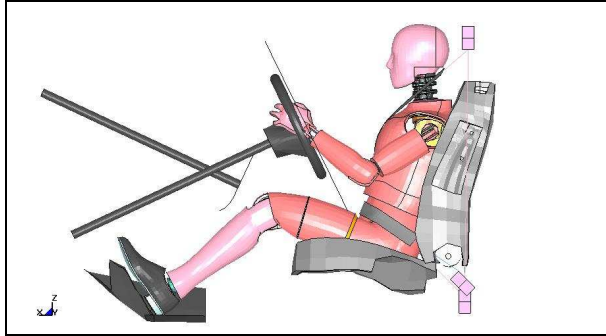


Figure 1. Model with HIII Dummy

The model was validated by means of results from mechanical sled tests at 48 km/h [9]. The predictions and results that were used for evaluation were HIC15, chest acceleration and chest deflection.

RESULTS

For the reference pulse HIC15 varied from 74 to 998 (Table 2). When the pulse was active HIC15 was reduced with as much as 467 (HIC15). The average reduction for the 13 pulses was 133 (46%). For one crash pulse HIC15 increased from 74 to 78.

**Table 2
HIII HIC15 Results**

Δv (km/h)	Injury	Reference Pulse HIC15	Active Pulse HIC15
72,3	AIS1	524,0	335,0
55,3	AIS1	998,0	531,0
53,1	AIS1	769,0	378,0
52,9	AIS2	548,0	460,0
52,1	AIS1	574,0	487,0
51,3	AIS1	512,0	398,0
49,7	AIS0	196,0	154,0
48,0	AIS1	88,0	78,0
44,3	AIS1	408,0	318,0
43,9	AIS1	267,0	207,0
43,7	AIS2	232,0	109,0
41,5	AIS2	74,0	78,0
40,2	AIS2	286,0	211,0

For the reference pulse, chest acceleration varied from 490 to 175 m/s² (Table 3). When the pulse was active chest acceleration was reduced with as much as 124 m/s². Average reduction was 67 m/s² (18%). Least reduction was 7 m/s².

**Table 3
HIII Chest Acceleration Results**

Δv (km/h)	Injury	Reference Pulse Chest Acc (m/s ²)	Active Pulse Chest Acc (m/s ²)
72,3	AIS1	396,0	360,0
55,3	AIS1	486,0	362,0
53,1	AIS1	429,0	332,0
52,9	AIS2	490,0	370,0
52,1	AIS1	427,0	356,0
51,3	AIS1	370,0	315,0
49,7	AIS0	269,0	247,0
48,0	AIS1	222,0	215,0
44,3	AIS1	392,0	317,0
43,9	AIS1	334,0	250,0
43,7	AIS2	335,0	230,0
41,5	AIS2	175,0	166,0
40,2	AIS2	345,0	281,0

For the reference pulse peak chest deflection was 33 mm (Table 4). It was for the pulses with 53 km/h in Δv . For active crash pulses the greatest reduction in chest deflection was 4 mm. It was for the crash pulse with 40 km/h Δv . The average reduction was 1.3 mm (5%). There were a number of crashes in which no reduction in chest deflection was obtained for the active crash pulse.

**Table 4
HIII Chest Deflection Results**

Δv (km/h)	Injury	Reference Pulse Chest Def (mm)	Active Pulse Chest Def (mm)
72,3	AIS1	31,0	29,0
55,3	AIS1	32,0	32,0
53,1	AIS1	33,0	32,0
52,9	AIS2	33,0	31,0
52,1	AIS1	32,0	32,0
51,3	AIS1	31,0	31,0
49,7	AIS0	27,0	25,0
48,0	AIS1	17,0	17,0
44,3	AIS1	30,0	28,0
43,9	AIS1	28,0	27,0
43,7	AIS2	18,0	16,0
41,5	AIS2	19,0	18,0
40,2	AIS2	31,0	27,0

For the diagonal belt generally the peak force was reduced when the pulse was active (Table 5). The force was reduced for all Δv :s but 2. For the

configuration with ΔV 48 km/h the force increased. Greatest reduction was 0.6 kN. This was for the pulse with a ΔV of 43.7 km/h. Average reduction was 0.2 kN (5%).

Table 5
Diagonal Belt Force

Δv (km/h)	Injury	Reference Pulse Diag Belt Force (kN)	Active Pulse Diag Belt Force (kN)
72,3	AIS1	4,2	4,0
55,3	AIS1	4,4	4,1
53,1	AIS1	4,4	4,0
52,9	AIS2	4,2	4,1
52,1	AIS1	4,1	4,1
51,3	AIS1	4,3	4,0
49,7	AIS0	3,8	3,7
48,0	AIS1	3,7	3,8
44,3	AIS1	4,2	4,0
43,9	AIS1	3,9	3,8
43,7	AIS2	4,1	3,5
41,5	AIS2	3,2	3,0
40,2	AIS2	3,9	3,5

NIJ was generally reduced when the pulse was active (Table 6). The pulse was reduced for all ΔV :s but one. Greatest reduction was 0.17. This was for the pulse with 55.3 km/h in ΔV . Average reduction was 0.11 (22%).

Table 6
NIJ

Δv (km/h)	Injury	Reference Pulse NIJ	Active Pulse NIJ
72,3	AIS1	0.61 NTE	0.52 NTE
55,3	AIS1	0.69 NTE	0.52 NTE
53,1	AIS1	0.63 NTE	0.47 NTE
52,9	AIS2	0.66 NTE	0.54 NTE
52,1	AIS1	0.64 NTE	0.53 NTE
51,3	AIS1	0.53 NTE	0.46 NTE
49,7	AIS0	0.46 NTE	0.34 NTE
48,0	AIS1	0.17 NTF	0.15 NTF
44,3	AIS1	0.59 NTE	0.49 NTE
43,9	AIS1	0.52 NTE	0.38 NTE
43,7	AIS2	0.49 NTE	0.29 NTE
41,5	AIS2	0.19 NTE	0.20 NTE
40,2	AIS2	0.55 NTE	0.39 NTE

DISCUSSION

For none of the evaluated crash pulses chest acceleration and chest compression reached the FMVSS208 injury criteria levels of 60 g and 63 mm. However, for two of the crash pulses HIC15 was greater than the FMVSS208 injury criteria level of 700. However, in the data no head injuries were obtained in those crashes. For the configurations with an active pulse HIC15 was less than 700 for all evaluated crashes.

In a number of cases the belt force and not the chest deflection was reduced for the active pulse. In those cases when the belt forces were reduced an increased force from the airbag contact with the chest was obtained that compensated for the reduced belt force.

Many vehicles on the roads today have an available stopping distance of approximately 0.6 m [10 and 11]. The vehicles are designed for high-speed impacts to use the stopping distance as efficiently as possible. Therefore the initial acceleration in a crash is significant. In moderate impacts the acceleration of the vehicle is therefore also significant resulting in short stopping distances. For an initial acceleration of the vehicle of 160 m/s^2 the stopping distance in a 40 km/h crash is 0.4 m with a square wave pulse. However, a small city car designed for rigid barrier impact at 50 km/h and a crush zone of 0.5 m as described by Walz [12] would exhibit an acceleration of 270 m/s^2 with a square wave pulse at 50 km/h. In a 40 km/h crash that acceleration level corresponds to a crush of 0.260 m. Such vehicle accelerations in low speed impacts may cause injuries. In particular for the elderly such acceleration levels can be injurious. For a majority of the crashes evaluated peak acceleration was greater than 270 m/s^2 .

In many modern cars the load limiter in the seat belt is set to a level of 4.0 kN in order to limit the belt loading on the chest [13 and 14]. (3.6 kN was used in this study). However increasing the ride down of the occupant by using a load limiter has two major drawbacks. The forward displacement of the occupant inside the occupant compartment is increased and the efficiency of the load limiter in spooling out webbing is dependent on the mass of the occupant. The heavier the occupant is, the greater the forward displacement. The lighter the occupant is, the smaller the effect of the load limiter. One of the benefits with an adaptive crash pulse is that the input inertia field (crash pulse) can be adjusted based on the impact speed. An adaptive crash pulse can therefore reduce the loads on all occupants regardless

of the mass of the occupant. Adaptive crash pulse technology has the potential of decreasing the demands on the “tuning” of the interior restraint systems for the individual occupants and to produce low occupant loadings in a majority of crashes.

Kent [15] has published injury risk curves (AIS3+) for different age categories as a function of chest deflection. In the simulations in this study with the 50%-ile HIII dummy and an impact velocity of 40 km/h chest deflection was in one case reduced from 31 mm to 27 mm when the crash pulse was made active. This would correspond to a decrease in risk of chest injury (AIS 3+) from 21% to 11% for a 60+ year car occupant.

In 81% of the vehicle frontal crashes at least one of the longitudinal members is loaded [10]. In addition the main longitudinal members generally absorb a significant amount of the crash energy. Therefore a system that adapts the force level on the main longitudinal members addresses the majority of the frontal impacts. A technical solution to vary the crush force in the vehicle front can be to pressurize the main longitudinal members. Tests were carried out in which 600 mm long tubes with a wall thickness of 1.0 mm were crushed axially (Figure 2). The diameter of the tubes was 80 mm.

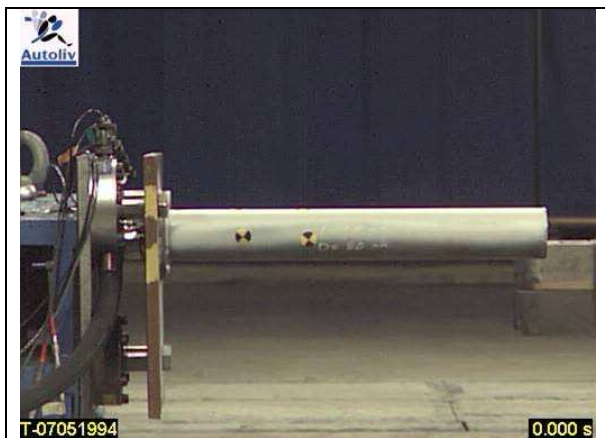


Figure 2. Test Set Up Tube Crush Tests

The tests were carried out at an impact velocity of 17 km/h (4.8 m/s). Tests were carried out with both reference tubes (unpressurized), pressurized sealed tubes and pressurized ventilated tubes.

In the results it can be observed that for the reference tubes the crush force was 40 kN (Figure 3). For the pressurized tubes the crush force was 70 kN. For the

pressurized ventilated tubes the crush force was 60 kN.

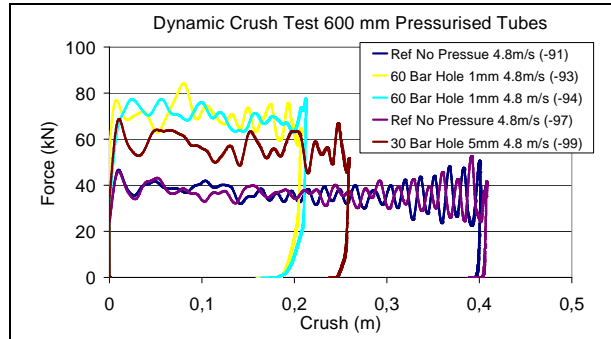


Figure 3. Force vs Deformation for Crushed Tubes

By pressurization a significant increase in the energy absorbed was obtained (Figure 4). At 200mm deformation of the tubes the reference tubes absorbed 7.7 kJ. The pressurized tubes absorbed 14 kJ. By pressurization the energy absorbed was increased by 82%.

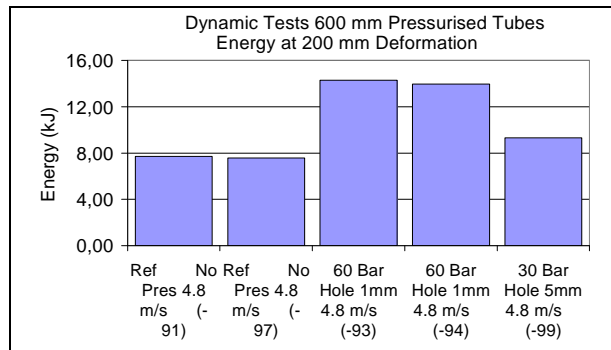


Figure 4. Energy Absorbed by the Tubes

The increased crush force from pressurization depends linearly on the cross sectional area of the tubes (Figure 5), the greater the cross sectional area of the tube, the greater the increase in crush force by pressurization.

Significant weight reductions can be achieved with a thin-walled beam with a large cross sectional area that is pressurized. For a tube with a diameter of 160 mm that is pressurized the increase in crush force is 80 kN.

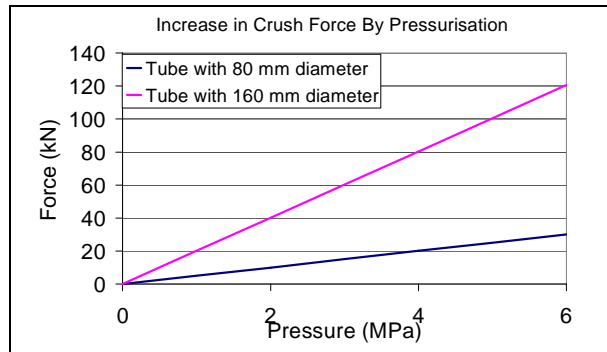


Figure 5. Increase in Crush Force

This concept can then be used in other types of crashes in order to achieve effective protection in other crash velocities and also to improve vehicle compatibility.

CONCLUSIONS

An active crash pulse can reduce HIC15 by 46%, chest acceleration by 18%, chest deflections by 5% and NIJ by 22% in accidents with 72 – 40 km/h in Δv .

Pressurising thin-walled tubular structures can significantly increase the crush force and energy absorption.

REFERENCES

- [1] Witteman W.J., Kriens R.F.C. “The necessity of an adaptive vehicle structure to optimise deceleration pulses for different crash velocities”. Technische Universiteit Eindhoven, 1999
- [2] Shi Y., Wu J., Nusholtz G. “Optimal Frontal Vehicle crash Pulses- A numerical method for design”. Paper 514. 18th Technical Conference on the Enhanced Safety of Vehicles, Nagoya, Japan. 2003
- [3] Mellander H., Pipkorn B., Håland Y. “Driver protection potentials in high severity frontal impacts with up to 50 mph delta-V”. Safety 2004 conf., Institution for Mechanical Engineers, London 2004
- [4] Pipkorn B., Mellander H., Håland Y. “Car driver protection at frontal impacts up to 80 km/h (50 mph)”. Paper Number 05-0102. ESV Conference 2005
- [5] Pipkorn B., Mellander H., Olsson J., Håland Y. “On the combined effect of the variation of driver restraint configuration and crash pulse for high and very high impact velocities”. IRCOBI 2006
- [6] Kamrén B, Krafft M, Kullgren A, Lie A, Nygren Å, Tingvall C. Advanced Accident Data Collection - Description and Potentials of a Comprehensive Data Collection System. Proc. of the 13th ESV Conf., Paris, 1991: Vol1:41-45
- [7] Kullgren A. Validity and Reliability of Vehicle Collision Data: Crash Pulse recorders for Impact Severity and Injury Risk Assessments in Real-Life Frontal Collisions. Thesis for the degree of Doctor in Philosophy, faculty of Medicine, Folksam Research 106 60 Stockholm, 1998.
- [8] AAAM, Abbreviated Injury Scale 2005, AAAM Des Plaines, IL, USA, 2005.
- [9] Pipkorn, B., Mroz K. “Validation of a Human Body Model for Frontal Crash and its Use for Chest Injury Prediction”. SAE Paper No 08DHM-0015. Digital Human Body Modelling Conference, 2008, Pittsburgh, USA
- [10] Ng, E., Hassan, A., Cuerden R. “Effectiveness of Longitudinal in Frontal Impacts”, Paper No: 2008-099, IJ Crash Conference 2008, Japan
- [11] Ono Y, Kimura Y; Mizuno K. “What we learned from JNCAP and our proposals”. ESV 2003 paper 244
- [12] Walz F., Kaeser R., Niederer P. “Occupant and Exterior safety of low mass cars”. IRCOBI 1991
- [13] Bendjellal F., Walfish G., Steyer C., Ventre P., Foret-Bruno J-Y.. “The Programmed restraint system – A lesson from accidentology”. SAE 973333 Stapp conf., 1997
- [14] Foret-Bruno J-Y., Troisseille X., Le Cox J-Y. “Thoracic Injury Risk in Frontal Car Crashes with Occupant Restrained with Load Limiter”. Stapp Conf., 1998
- [15] Kent R., Patrie J., Poteau F., Matsuoka F., Mullen C.. “Development of an age-dependent thoracic injury criterion for frontal impacts restraint loading”. Paper 72, 18th Technical Conference on the Enhanced Safety of Vehicles, Nagoya, Japan. 2003

APPENDIX A

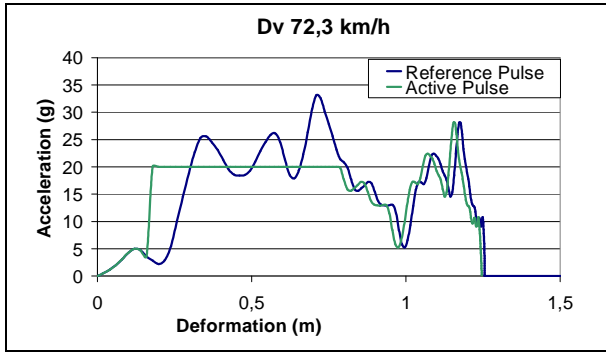


Figure A1. Dv 72,3 km/h

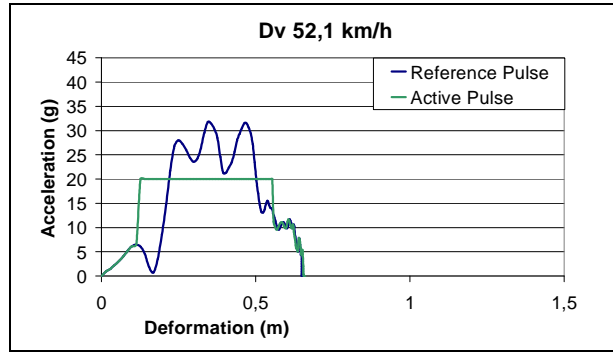


Figure A5. Dv 52,1 km/h

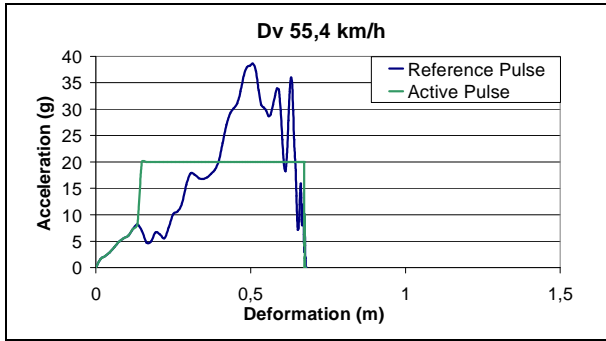


Figure A2. Dv 55,4 km/h

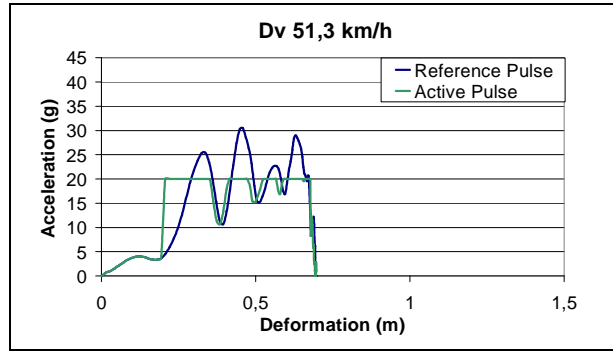


Figure A6. Dv 51,3 km/h

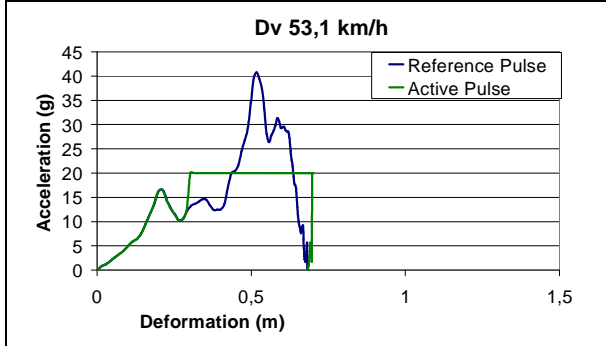


Figure A3. Dv 53,1 km/h

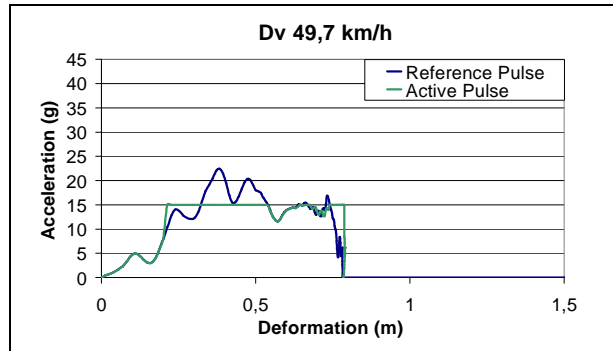


Figure A7. Dv 49,7 km/h

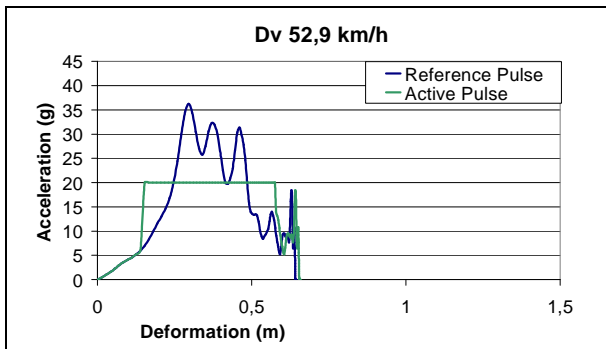


Figure A4. Dv 52,9 km/h

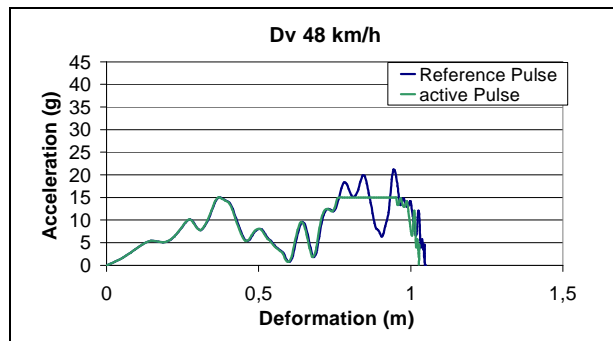


Figure A8. Dv 48,0 km/h

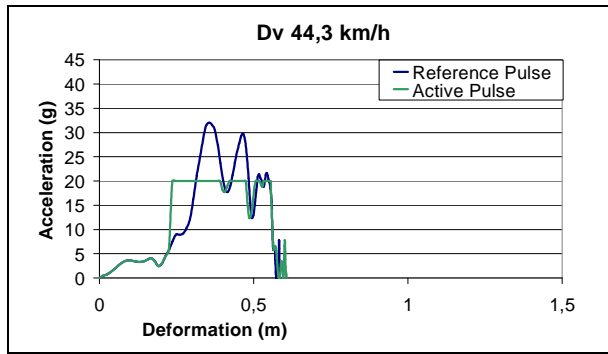


Figure A9. Dv 44,3 km/h

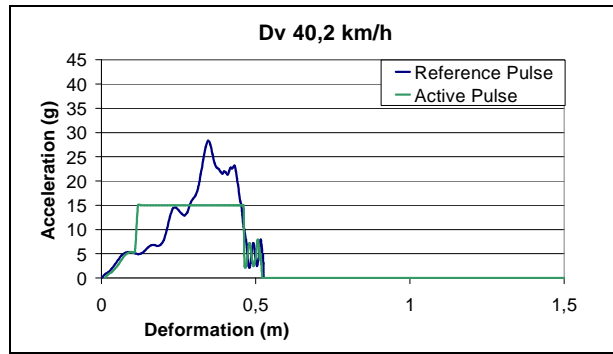


Figure A13. Dv 40,2 km/h

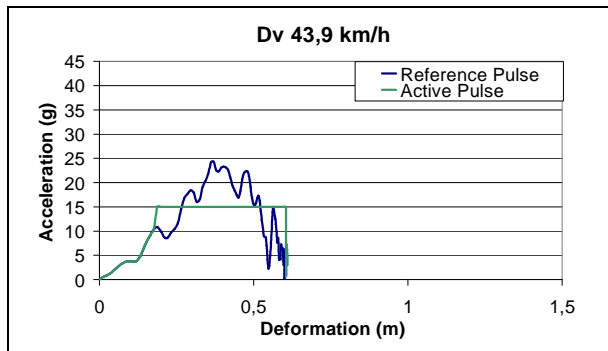


Figure A10. Dv 43,9 km/h

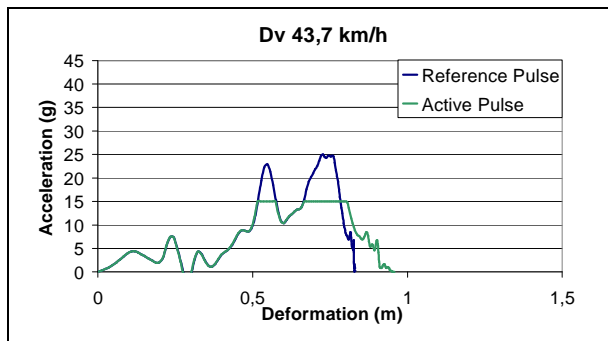


Figure A11. Dv 43,7 km/h

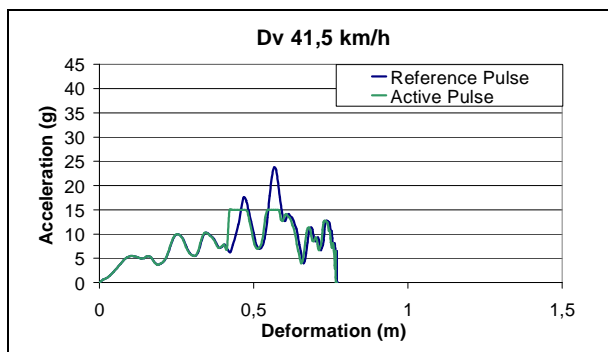


Figure A12. Dv 41,5 km/h

DETAILED ANALYSIS OF TARGET CRASHES FOR PRE-CRASH SENSING APPLICATIONS

Ana Maria Eigen

National Highway Traffic Safety Administration

Wassim G. Najm

Volpe National Transportation System Center

United States

Paper 09-0248

ABSTRACT

Target pre-crash scenarios, crash modes, and occupant injury mechanisms are statistically described for crash imminent braking (CIB) and advanced restraint system (ARS) applications based on pre-crash sensing. Vehicle-object and vehicle-vehicle crashes are distinguished between single-impact and multiple-impact crashes. This analysis focuses on light vehicles of model year 1998 or higher that suffered frontal damage from the first most harmful event. An in-depth examination of candidate crash cases from target crashes was conducted to understand crash mechanisms and circumstances as well as occupant injury scenarios. Consideration was given to pre-crash conditions for CIB applications and to injury source for ARS applications. Results will be used in subsequent research to assess candidate CIB and ARS technologies, develop system functional requirements, devise test procedures, and estimate safety benefits.

INTRODUCTION

Pre-crash sensing applications encompass active safety measures aimed at reducing injuries once the crash is deemed unavoidable. These applications detect a crash earlier than accelerometer-based approaches with anticipatory sensors, communicate this information to the vehicle and its occupant protection systems, and take appropriate actions to reduce the crash severity or alleviate the severity of crash injury [1]. Crash avoidance systems are now appearing on new vehicle models in the United States (US). These systems offer the opportunity to improve vehicle crashworthiness by providing environmental awareness data so that automatic braking and crashworthiness protection systems can be activated when a crash becomes imminent and before the vehicles contact each other. Today's airbag and seatbelt systems will be more effective if advanced occupant sensors are added to pre-crash sensors, creating occupant protections with advanced restraints that adapt to whoever happens to be sitting in the vehicle and to the demands of a variety of crash scenarios.

This paper describes crash scenarios based on an in-depth examination of applicable crash cases for

full-authority last-second crash imminent braking (CIB) and advanced restraint systems (ARS). The CIB system is designed to reduce impact severity by dissipating energy from the crash. ARS are intended to improve the coupling of occupants to the vehicle, reducing firing times of airbags, among others. This crash analysis supports two joint research efforts on CIB and ARS between the US Department of Transportation and the Crash Avoidance Metrics Partnership comprised of three automakers and major suppliers [2, 3]. These two research efforts have common objectives:

- Develop and validate minimum performance requirements and objective test procedures for CIB and ARS that appear to provide an opportunity to reduce the societal harm resulting from light-vehicle crashes in the US.
- Identify and fabricate the most promising CIB and ARS prototypes, and complete objective testing to evaluate their performance.
- Obtain preliminary estimates of potential safety benefits of these prototype systems.

Development and integration of internal and external sensors, advanced braking systems, and restraints systems focus on the time period when a crash becomes unavoidable. Priority of these research efforts is given to the development and evaluation of autonomous vehicle systems, crash types causing the most societal harm, and systems considered technically feasible for near-term deployment (3-5 years from project completion).

This paper presents results of the crash analysis conducted in support of the cooperative CIB and ARS projects. Target crashes were identified and prioritized for CIB and ARS applications using the National Automotive Sampling System's Crashworthiness Data System (CDS) and General Estimates System (GES), Fatality Analysis Reporting System (FARS), and data from event data recorders [4]. Most common and harmful pre-crash scenarios were correlated with impact crash modes to produce target crashes to be addressed within these two projects. From these crashes, candidate crash cases were selected for in-depth examination to understand crash mechanisms and circumstances as well as occupant injury scenarios. This research step

determined applicable crashes and served to filter out crash cases that are not amenable to CIB or ARS applications. The crash scenarios for the applicable collision cases provide the crash context that can be used for the development of pre-crash sensor specifications, minimum performance requirements, and objective test methods. This paper summarizes the results from the in-depth examination of applicable crash cases.

Next, this paper describes the crash analysis approach and highlights the results of the prioritized target crash scenarios. After that, results from the analysis of the CIB applicable crash cases are presented. This is followed by results from the in-depth examination of ARS applicable crash cases. This paper concludes with a summary of key results.

CRASH ANALYSIS APPROACH

A two-stage crash analysis approach was adopted to identify target crash scenarios and statistically describe applicable crash cases that could be amenable to CIB and ARS applications. As illustrated in Figure 1, the first stage consists of a top-down analysis that involved data queries of national crash databases to identify and prioritize crash scenarios for further examination in the second stage named the bottom-up analysis. These analyses targeted light vehicles of model year 1998 or higher (MY98⁺) that sustained frontal damage from the first harmful event. The model year served as the surrogate for modern restraint systems including three-point lap and shoulder belts, presence of pretensioners, load limiters, the advent of the second generation, de-powered airbags, and more advanced seatbelt and airbag technology. The first harmful event was considered to accommodate the development of functional requirements for forward-looking pre-crash sensors that would enable the CIB application and augment advanced restraints. The ARS analysis focused on understanding the injury suffered by the driver and the front seat passenger of 13 years of age or older (FSP13⁺). The age restriction placed upon the front seat occupant is consistent with the position in the US that child passengers should ride in the rear seating positions until they are 12 years. The CIB analysis considered all persons in crashes that involved at least one target vehicle.

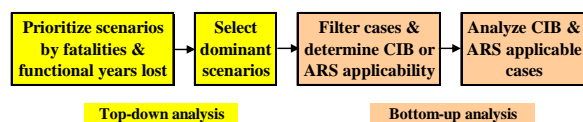


Figure 1. Crash Analysis Approach

The analysis distinguished crashes between vehicle-object and vehicle-vehicle crash types by the type of obstacle struck during the first harmful event based on whether or not the obstacle was a vehicle in transport. As seen in Figure 2, vehicle-object crashes are characterized by a vehicle in transport contacting a “not vehicle in transport” obstacle. Obstacle categories include tree, pole, ground, structure, person, vehicle, animal, not-fixed object, non-collision, and unknown. Attention is paid to whether the target vehicle is involved in a single- or multi-impact crash. In single-vehicle crashes, the target vehicle does not hit a vehicle in transport. However, in a multi-impact crash, it is important to identify the object type that was contacted during the first harmful event. In vehicle-vehicle or multi-vehicle crashes, the target vehicle contacts a vehicle in transport. In a multi-impact crash, it is possible for the target vehicle to strike an object first before hitting another vehicle in transport. Thus, the analysis separates multi-vehicle crashes based on the first harmful event into vehicle-object and vehicle-vehicle crashes as shown in Figure 2.

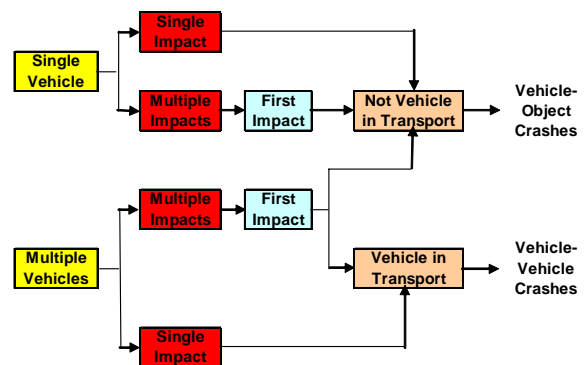


Figure 2. Breakdown of Target Crash Types

The top-down analysis correlated pre-crash scenarios to the manner of collision such as pole in vehicle-object crashes and front-back in vehicle-vehicle crashes. These correlations of crash scenarios were then prioritized and ranked by severity. The number of fatalities from FARS and the number of functional years lost (FYL) derived from CDS and GES injury data were selected to quantify crash severity. The FYL measure sums the years of life lost to fatal injury and the years of functional capacity lost to nonfatal injury using the Maximum Abbreviated Injury Scale (MAIS) [5]. The ARS analysis only counted MAIS levels 3 through 6 by the driver and FSP13⁺ in target vehicles, while the CIB analysis incorporated all persons involved in the crash with MAIS levels 2 through 6. Results of the top-down analysis are summarized in the next section and are described in Reference [4].

The bottom-up analysis encompassed detailed examinations of individual filtered cases to determine the applicability of CIB and to understand why and how the target occupants were at least seriously injured for ARS application. The top-down analysis identified lists of case numbers from the CDS for the dominant crash scenarios. Researchers then reviewed these CDS cases and assessed their usefulness for the bottom-up analysis. This paper discusses the bottom-up analysis and presents the results for CIB and ARS in the following sections.

TARGET CRASH SCENARIOS

The top-down analysis identified and prioritized target crash scenarios for CIB and ARS applications based on injury statistics from the 1997-2006 CDS databases. Ranking of scenarios was established using the FYL measure that integrated the MAIS levels 3-6 of the driver and FSP 13⁺ in target vehicles for ARS and the MAIS levels 2-6 of all persons involved in the crash for CIB.

Road departure was the dominant pre-crash scenario in vehicle-object crashes for CIB and ARS. In this scenario, the vehicle is typically going straight and then departs the edge of the road due to driver inattention, drowsiness, or under the influence or alcohol impairment. The vehicle may also be negotiating a curve, turning left or right at a junction, changing lanes or passing, or entering or leaving a parking position. Road departure with different struck obstacle combinations had the same order of severity for CIB and ARS, as shown below in a descending order:

1. Road departure – ground
2. Road departure – pole
3. Road departure – structure
4. Road departure – tree

Table 1 lists the ranking of vehicle-vehicle crash scenarios for CIB and ARS. There are five dominant pre-crash scenarios:

- Opposite direction (OD): vehicle is typically going straight, drifts at a non-junction, and then encroaches into another vehicle traveling in the opposite direction. Vehicle may also be negotiating a curve or passing.
- Rear-end (RE): vehicle is typically going straight and then closes in on a lead vehicle that may be stopped, decelerating, accelerating, or moving at slower constant speed. Vehicle may also be starting in traffic, changing lanes, passing, or turning and then closes in on a lead vehicle.

- Left turn across path/opposite direction (LTAP/OD): vehicle is turning left at a junction and then cuts across the path of another vehicle traveling from the opposite direction.
- Straight crossing paths (SCP): vehicle is going straight through a junction and then intersects the path of another straight crossing vehicle from lateral direction. Vehicle may also stop and proceed against crossing traffic or both vehicles first stopping and then proceeding on straight crossing paths.
- Turning: these scenarios refer to any crossing-paths turning maneuvers other than the LTAP/OD scenario.

Table 1. Vehicle-Vehicle Crash Scenario Ranking

Crash Scenario	CIB	ARS
Opposite-Direction - Front-Front	1	1
Rear-End - Front-Back	2	2
LTAP/OD - Front-Front	3	3
SCP - Front-Left Side	4	5
Turning - Front-Left Side	5	4
SCP - Front-Right Side	6	6

ANALYSIS OF CIB CRASH CASES

The filtering scheme is first outlined to select crash cases from target crashes for further examination. Applicable CIB cases from vehicle-object and vehicle-vehicle crashes are later described separately. This description includes CDS statistics on the breakdown of target vehicles by vehicle type (i.e., passenger car or light truck or van), attempted avoidance maneuver by the target vehicle, environmental conditions, and Delta V (ΔV).

Selection of CIB Applicable Cases

The following five filters were applied to identify the final set of target vehicle cases that might be amenable to CIB applications:

1. Include crash cases where at least one occupant in any vehicle suffered an injury level of MAIS2⁺.
2. Exclude crash cases in which the target vehicle attempted any braking maneuver. It is assumed that brake assist, a different countermeasure than CIB, would apply if brakes were applied in the target vehicle.
3. Exclude crash cases in which the target vehicle lost control as a result of an evasive maneuver. Stability control systems help in this situation.
4. Include crash cases in which the target vehicle had at least one of the following information:

longitudinal ΔV or estimated highest ΔV values from the CDS [6], or ΔV available from event data recorders [7].

- Exclude crash cases in which the target vehicle experienced longitudinal ΔV over 45 mph (72 Km/h).

After the five filters were applied, remaining cases were individually analyzed to determine their applicability to CIB. Tables 2 and 3 provide the results of this filtering process for vehicle-object and vehicle-vehicle crashes, respectively. Out of 1,903 target vehicle cases from vehicle-object crashes, only 99 cases were determined to be amenable to CIB. Using the corresponding CDS weights for these cases, CIB addresses only 2% of the target vehicles. For vehicle-vehicle crashes, CIB addresses 871 target vehicle cases out of a total of 8,807 cases. Using weighted values, CIB could help only 4.3% of all target vehicles involved in vehicle-vehicle crashes. In total, intervention opportunity for CIB exists in about 4% of all target vehicles based on the total weighted counts in Tables 2 and 3.

Table 2. Applicable CIB Vehicle-Object Cases

Obstacle	Raw Count			Weighted Count		
	Initial	CIB	Ratio	Initial	CIB	Ratio
Pole	532	39	7.3%	203,582	7,928	3.9%
Tree	395	31	7.8%	95,033	3,231	3.4%
Ground	364	0	0.0%	197,139	0	0.0%
Structure	612	29	4.7%	183,902	2,363	1.3%
Total	1,903	99	5.2%	679,656	13,522	2.0%

Table 3. Applicable CIB Vehicle-Vehicle Cases

Crash Scenario	Raw Count			Weighted Count		
	Initial	CIB	Ratio	Initial	CIB Cases	Ratio
OD - FF	1,072	218	20.3%	222,638	58,904	26.5%
RE - FB	2,427	62	2.6%	1,637,691	16,343	1.0%
LTAP/OD - FF/FRS	2,414	293	12.1%	964,399	61,829	6.4%
SCP - FLS/FRS	2,005	218	10.9%	801,240	26,331	3.3%
Turning - FLS	889	80	9.0%	458,589	12,286	2.7%
Total	8,807	871	9.9%	4,084,557	175,693	4.3%

FF: Front-Front, FB: Front-Back, FLS: Front-Left Side
FRS: Front-Right Side

Description of CIB Vehicle-Object Cases

Statistical description of CIB vehicle-object cases is provided using CDS weighted values. About 63% of the target vehicles were light trucks or vans. Figure 3 shows statistics of attempted avoidance maneuver by the target vehicle in CIB-applicable vehicle-object crashes, excluding braking. Steering was noted for 22.4% of the target vehicles. Table 4

presents statistics on environmental conditions including atmospheric, lighting, and roadway surface conditions. In vehicle-object crashes, 96% of target vehicles were driving under clear weather, 91% were traversing dry road surfaces, and 56% were traveling in non-daylight conditions. Figure 4 plots the cumulative percentage of target vehicles by total ΔV . Almost two thirds of the vehicles (65%) suffered ΔV under 40 Km/h. Moreover, 95% of the vehicles experienced total ΔV under 55 Km/h. It should be noted that vehicles with longitudinal ΔV over 72 Km/h were excluded from this analysis.

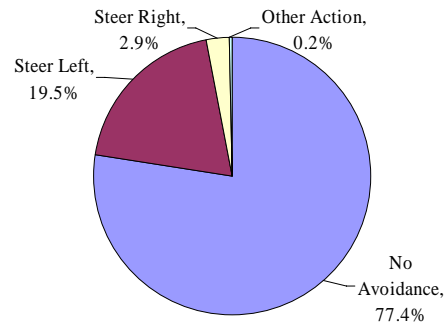


Figure 3. Avoidance Maneuver in CIB Vehicle-Object Crashes

Table 4. Environmental Conditions in CIB Vehicle-Object Crashes

		Weight	%
Atmospheric Condition	Clear	12,975	96.0%
	Adverse	547	4.0%
Total		13,522	100.0%
Lighting Condition	Daylight	5,972	44.2%
	Dark	4,922	36.4%
	Dark/Lighted	2,466	18.2%
	Dawn	133	1.0%
	Dusk	27	0.2%
Total		13,522	100.0%
Roadway Surface Condition	Dry	12,356	91.4%
	Slippery	1,165	8.6%
Total		13,522	100.0%

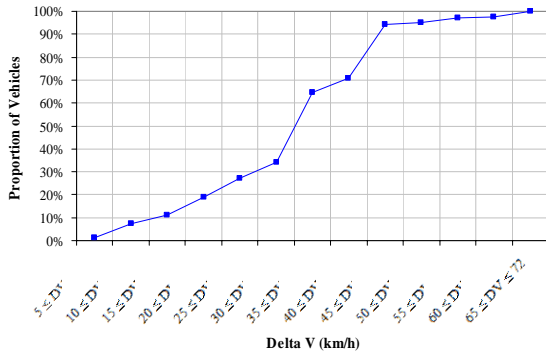


Figure 4. Cumulative Distribution of Vehicles by Total ΔV in CIB Vehicle-Object Crashes

Description of CIB Vehicle-Vehicle Cases

About 53% of the target vehicles involved in vehicle-vehicle crashes were light trucks or vans. Table 5 shows statistics of attempted avoidance maneuver by the target vehicle in CIB-applicable vehicle-vehicle crash scenarios, excluding braking. Steering was noted for 17.4% of the target vehicles. Rear-end crash scenario had the highest steering percentage (56%) among other vehicle-vehicle crash scenarios. On the other hand, opposite direction crash scenario had the least steering maneuvers (11%) by target vehicles. Table 6 provides CDS statistics on environmental conditions including atmospheric, lighting, and roadway surface conditions. In vehicle-vehicle crashes, 94% of target vehicles were driving under clear weather, 92% were traversing dry road surfaces, and 58% were traveling in daylight. Figure 5 plots the cumulative percentage of target vehicles by total ΔV in vehicle-vehicle crash scenarios. Almost two thirds of the target vehicles (66%) suffered ΔV under 25 Km/h. Moreover, 95% of the vehicles experienced total ΔV under 45 Km/h. It should be noted that vehicles with longitudinal ΔV over 72 Km/h were excluded from this analysis. Table 7 presents statistics on the relative direction of vehicles when they crashed. This information is relevant to the development of performance requirements for the field-of-view of pre-crash sensors.

Table 5. Avoidance Maneuver Statistics in CIB Vehicle-Vehicle Crash Scenarios

Attempted Avoidance Maneuver	OD	RE	LTAP/OD	SCP	Turning	All
No Avoidance	89%	44%	87%	85%	64%	82%
Steering Left	4%	0.3%	1%	9%	24%	5%
Steering Right	7%	56%	11%	5%	9%	13%
Accelerating & Steer Left	0.1%		0.2%	0.03%	1%	0.2%
Accelerating			1%	0.1%		0.4%
Other Action	1%		0.1%		2%	0.3%
Total	100%	100%	100%	100%	100%	100%

Table 6. Statistics of Environmental Conditions in CIB Vehicle-Vehicle Crash Scenarios

		OD	RE	LTAP/OD	SCP	Turning	All
Weather Condition	Clear	91%	99%	93%	96%	96%	94%
	Adverse	9%	1%	7%	4%	4%	6%
Total		100%	100%	100%	100%	100%	100%
Lighting Condition	Dark	5%	10%	14%	5%	3%	8%
	Dark/Lighted	68%	12%	17%	14%	6%	32%
	Dawn	0%	3%	1%	1%	0%	1%
	Daylight	26%	73%	67%	80%	91%	58%
	Dusk	1%	3%	1%	0%	0%	1%
	Total	100%	100%	100%	100%	100%	100%
Roadway Surface Condition	Dry	91%	99%	91%	93%	89%	92%
	Slippery	9%	1%	9%	7%	11%	8%
Total		100%	100%	100%	100%	100%	100%

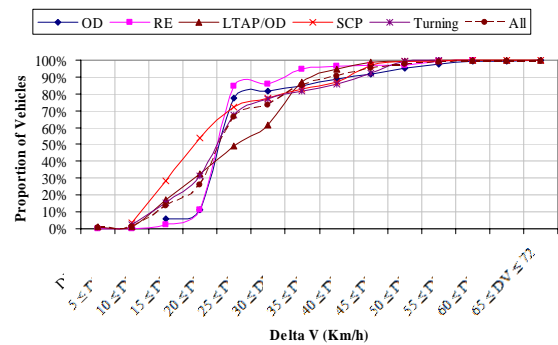


Figure 5. Cumulative Distribution of Vehicles by Total ΔV in CIB Vehicle-Vehicle Crash Scenarios

Table 7. Relative Direction Statistics in CIB Vehicle-Vehicle Crash Scenarios

Relative Clock	OD	RE	LTAP/OD	SCP	Turning	All
1	2%		18%			7%
10	0.2%		5%	0.1%		2%
10-11	5%		24%			10%
11	4%		4%	0.1%		3%
11-12	75%		6%			28%
1-2	0.2%		16%		13%	7%
12, head on	4%					1%
12-1	8%		14%			8%
2			2%	0.4%	5%	1%
9-10	1%					0.2%
2-3	0.2%		1%	3%	61%	5%
3, angle		0.1%		43%	4%	7%
3-4				11%	13%	3%
4					0.1%	0.01%
4-5					0.4%	0.03%
5					2%	0.1%
5-6		92%			2%	9%
6-7		8%				1%
7-8						0%
8			0.1%			0.04%
8-9			1%	5%		1%
9, angle			1%	36%		6%
9-10			8%	2%		3%
Total	100%	100%	100%	100%	100%	100%

Figure 6 illustrates the configurations of the relative direction for head-on/angle and rear-end/angle collisions. In rear-end pre-crash scenarios, the front of the target vehicle struck the back of the other vehicle within ± 30 degrees in 100% of the cases, relative clock between 5 and 7 as indicated in Table 7. In opposite direction pre-crash scenarios, the front of the target vehicle struck the front of the other vehicle within ± 30 degrees in 94% of the cases, relative clock between 1 and 11. In straight crossing path pre-crash scenarios, the front of the target vehicle struck the side of the other vehicle at 90 degrees in 79% of the cases, relative clock at 3 or 9. In LTAP/OD pre-crash scenarios, the relative angle of collision between the target vehicle and the other vehicle was between 30 and 60 degrees in 69% of the cases, relative clock between 1 and 2 and between 10 and 11. In all CIB vehicle-vehicle crash scenarios, 56% and 76% of the target vehicles experienced a relative angle of collision respectively within ± 30 and ± 60 degrees.

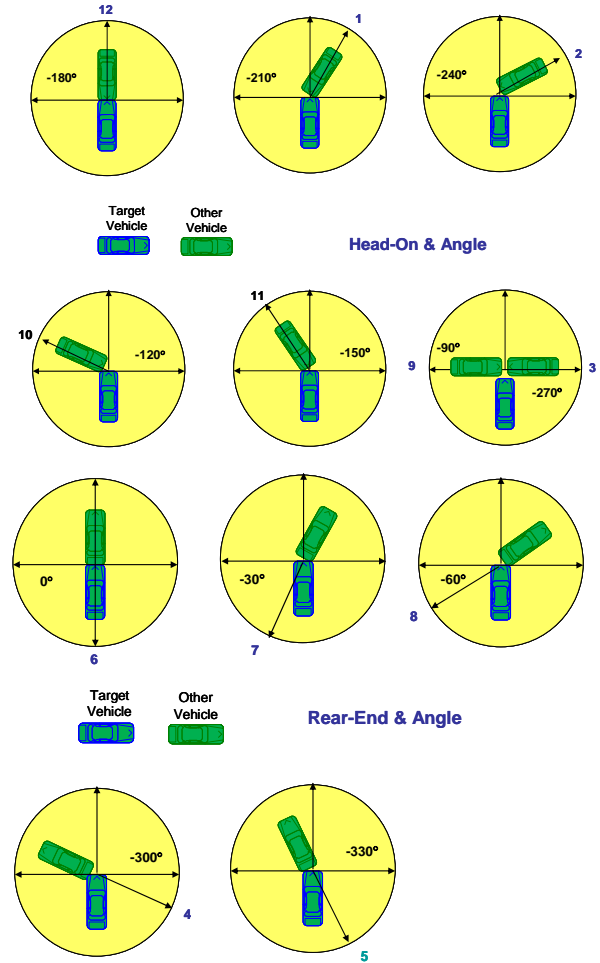


Figure 6. Configurations of Relative Directions

ANALYSIS OF ARS CRASH CASES

Results are presented from a detailed examination of individual crash cases deemed as priority for intervention opportunities by ARS with pre-crash sensing capability. This analysis included target vehicles in which the driver or FSP13⁺ suffered an injury level of MAIS3⁺. All relevant cases belonging to the following five crash scenarios were selected from the 1997-2006 CDS databases for further examination:

- Opposite direction pre-crash scenarios with different impact modes
- Rear-end pre-crash scenarios with front-to-back impact mode
- LTAP/OD pre-crash scenarios with different impact modes
- Road departure pre-crash scenarios
- Control loss pre-crash scenarios

The selection and review of candidate cases are first delineated. This will be followed by a statistical description of the target occupants in terms of their breakdown by crash scenario, number of impact events, ΔV , and vehicle damage location and offset. In addition, statistics are provided about the distribution of injured body regions by crash scenario and injury source.

Selection and Review of Occupant Cases

All relevant cases from the CDS were divided and assigned to different reviewers. Cases lacking clarity or missing information were subjected to a group review or discarded. Reviewers were asked to consider coded, photographic, graphic, and supplementary unedited data sources, resident on the NASS CDS case access viewer [8]. Instructions were given to reviewers prior to accessing this viewer to encourage uniformity in consideration and synthesis of analysis. As a result, some cases were excluded from the analysis due to insufficient data, incorrect crash modes, and unique modes not applicable to this study such as A-pillar contact with predominant side impact damage. Also excluded were cases that had losses in passenger compartment integrity. This constraint was placed on the analysis owing to the technologies contemplated and their potential countermeasures.

During the review, consideration was given to the role of active and passive restraint systems resident in the target vehicle. The applicability of newer generation restraint systems was assessed in terms of their potential capability to mitigate or avoid injuries produced in the various crash types. In each vehicle case, the driver and FSP13⁺ with AIS3⁺ injuries were examined separately. This examination focused on injured occupants who were restrained using a lap and shoulder belt and their airbag was deployed. All AIS3⁺ injuries were included; however, many lower extremity cases exist in which the present restraint or an advanced restraint would have been superfluous based upon the specific crash parameters. Consideration, however, was given to the potential presence of knee airbags and their role in injury mitigation or prevention. Each body region was analyzed separately if a driver or FSP13⁺ had AIS3⁺ injuries to more than one body region. If a single body region sustained multiple AIS3⁺ injuries, the analysis then focused on the most severe injury.

Injury information was based on vehicle inspection and injury assessment records. Vehicle inspection involved an examination of the vehicle and evidence of relevant occupant contact. This was tempered by a review of medical records and vehicle contact assessment. The case reviewer consulted the

various photographs taken in support of the crash investigation, scene diagram, and the unedited text version of crash events. Table 8 lists the number of relevant vehicle and occupant files reviewed and disaggregates them by reviewer disposition. Counts of vehicles and occupants were weighted to reflect national CDS representation. These dispositions were assessed relevant to the injuries sustained and the applicability of a restraint system. It should be noted that the majority of relevant occupants was submitted to the automotive partners as candidate members of advanced restraints systems. Overall, 71% of the weighted number of vehicles and occupants (63% of counts) were accepted for further examination. The following analyses were conducted on target occupants who were accepted by case reviewers as candidates for ARS applications.

Table 8. Number of Relevant Vehicles and Occupants by Reviewer Disposition

Reviewer Disposition	Vehicles		Occupants	
	Weighted	Count	Weighted	Count
Accepted	32,134	389	33,006	407
Rejected	12,739	226	13,434	239
Questionable	145	1	145	1
Total	45,018	616	46,585	647

Breakdown of Occupants by Crash Scenario and Number of Events

Figure 7 shows a breakdown of the weighted number of accepted occupant cases by the five crash scenarios. About 61% of the occupants were traveling in vehicles that were involved in single-vehicle crashes: road departure and control loss. Of these occupants involved in single-vehicle crashes, 72% of the occupants were in a single impact or a multi-impact crash in which the first event was the most harmful. In contrast, 93% of the occupants who were involved in multi-vehicle crashes were traveling in vehicles sustaining a single impact or a most harmful first event in a multi-impact crash. In general, only 20% of target occupants were involved in multi-impact crashes where the most harmful event resulted from secondary impacts.

Figure 8 shows the breakdown of target occupant cases by the crash scenario and event category. The following results can be observed:

- Opposite direction crashes had the highest rate of occupants in single events (59% of all occupants in opposite direction crashes).
- Rear-end crashes had the highest rate of occupants in multi-impact, most harmful first events (53% of all occupants in rear-end crashes).

- Road departure crashes had the highest rate of occupants in multi-impact, most harmful secondary events (30% of all occupants in road departure crashes).

In multi-impact crashes in which the most harmful event happened in secondary events, about 87% of the target occupants were in vehicles experiencing frontal damage in the most severe event. Damage to the undercarriage was reported as the most severe event for 6% of the occupants. The remaining 7% of the occupants were evenly split between right and left damage areas of the vehicles in the most severe event. Overall, 98% of the target occupants were in vehicles suffering frontal damage in the most harmful event in single- and multi-impact crashes. Thus, the remainder of this section presents occupant results independent of the number of impact events.

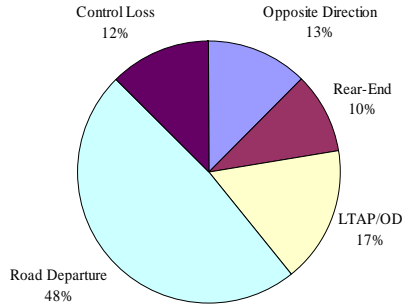


Figure 7. Breakdown of Occupants by Crash Scenario

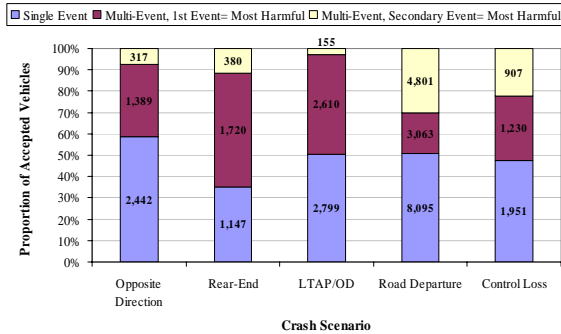


Figure 8. Breakdown of Occupants by Crash Scenario and Event

Breakdown of Occupants by Delta V, Damage Location, and Offset

Figure 9 shows the cumulative distribution of occupants by ΔV , representing a proportional

redistribution of vehicles with only calculated ΔV values. Not included were 24% of the occupants in vehicles that had other or unknown information coded in the CDS. About 96% of the occupants were in vehicles that experienced ΔV below 70 Km/h. Moreover, 49% of the occupants were in vehicles having ΔV values below 30 Km/h.

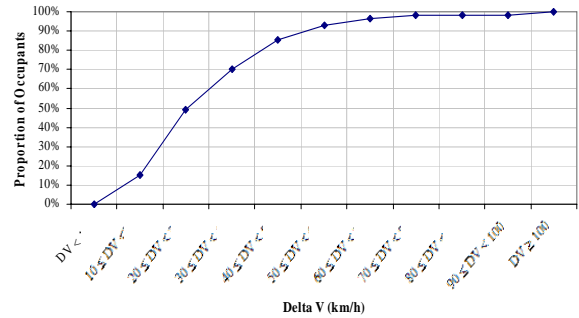


Figure 9. Cumulative Distribution of Occupants by Delta V

Breakdown of the number of occupants by vehicle damage location and offset percentage in Figure 10 shows:

- 50% of the occupants were in vehicles sustaining left frontal damage with offset percentage of 50% or less.
- 23% of the occupants were in vehicles suffering center frontal damage with offset percentage greater than 50%.
- 17% of the occupants were in vehicles experiencing right frontal damage with offset percentage of 50% or less.

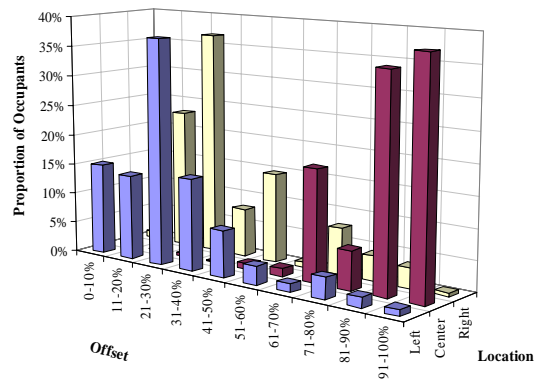


Figure 10. Distribution of Occupants by Vehicle Damage Location and Offset

Examination of Injuries

Figure 11 shows the distribution of 42,000 MAIS3+ injuries by injured body region. The highest

injured body region was the chest at 36% of all MAIS3+ injuries. This was followed by the lower extremity. About 48% of MAIS3+ injuries were associated with extremities. Figure 12 provides a distribution of MAIS3+ injuries by crash scenario. Road departure resulted in most MAIS3+ injuries at 49%. Overall, single-vehicle crashes and multi-vehicle crashes accounted respectively for 61% and 39% of all MAIS3+ injuries to target occupants. Table 9 lists the weighted counts of MAIS3+ injuries by injured body region and crash scenario.

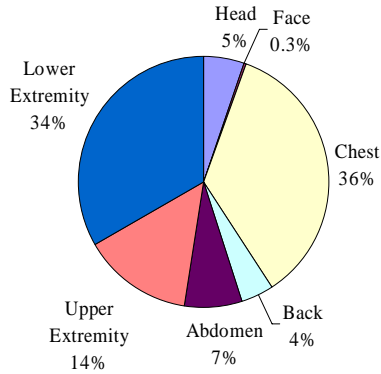


Figure 11. Distribution of MAIS3+ injuries by Body Region

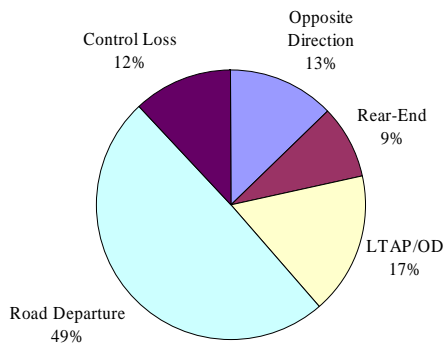


Figure 12. Distribution of MAIS3+ injuries by Crash Scenario

Table 9. Breakdown of MAIS3+ Injury Counts

Crash Scenario	Head	Face	Chest	Back	Abdomen	Upper Extremity	Lower Extremity	Total
Opposite Direction	178	18	1,538	125	702	535	2,301	5,398
Rear-End	191	0	297	204	42	804	2,205	3,743
LTAP/OD	526	4	1,961	108	272	1,944	2,312	7,127
Road Departure	1,088	60	8,558	776	1,838	2,358	6,243	20,921
Control Loss	278	58	2,463	605	245	344	1,064	5,057
Total	2,262	140	14,817	1,817	3,099	5,985	14,125	42,246

Analysis of Injury Sources

Figure 13 shows the distribution of MAIS3+ injuries by the source of injury in the vehicle as identified by the case reviewer. Other non-specific sources of injury were reported as the highest rate at 23% of MAIS3+ injuries. Instrument panel, seatbelt, and steering wheel were the three other sources of injury each at a rate over 10%, respectively at 18%, 16%, and 15% of MAIS3+ injuries. Airbag and knee bolster followed respectively at 8% and 7% of MAIS3+ injuries.

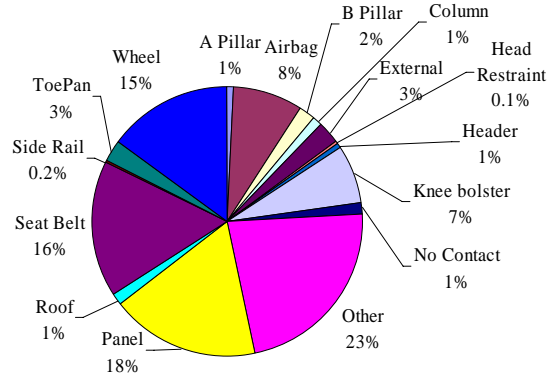


Figure 13. Distribution of MAIS3+ Injuries by Source of Injury

Table 10 provides percentage values of MAIS3+ injury source contribution rates to each body region. The highest rate to each body region is highlighted in yellow. The steering wheel had the highest contribution rate in chest, head, and upper extremity body regions. Injury to the abdomen was caused predominantly by the seatbelt at an extreme rate of 83%. It should be noted that target occupants were all belted. Instrument panel caused the highest rate of injury to the lower extremity at 40%.

Table 11 provides percentage values of MAIS3+ injury source contribution rates in each crash scenario. The highest rate to each body region is highlighted in yellow and the second highest rate is highlighted in tan. Injury sources indicated by the reviewers as “other” were the most dominant in multi-vehicle crashes. Seatbelt was the second highest contributor to MAIS3+ injury in opposite direction and rear-end crashes. On the other hand, knee bolster was the second highest injury source in LTAP/OD crashes. It is interesting that the instrument panel was the most dominant injury source in road departure crashes while the steering wheel was the most prevalent in control loss crashes. Control loss is usually associated with high speeds while road departure is associated with lower speeds and impaired drivers. Based upon these findings, it is possible that high

speed crashes cause drivers to strike steering wheel at a higher force.

Table 10. Percentage of MAIS3+ Body Region Injuries by Injury Source

Injury Source	Abdomen	Back	Chest	Face	Head	Lower Extremity	Upper Extremity
A Pillar				20%	8%		2%
Airbag		10%	19%		8%	3%	9%
B Pillar		7%			20%		1%
Column			4%				1%
External				35%	5%	2%	11%
Head Restraint					1%		
Header				10%	3%		3%
Knee bolster						19%	
No Contact		19%			3%		
Other	14%	24%	19%	19%	14%	28%	25%
Panel			1%		5%	40%	16%
Roof		22%			3%		
Seat Belt	83%	4%	28%		3%		1%
Side Rail					3%		
ToePan							7%
Wheel	3%	14%	29%	16%	23%	1%	33%
Total	100%	100%	100%	100%	100%	100%	100%

Table 11. Percentage of MAIS3+ Injuries in Crash Scenarios by Injury Source

Injury Source	Opposite Direction	Rear-End	LTAP/OD	Road Departure	Control Loss
A Pillar		2%		2%	1%
Airbag		11%	10%	2%	
B Pillar			1%	7%	4%
Column		3%		1%	1%
External					3%
Head Restraint					11%
Header		1%	5%		
Knee bolster		14%		25%	
No Contact		3%	9%		
Other	34%	50%	27%	13%	23%
Panel	3%	9%	10%	30%	11%
Roof				2%	2%
Seat Belt	16%	12%	11%	20%	14%
Side Rail			1%		
ToePan		5%	1%	6%	1%
Wheel		6%	4%	9%	19%
Total	100%	100%	100%	99%	100%

CONCLUSIONS

Based on results from general data queries that prioritized pre-crash scenario and impact mode combinations, individual CDS cases were selected for review for potential mitigation by CIB and ARS. Different filtering schemes were adopted to determine the applicability of CIB and ARS to selected cases. Descriptive statistics using weighted CDS data were provided to the CIB and ARS applicable case sets.

The CIB analysis identified 99 cases out of 1,903 target vehicle cases from vehicle-object crashes and 871 cases out of 8,807 target vehicle cases from vehicle-vehicle crashes to be amenable to CIB intervention. Brake assist or stability control was assumed to address some of the other cases. Using CDS weights for these cases, CIB addresses about

4% of all target vehicles. The analysis of CIB applicable vehicle cases revealed:

- About 63% of the target vehicles involved in vehicle-object crashes were light trucks or vans. By excluding braking from CIB applicable cases, steering was noted as the avoidance maneuver for 22% of the target vehicles. In vehicle-object crashes, 96% of target vehicles were driving under clear weather, 91% were traversing dry road surfaces, and 56% were traveling in non-daylight conditions. Almost two thirds of the vehicles suffered total ΔV under 40 Km/h. Moreover, 95% of the vehicles experienced total ΔV under 55 Km/h. Vehicles with longitudinal ΔV over 72 Km/h were excluded from the CIB applicable case set.
- About 53% of the target vehicles involved in vehicle-vehicle crashes were light trucks or vans. Excluding braking from CIB applicable cases, 17% of target vehicles attempted steering before the crash. In vehicle-vehicle crashes, 94% of target vehicles were driving under clear weather, 92% were traversing dry road surfaces, and 58% were traveling in daylight. Almost two thirds of the target vehicles (66%) suffered ΔV under 25 Km/h and 95% of the vehicles experienced total ΔV under 45 Km/h. In all CIB vehicle-vehicle crash scenarios, 56% and 76% of the target vehicles experienced a relative angle of collision respectively within ± 30 and ± 60 degrees.

The ARS analysis restricted target occupants to belted drivers and FSP13+. Overall, 71% of the number of occupants were accepted for further examination. The raw number of CDS cases was 407 occupants. Results showed:

- 72% of occupants in single-vehicle crashes were in a single- or multi-impact crash in which the first event was the most harmful. In contrast, this rate was 93% in multi-vehicle crashes.
- 96% of occupants were in vehicles with ΔV below 70 Km/h.
- 50% and 17% of occupants were in vehicles sustaining left and right frontal damage, respectively, with offset percentage of 50% or less. The remaining 23% were in vehicles with center frontal damage at offset percentage greater than 50%.
- Single- and multi-vehicle crashes accounted respectively for 61% and 39% of all MAIS3+ injuries to occupants.
- The body region most likely to be injured at MAIS3+ was the chest, accounting for 36% of

all MAIS3⁺ injuries. About 48% of MAIS3⁺ injuries were associated with lower and upper extremities.

- Other non-specific sources of injury were reported as the highest rate at 23% of MAIS3⁺ injuries. Instrument panel, seatbelt, and steering wheel followed respectively at 18%, 16%, and 15% of MAIS3⁺ injuries. Airbag and knee bolster were noted at 8% and 7% of MAIS3⁺ injuries.
- Steering wheel had the highest contribution rate to injury in chest, head, and upper extremity body regions. Injury to the abdomen was caused predominantly by the seat belt at an extreme rate of 83%. Instrument panel caused the highest rate of injury to the lower extremity at 40%.

Results from these crash analyses were used by the automotive partners and their suppliers to devise potential countermeasure concepts for CIB and ARS based on pre-crash sensing, and to develop preliminary functional requirements. Development of objective test procedures and estimation of safety benefits constitute next research steps.

REFERENCES

- [1] Crash Avoidance Metrics Partnership, Task 3 Final Report – Identify Intelligent Vehicle Safety Applications Enabled by DSRC. Vehicle Safety Communications Project, DTFH61-01-X-0001, Federal Highway Administration, May 2004.
- [2] Crash Avoidance Metrics Partnership, Objective Tests for Crash Imminent Automatic Braking Systems. Task 2, DTNH22-05-H-01277, National Highway Traffic Safety Administration, 2008.
- [3] Crash Avoidance Metrics Partnership, Objective Tests for Advanced Restraint Systems. Task 3, DTNH22-05-H-01277, National Highway Traffic Safety Administration, 2008.
- [4] A.M. Eigen and W.G. Najm, Prioritization of Crash Scenarios for Pre-Crash Sensing Applications. Paper No. 2009-01-1248, SAE 2009 World Congress, Detroit, MI, April 2009.
- [5] T. Miller, J. Viner, S. Rossman, N. Pindus, W. Gellert, J. Douglass, A. Dillingham, and G. Blomquist, The Costs of Highway Crashes. FHWA-RD-91-055, Federal Highway Administration, October 1991.
- [6] National Center for Statistics and Analysis, National Automotive Sampling System Crashworthiness Data System 2000 Coding and Editing Manual. National Highway Traffic Safety Administration, 2001.
- [7] ftp://ftp.nhtsa.dot.gov/NASS/EDR_Reports/
- [8] <http://www.nass.nhtsa.dot.gov/BIN/NASSCASELIST.EXE/SETFILT>

Investigation for New Side Impact Test Procedures in Japan

Hideki Yonezawa

Naruyuki Hosokawa

Yoshinori Tanaka

Yasuhiro Matsui

Shunsuke Takagi

National Traffic Safety and Environment Laboratory

Takahiro Hirasawa

Hitoshi Kanoshima

Ministry of Land, Infrastructure and Transport

Koji Mizuno

Nagoya University

Japan

Paper Number 09-0369

ABSTRACT

Side impact regulations have been introduced in many countries to improve occupant protection in side collisions. As a result, car structures have been improved significantly. However, the number of fatalities and serious injuries in side collisions is still large. To understand the causes of these injuries and to identify their potential countermeasures, accident analyses of side collisions were newly conducted.

From the accident data analysis, it was shown that the contacts with the head and chest during side crashes are still a major cause of serious injuries and death. The impact vehicle type affected the injured body regions of the occupant in the struck vehicle, and the chest was frequently injured in the struck car when impacted by an 1BOX type vehicle. Occupant seating postures were surveyed in vehicles on the roads, and it was found that from a side view that the head location of 50% of the drivers was in line or overlapped with the vehicle's B-pillar. This observation suggests that in side collisions head injuries may occur frequently due to contacts with the B-pillar.

A series of side impact tests were conducted to examine test procedures that would be beneficial for improving occupant protection. When the 1BOX was a striking vehicle, the chest deflection of the ES-2 dummy was large. The crash tests also included car-to-car crash tests in which either (1) both cars are moving or (2) one car is stationary, i.e., an ECE R95 test. The injury measures of the ES-2 dummy were substantially smaller if the struck car was moving.

The tests also were conducted for an occupant seating position where the head would make contact with the B-pillar. To investigate the effectiveness of curtain side airbags for head protection in car-to-car crashes, these test were conducted for struck cars with and without a curtain side airbag. It was demonstrated that

the curtain side airbag was effective for reducing the number of head injuries in car-to-car crashes.

INTRODUCTION

Though the number of vehicle accidents is decreasing recently, in 2008 it was 760,000 or more, and the number of injuries was 940,000 or more. Considering this traffic accident situation, regulations for occupant protection including the side impact protection [1] have been introduced in Japan. Additionally, The Japan New Car Assessment Program (JNCAP) conducts safety evaluation of new cars.

In traffic accidents in Japan, intersection collisions and rear-end collisions account for about 60% when classified by collision configuration and vehicle-to-vehicle collisions account for 80% or more when classified by crash objects. In fatal and serious injuries to drivers, vehicle-to-vehicle collisions account for a large proportion. In vehicle-to-vehicle side collisions, since the crash configurations are widely varied (such as a large array of impact velocities and angles), an investigation of representative crash test procedures is necessary in order to effectively reduce the number of fatal and serious injuries in side crashes, and to protect the occupants most frequently seriously injured body regions.

In this study, building on the bases of our past studies [2][3][4][5][6][7], side accident analyses, field surveys of occupant postures, and car-to-car side impact tests were conducted. Based on the results of these studies, the trend for a representative side impact test procedure for the future was investigated. In accident analyses, the general trend of side collisions were investigated based on the Institute for Traffic Accident Research and Data Analysis (ITARDA) global accident data for 3 years (2006-2008). In the occupant posture investigation, the relative positions of the head of the driver and passenger with respect to the B-pillar were examined to understand the potential of injury

causation by the B-pillar in side collisions. Several car-to-car crash tests were conducted to investigate potential side impact test procedures for the future. Taking the results of seating posture investigation into account, the crash tests were conducted to understand the effects of curtain side airbag (CSAB) and side air bag (SAB) which were installed recently on many cars.

STUDY ON SIDE IMPACT ACCIDENT IN JAPAN

In this study, the accident analyses in Japan were examined using the police data. From the data, in 2008, the number of traffic accidents in Japan was 766,147, the number of injuries was 950,659, and the number of fatalities (i.e., fatalities within 30 days after an accident) was 6,023.

General Trend of Side Impact Accidents

The number of traffic accidents in which occupants of four-wheel vehicles were involved was 1.4 million from 2005 to 2007. Figure 1 shows the crash configurations as classified by impact locations. A large portion of the total accidents were rear-end collisions. In the fatal and serious accidents, the percentage of frontal collisions was large. Side collisions occupy about 20% of fatal accidents as well as fatal and serious accidents. These findings indicate that, when considering the potential safety benefit of a crash configuration, the side collision is next in importance to the frontal collision, of which the risk of fatal and serious injury to occupants was high.

The fatal and serious injuries of front seat occupants were examined for side collisions which included vehicle-to-vehicle intersection collisions and single vehicle collisions. Multiple collisions were excluded. Figure 2 shows the percentage of striking vehicle and object types by seat position (struck-side or non struck-side) of the front seat occupants in the struck vehicle. Sixty percent of the fatal and serious injuries in side collisions are on the struck side occupants, and 40% are the non-struck side occupants. Eighty percent of the striking objects were vehicles, which account for the largest source of striking objects. Among these, the mini passenger cars and passenger cars account for 60%. Narrow objects (e.g., signals, telephone poles, and road signs) account for 6% or less.

Figure 3 shows the injured body regions of the occupants by striking objects. When struck by an 1BOX or SUV, and a Large vehicle or Truck, the percentage of head and chest injuries was large, whereas that of neck injury decreases. When struck by a pole, the percentage of head injuries is large. The percentage of abdomen injuries is lowest, irrespective of striking objects.

Figure 4 shows the relation between injured body regions to the struck-side occupants and injury causes. The door and window account for the largest percentage of injury causes. Seats account for 60% of the injury causes for the neck. The pillars, which have probably high injury potentials in the passenger compartment, account for only small percentages of injury causes. To understand the injury causes in side impact collisions in more detail, it is necessary to examine the injury causes using in-depth accident data.

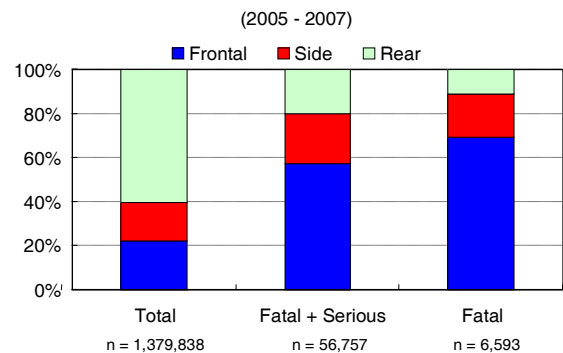


Figure 1 Impact configuration of vehicle accidents

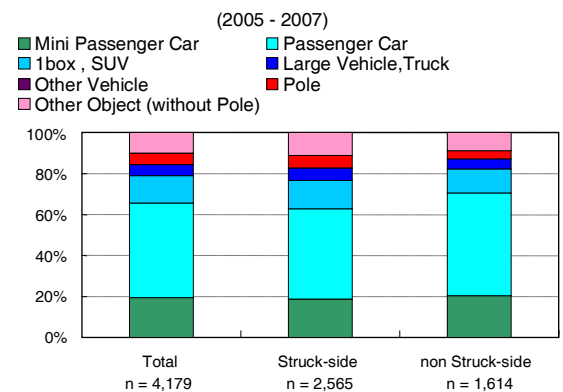


Figure 2 Type of striking vehicle and object involved in side impact accidents (fatal and serious injuries).

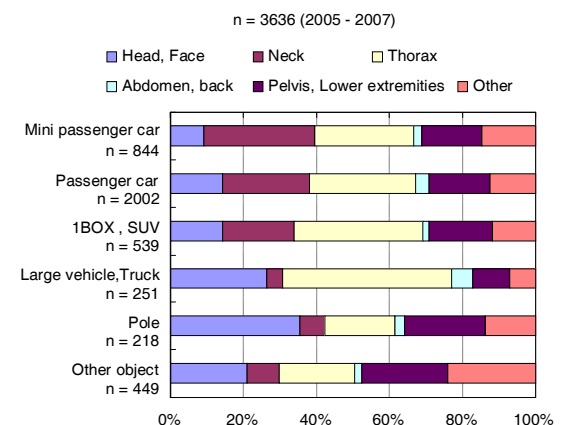


Figure 3 Injured body regions for fatal and serious injuries in side impact accidents by striking object.

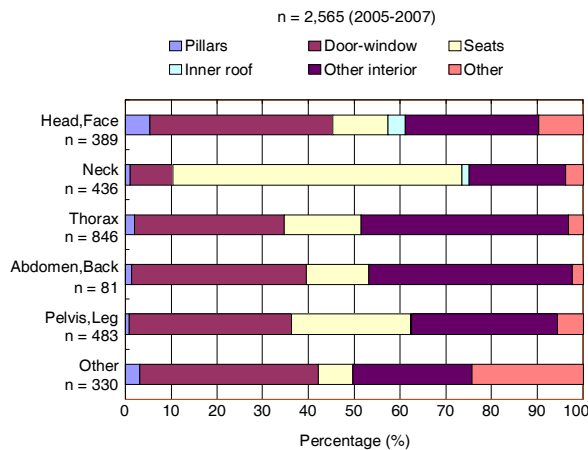


Figure 4 Contact parts for injuries in side impact accidents (struck-side occupant)

INVESTIGATION OF RIDING POSTURE POSITION

The postures of the driver and front passenger in the real-world were surveyed in order to provide a basis to predict injury causes of the car interior in side impact accidents. The pictures of the position of a front seat occupant were recorded by a video camera from a side view of the vehicle, and the occupant head's position was observed. From the accident analyses, the head was a frequently injured body region in side impact accidents. Therefore, the percentage of occupants whose head location overlapped with the vehicle's B-pillar was examined. By analyzing the results, the conditions for which occupant protection devices effectively work (i.e., the area to be covered by the occupant protection device) also could be estimated.

Investigation on Driver and Passengers Seating Position in Real World

Side views of vehicles traveling in both directions of the road near an intersection were filmed with a video recorder. From the side view of the occupants, the percentage of the occupants whose head overlapped with the B-pillar was examined. The head positions of drivers (right side) and front passengers (left side) were surveyed. The surveyed vehicles were passenger cars (sedan, wagon, and 1BOX) and mini passenger cars. The large vehicles such as truck and bus, and 2-door cars were excluded from the survey. In total, 377 cars were surveyed from driver side, and 256 cars were surveyed from the front passenger side. However, note that only 45 front passengers were examined since front passenger seating frequency was observed to be 18%. Figure 5 shows the criterion used to evaluate whether the head overlapped the B-pillar. Even if only a part of the head overlapped with the B-pillar, it was defined as head/B-pillar overlap.

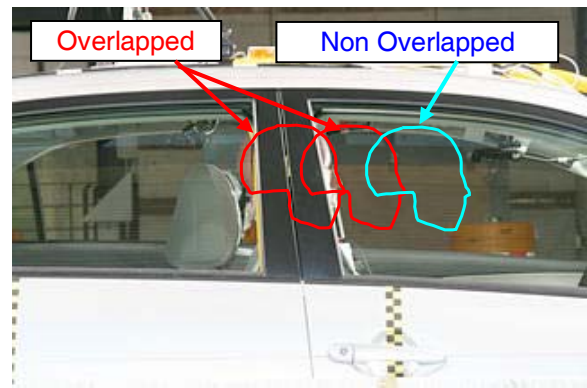


Figure 5 The criterion of judgment for the head overlapping B-pillar

Figure 6 shows the percentages of head/B-pillar overlap for the driver and front passenger. Fifty percent of drivers and 70% of front passengers were determined to have head/B-pillar overlap. The percentage of front passengers was large probably because front passengers have the freedom to change their seat positions, whereas the driver must adjust the seat to accommodate reaching the steering wheel and floor pedals. Figure 7 shows the percentages of the head/B-pillar overlap of drivers by male and female. The percentage of head/B-pillar overlap for female was about half of that for male. It is likely that the body size of the driver affects the overlap percentages.

Figure 8 shows the percentage of the head/B-pillar overlap of the driver by car type. The percentage of head/B-pillar overlap for 1BOX was larger than that for the sedan and wagon. This is probably because the B-pillar of the 1BOX is located more forward as compared to the sedan due to its vehicle design.

Based on the survey, it was found that 50% of the driver heads overlapped the B-pillar. The male has a high frequency of head and B-pillar overlap. The driver head overlaps more frequently with the B-pillar of 1BOX as compared to that for the sedan. Accordingly, it is predicted that the head is likely to contact the B-pillar during side crashes, and thereby lead to head injuries.

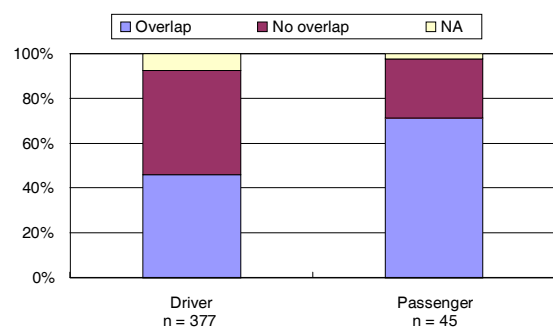


Figure 6 Seat location for the head and B-pillar overlapped.

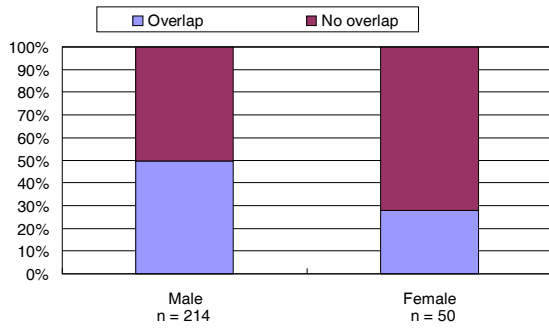


Figure 7 Gender for the head and B-pillar overlapped (Driver).

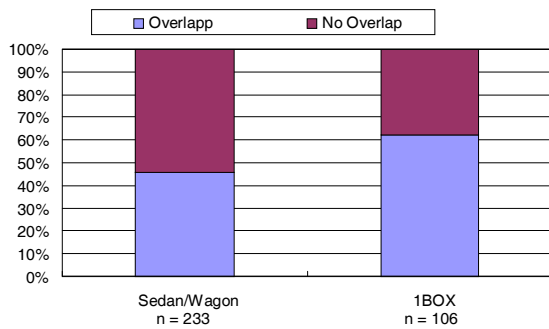


Figure 8 Type of vehicle for the head and B-pillar overlapped (Driver).

In Tests 5 and 6, the effectiveness of the CSAB was examined. The ECE R95 MDB impacted the Sedan 2 at 50 km/h. Considering the occupant posture survey that the head can contact with B-pillar, Tests 5 and 6 were prescribed to investigate the effect of the CSAB and SAB (torso side airbag) to when the occupant head would make contact with the B-pillar with and without these devices. Therefore, for Tests 5 and 6, the seat position was adjusted so that the dummy head overlapped the B-pillar. The CSAB was not equipped in the Sedan 2 in Test 5 and was equipped in the Sedan 2 in Test 6. Test 7 is the JNCAP test of Sedan 2, from which data was used for reference, though the impact velocity of the MDB was 55 km/h. In this paper, results of only the front seat dummy are discussed even though there were rear seat occupants in some tests.

Table 3 Specification of tested vehicles

Type	MDB (ECE/R95)	Sedan 1	Sedan 2	1BOX
Kurb mass	948 kg	1100 kg	1130 kg	1370 kg
Engin displacement	-	1498 cc	1496 cc	1789 cc
Dimension (L x W x H)	500 x 1500 x 500 (Barrier Face)	4395 x 1695 x 1535	4410 x 1695 x 1460	4285 x 1635 x 1980

Table 4 Test configurations

Test No.	1	2	3	4
Test config.				
Impact velocity	50 km/h	50 km/h	50 km/h	48 x 24 km/h
Impact Point	Vehicle C/L	Vehicle C/L	Vehicle C/L	Vehicle C/L
Struck car	SRP	SRP	SRP	SRP
Striking vehicle	Type: ECE/R95 MDB	Car (Sedan 1)	Vehicle (1BOX)	Car (Sedan 1)
Mass	948 kg	1257 kg	1553 kg	1195 kg
Struck car	Type: Car (Sedan 1)	Car (Sedan 1)	Car (Sedan 1)	Car (Sedan 1)
Curtain air bag	without	without	without	without
Mass	1194 kg	1257 kg	1240 kg	1240 kg
Front Dummy	ES-2	ES-2	ES-2	ES-2
Rear Dummy	SID-IIs	ES-2	SID-IIs	SID-IIs

C/L: Center line
SRP: Seating reference point of driver in front seat

Test No.	5	6	7
Test config.			
Impact velocity	50 km/h	50 km/h	55 km/h
Impact Point	Vehicle C/L	Vehicle C/L	Vehicle C/L
Struck car	SRP	SRP	SRP
Striking vehicle	Type: ECE/R95 MDB	ECE/R95 MDB	ECE/R95 MDB
Mass	948 kg	948 kg	948 kg
Struck car	Type: Car (Sedan 2)	Car (Sedan 2)	Car (Sedan 2)
Curtain air bag	without	with CSAB and SAB	without
Mass	1253 kg	1279 kg	1192 kg
Front Dummy	ES-2	ES-2	ES-2

C/L: Center line
SRP: Seating reference point of driver in front seat

FULL-SCALE SIDE IMPACT TEST

Test Method

In order to understand the injury situation in side collision accidents and to investigate the occupant protection in side collisions, two series of crash tests were carried out using a car. In test series of Tests 1 to 4, Sedan 1 was used as a struck car. In the test series of Test 5 to 7, Sedan 2 was used. Table 3 presents the test car specifications, and Table 4 presents the test matrix. Tests were conducted based on the specifications of Regulation ECE/R95. An ES-2 dummy was seated in the stuck side of the front seat. Figure 9 shows the car test configurations and conditions. Figures 10 and 11 show the dummy postures before and after test, respectively. In Tests 1, 2, 3, and 4, the influence of car types on the occupant injury measures was examined. In Test 1 to 4, an ECE R95 moving deformable barrier (MDB), Sedan 1 (same car model as used for the struck car), and 1BOX vehicle were used as the striking cars. The impact velocity ranged from 48 to 50 km/h (Tests 1 to 6). A side impact test with two moving cars using the same car model (Sedan 1) for the striking and struck vehicles also was conducted to simulate a real car-to-car accident (Test 4). In Test 4, the velocities of the striking car and struck car were 48 and 24 km/h, respectively.

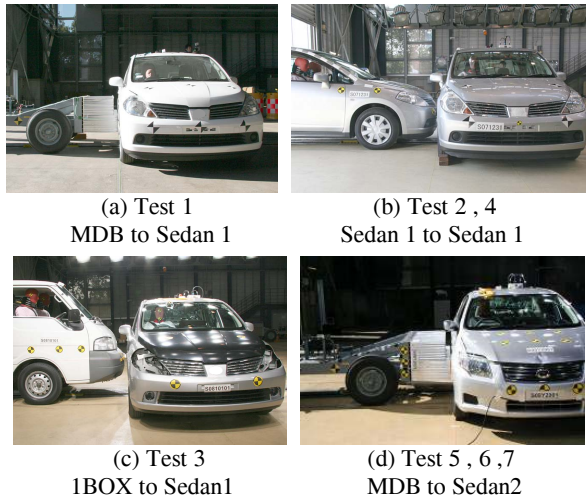


Figure 9 Test vehicles before crash tests

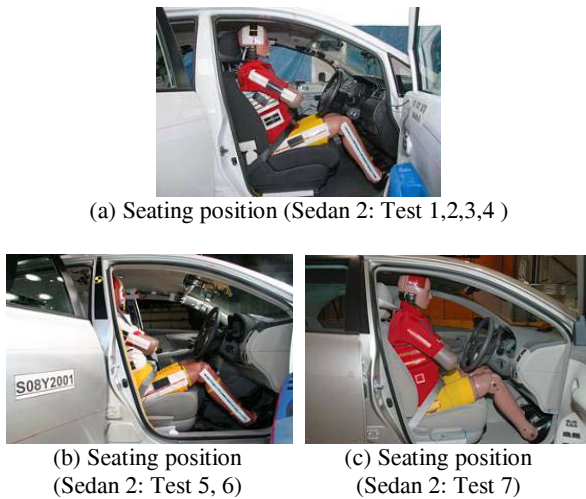


Figure 10 Photo of dummy seating position before tests. Parenthesis indicates the struck car

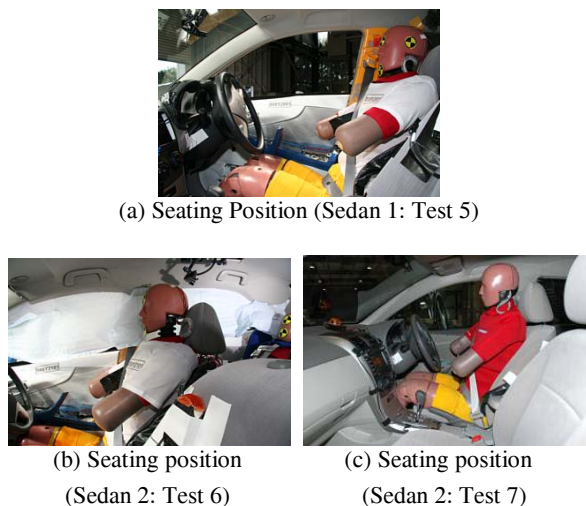


Figure 11 Photo of dummy seating position after tests. Parenthesis indicates the struck car

Test Results

Comparison by striking cars (Test 1 to 4)

The struck car deformation and dummy injury measures were compared from Test 1 to 4. Figure 12 shows the car exterior deformation at the dummy thoracic level, H-point level, and side sill level. In the front seat location (2170 mm) at the thoracic level for the struck car, the deformation increased in the ascending order of the striking vehicle being the Sedan 1 (both cars moving, Test 4), MDB (Test 1), Sedan 1 (Test 2), and 1BOX (Test 3). At the hip point level, the deformation was smallest when the Sedan 1 (Test 4) was the striking vehicle, whereas the deformations were similar when impacted by 1BOX (Test 3), MDB (Test 1) and Sedan 1 (Test 2). At the side sill level, the deformation increased in the ascending order of the striking vehicle being the Sedan 1 (Test 4), Sedan 1 (Test 2), MDB (Test 1) and 1BOX (Test 3). Accordingly, overall the deformation of the struck car was largest when struck by the 1BOX. The flat shape and stiffness of the 1BOX probably affected the deformation of the struck car. The deformation of the struck car was comparable when struck by the MDB and Sedan. When the struck car was moving (Test 4), the deformation of the struck car was smallest among the test series.

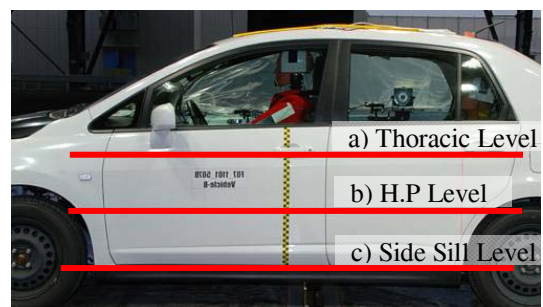
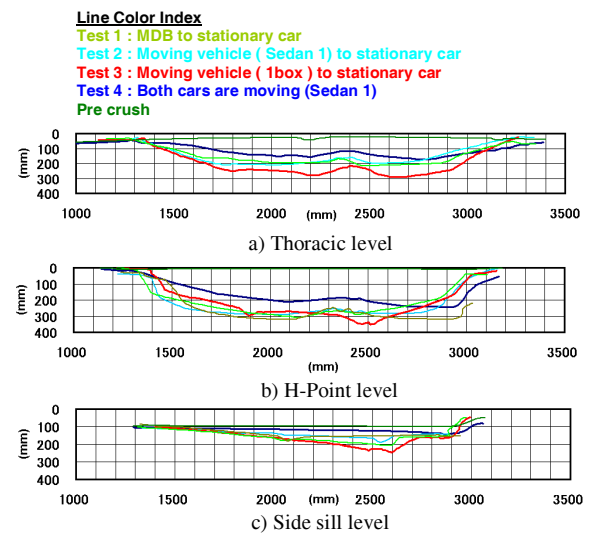
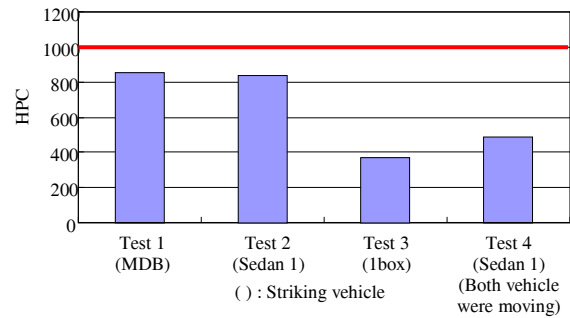


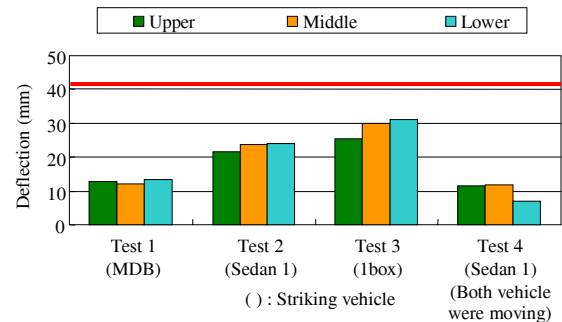
Figure 12 Exterior panel deformation of Sedan 1

Figure 13 shows the injury measures of the front seat ES-2 dummy in the Sedan 1 with the various striking vehicles. In Tests 1 and 4, all injury measures of the ES-2 were less than the acceptance levels of ECE R95. The HPC of the dummy in Sedan 1 struck by the 1BOX (Test 3) and Sedan 1 (both car moving, Test 4) were about 400, which were smaller than the values when struck by the Sedan 1 (Test 2) and MDB (Test 1). The thoracic rib deflection was larger in the ascending order of the striking vehicle being the Sedan 1 (both car moving, Test 4), MDB, Sedan 1, and 1BOX. The lower rib deflection was larger than the upper and middle rib deflection except in Test 4 for the moving vehicle to moving vehicle test. The V*C exhibited a similar trend as the rib deflection. The abdominal force and pubic force of the ES-2 were comparable when struck by Sedan 1, irrespective of whether the struck car was moving (Test 2 and Test 4). The V*Cs were smaller than in these two tests then those measured when the striking vehicles were the 1BOX and MDB.

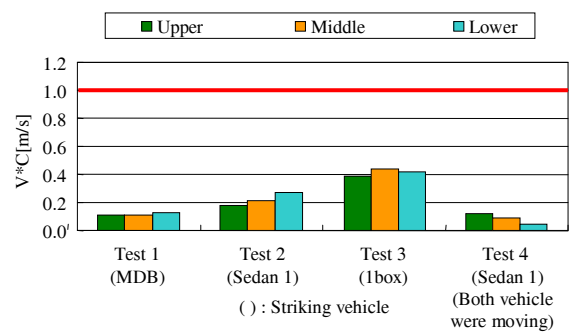
Figure 14 shows the ES-2 dummy kinematic behavior at the time the head resultant acceleration was maximal. When struck by the 1BOX (Test 3), the head of the ES-2 rotated around the x- (anterior-posterior) axis toward the striking vehicle, whereas the head orientation was close to a vertical position in the other tests. In the impact by the 1BOX, the door deformation of the struck car at the thoracic level was large, which led to a large displacement of the ES-2 torso. Then, the head moved toward the inboard side of the car, and it is likely that the head contact velocity with the roof side rail was small. As a result, the HPC was small while the rib deflection was large when struck by 1BOX.



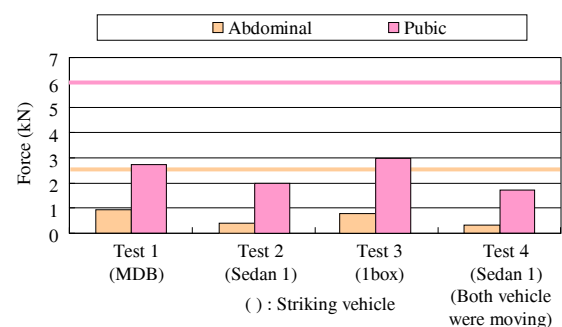
(a) HPC



(b) Thoracic rib deflection



(c) Thoracic rib V*C



(d) Abdominal and public forces

Figure 13. Injury measures of ES-2 in front driver seat in struck car (Sedan 1).

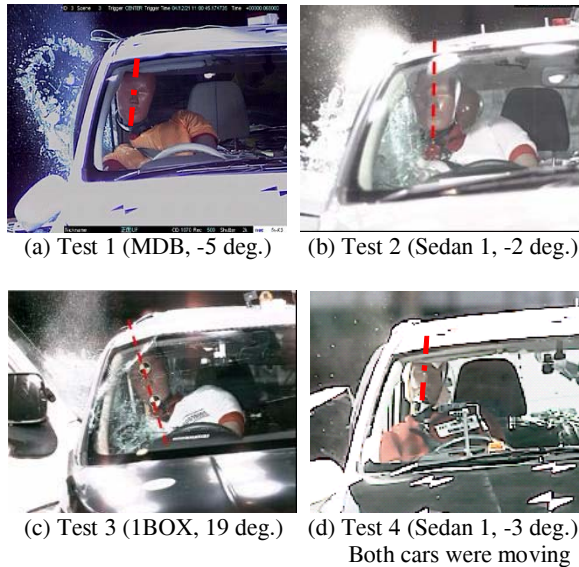


Figure 14 Dummy behavior at the time of maximum resultant head acceleration; parenthesis indicates striking vehicle and inclination angle of dummy head

Comparison by moving and stationary struck cars (Test 2 and 4)

In Tests 2 and 4, the car-to-car tests were conducted using the same models (i.e., both the striking and the struck vehicles were a Sedan 1). In Test 2, the struck car was stationary, and in Test 4 the struck car was traveling at 24 km/h. The influence of a moving struck car was examined based on the results of these two tests. Figure 15 shows the head contact locations in the struck cars for Test 2 and Test 4. The head contact locations in the struck car were similar in both tests, which demonstrate that the head contact velocity in the A-P direction was relatively small even though the struck car was moving in Test 4. The HPC and rib deflection was large when the struck car was stationary (see Figure 13).

Figure 16 shows the struck car deformations in Tests 2 and 4. The deformation of the striking car was larger when the struck car was moving. On the other hand, the deformation of the struck car was larger when the struck car was stationary. In Test 4, the longitudinal member bent laterally in the direction that the struck car was moving. Accordingly, it is likely that the effective stiffness of the striking car was smaller when the struck car was moving than when the struck car was stationary. In Test 4, where both cars were moving, the deformation of the struck car was relatively small but was distributed more widely in the struck car's longitudinal direction (Figure 12 and 16).



Figure 15 Head contact location in the struck car when struck car was stationary (Test 2) and moving (Test 4)



Figure 16 Car deformation when struck car was stationary (Test 2) and moving (Test 4)

Comparison between a curtain side air bag equipping car and a non-equipping car

Based on Tests 5, 6, and 7, the effect of a CSAB was examined. In Tests 5 and 6, the dummy's head was aligned to overlap the B-pillar, and the CSAB and SAB were installed in Test 6. In Test 7 (i.e., the JNCAP test), the impact velocity of the MDB was 55 km/h and the dummy torso made contact with the door.

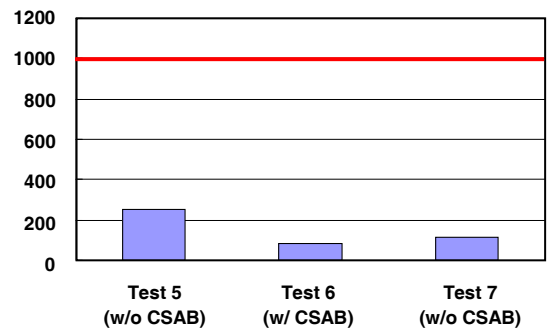
Figures 17 and 18 show the dummy injury measures and the time histories of the dummy readings. The HPC in Test 6 where the CSAB deployed and made contact with the head was 86, which was less than those for Test 5 (255) and Test 7 (113), which were conducted without a CSAB installed. As shown in the head resultant acceleration-time histories [see Figure 18(a)], in the case with a CSAB installed (Test 6), the CSAB deployed between the head and the B-pillar within 20 ms after the collision, the head was accelerated earlier in the crash event, and the peak acceleration was small. In contrast, in the case of the

struck car not having a CSAB installed (Test 5), the head made contact with the B-pillar at the velocity of the B-pillar intrusion, the head acceleration increased suddenly, and the peak was relatively high.

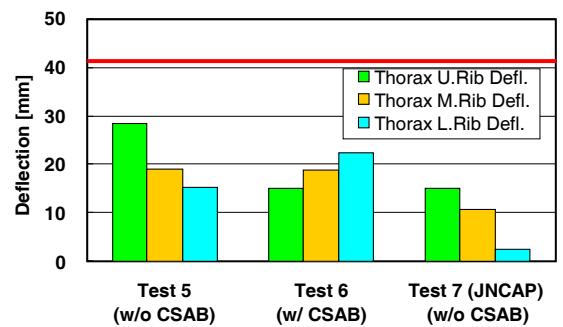
The rib deflection was smaller in the test with the CSAB installed than that without the CSAB. The rib deflection was smallest in JNCAP test where the chest made contact the door (Test 7). Accordingly, it is likely that the B-pillar has a higher potential of causing thoracic injuries than the door with respect to the rib deflection. The lower rib deflection was larger than the upper rib deflection in Test 6 probably because the SAB deployed. As shown in the time history of rib deflections [see Figure 18(b)], the lower deflection increased earlier during the crash event as compared to the upper rib. The rib deflection could be smaller with an optimization of the SAB design.

The V*C of thoracic upper rib, middle rib, and lower rib was compared in Figure 17(c). The trend of the V*C responses in these tests were comparable to those of the rib deflections.

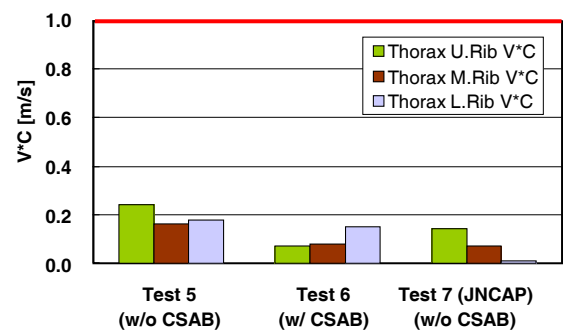
Figure 17(d) shows the abdominal and pubic forces. The abdominal force and pubic force do not change appreciably, irrespective of the CSAB equipment. In Test 7 (i.e., the JNCAP test), the abdominal force was larger and the pubic force was smaller as compared to Tests 5 and 6. Therefore, it is likely that the B-pillar has more of an injury potential to the upper torso as compared to the lower torso. Figures 18(c) and 18(d) show the time histories of abdominal force and pubic forces. Although there were differences in the abdominal force in Tests 5, 6, and 7, the pubic forces in these tests were comparable. Since the pelvis was not covered with the SAB, and the gap between the pelvis and B-pillar (Tests 5 and 6) and that between the pelvis and door (Test 7) would be comparable.



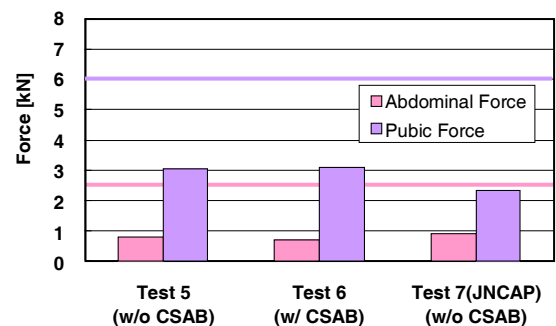
(a) HPC



(b) Thoracic rib deflection

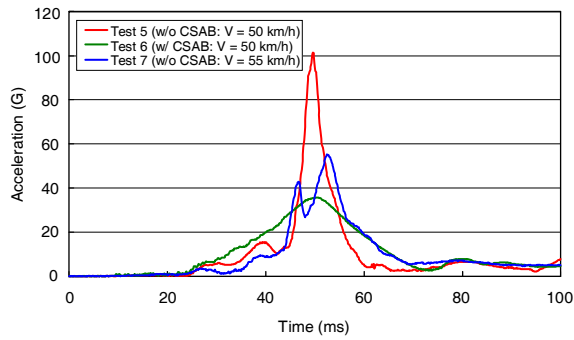


(c) Thoracic rib V*C

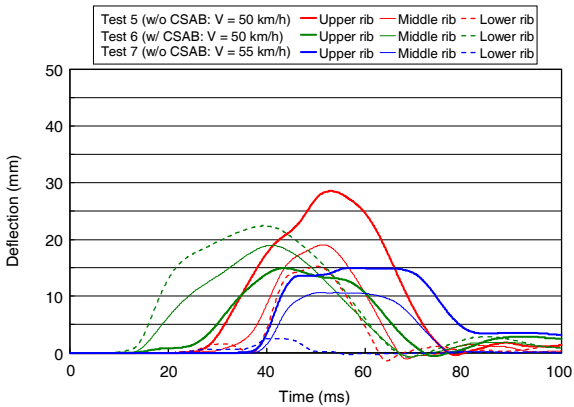


(d) Abdominal and pubic force

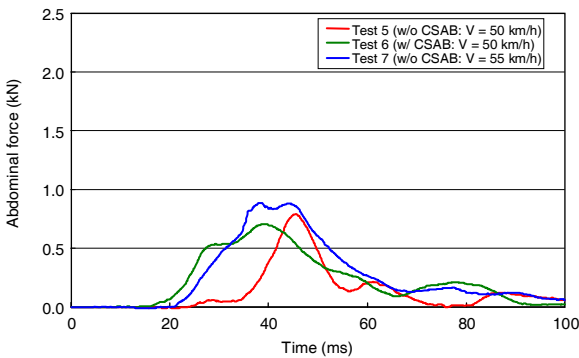
Figure 17 Injury criteria of ES-2 seated in front seat (Test 5, 6 and 7).



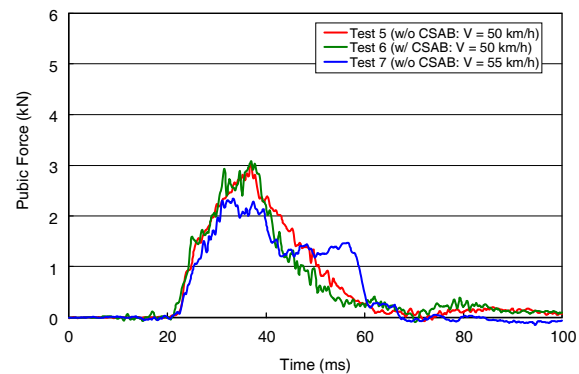
(a) Head resultant acceleration



(b) Thoracic rib deflection



(c) Abdominal force



(d) Pubic force

Figure 18 Injury parameter time histories of ES-2 in Test 5, 6, and 7.

DISCUSSION

Accident analyses were conducted using police data. Sixty percent of the fatal and serious injuries to front seat occupants in side collisions were to those seated on the struck side, and 40% were to those seated on the non-struck side. The percentage of thoracic injuries was large, whereas that of the neck injuries was small when the striking vehicle was an IBOX, SUV, or truck. The percentage of pillars being among the injury causes for head injuries was only 5.4%. A field survey of the occupant posture was conducted, and it was shown that 50% of the driver head locations overlapped the B-pillar. In order to understand this difference in the percentage of B-pillar as injury causes of the head, it is necessary to conduct further in-depth accident analyses.

The deformation and injury risk of the occupants in the struck cars are affected by the striking vehicles. Based on the accident analysis, the percentage of chest injuries was large when the struck vehicle was impacted by an IBOX. In Test 3, the IBOX impacted the Sedan 1. Since the IBOX has a high leading edge, the loading and the deformation of the struck car at the thoracic level was large. This deformation mode of the struck car led to large thoracic deflection of the dummy.

The effect of struck car movement was examined by conducting car-to-car tests (Tests 2 and 4). In Test 2, the struck car was stationary, and in Test 4 struck car was traveling at 24 km/h. The injury measures of the ES-2 seated in the struck car were smaller when the struck car was traveling compared to those when the struck car was stationary. In the car-to-car crash, when the struck car was traveling, the longitudinal members of the striking car bent laterally. As a result, the stiffness of the front structure of the striking car possibly may be less stiff than that for the striking car in Test 2. (In Test 2, the struck car was stationary and the longitudinal members of the striking car collapsed in an axial mode.) In Test 4, where both cars were moving, the deformation of the struck car was distributed widely in the struck car's longitudinal direction. The delta-V in the lateral (i.e., L-R) direction of the struck car was lower when the struck car was moving than when the struck car was stationary. The less stiff deformation mode of the striking car and the wide distribution of the struck car deformation led to a lower intrusion velocity and smaller intrusion of the struck car. As a result, the injury measures of the dummy in the struck car were smaller. In Test 4, because the impact force applied by the striking car to the struck car was small, the acceleration in the longitudinal direction of the struck car was small. Accordingly, the dummy movement in the A-P direction in the struck car was small in Test 4, and the dummy behavior was comparable between Tests 2 and 4.

Based on the field survey of occupant posture, it is probable that the occupant head makes contact with the B-pillar in side impact accidents. To understand the head injury risk in contact with B-pillar and its protection by the CSAB, Tests 5 and 6 were carried out with a dummy posture that the head overlapped the B-pillar. In Test 5, the head was impacted by the B-pillar at the intrusion velocity of the B-pillar, and the peak of the head acceleration was high. The HPC in the Test 5 was less than the injury assessment reference value possibly because of the energy absorbing structure in the B-pillar. In Test 6, the struck vehicle was equipped with a CSAB and SAB. The CSAB deployed and decelerated the head at an early stage of the impact, and thereby effectively reduced the head acceleration. It is likely that the CSAB is effective for reducing head injury risk in the case where the head would make contact with B-pillar.

CONCLUSIONS

In order to discuss potential side impact test procedures for the future and to identify the issues in side collisions, accident analyses, a field survey of occupant posture, and crash tests were carried out. The results are summarized as follows:

1. From accident analyses using police data, 60% of the fatal and serious injuries to front seat occupants in side collisions were to the struck side occupants, and 40% were to the non-struck side occupants. The percentage of thoracic injuries was larger as the striking vehicle was the IBOX, SUV, or truck.
2. Based on the field survey on the road, it was shown that 50% of driver heads overlapped the B-pillar. Accordingly, it is predicted that the head will make contact with the B-pillar which can lead to head injuries.
3. The deformation and injury measures of the dummy of the struck car were affected by the properties of the striking car. When the IBOX vehicle, which has a flat front shape and a stiff front structure, impacted the side of the car, the thorax was impacted because of the large deformation of the belt-line of the struck car. As a result, the HPC of the dummy in the struck car was small and the chest deflection was large.
4. The effect of struck car movement was examined from the car-to-car tests. When the struck car was moving, the loading and the deformation of the struck car was small, and the injury measures of the dummy in the struck car were smaller than those for when the test was conducted with the struck car being stationary.
5. The effect of CSAB was examined in the case where the dummy placement resulted in the dummy head being overlapped with the B-pillar. The CSAB decelerated the head at the early stage of the impact, and thereby effectively reduced the head acceleration. It is likely that the CSAB is effective for reducing head injury risk as compared to the case where the head otherwise would make contact with the B-pillar.

ACKNOWLEDGEMENT

This study project was carried out under contract between the Japan Ministry of Land, Infrastructure and Transport (Japan MLIT) and the National Traffic Safety and Environment Laboratory (NTSEL). The side impact occupant protection working group was established and this study was conducted according to the opinions within the working group. The authors thank the members in the WG and researchers and engineers who cooperated in the experiments and for their support. These include members from the National Agency for Automotive Safety & Victim's Aid, Japan Automobile Research Institute (JARI), and Japan Automobile Transport Technology Association (JATA).

REFERENCES

1. ECE Regulation No.95, "Uniform provisions concerning the approval of vehicles with regard to the occupants in the event of a lateral collision" (1995)
2. Newland C., "International Harmonised Research Activities Side Impact Working Group Status Report" 19th ESV, Paper Number ,05-0460 (2005)
3. Seyer, K., "International Harmonized Research Activities Side Impact Working Group Status Report," 18th ESV, Paper Number 579 (2003)
4. Matsui, Y., et al. "Investigation for New Side Impact Test Procedure in Japan", 20th ESV, Paper Number ,07-0059 (2007).
5. Yonezawa, Y., et al. "Investigation of New Side Impact Test Procedures in Japan" 19th ESV, Paper Number ,05-0188 (2005).
6. Yonezawa, H., et al. "Investigation of New Side Impact Test Procedures in Japan," 18th ESV, Paper Number 328 (2003).
7. Yonezawa, H., et al. "Japanese Research Activity on Future Side Impact Test Procedures," 17th ESV, Paper Number 267 (2001).